Molecular Characterization of EGFR Signaling in *Drosophila melanogaster*

Dissertation

zur Erlangung des Doktorgrades
der Mathematisch-Naturwissenschaftlichen Fakultät
der Christian-Albrechts-Universität zu Kiel

vorgelegt von
Tasja Rahn

Kiel, 2012

Referent:	Prof. Dr. Matthias Leippe
Korreferent:	Prof. Dr. Thomas Roeder
Tag der mündlichen Prüfung:	07.11.2012
zum Druck genehmigt:	07.11.2012

_____

Prof. Dr. Wolfgang J. Duschl, Dekan

TABLE OF CONTENTS

LIST OF ABBREVIATIONS

°C	degree Celsius
µg	microgram
µl	microliter
aa	amino acids
aaRNA	aminoallyl ribonucleic acid interference
aaUTP	aminoallyl uridin triphosphate
AC	adenylyl cyclase
ACT	constitutively active
AD	activation domain
aFB	abdominal fat body
AL	antennal lobe
AM	amyl acetate
AMP	antimicrobial peptide
AN	antennal nerve
BL	brain lobe
BODIPY	4,4-difluoro-1,3,5,7,8-pentamethyl-4-bora-3a,4a-diaza-s-indacene
bp	base pairs
Ca	calyx
$CaCl_2*2H_2O$	Calciumchlorid-dihydrat
cAMP	cyclic adenosine monophosphate
CB	cell bodies
CC	central complex
CCA	coupled colorimetric assay
cDNA	complementary deoxyribonucleic acid
cm	centimeter
CNS	central nervous system
C_t	cycle threshold
ctrl	control
DAPI	4',6-diamidino-2-phenylindole
DBD	deoxyribonucleic acid binding domain
DGRC	*Drosophila* Genomics Resource Center

DIC	differential interference contrast
dM	distal medulla
Dm	distal amacrine neurons
DMSO	dimethyl sulfoxide
DN	dominant negative
DNA	deoxyribonucleic acid
dNTP	deoxynucleoside triphosphate
E	ejaculatory duct
E. coli	*Escherichia coli*
EB	enteroblast
EC	enterocyte
EDTA	ethylenediaminetetraacetic acid
EE	enteroendocrine
EGF	epidermal growth factor
EGFR	epidermal growth factor receptor
ER	endoplasmic reticulum
ErbB	erythroblastic leukemia viral (v-erb-b) oncogene homologue
Eso	esophagus
FB	fan-shaped body
FRU	fructose
fwd	forward
g-3-p	glycerin-3-phosphate
GFP	green fluorescent protein
gpo-1	glycerophosphate oxidase-1
Grb2	growth factor receptor binding protein 2
Gs	G protein subunit α_s
GS	GeneSwitch
h	hour
H_2O	water
HCl	hydrochloric acid
HER	human epidermal growth factor receptor
HL3	hemolymph-like buffer
hPR BD	human progesterone receptor binding domain
Ig	immunglobulin

ISC	intestinal stem cell
KCl	potassium chloride
KH_2PO_4	orthophosphate potassium dihydrogen
l	liter
LB	Lauria Bertani
LC	lobula complex
LI	learning index
Lo	lobula strata
M	medulla
mA	milliampere
MAPK	mitogen-activated protein kinase
MB	mushroom body
MEK	mitogen-activated protein/extracellular signal-regulated kinase kinase
mg	milligram
$MgCl_2$	magnesium chloride
$MgSO_4$	magnesium sulfate
mife	mifepristone
min	minute
ML	medial lobe
mM	millimolar
mm	millimeter
$MnCl_2 * 4\ H_2O$	manganese(II) chloride tetrahydrate
mRNA	messenger ribonucleic acid
Na_2HPO_4	potassium dihydrogen orthophosphate
NaCl	sodium chloride
$NaHCO_3$	sodium hydrogen carbonate
NaOH	sodium hydroxide
NEU	neutral
NF1	neurofibromin 1
nm	nanometer
NRG	neuregulin
ns	not significant
OCT	1-octanol

OD	optical density
OL	optic lobe
PBS	phosphate buffered saline
PCR	polymerase chain reaction
PI	pars intercerebralis
PI3K	phosphatidylinositol 3-kinase
PKA	protein kinase A
PR	photoreceptor
Pref	preference
prom-gal4	*promoter-gal4*
qRT-PCR	quantitative real-time polymerase chain reaction
QUI	quinine
RAF	rapidly accelerated fibrosarcoma
RAS	rat sarcoma
rev	reverse
Rho	Rhomboid
RNAi	ribonucleic acid interference
rpm	rounds per minute
RT-PCR	reverse-transcriptase polymerase chain reaction
Rut-AC	Rutabaga-AC
SCN	suprachiasmatic nucleus
sec	second
SOC	super optimal broth with catabolite repression
SOG	subesophageal ganglion
SOS	son of sevenless
Spi	Spitz
TAG	triacylglyceride
TARGET	temporal and regional gene expression targeting
TGF α	transforming growth factor α 1-4
Tm	transmedullary neurons
TriC	tritocerebrum
tRNA	transfer ribonucleic acid
UAS	upstream activating sequence
v/v	volume/volume

VDRC	Vienna *Drosophila* RNAi Center
VL	ventral lobe
VM	visceral muscle
VNC	ventral nerve cord
w/v	weight/volume
× g	x-fold gravity

1 INTRODUCTION

1.1 EPIDERMAL GROWTH FACTOR RECEPTOR SIGNALING

Epidermal growth factor receptor (EGFR) signaling is found throughout the animal kingdom (Stein and Staros, 2006). It plays essential roles in development and in the maintenance of adult tissues by regulating cell proliferation, survival, differentiation, migration, and growth (Wieduwilt and Moasser, 2008). In general, EGFR signaling transduces signals from the extracellular environment to the nucleus, where it influences diverse genetic programs (Fig. 1).

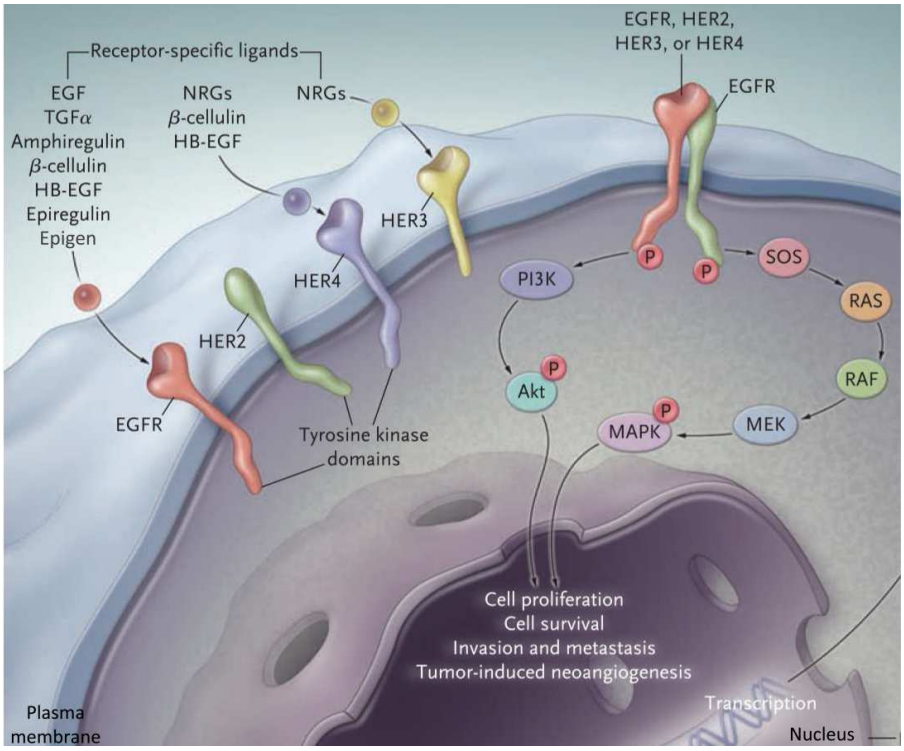

Fig. 1. EGFR signaling in humans. On the left side, the four ErbB family members EGFR (ErbB1), HER2 (ErbB2), HER3 (ErbB3), and HER4 (ErbB4) are displayed as transmembrane proteins with their specific ligands epidermal growth factor (EGF), transforming growth factor α (TGF α), amphiregulin, β-cellulin, heparin-binding EGF-like growth factor (HB-EGF), epiregulin, epigen, and neuregulin 1-4 (NRGs). On the right side, the formation of homo- or heterodimers upon ligand binding is shown (ligand not visible). The dimerization triggers phosphorylation (P) of tyrosine residues at the cytoplasmic domain of the receptors, which subsequently activates two major intracellular pathways: RAS/RAF/MEK/MAPK pathway or phosphatidylinositol 3-kinase (PI3K)-AKT pathway. HER, human epidermal growth factor receptor; MAPK, mitogen-activated protein kinase; MEK, mitogen-activated protein/extracellular signal-regulated kinase kinase; RAF, rapidly accelerated fibrosarcoma; RAS, rat sarcoma; SOS, son of sevenless. Modified from Ciardiello and Tortora (2008).

In vertebrates, EGFR is the founding member of the erythroblastic leukemia viral (v-erb-b) oncogene homologue (ErbB) receptor family, which also includes ErbB2/HER2, ErbB3/HER3, and ErbB4/HER4 (Yarden and Schlessinger, 1987).

These receptors have three distinct domains, which are an extracellular ligand binding domain, a hydrophobic transmembrane region, and a cytoplasmic tyrosine kinase domain (Yarden and Ullrich, 1988). At the plasma membrane, the unstimulated EGFR is present as a monomer (Fig. 1, left side). Eleven ligands can induce the formation of homo- or heterodimers, which leads to phosphorylation on tyrosine residues of the cytoplasmic domain (Fig. 1; Holbro and Hynes (2004)). A variety of signaling molecules interact with these phosphorylated residues and subsequently control diverse genetic programs by several intracellular signaling cascades, mostly via the RAS/RAF/MEK/MAPK pathway or the phosphatidylinositol 3-kinase (PI3K)-AKT pathway.

Dysregulation of EGFR signaling has been causally implicated in several severe human diseases, most notably cancer (Dhomen *et al.*, 2012) and neurological disorders (Bublil and Yarden, 2007). To elucidate the molecular mechanisms underlying dysfunctions of EGFR signaling, the pathway is also intensively studied in simpler model organisms, such as mice or the fly *Drosophila melanogaster.*

1.1.1 EGFR SIGNALING IN *DROSOPHILA MELANOGASTER*

In contrast to vertebrates, *Drosophila melanogaster* owns only one EGFR and four activating ligands. A fifth ligand unique to *Drosophila* inhibits EGFR activation (Shilo, 2003). However, the EGFR pathways in vertebrates and *Drosophila* share the basic machinery (Fig. 2; Schejter *et al.* (1986); Bogdan and Klämbt (2001); Vivekanand and Rebay (2006)).

Unlike vertebrates, which own two major downstream signaling pathways, transcriptional activation in *Drosophila* is transduced exclusively by a RAS/RAF/MEK/MAPK cascade that influences gene expression mostly through the transcriptional activator Pointed and the transcriptional repressor Yan to maintain signaling homeostasis (Gabay *et al.*, 1996).

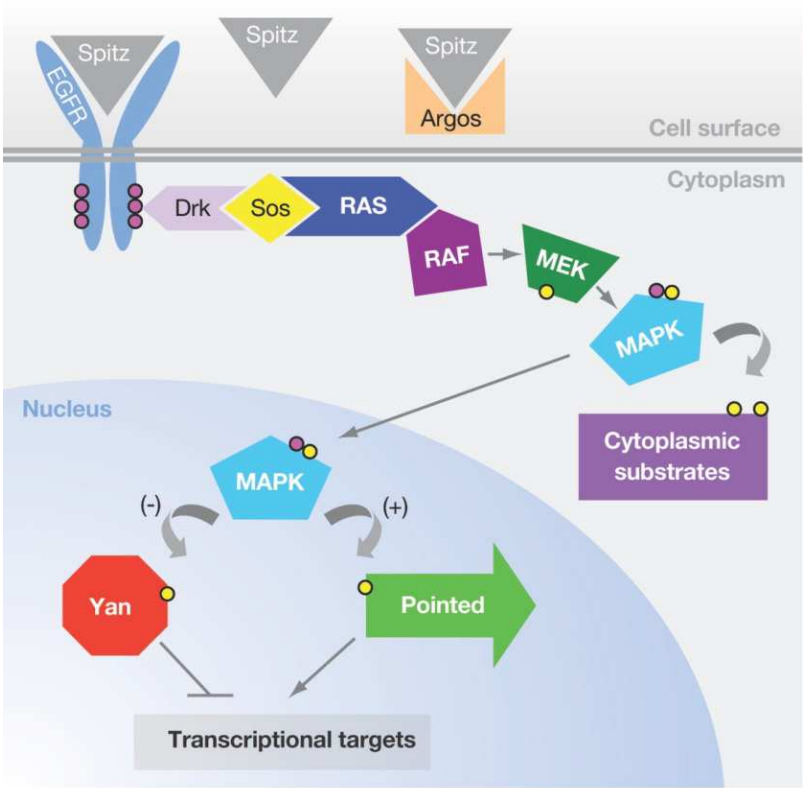

Fig. 2. The EGFR signaling pathway in *Drosophila*. Exemplary for activation of EGFR signaling, the ligand Spitz is shown. Upon ligand binding, an EGFR homodimer is built, which results in trans- and autophosphorylation of tyrosines in the cytoplasmic receptor domain. Via the adaptor protein Drk and son of sevenless (SOS), a RAS/RAF/MEK/MAPK pathway is activated. Subsequently, the MAPK targets the repressing (-) transcription factor Yan and activating (+) transcription factor Pointed to maintain signaling homeostasis. Phosphorylation is shown in violet circles (tyrosines) or yellow circles (serine/threonine). Not all phosphorylation events are displayed (Vivekanand and Rebay, 2006).

The activating EGFR ligands Spitz, Keren, Gurken, and Vein differ in their systemic availability (Fig. 3). Spitz, Keren, and Gurken are produced as membrane-bound precursor proteins that have to be proteolytically cleaved before they become systemically available and, subsequently, activate the pathway (Urban *et al.*, 2002). By contrast, Vein is produced as a secreted protein that does not need any processing (Schnepp *et al.*, 1996).

The transforming growth factor (TGF) α homologue Spitz (Fig. 3 A) is the most prominent ligand and has been analyzed in detail. Spitz is transported by the chaperone Star from the endoplasmic reticulum to the Golgi apparatus, where it is cleaved by the intra-membrane serine protease Rhomboid (Fig. 3 B). In the embryo, Spitz is broadly expressed and is involved in a variety of developmental processes, such as dorsal-ventral axis formation (Rutledge *et al.*, 1992), patterning of the dorsal midline (Dumstrei *et al.*, 1998), and formation of the Malpighian tubules (Sudarsan *et al.*, 2002). In post-embryonic development, it is involved in many events, like determination of the veins in wing discs (Sturtevant *et al.*, 1993), neuronal differentiation in the lamina (Huang *et al.*, 1998), and restriction of stem cell renewal capacity in somatic cyst cell during spermatogenesis (Kiger *et al.*, 2000).

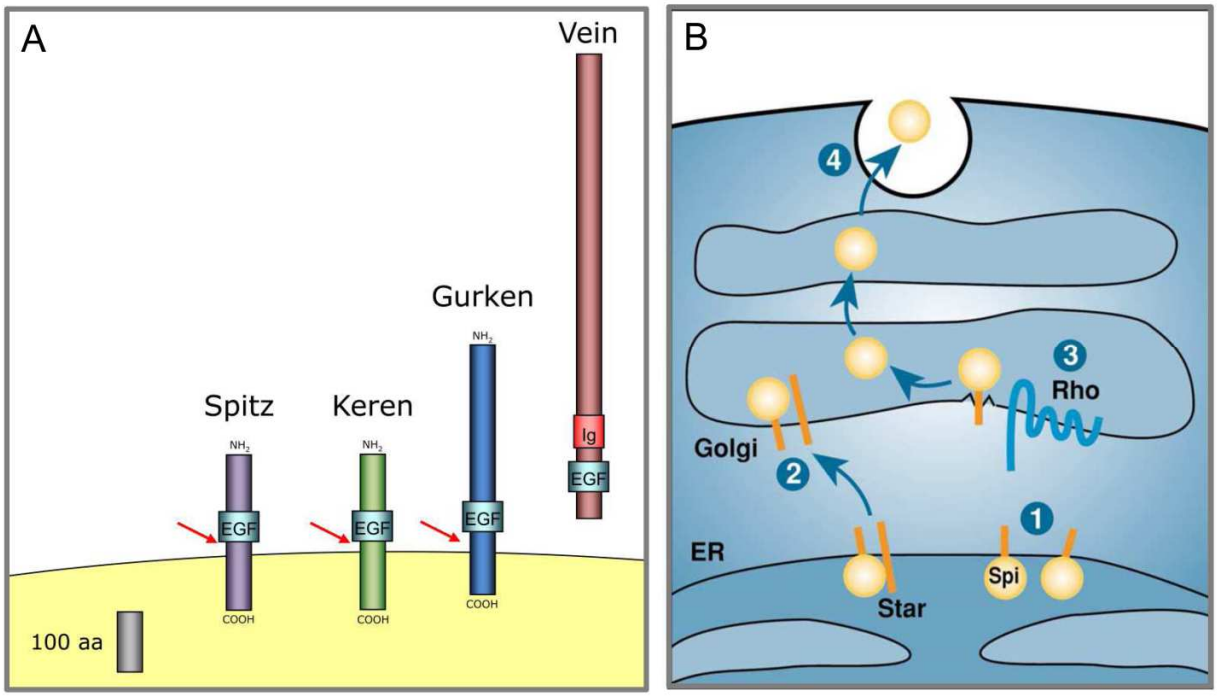

Fig. 3. EGFR signaling ligands and their proteolytic processing. (A) Spitz, Keren, and Gurken are produced as membrane-bound precursor proteins with an epidermal growth factor domain (EGF). Red arrows indicate the cleavage sites. Vein is produced as a secreted protein. Additional to the EGF domain, Vein owns an immunglobulin domain (Ig). (B) Exemplary for the three membrane-bound EGFR ligands, the transport and processing of Spitz is displayed. (1) The membrane-bound precursor Spitz (Spi) is situated in the endoplasmic reticulum (ER). (2) The chaperone Star transports Spitz to the Golgi, (3) where it is cleaved by the intra-membrane serine protease Rhomboid (Rho). (4) Finally, the extracellular domain of Spitz is secreted. Aa, amino acids. Modified from Shilo (2003)**.**

Keren (Fig. 3 A) is the functional homologue of Spitz but also possesses a Rhomboid/Star independent ability to undergo low-level cleavage (Reich and Shilo, 2002). It is involved in the migration of border cells in the embryo (McDonald *et al.*, 2006) and it controls cell clustering, cell survival and spacing of the photoreceptor (PR) R8 (Brown *et al.*, 2007).

The secreted ligand Vein (Fig. 3 A) is structurally similar to vertebrate neuregulin and has a restricted expression pattern in the embryo (Schnepp *et al.*, 1996), where it is involved in the patterning of the ventral ectoderm (Schweitzer *et al.*, 1995), specification of muscle precursors (Buff *et al.*, 1998), and maintenance of glia cell survival and axon guidance (Hidalgo *et al.*, 2001).

Like Spitz, the ligand Gurken (Fig. 3 A) is a TGF-α homologue and needs to be proteolytically processed. It plays multiple roles during oogenesis, such as the establishment of the anterior-posterior and the dorsal-ventral polarities (Neuman-Silberberg and Schüpbach, 1993) and the migration of border cells (Duchek *et al.*, 2001).

An additional EGFR signaling ligand, called Argos, blocks the activation of the pathway by ligand sequestration of Spitz (Golembo *et al.*, 1996; Klein *et al.*, 2004;

Shilo, 2005). As well as Vein, Argos is produced as a secreted protein. It is involved in many processes during embryonic and post-embryonic development. Examples are the segmentation of midline cells (O'Keefe *et al.*, 1997) and determination of pigment cells in the eye disc (Freeman, 1996). Importantly, Argos is only expressed when the EGFR is activated at high levels and is thus part of a negative feedback loop that restricts signaling to a small region (Golembo *et al.*, 1996). Its function is the inhibition of EGFR signaling in cells that are more distant from the source. In this way, a signaling mode that is restricted to the surrounding area is supported, irrespective the tissue, in which signaling takes place (Shilo, 2005).

1.2 Non-Developmental Roles of EGFR Signaling in *Drosophila*

In contrast to the attribution of EGFR signaling to a variety of functions in development, little is known about the non-developmental roles of this signaling system. These known functions comprise the involvement in maintenance of gut homeostasis and some neuronal functions.

Buchon *et al.* (2010) and Jiang *et al.* (2011) reported that EGFR signaling is important for gut homeostasis after bacterial infection in adult flies. It was shown that EGFR signaling promotes intestinal stem cell (ISC) proliferation, delamination, and anoikis of damaged enterocytes (ECs) after infection with *Erwinia carotovora* or *Pseudomonas entomophila*. Moreover, they analyzed *spitz*, *vein*, and *keren* expression in guts of adult flies via *in situ* hybridisation, *vein*-lacz, *spitz* enhancer-trap-*gal4*, and RNAi experiments. *Spitz* expression was detected in precursor cells, i.e. ISCs and enteroblasts (EBs), and ECs, *vein* expression was detected in the visceral muscle and ECs, and *keren* expression in precursor cells and ECs.

Jiang and Edgar (2009) found that signaling through the EGFR pathway is necessary and limiting for adult midgut progenitor cell proliferation in larvae. These progenitor cells express the ligands *spitz* and *keren*, whereas *vein* is expressed in the visceral muscle of the gut.

Another non-developmental role of EGFR signaling is the regulation of sleep levels in adult flies (Foltenyi *et al.*, 2007). Induction of enhanced EGFR signaling by the expression of *rhomboid-1* and *star* or a gene coding for the active form of Spitz resulted in increased sleep levels. On the contrary, constitutively and pan-neuronally

reduced EGFR signaling by silencing of *rhomboid-1* resulted in decreased sleep levels and abnormally low locomotor activity.
In addition, Corl *et al.* (2009) showed that EGFR signaling regulates ethanol sensitivity in adult flies. Enhanced EGFR signaling in the nervous system resulted in resistance to sedating effects of ethanol.

1.3 Anatomy of *Drosophila* Larvae and adult Flies

Although phylogenetically distantly related, *Drosophila* has organs that perform the equivalent functions of several mammalian organs, e.g. gut, kidney, liver, reproductive tract, and brain (Pandey and Nichols, 2011). Therefore, larvae and adult flies are suited to study the physiology of organs in a comparatively simple model organism.
Anatomy and functions of several organs of the fruit fly are introduced in the following paragraphs.

1.3.1 Anatomy and Functions of the Digestive System

The *Drosophila* digestive tract is necessary for the absorption of nutrients. From anterior to posterior, it consists of the pharynx, esophagus, proventriculus, midgut, and hindgut with the salivary glands and the attached Malpighian tubules (Fig. 4 A and D). The proventriculus is located at the foregut/midgut junction (Lehane, 1997). Its main function is the secretion of the peritrophic matrix, an acellular sheath that lines the entire intestine and plays a major role in food digestion and absorption. The larval and the adult midgut are composed of a single layer of epithelial cells with two layers of visceral muscle wrapped outside (Jiang *et al.*, 2011). The larval and the adult *Drosophila* midgut, like the mammalian intestine, are made up of digestive ECs and hormone-producing enteroendocrine cells (EEs; LaJeunesse *et al.* (2010)).

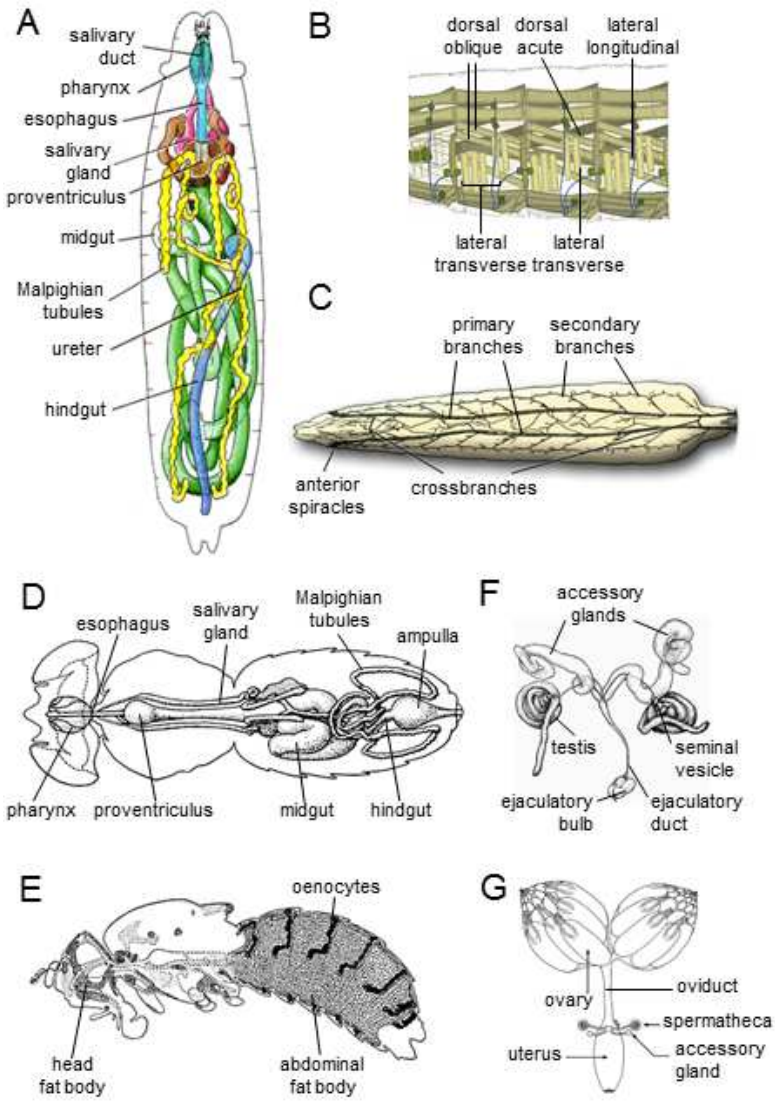

Fig. 4. Anatomy of larvae and adult flies. (A) Overview of a larva with digestive system and glands (anterior is up; modified from www.doctoc.com); (B) dorso-lateral view on the larval abdominal body wall muscles (anterior is left; modified from Hartenstein (1993)); (C) dorsal view on the larval tracheal system (anterior is left; www.flymove.uni-muenster.de); (D) dorsal view on the adult digestive system with glands (anterior is left; modified from Miller (1950)); (E) lateral view on the adult fat body (modified from Miller (1950)); (F) male reproductive tract (modified from (Patterson, 1943)); and (G) female reproductive tract (modified from Bloch Qazi *et al.* (2003)).

The larval midgut also contains undifferentiated adult midgut progenitor cells, which appear as scattered islets of cells and give rise to the new adult midgut epithelium during pupal development (Jiang and Edgar, 2009). Instead of these cells, the adult midgut owns ISCs and EBs. The latter subsequently become ECs or EEs to maintain gut homeostasis (Ohlstein and Spradling, 2007).

The salivary glands secrete fluids and proteins for digestion, whereas the Malpighian tubules are necessary for excretion and are analogous to the vertebrate kidney (Singh *et al.*, 2007).

1.3.2 Anatomy and Functions of the Fat Body and the Reproductive Tract

The fat body in larvae and adult flies (Fig. 4 A and E) is an organ unique to insects (Law and Wells, 1989). However, because of its variety of essential roles in metabolism, it is often compared with the mammalian liver (Søndergaard, 1993). It is made up of adipose tissue attached to the internal surface of the exoskeleton. Its main cells are the adipocytes, which are characterized by the presence of lipid droplets (Arrese and Soulages, 2010). These lipid droplets store triacylglycerides (TAGs) and to a less extend glycogen. In close contact with the fat body are the so-called oenocytes. These cells have a role in lipid mobilization during starvation (Gutierrez *et al.*, 2007).

The major functions are the secretion of antimicrobial peptides (AMPs; Imler and Bulet (2005)) and the energy metabolism, which includes storage and release of fat (Law and Wells, 1989). Furthermore, the fat body is an endocrine organ (Geminard *et al.*, 2009) and participates in detoxification (Misra *et al.*, 2011).

The male reproductive tract consists of the sperm-producing testes as well as different accessory tissues, which are the seminal vesicles, accessory glands, the ejaculatory duct, and the ejaculatory bulb (Fig. 4 F). These accessory tissues produce the seminal fluid, which is together with the sperm transferred to the female reproductive tract during mating (Ravi Ram and Wolfner, 2007).

The paired ovaries of the female reproductive tract produce the oocytes (Fig. 4 G). The mature oocytes leave the ovaries via the oviduct into the uterus, where they will be fertilized (Middleton *et al.*, 2006). In the spermathecae, sperm can be stored for later fertilization.

1.3.3 Anatomy and Functions of the Central Nervous System

The *Drosophila* central nervous system (CNS) and the human brain present common features (Davis, 2004; Lessing and Bonini, 2009). Especially the olfactory systems of humans and insects have striking design similarities. They share the basic hierarchy with first, second, and third order olfactory neurons and the synaptic connections in brain centers are comparable (Davis, 2004). Significantly, the response of flies to

many drugs that act within the CNS is similar to the effects observed in mammalian systems (Pandey and Nichols, 2011).

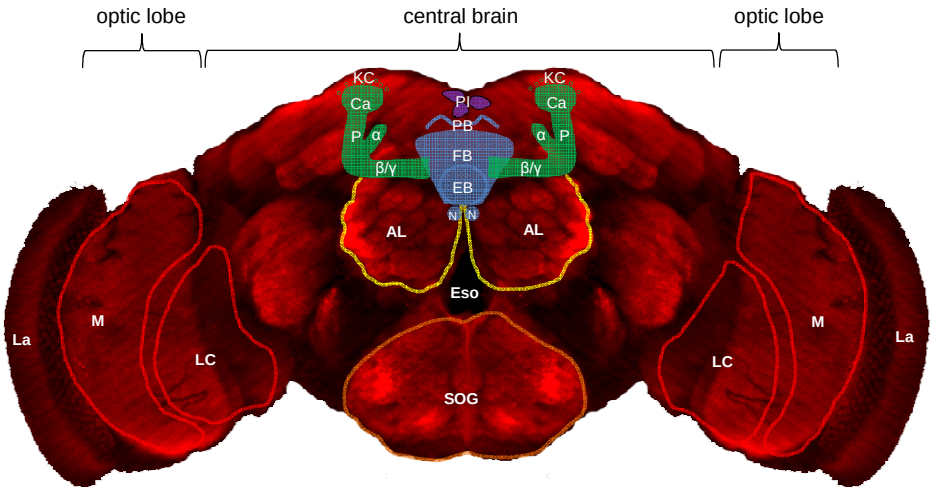

Fig. 5. Scheme of the *Drosophila* adult brain. The neuropil (red) of the central brain and the optic lobes with the lamina (La) are shown. The most prominent substructures of the supraesophagial ganglion are displayed: mushroom bodies (green) with Kenyon cells (KC), calyx (Ca), pedunculus (P), and α and β/γ lobes; central complex (blue) with protocerebral bridge (PB), fan-shaped body (FB), ellipsoid body (EB), and noduli (N) as well as the antennal lobes (ALs, framed yellow). The supraesophageal ganglion also contains the pars intercerebralis (PI) with neurosecretory cells (violet). The optic lobes contain the medulla (M, framed red) and the lobula complex (LC, framed red). Eso, esophagus; SOG, subesophageal ganglion (framed orange).

However, the larval and the adult brain of *Drosophila* differ in their complexity. The larval brain possess about 10,000 to 15,000 neurons, a value 10 to 20-fold lower than the number of neurons in the adult brain (Scott *et al.*, 2001). The more than 100,000 neurons of the adult brain form discreet circuits and neuropils (Fig. 5) that mediate complex behaviors, including circadian rhythm, sleep, learning and memory, and feeding (Pandey and Nichols, 2011).

The adult central brain region is divided in a small subesophageal ganglion (SOG) below the esophagus and a large supraesophageal ganglion above the esophagus (Fig. 5).

The SOG (Fig. 5) is important for taste behavior. Gustatory receptors of taste neurons on the labellum detect tasting agents in the environment. The axons of these gustatory receptor neurons innervate the SOG (Marella *et al.*, 2006). Additionally, dendrites of motor neurons branch in the SOG and send their axon to the proboscis. These motor neurons mediate the behavioral response to the perceived taste (Gordon and Scott, 2009).

The supraesophageal ganglion is structured into characteristic neuropil regions (Fig. 5) including antennal lobes (ALs), adult mushroom bodies (MBs), and the central complex (CC).

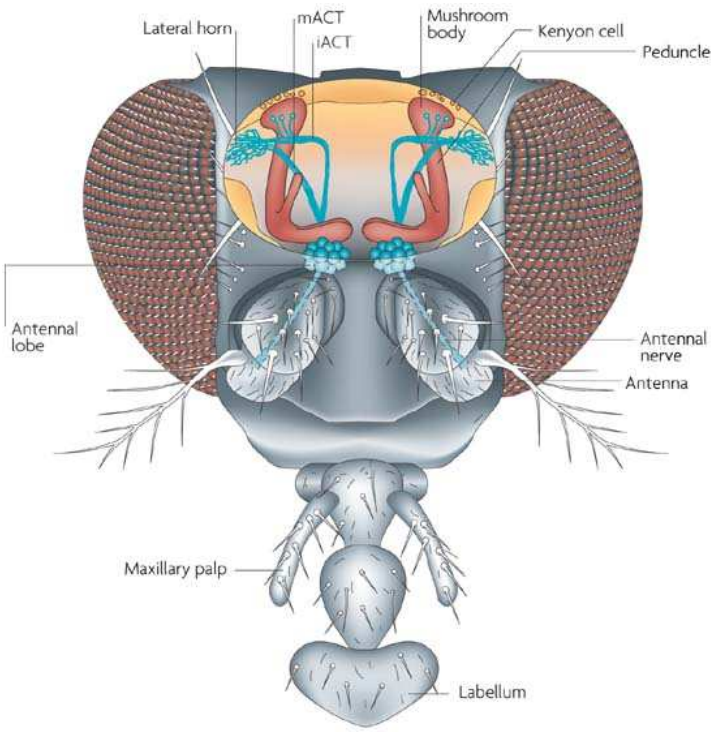

Fig. 6. Dorsal view of a cutaway fly head showing the main elements of the olfactory pathway. Odors are sensed by olfactory receptor neurons in the antennae and maxillary palps. These neurons project axons along the antennal nerve to the antennal lobe glomeruli. From there the information is relayed by projection neurons to the mushroom bodies (displayed with Kenyon cells and peduncle) and to the lateral horn via the inner and medial antennocerebral tract (iACT and mACT). Gustatory stimuli are sensed by gustatory receptor neurons in the labellum on the tip of the proboscis (Keene and Waddell, 2007).

The ALs are the primary centers for olfactory processing that have equivalent functions as the olfactory bulb in mammals (Fishilevich *et al.*, 2005). They receive input from the antenna via the antennal nerve and from the maxillary palp and the labellum via the labiomaxillary nerve. Each antenna contains approximately 1,200 olfactory receptor neurons, whereas the maxillary palp comprises only 120 (de Bruyne *et al.*, 1999). The main elements of the olfactory system are displayed in Fig. 6.

Olfactory receptors on the antenna bind to free-floating molecules like odors and pheromones. The neurons that possess these receptors are called olfactory receptor neurons. These first order olfactory neurons synapse with two types of second order olfactory neurons, named local interneurons and projection neurons, in the glomerular neuropil of the ALs. Subsequently, the projection neurons connect to third order olfactory neurons located in the lateral horn and the MBs (Fig. 6) that identify the odor (Das *et al.*, 2008; Hummel *et al.*, 2003). These higher brain centers share similarities with the mammalian amygdaloid cortex and the piriform cortex (Davis, 2004).

The MBs are mainly formed of intrinsic neurons named Kenyon cells. The axons of these cells form the substructures of the MBs, which are roughly classified into calyx, pedunculus as well as α and β/γ lobes (Lee *et al.*, 1999). They are not only required for odor identification but also for olfactory learning and memory by processing

olfactory and gustatory information (Busto *et al.*, 2010). At the molecular level, the rutabaga adenylyl cyclase (AC) is assumed to function as a coincidence detector capable of associating information from both stimuli. This enzyme can be activated synergistically by odor-induced Ca^{2+} and by taste-induced G-protein coupled receptor signaling (Gervasi *et al.*, 2010). Subsequent cAMP/PKA pathway activation plays a crucial role in synaptic plasticity and memory storage (Blum *et al.*, 2009; Tomchik and Davis, 2009). In addition, the MBs are involved in the regulation of locomotor activity and circadian rhythms (Joiner *et al.*, 2006).

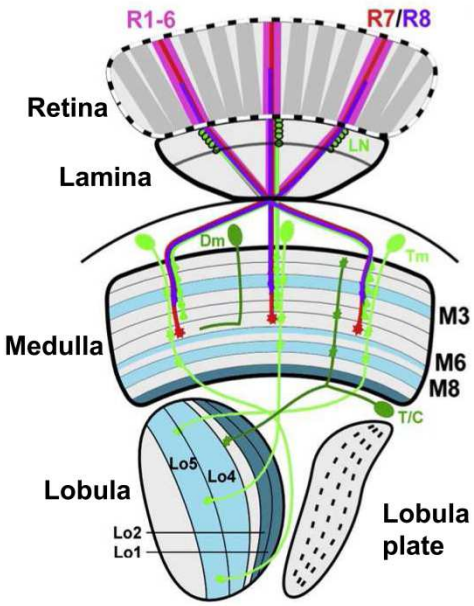

Fig. 7. *Drosophila* adult visual system. In the adult retina, each ommatidium consists of six outer photoreceptors (R1–R6) and two inner photoreceptors (R7 and R8). R1–R6 (pink) extend their axons into the lamina and synapse with lamina neurons (LN). R7 (red) and R8 (violet) terminate in the medulla strata M3 and M6, respectively. Three types of medulla neurons are displayed: Transmedullary neurons (Tm), distal amacrine neurons (Dm), and T and C (T/C) neurons. The axons of Tm neurons reach through the medulla and the lobula. Dm neurons (Dm) synapse in the medulla, and T/C neurons extend axons into the medulla and lobula. Lobula and lobula plate can be summarized as the lobula complex. Lo, lobula strata. Modified from Gao *et al.* (2008).

The CC lies in the middle of the central brain and is built of the four substructures of the protocerebral bridge, the fan-shaped body, the ellipsoid body and the noduli (Hanesch *et al.*, 1989). The CC is a characteristic neuropil of adult brains and is important for locomotor behavior (Strauss and Heisenberg, 1993).

In addition to these three characteristic regions, the supraesophageal ganglion contains the pars intercerebralis (PI), which is one of the centers of the central neuroendocrine system. It contains large neurosecretory cells with axons along the median midline innervating the ring gland, which surrounds the aorta (de Velasco *et al.*, 2007).

The visual system flanks the central brain region on the left and on the right side. It consists of the optic lobes (OLs) and the retina (Fig. 5 and Fig. 7). The OLs are organized in parallel, retinotopically organized columns and consist of four neuropil regions: lamina, medulla, lobula and lobula plate. Lobula and lobula plate are also

called lobula complex and are involved in higher processing of motion detection and color vision (Fig. 7).

The retina is situated distal of the OLs (Fig. 7). It owns about 800 ommatidia each containing eight photoreceptor (PR) cells. The PRs R1-R6 lie peripheral in the ommatidium, range over the entire length of the ommatidium, and terminate in the lamina. By contrast, PR R7 and PR R8 lie in the center of the ommatidium, have a smaller length, and terminate in the medulla neuropil. R7 is located distal of R8. The function of PR R1-R6 is the detection of motion, while R7 and R8 perceive colors (Fig. 7; Morante and Desplan (2004)).

The connections between lamina and medulla as well as between medulla and lobula complex transduce visual information (Fig. 7; Blagburn and Bacon (2004)). They connect the PR cells with layers specialized for processing visual information.

The lower complexity of the larval brain is not only demonstrated by a smaller number of neurons but also by fewer functional regions (Fig. 8). However, the two basic parts, the brain lobes (BLs) and the ventral nerve cord (VNC), can be subdivided in several sections. The BLs and the VNC contain a central fibrous neuropil (Fig. 8), which is surrounded by an outer shell of neuronal cell bodies and glial cells.

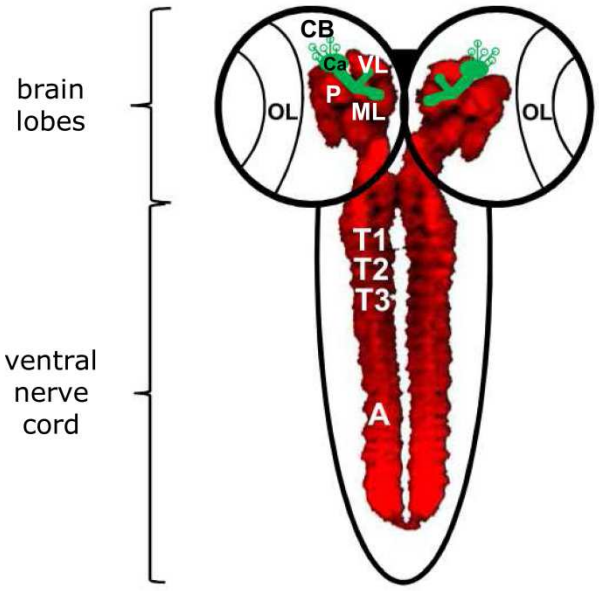

Fig. 8. Scheme of the *Drosophila* larval brain. The two main parts of the larval brain are the brain lobes and the ventral nerve cord. Both contain the neuropil, which is stained with the nc82 antibody as a reference for brain morphology (red). The most prominent region of the brain lobes is the mushroom body complex (green). Several substructures of this complex are displayed: cell bodies (CBs), calyx (Ca), pedunculus (P), ventral lobe (VL), and medial lobe (ML). The ventral nerve cord comprises of hemisegments in both the thoracic region (T1-T3) and the abdominal region (A). OL, optic lobes.

The whole CNS is bilaterally symmetrical, which means that neurons are organized in right and left mirror images. There are also medial neurons that mediate considerable communication between right and left side. The most prominent region of the BLs is

the MB complex. Like the adult MBs, the larval MBs are important for olfactory learning and memory and consist of five main compartments (Pauls *et al.*, 2010). These compartments are cell bodies, calyx, pedunculus, and vertical and medial lobe. Additional to the MBs, the BLs contain the OL region, where neuroblasts develop, which subsequently generate the medulla neurons (Wang *et al.*, 2011).
The VNC can be divided in thoracic region and abdominal region, which are composed of hemisegments. Each hemisegment contains about 200 neurons. Most neuronal cell bodies are relatively inaccessible within the VNC, which is ensheated by glia and connective tissue. In general, VNC cells are difficult to identify (Rohrbough and Broadie, 2002).

1.4 *DROSOPHILA* AS A MODEL ORGANISM

Since 1901, when William E. Castle started working with *Drosophila melanogaster*, the fruit fly has been a convenient invertebrate model organism to study evolution, genetics, and development. Its main attributes are the same as they were at the beginning of 20th century: short generation time, ease and robustness of culturing, and low maintenance costs. Additionally, sequencing of the fly's genome in 2000 created many new opportunities to investigate this organism (Adams *et al.*, 2000). However, already since 1910, *Drosophila* has highly contributed to genome research. At that time, Thomas H. Morgan started working on the chromosome theory of heredity (Rubin and Lewis, 2000). Since then, many basic findings of eukaryotic genetics were revealed in the fruit fly. The facts that genes are arranged in a linear order (Sturtevant, 1913) and that chromosomes contain genes were only the first discoveries that had a general meaning (Bridges, 1914). Often *Drosophila* served as the organism, in which a new genetic method was established. For example, in the 1970s, Lindsley *et al.* (1972) formed the basis for the concept of whole-genome scanning in metazoans for phenotypic perturbations and Bender *et al.* (1979) achieved the first positional cloning. Since 1980, *Drosophila* is used to identify genes involved in fundamental processes like embryonic development by genome-wide mutation screens (Nusslein-Volhard and Wieschaus, 1980). Around that time, the first transgenic flies were made using transposable elements vectors (Spradling and Rubin, 1982). Basically, this technique is still used today. The desired sequence, for example a promoter-*gal4* construct, is cloned into a special plasmid, which is injected

into posterior germ cells of the *Drosophila* embryo. Using the transposon-based approach, the sequence is integrated in the fly's genome at a random insertion site (Bachmann and Knust, 2008). An improvement offers the bacteriophage PhiC31 integrase, which provides sequence-directed and highly-efficient integration (Venken and Bellen, 2012).

Particularly, the two-component Gal4/UAS system makes genetic manipulation in *Drosophila* very convenient (Brand and Perrimon, 1993). This gene targeting system allows the expression of a gene of interest in a spatially controlled manner by mating two different transgenic fly lines, called driver line and responder line (Fig. 9 A). In the driver line, the yeast transcription activator protein Gal4 is set under the control of a tissue or cell specific promoter. In the unmated fly, *gal4* expression has no effects. In the responder line, the gene of interest is placed under the control of a specific promoter region, the upstream activating sequence (UAS), which can only be activated by Gal4. Thus, the gene of interest is not expressed in the unmated responder line. Mating of driver line and responder line results in an F_1 generation with the desired genotype. The progeny expresses the gene of interest in the specific tissue or cell defined by the *gal4* promoter (Fig. 9 A).

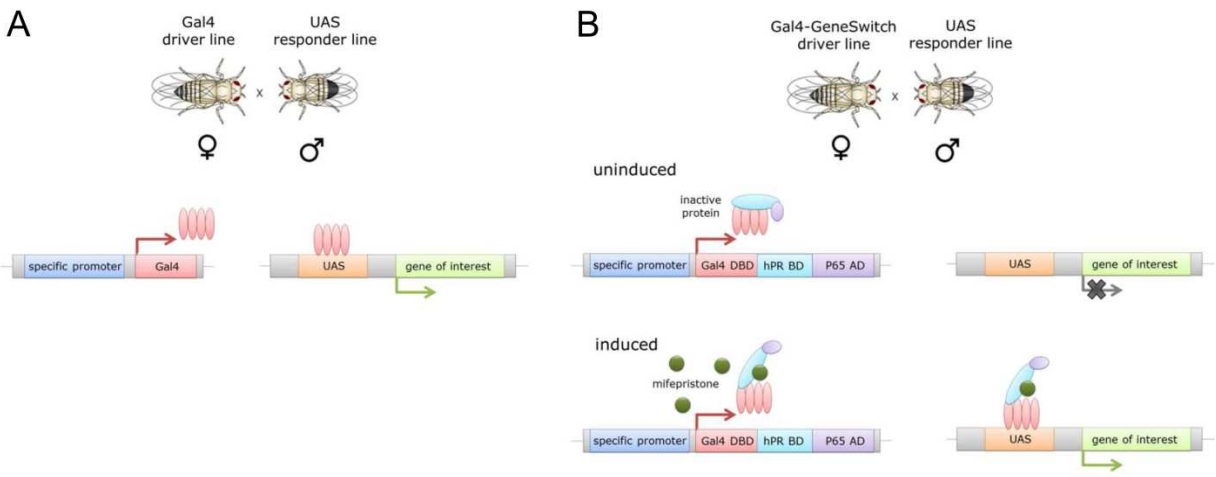

Fig. 9. Gal4/UAS system and GeneSwitch system. (A) The Gal4/UAS system allows spatial control of expression of a gene of interest, whereas (B) the inducible GeneSwitch system additionally controls expression temporally. UAS, upstream activating sequence; DBD, DNA binding domain; hPR BD, human progesterone receptor binding domain; AD, activation domain. Modified from Nicholson *et al.* (2008) and Muqit and Feany (2002).

To permit not only spatial but also temporal control of expression, the temporal and regional gene expression targeting (TARGET) system and the GeneSwitch system are applied (McGuire *et al.*, 2004). In the TARGET system, the temperature-sensitive

Gal80 protein is used as a repressor of Gal4 that inhibits activation of transcription of the gene of interest at permissive temperatures.

The GeneSwitch system is based on a chimeric Gal4 protein. The Gal4 binding domain is linked to the human progesterone receptor binding domain and the human protein P65 activation domain (Fig. 9 B). Only in the presence of the antiprogestin mifepristone, expression of the gene of interest is induced (Osterwalder *et al.*, 2001).

Since the generation of new transgenic *Drosophila* lines is easy and cost-effective, many mutants are available. For example, the Bloomington Stock Center offers more than 50,000 fly mutants and the Vienna Drosophila Research Center has a collection of UAS-RNAi strains targeting about 90% of the entire fly genome (Dietzl *et al.*, 2007). Thus, overexpression or silencing of most of the 14,000 *Drosophila* genes in a great number of tissues or cells is possible.

The fruit fly has been extensively studied concerning developmental and physiological processes. Since fly and human share many key systems at the molecular level, *Drosophila* additionally contributed to the elucidation of transient receptor potential channels (Montell, 2005) and signaling pathways such as ras (Nagaraj and Banerjee, 2004), among many other processes (Lessing and Bonini, 2009).

Nearly 75% of disease-related genes in humans have functional orthologs in the sequenced fly genome (Reiter *et al.*, 2001). Thus, *Drosophila* has also evolved as a good model organism to investigate several human diseases. These diseases include cancer, cardiovascular and infectious diseases, as well as metabolic disorders and Diabetes (Pandey and Nichols, 2011). Significantly, the response of flies to many drugs is similar to the effects observed in mammalian systems (Pandey and Nichols, 2011).

Also neurological disorders, like Alzheimer's disease (Finelli *et al.*, 2004), Parkinson's disease (Whitworth, 2011), and Huntington's disease (Weiss *et al.*, 2012), are investigated using the fruit fly because the *Drosophila* CNS and the human brain share common features (Davis, 2004). These neurological disorders are among others associated with impairments in learning and memory. *Drosophila* is well suited to investigate these behaviours since the same genetic pathways underlying learning and memory have been shown to be relevant in flies and in humans (Dubnau, 2003). In *Drosophila,* olfactory conditioning assays can be used to quantify learning in larvae (Selcho *et al.*, 2009) and adult flies. (Akalal *et al.*, 2010). According to classical

conditioning, different odors are presented in these assays as conditional stimuli that must be associated with aversive (punishment) or appetitive (reward) stimuli, which are in turn defined as unconditional stimuli (Pavlov, 1927).

For neurodegenerative disorders, sleep disturbances are clinical features (Arnulf *et al.*, 2008a; Arnulf *et al.*, 2008b; Gagnon *et al.*, 2008). Since *Drosophila* exhibits many of the behavioral characteristics of mammalian sleep, it serves as a good invertebrate model for the investigation of sleep problems (Cirelli, 2009). For example, forward genetics are used to identify genes involved in the maintenance of sleep rhythms.

1.5 AIMS

EGFR signaling has been extensively studied concerning its role during development in the *Drosophila* embryo, larva, pupa, and adult fly. On the contrary, its non-developmental functions are less understood. However, these non-developmental functions are of particular importance because EGFR signaling can be connected to many human diseases. These diseases include cancers of the stomach (Dragovich and Campen, 2009), colon (Enrique *et al.*, 2012), lung (Katzel *et al.*, 2009), liver (Sung *et al.*, 2012), and brain (Zhu *et al.*, 2009) as well as neurological disorders like Parkinson's disease (Chen-Plotkin *et al.*, 2011), Alzheimer's disease (Fleck *et al.*, 2011; Hochstrasser *et al.*, 2011), schizophrenia (Harrison and Law, 2006), and multiple sclerosis (Aguirre *et al.*, 2007). Notably, *Drosophila* is a suitable system to study the basis of these diseases because it has all the advantages of a comparatively simple model organism with functional homologous organs (Pandey and Nichols, 2011). The remarkable design similarities between the *Drosophila* and the human brain (Lessing and Bonini, 2009) are another advantage for the investigation of neurological diseases in the fruit fly. Studying these EGFR related diseases in fruit flies is especially convenient because *Drosophila* EGFR signaling is less complex compared to humans (Stein and Staros, 2000).

The aim of this study was to reveal new non-developmental EGFR signaling functions in *Drosophila*. The elucidation of expression patterns of the main EGFR pathway components should be the basis for further analyses. Different tissues or cells are related to certain physiological roles and thus spatial identification of EGFR pathway component gene expression gives a first hint for further functions. Based on the expression patterns, signaling manipulations can be specifically targeted to cells, in which EGFR pathway components are naturally present. Thus, ectopic manipulation of EGFR signaling is excluded.

For both identification of the expression patterns and signaling manipulations, the Gal4/UAS gene expression system should be used. First, *promoter-gal4* driver lines should be generated and mated to *gfp* (green fluorescent protein) expressing responder lines to analyze promoter activity patterns of several EGFR pathway component genes by immunohistochemistry. Second, several tissue or cell specific manipulations of EGFR signaling should be performed based on the expression patterns. Classical Gal4 lines should be used for constitutive expression, whereas GeneSwitch lines should be applied for induced temporally controlled expression.

The effects of reduced and enhanced EGFR signaling should be investigated. Reduction and enhancement of pathway activity should be performed targeting both, either ligands or the receptor. Manipulations on ligand level should be done using RNAi-mediated silencing or overexpression of a gene coding for the active form of the ligand Spitz. For changes in pathway activity on receptor level, a dominant-negative strategy and a constitutively active version of EGFR should be applied.
Subsequently, the effects of these EGFR signaling manipulations on phenotypes and different physiological parameters should be investigated to find so far unknown functions of the pathway.

2 MATERIALS

2.1 GENERAL MATERIALS

If not otherwise mentioned, general materials were purchased from Sarstedt.
Ceramic Beads 2.8 mm: Biolab Products; **Ceapren plugs (Ø 22, 27, 36 mm):** Greiner Bio-One GmbH; ***Drosophila* vials (16, 28, 68 ml):** Greiner Bio One GmbH); ***Drosophila* wide vials:** Genesee Scientific; **MicroAmp Fast Optical 48-Well Reaction Plate:** Ambion, Life Technologies GmbH; **MicroAmp 48-Well Optical Adhesive Film:** Ambion, Life Technologies; **microarray Oligo14kv2:** Canadian *Drosophila* Microarray Center; **micro tissue grinder 0.2 ml:** Wheaton; **mite plugs:** K.TK e.K.; **Orginal Swiss Dumont forceps #5:** Dumont & Fils.

2.2 EQUIPMENT

Activity monitoring system: Drosophila Activity Monitor DAM2, Trikenetics; **agarose gel electrophoresis documentation system:** transilluminator CN-1000.26, biostep; camera: Foculus IEEE 1394, biostep, printer: Digital Graphic Printer UP-D897, Sony; **analytical balance ABS/AB:** Kern & Sohn GmbH; **ApoTome:** Zeiss; **Axioplot Imager Z1:** Zeiss; **Axiocam mRM camera:** Zeiss; **Centrifuge 5415D:** Eppendorf AG; **Centrifuge 5417R:** Eppendorf AG; **Centrifuge mini spin:** Eppendorf AG; **Centrifuge Rotanta 460R:** Hettich; **MasterCycler® ep gradient thermal cycler:** Eppendorf AG; **micro plate reader LEDETECT 96:** Deelux Labortechnik GmbH; **microarray equipment:** Hybridization chamber: QInstruments; thermoshaker Inhenco: Series 96, Waltlow; scanner: Gene Pix 4000B scanner, Axon Instruments, Biozym Scientific; **NanoDrop ND-1000 UV/Vis-Spectrophotometer:** Thermo Fisher Scientific; **Omni Bead Ruptor 24:** Omni International Inc.; **PCR working station:** Ultraviolet sterilizing PCR working station, peqlab; **pipettes:** Eppendorf and Gilson; **stereo-microscope Leica M80:** Leica Camera AG; **stereo-microscope Olympus SZX12 with camera DP 71:** Olympus; **StepOne Real-time PCR system:** Applied Biosystems, Life Technologies GmbH; **Thermomixer comfort:** Eppendorf AG; **Ultrospec 1100 pro:** Amersham Biosciences Europe GmbH; **UV-table TI3:** Biometra

Biomedizinische Analytik GmbH; **Varioklav:** Thermo scientific (Dreieich); **VortexGenie2:** Scientific Industries.

2.3 General Chemicals

If not otherwise mentioned, chemicals were obtained from Carl Roth GmbH.

1-octanol: Fluka; **aminoallyl UTP Ambion:** Life Technologies GmbH; **ampicillin:** Applichem; **amyl acetate:** SAFC; **β-mercaptoethanol:** Applichem; **BODIPY (493/503):** Molecular Probes life technologies; **bovine serum albumin (BSA):** Serva; **bromophenol blue:** Applichem; **calcium chloride ($CaCl_2$):** Applichem; **corn meal:** Muhle Schlingemann; **DIG easy Hyb:** Roche Diagnostics GmbH; **dNTPs:** Fermentas GmbH; **ethidium bromide:** Applichem; **Focus Clear:** CelExplorer Labs CO (Taiwan); **formaldehyd, 37%:** Applichem; **Glyceryl trioleate (triolein):** Sigma-Aldrich; **GeneRuler^{TM} DNA Ladder Mix (100–10,000 bp):** Fermentas GmbH; **glycogen:** Boehringer Mannheim; **goat serum:** Sigma-Aldrich; **Infinity Triglyceride Reagent:** ThermoScientific; **magnesium chloride ($MgCl_2$):** Fermentas GmbH; **magnesium sulfate ($MgSO_4$):** Merck; **manganese(II) chloride tetrahydrate (MnCl2 * 4 H2O):** Sigma-Aldrich; **mifepristone:** Sigma-Aldrich; **molasse:** Biohof-Heidelicht GbR; **MOPS:** Applichem; **Nipagin (methyl-4-hydroxybenzoate):** Sigma-Aldrich; **paraffin oi**l: pharmacy; **Taq buffer with KCl (10x):** Fermentas GmbH; **paraformaldehyde:** Applichem; **potassium acetate (CH_3CO_2K):** Applichem; **potassium dihydrogen orthophosphate(Na_2HPO_4):** Applichem; **potassium chloride (KCl):** Applichem; **quinine hemisulfate:** Sigma-Aldrich; **RNase inhibitor:** Invitrogen; **salmon testis DNA:** Sigma-Aldrich; **sugar beet molasses:** Kanne BrottrunkR GmbH & Co.KG; **Triton X-100:** Serva; **Tween 20:** Applichem; **UltraPure agarose:** Invitrogen; **yeast:** Leiber GmbH; **yeast tRNA:** Ambion, Life Technologies GmbH.

2.4 ANTIBODIES

2.4.1 PRIMARY ANTIBODIES

rabbit anti-GFP: Invitrogen; **mouse anti-prospero:** Developmental Studies Hybridoma Bank (DSHB); **mouse anti-delta:** DSHB; **mouse anti-notch, extracellular domain, EGF repeats #5-7:** DSHB; **mouse anti-armadillo:** DSHB; **mouse anti-nc82:** DSHB; **mouse anti-repo:** DSHB.

2.4.2 SECONDARY ANTIBODIES

DyLight488-conjugated goat anti-rabbit: Jackson ImmunoResearch; **DyLight549-conjugated goat anti-mouse:** Jackson ImmunoResearch.

2.5 ENZYMES AND KITS

Alexa Fluor 555 Reactive Dye decapack: Invitrogen**; Alexa Fluor 647 Reactive Dye decapack:** Invitrogen**; DyNAmo Flash SYBR Green qPCR Kit:** Finnzymes; **Gateway® LR and BP Clonase™ II enzyme mix:** Invitrogen; **Genomic DNA Purification Kit:** Fermentas; **LA taq polymerase:** TAKARA; **NucleoSpin Gel and PCR Clean-up kit:** Macherey-Nagel; **NucleoSpin Plasmid QuickPure kit:** Macherey-Nagel; **MEGAscript T7 kit:** Ambion life Technologies GmbH (Darmstadt); **my-Budget RNAmagic:** Biobudget (Krefeld); **NucleoSpin RNA II:** Macherey-Nagel; **Plasmid Maxi kit:** Quiagen; **PrimeScript reverse transcriptase:** TAKARA; **RNaseOUT Ribonuclease (RNase) Inhibitor:** Invitrogen; **SureClean:** Bioline; **Taq polymerase:** Fermentas; **TRITC-conjugated phalloidin:** Sigma-Aldrich; **Quiagen Plasmid Maxi kit:** Quiagen.

2.6 VECTORS

pDONR221: Invitrogen; **pBPGUw:** Addgene.

2.7 BACTERIAL STRAIN

E. coli DH5α

2.8 BUFFERS AND SOLUTIONS

1× SSC	3 M NaCl, 300 mM trisodium citrate dihydrate; pH 7 with HCl
4% paraformaldehyde	4% (w/v) paraformaldehyde in PBS (pH 7.3), heat at 50-60 °C, add 0.3% Triton X-100
6× DNA loading dye	50% glycerol; 60 mM EDTA; 6% SDS; 0.9% bromophenol blue; pH 8.0
HL3	70 mM NaCl, 5 mM KCl, 1.5 mM $CaCl_2$ x 2 H_2O, 20 mM $MgCl_2$ x 6 H_2O, 10 mm $NaHCO_3$, 5 mM trehalose, 115 mM sucrose, 5 mM HEPES; pH 7.1 and autoclaved
$NaHCO_3$	0.3 M, pH 9.0
Nipagin	10% (w/v) in 70% ethanol
PBS	136 mM NaCl, 2.7 mM KCl, 1.5 mM KH_2PO_4, 7 mM Na_2HPO_4; pH 7.3
Propionic acid	10% propionic acid
TAE buffer	40mM Tris, 20 mM acetic acid, 1 mM EDTA (pH 8.0)
TE buffer	1 mM Tris (pH 8.0), 0.1 mM EDTA
TfB I	30 mM CH_3CO_2K, 100 mM KCl, 10 mM $CaCl_2$, 15% glycerin; filter sterilized

TfB II	10 mM MOPS, 75 mM $CaCl_2$, 10 mM KCl, 15% glycerin; adjust to pH 7.0 with NaOH; filter sterilized

2.9 CULTURE MEDIA

Apple juice agar plates	2% (w/v) agar-agar in apple juice; mixed and boiled up
LB medium	10 g NaCl, 10 g tryptone, 5 g yeast extract; ad 1 l H_2O; autoclaved
LB agar plates	LB medium with 15 g agar-agar; autoclaved
SOC medium	0.5% (w/v) yeast extract, 2% tryptone, 10 mM NaCl, 2.5 mM KCl, autoclave, add 10 mM $MgCl_2$, 10 mM $MgSO_4$, 20 mM glucose; filter sterilized
Standard food medium for flies	31.25 g corn meal, 31.25 g yeast, 5 g agar-agar, 10 g glucose, 15 g melasse, 15 g sugar beet molasses, 500 ml H_2O; mixed and heated for 15 min. Autoclaved for 15 min, cooled down to 60 °C, and 15 ml propionic acid and 5 ml 10% nipagin were added
Starvation medium	2% agar in H_2O; boiled up

2.10 OLIGONUCLEOTIDES

Tab. 1. Oligonucleotides used for the amplification of the putative promoter region. (*att*B1 site, red: GGG GAC AAG TTT GTA CAA AAA AGC AGG CT; *att*B2 site, blue: GGG GAC CAC TTT GTA CAA GAA AGC TGG GT).

genomic region	oligonucleotide	sequence (5' to 3')
promoter *spitz* no. 1	I_Spitz_F1	*att*B1CAT ACA TAA ATG CGC GAG TGT G
	I_Spitz_R2	*att*B2GAG CGA CAA AGT CTC TCC TC
promoter *spitz* no. 2	P_Spitz_F1	*att*B1CTC GTC TGG GTT TCA TCC TG
	P_Spitz_R1	*att*B2GTA GCG TAT CGG CTT GTT CG
promoter *vein*	P_Vein_F1	*att*B1GAT GAT ACA ATG ACG CTG CGC
	P_Vein_R1	*att*B2CCA AAG TTG TTG CTG CTA TTG C
promoter *keren*	P_Keren_F1	*att*B1CGT CAA TTC GGC TTG AAT TTG C
	P_Keren_R1	*att*B2GGA ATT CTT GGC TTT GGC TG
promoter *gurken*	P_Gurken_F1	*att*B1GTT TCA GCT TAA CCG ACA TGG
	P_Gurken_R1	*att*B2GTC GCA ACA GAA GCT GAA AC
promoter *argos*	P_Argos_F1	*att*B1GGA CGA AAG GTA AGC CTA ATT G
	P_Argos_R1	*att*B2GAT TTA TGA CTC TGA CTC TGG C
promoter *EGFR*	P_EGFR_F1	*att*B1GTA ACA TCG AAC CGG CTG AG
	P_EGFR_R1	*att*B2CGT TGT GGT GCC TAG TCA AG

Tab. 2. Oligonucleotides used for RT-PCR analyses.

gene	oligonucleotide	sequence (5' to 3')
spitz	Spitz_fwd	GAT CTA CCG GTT TAC AGC TG
	Spitz_rev	GAA GGC CAG GCA GAC AAA C
vein	Vein_fwd	GCA GGC GTC GGA TAT ATC C
	Vein_rev	GTG ACC TCT GCG TTC TGT G
keren	Keren_fwd	GCG AAC GCA ATC GCA ATC G
	Keren_rev	GGC TCG CAT CTT GAT CTT AAC
gurken	Gurken_fwd	GTG GAC AAT CGG TCC ACC
	Gurken_rev	GAA GTA AGA TTC GGC TCG AAC
argos	Argos_fwd	GCG CAT CCT CTA CCA AGT G
	Argos_rev	GAT CAC ATT GTT GGG CAT GC
egfr	EGFR_fwd_5	CTG CTA CGT AAG CAA TAT CCG
	EGFR_rev_5	CTT GCA GGT AAG GCA CTG AT
RPL32	RPL32_Forw	CCG CTT CAA GGG ACA GTA TC
	RPL32_Reve	GAC AAT CTC CTT GCG CTT CT

Tab. 3. Oligonucleotides used for cDNA first strand synthesis and amplification.

application	oligonucleotide	sequence (5' to 3')
First strand cDNA synthesis	Oligo dT T7 I	GAG AGA GG ATC CAA GTA CTA ATA CGA CTC ACT ATA GGG AGA $(T)_{25}$
	CF-Sp6rG1	CAG CGG CCG CAG ATT TAG GTG ACA CTA TAG ArG rGr G
cDNA amplification	Adaptor-SP6-PCR	GAC GCC TGC AGG CGA TGA ATT TAG G
	Oligo dT T7 II	GAG AGA GGA TCC AAG TAC TAA TAC GAC TCA CT

Tab. 4. Oligonucleotides used for qRT-PCR analyses.

gene	oligonucleotide	sequence (5' to 3')
RPL32	RPL32_fwd	TTG GCT TCG GTT TCC GGC AAG
	RPL32_rev	ATC GAT CCG ACT GGT GGC GGA T
attacin A	attacinA_fwd	CAA TCT GGA TGC CAA GGT CT
	attacinA_rev	TCC CGT GAG ATC CAA GGT AG
defensin	defensin_fwd	GCT ATC GCT TTT GCT CTG CT
	defensin_rev	GCC GCC TTT GAA CCC CTT GG
diptericin	diptercin_fwd	GCA ATC GCT TCT ACT TTG GC
	diptericin_rev	TAG GTG CTT CCC ACT TTC CA
drosomycin	drosomycin_fwd	ACC AAG CTC CGT GAG AAC CTT
	drosomycin_rev	TTG TAT CTT CCG GAC AGG CAG
cecropin C	cecropinC_fwd	AAG ATC TTC GTT TTC GTC GC
	cecropinC_rev	GTT GCG CAA TTC CCA GTC
metchnikovin	metchnikovin_fwd	CCA CCG AGC TAA GAT GCA A
	metchnikovin_rev	AAT AAA TTG GAC CCG GTC TTG
drosocin	drosocin_fwd	GTT CAC CAT CGT TTT CCT GC
	drosocin_rev	GGC AGC TTG AGT CAG GTG AT

Tab. 5. Oligonucleotides used for colony checks and sequencing of vectors.

vector	oligonucleotide	sequence (5' to 3')
pDONR221	M13F(-20)	GTA AAA CGA CGG CCA GT
	M13R(-29)	CAG GAA ACA GAT GAC C
pBPGUw	pBPGUw_fwd	GCC CTT TCG TCT TCA AGA ATT CG CTC
	pBPGUw_rev	GAA CAT TCA TTC ACA ACT GAT GC

2.11 *DROSOPHILA MELANOGASTER* STRAINS

The used fly strains are displayed in Tab. 6. The strains were purchased from the Vienna *Drosophila* RNAi Center (VDRC; Vienna), the *Drosophila* Genomics Resource Center (DGRC), the Bloomington stock center (Bloomington), or were a gift from the mentioned person.

Tab. 6. Fly strains.

stock name	genotype	donator
CantonS	CantonS	Bloomington
w^{1118}	w{1118}	Bloomington
nsyb-Gal4	w*; nsyb-gal4	Julie Simpson
elav-GeneSwitch	yw*; P{elav-GeneSwitch}	Haig Keshishian
aFB-GeneSwitch	w*; P{Switch1}106 GS	Ronald Kühnlein
RKF 125	w[*]; P{w[+mW.hs]=GawB}FB/SNS	Ronald Kühnlein
spitz-enhancer-trap-Gal4	yw*; P{GawB}spi(NP0261) / CyO, P{UAS-lacZ.UW14} UW14	DGRC
UAS-*egfr*^{DN}	yw*; P{w(+mC)=UAS-Egfr.DN.B}29-77-1; P{w(+mC)=UAS-Egfr.DN.B}29-8-1	DGRC
UAS-*egfr*^{ACT}	w*; P{w[+mC]=Egfr.1.A887T.UAS}12-4	Bloomington
UAS-*spitz*^{RNAi}	yw*; UAS-*spitz*^{RNAi}	VDRC
20XUAS-IVS-mCD8::GFP	w*; P{20XUAS-IVS-mCD8::GFP}attP2	Bloomington
UAS-GFP.S65T	w*; P{UAS-GFP.S65T}T10	Bloomington
UAS-*keren*^{RNAi}	yw*; UAS-*keren*^{RNAi}	VDRC
UAS-*vein*^{RNAi}	yw*; UAS-*vein*^{RNAi}	VDRC
UAS-sSpi::GFP	yw*; P{UAS-sSpi.CS.GFP}	Ben Shilo

2.12 Computer Programs and Databases

2.12.1 Computer Programs

Acuity 4.0: Molecular Devices; **GenePix 6.0:** Molecular Devices; **GraphPad Prism 3.0:** GraphPad Software; **Microsoft Excel 2010:** Microsoft; **Microsoft Word 2010:** Microsoft; **Microsopft PowerPoint 2010:** Microsoft**; Photoshop CS:** Adobe; **Windows 7 Professional:** Microsoft.

2.12.2 Databases

Bloomington	http://flystocks.bio.indiana.edu/
DAVID	http://david.abcc.ncifcrf.gov/
DGRC	https://dgrc.cgb.indiana.edu/
Flybase	http://flybase.org/
NCBI	http://www.ncbi.nlm.nih.gov/
Oligo Calculator	http://www.bioinformatics.org/JaMBW/3/1/9/index.html
PubMed	http://www.ncbi.nlm.nih.gov/pubmed/
VENNY	http://bioinfogp.cnb.csic.es/tools/venny/index.html

3 METHODS

3.1 CULTURING OF *DROSOPHILA MELANOGASTER*

Experiments were performed with larvae and adult flies of the species *Drosophila melanogaster*. Flies were kept on standard food medium at temperatures ranging from 17–29 °C in clear plastic vials capped with mite plugs. Animals were fed with standard food medium, unless otherwise mentioned, and were transferred to new food medium every two to three weeks.

Using larvae, it was not distinguished between females and males; using adult flies, the used gender is mentioned in the respective experiment, if it was considered. A list of flies that were subject to this study is given in Tab. 6.

3.2 CROSSINGS

A range of crossings was performed to obtain the desired genotypes. For this purpose, the Gal4/UAS system was applied (Brand and Perrimon, 1993), which consists of two parts: the Gal4 driver line expressing the yeast transcription factor Gal4 and the UAS responder line with the UAS, an enhancer to which Gal4 specifically binds to activate gene transcription. This system provides the opportunity of spatially controlled gene expression. Using the mifepristone-dependent GeneSwitch-Gal4 system, gene expression can also be temporally controlled.

In general, virgin female flies were placed in one vial together with male flies. Either of them was the Gal4 line and the other the UAS line. The egg deposition and the culturing of the F_1 generation followed the standard culturing protocol as described in 3.1.

3.3 GENESWITCH EXPERIMENTS

For experiments with inducible expression of transgenes and RNAi constructs a tissue-specific GeneSwitch driver line was crossed with the UAS line of choice. For GeneSwitch experiments analyzing larval olfactory learning, a stock solution of

250 µg/ml mifepristone in 50% ethanol was added during fly food preparation to reach a final concentration of 10 µg/ml. For induction, F_1 generation second-instar larvae were transferred to food medium supplemented with mifepristone. Larvae placed on food medium without mifepristone but containing the appropriate amount of 2% ethanol served as controls. The olfactory learning experiments were performed with third instar larvae 24 h (+/- 1 h) after the transfer. For RNAi experiments, eggs were laid on apple juice agar plates overnight and subsequently transferred to mifepristone containing medium or control medium. Thus, induction of the expression started immediately after the hatching of the larvae.

For GeneSwitch experiments with adult flies, 100 µl of a stock solution of 3 mg/ml mifepristone in 80% ethanol was applied onto the surface of standard food medium in *Drosophila* wide vials. The mifepristone solution was allowed to sink into the medium overnight resulting in a final concentration of 120 µg/ml. Control food medium was prepared applying 100 µl 80% ethanol to the standard food medium. After adult flies were placed in the mifepristone containing vials, they were transferred to new vials after 3 or 4 days.

For survival assays under starved conditions, starvation medium was cooled down after boiling to about 50 °C and a stock solution of 3 mg/ml mifepristone in 80% ethanol or 80% ethanol were added to reach a final concentration of 120 µg/ml mifepristone or the respective ethanol concentration.

GeneSwitch experiments with larvae and with adult flies were performed at 25 °C.

3.4 General Molecular Methods

3.4.1 RNA Isolation

For RNA isolation, the tissue of choice was dissected in PBS on ice. The dissected tissue was transferred to the lysis buffer of the NucleoSpin RNA II kit and grinded in a micro grinder. The subsequent RNA isolation was performed with the NucleoSpin RNA II kit according to instructions of the manufacturer with an extended DNase treatment of 30 min.

3.4.2 Genomic DNA Isolation

Drosophila larvae (5–10) were grinded in 200 µl TE buffer. For genomic deoxyribonucleic acid (gDNA) isolation, the Genomic DNA Purification kit was used following the instructions of the manufacturer.

3.4.3 Plasmid DNA Isolation

The plasmid DNA was isolated from overnight cultures (3.4.13) using the NucleoSpin Plasmid QuickPure kit according to the instructions of the manufacturer.

3.4.4 Nucleic-Acid Ethanol-Precipitation

Ethanol precipitation was used to concentrate and purify RNA and DNA. For precipitation, 10% (v/v) 3 M sodium acetate, 2.5 volumes of 100% ethanol, and 0.5 µl glycogen (35 mg/ml) were added to the nucleic acid solution. After accurate mixing, the RNA was incubated at -20 °C for a minimum of 1 h. Then, centrifugation at 16,000 × g for 30 min at 4 °C was done and the RNA pellet was washed twice with 500 µl 70% ethanol. The RNA was dried at room temperature and finally dissolved in RNase-free H_2O.

3.4.5 Measurement of RNA or DNA Concentration with the NanoDrop

For the measurement of RNA or DNA concentrations, the NanoDrop ND-1000 Spectrophotometer was used. The volume of the sample was 2 µl. Absorption at a wave length of 260 nm was measured. By means of the absorption coefficient A_{260} = 1, which corresponds to a RNA content of 40 µg/ml and a DNA content of 50 µg/ml, respectively, at a layer thickness of d = 1 cm, the concentration of the nucleic acids sample was calculated.

The ratio of sample absorbance at 260 and 280 nm was used to assess the purity of the sample. A ratio of about 1.8 is generally accepted as “pure” for DNA; a ratio of about 2.0 is generally accepted as “pure” for RNA.

3.4.6 First Strand cDNA Synthesis

During the first strand complementary DNA (cDNA) synthesis, messenger RNA (mRNA) is transcribed to cDNA. The Prime Script reverse transcriptase was used for this procedure as instructed by the manufacturer but in a total volume of only 10 µl. As an RNase inhibitor RNaseOUT was applied. The oligonucleotides Oligo dT T7 I and CF-Sp6rG1 were added (50 pmol). Oligo dT T7 I binds to the poly-A tail of the mRNA and thus provides a starting point for the reverse transcriptase. In addition to the poly-T sequence, which is necessary for binding to the poly-A tail, this oligonucleotide contains a specific adapter sequence, that is subsequently situated at the 5` end of the newly generated cDNA (Schramm *et al.*, 2000). Furthermore, the cap finder binds to cytosin residues, which were added by the reverse transcriptase to the 7-methylguanine cap during reverse transcription. In addition to the sequence necessary for this binding, the cap finder CF-Sp6rG1 contains a specific adapter sequence. Binding of this oligonucleotide leads to extension of the newly transcribed cDNA by the reverse transcriptase complementary to the adapter sequence. Thus, a specific sequence is added to the 3` end of every cDNA first strand (Schramm *et al.*, 2000). This specific adapter sequence as well as the specific adapter sequence at the 5’ end are needed for second strand synthesis and cDNA amplification (3.4.7).

3.4.7 Second Strand Synthesis and cDNA Amplification

During the second strand synthesis, single stranded (ss) cDNA is transcribed to double stranded (ds) cDNA, which is more stable. Moreover, amplification was performed modified from Schramm *et al.* (2000) and is necessary to reach an adequate amount of cDNA. Oligonucleotides used for this amplification (Tab. 3) bind to the specific adapter sequences that were integrated during the first strand synthesis. The reaction mixture was the following:

5 µl LA buffer (5x)
8 µl dNTPs (2.5 mM)
1 µl Adaptor-SP6-PCR (10 µM)
1 µl Oligo dT T7 II (10 µM)
1 µl ss-cDNA
0.5 µl LA-taq

33.5 µl aqua bidest

The amplification was performed in the master cycler with the program displayed in Tab. 7.

Tab. 7. PCR program for second strand synthesis and cDNA amplification.

	duration	temperature	
Initial denaturation	1 min	95 °C	
Denaturation	20 sec	95 °C	35 cycles
Annealing	20 sec	58 °C	
Extension	2 min 30 sec	72 °C	
Final extension	5 min	72 °C	

3.4.8 Clean-Up of ds-cDNA

The ds-cDNA had to be purified after the amplification to remove dNTPs and oligonucleotides for further experiments. For RT-PCR analyses, ds-cDNA was cleaned with the NucleoSpin Gel and PCR Clean-up kit according to instructions of the manufacturer. For microarray analyses, ds-cDNA was purified using SureClean according to the manufacturer's protocol.

3.4.9 Polymerase Chain Reaction (PCR)

The polymerase chain reaction (PCR) is an *in vitro* method to amplify specific DNA sequences (Mullis, 1990). For that, the matrix DNA is denatured and specific oligonucleotides bind to their complementary sequences, which flank the region that will be amplified. By using a thermostabile DNA polymerase, the complementary strand is synthesized. The repetitive chain of matrix denaturation, oligonucleotide binding, and strand synthesis starting at the hybridized oligonucleotides by the polymerase leads to an exponential increase of the amplicon.

The composition of the PCR reaction mixture and the PCR program that were applied are dependent on the length of the amplicon, the concentration of the DNA template, and the stringency and melting temperature of the oligonucleotides. For amplification of short DNA fragments the Taq polymerase was used with the following PCR reaction mixture:

1 µl Taq buffer with KCl (10x)

1 µl dNTPs (1 mM)

1 µl oligonucleotide forward (10 mM)

1 µl oligonucleotide reverse (10 mM)

0.8 µl $MgCl_2$

X µl DNA

1 µl Taq polymerase

add aqua bidest to a final volume of 10 µl

The volume of the DNA template was dependent on the concentration of the DNA sample.

For the amplification of long DNA fragments the LA Taq polymerase was used with the following PCR reaction mixture:

2.5 µl LA PCR buffer (10x)

4 µl dNTPs (2.5 mM each)

0.5 µl oligonucleotide forward (10 mM)

0.5 µl oligonucleotide reverse (10 mM)

X µl DNA

0.25 µl LA Taq

add aqua bidest to a final volume of 25 µl

The volume of the DNA template was dependent on the concentration of the DNA sample.

The amplification was performed in the master cycler with the program displayed in Tab. 8.

Tab. 8. Protocol for standard PCR amplification.

	duration	**temperature**	
Initial denaturation	5 min	95 °C	
Denaturation	30 sec	95 °C	30–38 cycles
Annealing	20 sec	26–62 °C	
Extension	30 sec–4 min	72 °C	
Final extension	5 min	72 °C	

3.4.10 RT-PCR Analysis

To investigate the expression of different genes coding for EGFR pathway components in different larval and adult tissues of wild-type animals, reverse-transcriptase polymerase chain reaction (RT-PCR) was used.

For the gene expression analysis of different parts of the brain, RNA was isolated from brain lobes or ventral nerve cords of larval brains and from central region, optic lobes, or retinae of adult brains. For the analysis of larval tissues, guts, fat bodies, tracheae, Malpighian tubules, or the body walls were dissected, whereas for the analysis of adult tissues guts, fat bodies, Malpighian tubules, or male and female reproductive tracts were dissected. RNA was isolated according to the RNA isolation protocol (3.4.1), with the exception of the fat body tissues, from which RNA was isolated with RNA magic according to the instructions of the manufacturer. Subsequently, the RNA was purified by nucleic acid ethanol precipitation (3.4.4). Up to 500 ng RNA were transcribed in cDNA in the first strand cDNA synthesis (3.4.6) and amplified using the second strand systhesis and amplification (3.4.7). The RT-PCR was performed with the Taq polymerase standard protocol (3.4.9) for short DNA fragments with equal amounts of DNA template. The respective oligonucleotides are displayed in Tab. 2. Subsequently, the amplified samples were analysed by agarose gel electrophoresis (3.4.11).

3.4.11 Agarose Gel Electrophoresis

Agarose gel electrophoresis is used to separate nucleic acid fragments according to their size. The agarose gel functions as a fine-meshed net, in which the nucleic acids move along an electric field. For the production of the gels, 1.5% agarose were boiled in TAE buffer, cooled down to about 60 °C, and ethidium bromide (0.5 µg/ml) was added. After hardening, the samples that were previously mixed with 6× DNA loading dye were applied to the gel. As a marker, 4 µl GeneRuler ladder were also applied. The separation of the samples was performed at a potential of 20 to 100 volt. Since ethidium bromide stains nucleic acids, separated samples were analyzed with a UV-transilluminator.

3.4.12 Extraction of DNA from Agarose Gels

To extract separated PCR samples from agarose gels, ethidium bromide-bound DNA was visualized by UV-light using a UV-table and was subsequently cut out of the gel. To isolate the sample from the gel, the NucleoSpin Gel and PCR Clean-up kit was used according to the manual.

3.4.13 Overnight Culture

For overnight cultures, 5 ml LB medium with the desired antibiotic concentration were inoculated with a single bacterial colony. The culture was grown overnight at 37 °C and 220 rpm.

3.4.14 Generation of Chemically Competent *E. coli* DH 5 alpha

To generate chemically competent *Escherichia coli* (*E. coli*) DH 5 α, 1 ml overnight culture (3.4.13) was diluted 1:100 in LB medium. This culture was incubated at 37 °C and 220 rpm until it reached an OD_{600} = 0.48–0.5. After cooling down to 4 °C, the culture was centrifuged at 2,000 × g for 5 min. Per 50 ml culture, the pellet was resuspended in 15 ml ice cold TfB I. After 15 min on ice, the sample was centrifuged at 2,000 × g for 5 min. Each sample was resuspended in 4 ml TfB II. After 15 min on ice, 200 µl aliquots were stored at -80 °C.

3.4.15 Transformation of Chemically Competent *E. coli* DH 5 alpha

For the transformation of *E. coli* DH 5 α, the bacteria were thawed on ice. The DNA of choice was added and the bacteria were incubated 15 min on ice. After a 1-min heat shock at 42 °C, the bacteria were placed on ice again and 900 µl of 37 °C warm SOC medium were added. The bacteria grew for 40 min at 37 °C and 800 rpm and were subsequently plated on LB agar plates containing the antibiotic of choice.

3.4.16 DNA SEQUENCING

DNA sequencing was performed by GATC biotech. Plasmids were prepared in a concentration of 30–100 ng/µl in a total volume of 20 µl.

3.4.17 QUANTITATIVE REAL-TIME PCR

In principle, the quantitative real-time PCR (qRT-PCR) is a conventional PCR that amplifies nucleic acids and simultaneously quantifies the targeted DNA molecule. This quantification is performed via a non-specific fluorescent dye that intercalates with any double-stranded DNA. An increase in the DNA product during PCR leads to an increase in fluorescence intensity, which is measured at each cycle, and allows to quantify DNA concentrations.

RNA isolation and cDNA synthesis were performed as described in 3.7 and the following reaction mixture was used with oligonucleotides displayed in Tab. 4:

5 µl SYBR Green
0.25 µl ROX
0.5 µl oligonucleotide forward (20 mM)
0.5 µl oligonucleotide reverse (20 mM)
2.5 µl cDNA (5 ng/µl)
add aqua bidest to a final volume of 10 µl

The program used for qRT-PCR analysis is shown in Tab. 9.

Tab. 9. Protocol for qRT-PCR analysis.

	duration	temperature	
Initial denaturation	10 min	95 °C	
Denaturation	15 sec	95 °C	40 cycles
Annealing	15 sec	60 °C	
Extension	30 sec	72 °C	
Melting curve	15 sec	95 °C	
Melting curve	1 min	60 °C + 0.3 °C until 95 °C	

Fluorescence was quantified at 72 °C after each cycle. The Ct-value (cycle threshold) was used for relative quantification and the fold change of expression was calculated with the $\Delta\Delta C_t$-method (Pfaffl, 2001). This involves comparing the C_t-values of a

treated sample with the C_t-value of an untreated control. The C_t-values of both, the sample and the control, are normalized to an appropriate endogenous housekeeping gene, in this case *rpl32*. The formula for the calculation is the following:

$$\Delta C_t = C_{t\ \text{gene of interest}} - C_{t\ \text{housekeeping gene}}$$

$$\Delta\Delta C_t = \Delta C_{t\ \text{sample}} - \Delta C_{t\ \text{control}}$$

$$\text{Fold change} = 2^{-\Delta\Delta CT}$$

3.5 GENERATION OF *PROMOTER-GAL4* LINES

For the generation of the *promoter-gal4* lines, the presumptive promoter regions were cloned into the pBPGUw vector. This vector is suitable for sequence-directed, irreversible, and highly efficient integration of the *promoter-gal4* construct into the *Drosophila* genome. The constructs were injected into *Drosophila* embryos by the Embryo Injection Service of the BestGene Inc. Company (USA).

Cloning was performed using the Gateway technology by Invitrogen. This technique is a universal cloning method based on the site-specific recombination properties of bacteriophage lambda. The first step is the PCR amplification with *att*B site containing oligonucleotides. These attachment sites are necessary for the generation of the entry clone using the BP recombination. By this recombination the toxin gene *ccd*B is replaced by the insert, which is essential for negative selection in *E. coli*. The kanamycin resistance gene in the vector is also used for selection in *E. coli*. The *att*B1 site reacts specifically with the *att*P1 site and the *att*B2 site reacts with the *att*P2 site whereby the *att*L sites are generated.

PCR amplification was performed using the LA-taq according to instructions of the manufacturer and with gDNA as a template. The *att*B site containing oligonucleotides are listed in Tab. 1. The PCR products were separated using agarose gel electrophoresis (3.4.11) and extracted from the gel according to 3.4.12. DNA was precipitated to reach higher concentrations and to remove primer-dimers using ethanol-sodium acetate precipitation (3.4.4). DNA pellets were solved in TE buffer and DNA concentrations were measured using the NanoDrop. The BP reaction using the Gateway BP Clonase II Enzyme Mix and the pDONR221 vector was performed in accordance with the manufacturer's instructions. The BP reaction was done overnight. Competent *E. coli* DH5α were transformed with the BP reaction mix and selected for entry clones using LB plates containing kanamycin (50 µg/ml). A colony

check was performed using the standard PCR protocol with the M13F-20 and M13R-29 oligonucleotides (Tab. 5) and positive clones were cultured overnight in LB medium containing kanamycin (50 µg/ml). Plasmid DNA was isolated using the NucleoSpin Plasmid QuickPure kit (3.4.3). DNA concentration was measured using the NanoDrop. Subsequently, the LR reaction was performed using Gateway LR Clonase II Enzyme Mix and the pBPGUw vector according to instructions of the manufacturer. The LR reaction was done overnight. Competent *E. coli* DH5α were transformed with the LR reaction mix and selected for positive clones using LB plates containing ampicillin (50 µg/ml). Clones carrying the desired fragment of DNA were identified by colony check PCR (3.4.9) and were subsequently cultured overnight (3.4.13) in LB medium containing ampicillin (50 µg/ml). Plasmid DNA was isolated using the NucleoSpin Plasmid QuickPure kit (3.4.3) and sequenced to confirm the correctness of the insert (3.4.16). To prepare the samples for the PhiC31 injection, correct clone was cultured overnight and plasmid DNA was isolated using the Quiagen Plasmid Maxi kit as instructed by the manufacturer. Finally, plasmid DNA was sent to Embryo Injection Service of the BestGene Inc. Company (USA) to generate transgenic flies carrying the *promoter-gal4* construct.

The pBPGUw vector was used for transfection of the flies with white eyes (w*). This vector comprises a marker gene coding for red eye color (w+). As transfected flies had white eyes (w*), the eye color was used to identify positive transformants.

Flies that were submitted by the BestGene Inc. Company (USA), had either white or orange eyes. White eyed flies were negative transformants that do not carry the marker gene and the *promoter-gal4* sequence, whereas positive transformants had orange eyes. The latter flies carry the insertion only on one chromosome and, thus, are heterozygous for the *promoter-gal4* construct. To generate homozygous transformants, flies with orange eyes were selected and crossed with each other. Only flies with red eyes were selected from the progeny, since they carry the insertion on both chromosomes and, thus, are homozygous.

3.6 MICROSCOPY

3.6.1 LIVE IMAGING

Live imaging refers to the detection of fluorescence in an animal or tissue without fixation or staining with antibodies.

For live imaging experiments, each *promoter-gal4* line was crossed with the UAS-GFP.S65T line, which expresses cytosolic GFP. GFP in the cytosol shows a strong signal in the whole cell and reveals an intense staining.

As a control, the uncrossed UAS-GFP.S65T line was also analyzed to detect unspecific GFP fluorescence in all tissues. All microscopic analyses were done with the Axioplot imager Z1. In addition, for Z-projections the the ApoTome was used.

3.6.2 IMMUNOHISTOCHEMISTRY - LARVAL AND ADULT DIGESTIVE SYSTEMS

Immunohistochemistry refers to the process of detecting proteins in fixed tissues by using antibodies binding specifically to a certain antigen.

All steps were performed at room temperature, unless otherwise mentioned. The UAS-GFP.S65T line, which expresses a cytoplasmic GFP, was mated with the *promoter-gal4* lines to obtain the desired genotypes in the F_1 generation . As a control, the uncrossed UAS-GFP.S65T line was also analyzed to detect unspecific GFP fluorescence.

Adult flies were fed with a 5% sucrose solution for three days, whereas larvae were fed with a 10% sucrose solution for 4 h to lower the background fluorescence caused by the food medium present in the digestive tract. Guts were dissected in PBS and immediately fixed in 4% paraformaldehyde in PBS for at least 30 min. After three washes with blocking solution (PBS, 0.5% BSA, 0.15% Triton X-100), samples were incubated with primary antibodies in blocking solution at 4 °C overnight. Guts were washed three times with blocking solution for 30 min and then incubated with secondary antibodies in blocking solution for 2.5 h in the dark. After three washes with PBT (PBS, 0.1% Triton X-100) in the dark, guts were embedded in Roti Mount.

The following primary antibodies and concentrations were used: rabbit anti-GFP (1:500), mouse anti-prospero (1:10), mouse anti-delta (1:100), mouse anti-notch, extracellular domain, EGF repeats #5-7 (1:10), and mouse anti-armadillo antibody

(1:10). Secondary antibodies were DyLight488-conjugated goat anti-rabbit and the DyLight549-conjugated goat anti-mouse antibodies (both 1:400). The anti-prospero antibody detects a marker protein of enteroendocrine cells and the anti-delta antibody detects a marker protein of stem cells. The anti-notch antibody detects a marker protein of enteroblasts and the anti-armadillo antibody detects a protein present at the membrane of progenitor cells and, to a lesser extent, at the membrane of enterocytes.

3.6.3 Immunohistochemistry - Larval and Adult Brains

All steps were performed at room temperature, unless otherwise mentioned. For the analysis of gene specif promoter activity in brains, the *promoter-gal4* lines were mated with the UAS-mCD8::GFP.L line, which expresses a membrane-bound GFP. The advantage of the plasma membrane-bound GFP is the clear differentiation between small brain cells and unspecific signals since membrane-bound GFP leads to a staining of the characteristic cell shape.

Brains were dissected in PBS and immediately fixed in 4% paraformaldehyde in PBT (PBS, 0.3% Triton X-100) for at least 30 min. After three washes with PBT, the samples were blocked with blocking solution (PBT, 5% goat serum) for 30 min and then incubated with primary antibodies in blocking solution at 4 °C overnight. Brains were washed three times with PBT for 10 min. Subsequently, they were incubated with secondary antibodies in blocking solution at 4 °C and kept dark overnight. After three washes with PBT in the dark, brains were embedded in Focus Clear to clear the tissue.

The following primary antibodies were used: rabbit anti-GFP (1:500), mouse anti-nc82 (1:5), mouse anti-repo (1:5), and mouse anti-elav (1:5). Secondary antibodies used were DyLight488-conjugated goat anti-rabbit and the DyLight549-conjugated goat anti-mouse antibodies (both 1:400). The anti-nc82 antibody detects the neurotransmitter “Bruchpilot” and thus is a marker for all neuropils in the *Drosophila* brain. The anti-elav antibody recognizes the “embryonic lethal, abnormal vision” mRNA binding protein and, thus, stains the nuclei of neurons. The anti-repo antibody binds the “revers polarity” protein and stains the nuclei of glia cells.

As a control, the uncrossed UAS-mCD8::GFP.L line was also analyzed to identify unspecific GFP fluorescence.

3.6.4 Immunohistochemistry - Adult Retinae

All steps were performed at room temperature, unless otherwise mentioned. For the analysis of gene specific promoter activity in retinae the same fly crossings were used as for the immmunohistochemistry with larval and adult brains.
First, eyes were dissected in PBS and fixed in 10% formaldehyde in HL3 for 30 min. After three washes with PBT, the remaining fat and laminae were removed from the retinae. The samples were washed in PBT (PBS, 0.3% Triton X-100) overnight at 4 °C to remove red pigments. The subsequent protocol followed the immunohistochemistry protocol for brains. The rabbit anti-GFP (1:500) and the mouse anti-elav (1:5) antibodies were applied, as well as the DyLight488-conjugated goat anti-rabbit and the DyLight549-conjugated goat anti-mouse secondary antibodies (both 1:400). The anti-elav antibody was used to detect the single PRs in the ommatidia.

3.6.5 Immunohistochemistry - Phalloidin Staining

Phalloidin is a toxin from the fungus *Amanita phalloides*, which binds to F-actin in muscle cells. TRITC-conjugated phalloidin is used to label actin for histological applications.
Guts were dissected and immunohistochemistry was performed as described in 3.6.2. TRITC-conjugated phalloidin was added to a final concentration of 0.5 µg/ml together with the secondary antibody.

3.7 Microarray Analysis

For microarray analysis, commercially available Oligo14kv2 microarray was used, which contains more than 14,000 *Drosophila* genes.
The fat body-specific GeneSwitch driver line (aFB-GS) was mated to the UAS-*egfr*^{DN} line. Flies of the F_1 generation were treated with mifepristone for 24 h to induce expression of a gene coding for a dominant-negative form of EGFR, whereas control flies were fed with the corresponding control food (3.3). Fat body tissue of ten 5–7 days old experimental and control female flies was dissected in HL3 and transferred

to HL3 containing 800 U/ml to inhibit RNA degradation. RNA was isolated from the dissected fat body tissue with my-Budget RNAmagic according to the manual. The RNA was concentrated using the nucleic acid ethanol-precipitation (3.4.4). After measurement of the RNA concentration (3.4.5), first strand cDNA synthesis (3.4.6) and second strand synthesis with cDNA amplification (3.4.7) was performed. The ds-cDNA was cleaned with SureClean according to instructions of the manufacturer and the quality was analyzed by agarose gel electrophoresis (3.4.11). The ds-cDNA was used as a template for aminoallyl complementary ribonucleid acid (aa-cRNA) synthesis with the MEGAscript T7 kit according to the manufacturer's protocol. During the synthesis, aminoallyl uridine triphosphates (aaUTPs) were incorporated in the synthesized RNA. This base-modified nucleotide was necessary to subsequently label the aa-cRNA with the Alexa Fluor 555 reactive dye or the Alexa Fluor 647 reactive dye. The Alexa Fluor succinimidyl ester dyes react with the introduced amine groups to form a covalent bond. The control sample was labeled with the Alexa Fluor 555 reactive dye, whereas the mutant sample was labeled with the Alexa Fluor 647 reactive dye. The following labeling reaction mixture was used:

3.33 µl aa-cRNA (15–20 µg)

6.67 µl $NaHCO_3$

10 µl Alexa Fluor 555/647 reactive dye (solved in DMSO)

After labeling for 2 h at room temperature in the dark, samples were cleaned using the NucleoSpin RNA II kit (3.4.3) and concentrated by nucleic acid ethanol-precipitation (3.4.4). For measurement of fluorescence intensity of the labeled aa-cRNAs, the Microarray software of the NanoDrop was applied.

For hybridization, the two labeled samples were mixed with blocking reagents and hybridization buffer. The reaction mix for the hybridization was the following:

345 µl DIG easy Hyb

16.6 µl Salmon testis DNA

16.6 µl Yeast tRNA

X µl Alexa Fluor 555 labeled aa-cRNA (500-1,000 pmol)

Y µl Alexa Fluor 647 labeled aa-cRNA (500-1,000 pmol)

The reaction mix was applied to the microarray by adhesive film using the same fluorescence intensities (pmol) of control and sample. Hybridization was performed at 42 °C overnight. Subsequently, the adhesive film was removed and the microarray was washed for 1 h in 1× SSC in the dark. For the following stringency washing

steps, different concentrations of SSC/Triton X-100 at different temperatures were used.

1st washing: 2x 15 min with 1× SSC, 0.1% Triton X-100 at 60 °C

2nd washing: 2x 15 min with 0.1× SSC, 0.1% Triton X-100 at 37 °C

3rd washing: 30 s 0.1× SSC at room temperature

The microarray was rinsed with H_2O and quickly dried with nitrogen. For analysis of fluorescence intensities, the GenePixTM 4000B Scanner was used at a resolution of 10 µm.

3.8 Learning Experiments

Different pan-neuronal EGFR signaling pathway manipulations were used for the olfactory learning experiments. For constitutive reduction of pathway activity, mutant and control larvae were obtained by crossing the pan-neuronal driver line nsyb-*gal4* with the UAS-*egfr*^{DN} line or different ligand^{RNAi} lines or, as a control, with the w^{1118} line.

For inducible expression, the pan-neuronal mifepristone-inducible elav-GeneSwitch line was crossed with the respective UAS line. Expression was induced as described in 3.3.

3.8.1 Procedure of Olfactory Learning Experiments

Learning experiments were performed according to previously described protocols (Hendel *et al.*, 2005; Michels *et al.*, 2005; Neuser *et al.*, 2005; Scherer *et al.*, 2003).

Basically, the olfactory learning assay consists of two rounds with two phases: training phase and test phase. During the training phase, one odor is presented to the larvae with a reward and another odor with a punishment. During the test phase, the odor choice behavior is analysed. To calculate the amount of associative learning, the odors are switched in the second round. Thus, the odor that was presented with the reward in the first stage is presented with punishment in the second. Changes in the odor preference after the reciprocal trainings show associative learning because the exposure to both, odors and reward or punishment, were identical and only the combination of stimuli differs.

Petri dishes were filled with a thin layer of 1% agarose. During the training phase plates with or without gustatory reinforcers were used. These gustatory reinforcers were fructose ([FRU], 2 M) as a reward and quinine ([QUI], 0.2%) as a punishment to enhance the learning effect. Quinine was used as a negative reinforcer to enhance learning by the effect of aversive learning. During the test phase, only pure plates without gustatory reinforcers were used.

Odors were presented by adding 10 µl of 1-octanol ([OCT], undiluted) or amyl acetate ([AM], diluted 1:50 in paraffin oil) into the lids of 200-µl PCR tubes. These lids were placed on opposite sides of the plates containing a gustatory reinforcer. During training phase, lids with the same odor were used, whereas during the test phase lids with different odors were added to the plates to have a choice situation.

All experiments were performed at room temperature. Larvae were washed with tap water directly before the transfer to the training plate.

The general procedure of the training phase was the following. Larvae underwent either of two treatment conditions: Under one treatment condition, AM was paired with the positive and OCT with the negative reinforcer (AM+/OCT-), whereas the other treatment was performed reciprocally (AM-/OCT+). Both treatments were run alternately. Additionally, the order of the odors that were presented first was changed: whereas during the first (AM+/OCT-) and second (AM-/OCT+) training larvae were at first confronted with AM, they were first confronted with OCT in the third (OCT-/AM+) and fourth (OCT+/AM-) training.

To start the training for the individually-assayed animal test, a group of eight larvae was put on a training plate with a gustatory reinforcer and stayed on the plate for 1 min with closed lids. During the following inter-trial phase (Hendel *et al.*, 2005), the larva stayed on an empty plate without odors and reinforcers for 1 min. Thereafter, the larvae were allowed to move on the second training plate with the other odor and the opposed reinforcer for 1 min. This cycle was repeated four times.

After the training phase, the odor choice of the larva was tested individually. During this test phase, pure-agarose plates were used with AM on one side and OCT on the other side. After one larva was put in place in the center of each test plate, the position of the larvae was recorded for 5 min every 30 s as “AM” or “OCT”. Larvae that were in a 5-mm-wide zone along the middle of the assay plate were counted as neutral (“NEU”). In contrast to the individually-assayed animal test, 12–17 larvae

were trained and also tested together in the en mass assay. The position of the larva was recorded after 3 min on the test plate as “AM,” “OCT,” or “NEU”.
For data analysis of the individually-assayed animal test as well as the en mass assay, the preference (Pref) for “AM” was calculated for both treatment conditions using the following formula:

$$\text{Pref } AM_{AM+/OCT-} = (\text{number of observations}_{AM} - \text{number of observations}_{OCT}) / \text{number of observations}_{total}$$

$$\text{Pref } AM_{AM-/OCT+} = (\text{number of observations}_{AM} - \text{number of observations}_{OCT}) / \text{number of observations}_{total}$$

Next, preferences of each replicate were sorted in ascending order and the learning index (LI) was calculated:

$$LI = (\text{Pref } AM_{AM+/OCT-} - \text{Pref } AM_{AM-/OCT+}) / 2$$

Values are between 1 and -1. One means that all larvae preferred the odor presented with fructose, whereas -1 means that all larvae preferred the odor that was presented with quinine. 0 means no learning at all.

3.8.2 Gustatory Test

To test the ability to taste fructose and quinine, a gustatory choice assay as described in Hendel *et al.* (2005) was performed. In this assay, larvae could choose between the putative attractive taste of fructose (“FRU”) and pure agarose (“PURE”) or the putative repellent taste of quinine (“QUI”) and pure agarose (“PURE”).
Petri dishes were filled with 1% pure agarose on one side and either 2 M fructose or 0.2% quinine in 1% agarose on the other side. Ten larvae were placed along the border of tasting agent and pure agarose. After 15 min, the larvae were recorded as “FRU”, “QUI”, or “PURE”. The preference for fructose and quinine, respectively, was calculated by subtracting the number of larvae on the pure side from the number of larvae on the “tasty” side and dividing the difference by the total number of larvae on the plate.

3.8.3 Odor Sensing - Banana

To test the odor sensing, smashed banana was used as a source for attractive smell. A spoonful of banana (“BANANA”) was situated on one side of a Petri dish filled with 1% agarose, whereas the other side of the Petri dish was empty (“EMPTY”). One single larva was placed in the middle of the petri dish and was allowed to freely move around for 5 min. The position of the larva was noted every 30 sec as “BANANA” or “EMPTY”. The preference for the odor side was calculated by subtracting the number of counts on the empty side from the number of counts on the odor side and dividing the difference by the total number of counts.

3.8.4 Odor Sensing – AM or OCT

To analyze the odor sensing ability of larvae, the to-be-associated odors AM or OCT were situated on one side of a Petri dish filled with 1% agarose and were tested versus an empty (“EMPTY”) container. One experimentally naive larva was placed in the middle of the Petri dish and was allowed to move freely for 5 min. The position of the larva was noted every 30 sec as “AM,” “OCT,” “EMPTY,” or “NEU” (a 5-mm-wide zone along the middle of the assay plate). Preference for the odor side was calculated by subtracting the number of counts on the empty side from the number of counts on the odor side and dividing the difference by the total number of counts.

3.9 Locomotor Activity Assay and Sleep Analysis

Flies expressing *spitz*^{RNAi}, *vein*^{RNAi} or *keren*^{RNAi} constitutively and pan-neuronally were compared to a control (nsyb-*gal4* > w^{1118}) in the *Drosophila* Activity Monitoring System. After hatching, female virgins of the ligand^{RNAi} flies and of the control flies were collected. They were raised for 3–5 days at 25 °C in the monitoring incubator at the light and dark cycle, which later was used for the experiment.

The monitoring system comprises of a locomotor monitor with 32 glass tubes of 5-mm diameter connected to a recording unit. A single fly was placed into each tube, where its confined motion is detected and counted by infrared light beams. The monitoring system is connected to a computer and records the movements, i.e.

locomotor activity of individual flies. A maximum of 32 flies can be monitored in parallel. The activity of flies is summarized for every min. The locomotor monitor is placed inside an incubator with a temperature of 25 °C and a 12-h light and dark cycle.

Data were analyzed using Excel software. For the measurements of daytime and nighttime activity, the counts for 60 min per single fly were summarized to calculate counts per h. The mean of the counts per h during daytime (light on, 8:00 h to 20:00 h) and during nighttime (light off, 20:00 h to 8:00 h) were calculated per fly. The means of these daytime or nighttime activities of all monitored ligand^{RNAi} flies were compared with the means of all monitored control flies (3.13.2).

For the calculation of sleep levels, 1 min sleep was defined as 1 min without activity counts. Subsequently, sleep (min/h) was calculated by counting the minutes without activity recorded within one hour.

For the analysis of activity and sleep in the course of the day, median and range of the activity counts per hour or of sleep per hour of all monitored flies of one genotype at one time were calculated. Statistical analysis was performed to compare the activity or sleep level at each time point of ligand^{RNAi} expressing flies and control flies as described in 3.13.2.

3.10 GEOTAXIS ASSAY

In the geotaxis assay, the natural tendency of flies to move against gravity when agitated was analyzed. 5–7 days old female flies expressing *spitz*^{RNAi}, *vein*^{RNAi} or *keren*^{RNAi} constitutively and pan-neuronally and female control flies (nsyb-*gal4* > w^{1118}) were tested in a climbing apparatus. This climbing apparatus was self-made. Two empty *Drosophila* wide vials were vertically joined by tape facing each other. In the lower vial, a vertical distance of 8 cm above the bottom surface was measured and marked by drawing a line around the entire circumference of the vial. Groups of 7–14 flies were transferred into the vials. After 1 h of acclimatization, the flies were tapped down to the bottom and the number of flies that crossed the 8-cm mark within the next 10 sec was counted. This procedure was performed ten times for each group, with a 1-min rest period between the trials. The number of flies per group that crossed the 8-cm mark was recorded as percentage of total flies. The mean of the

ten trials was used to calculate the “average pass rate”. Statistical analysis was performed according to 3.13.2.

3.11 Fat Content Analysis

3.11.1 BODIPY (493/503) Staining

4,4-difluoro-1,3,5,7,8-pentamethyl-4-bora-3a,4a-diaza-s-indacene (BODIPY (493/503) is intrinsically lipophilic and specifically stains neutral lipids. Flies, in which EGFR signaling was reduced (aFB-GS > UAS-*egfr*^{DN}) or enhanced (aFB-GS > UAS-*egfr*^{ACT}) in the fat body for a period of seven days, and uninduced control flies (3.3) were frozen in liquid nitrogen in a 1.5 ml tube. After washing with PBS, the flies were fixed in 4% paraformaldehyde in PBS for 25 min. After washing, flies were incubated in BODIPY (493/503) working solution (1:1,000 BODIPY (493/503) in PBS) for 1 h in the dark. Subsequently, flies were washed and analyzed with the fluorescence stereo magnifying glasses.

3.11.2 Coupled Colorimetric Assay

The coupled colorimetric assay (CCA) relies on hydrolysis of TAGs by a lipoprotein lipase that results in glycerol. The glycerol is then phosphorylated and oxidized to produce hydrogen peroxide. The amount of the generated hydrogen peroxide is measured using a colour reaction catalyzed by peroxidase. The absorabance of the generated dye is proportional to the concentration of TAGs present in the sample.
Using CCA (Hildebrandt et al., 2011), the TAG content of 5–7 days-old female flies was analyzed. Reduced or enhanced EGFR signaling in the fat body (aFB-GS > UAS-*egfr*^{DN} or aFB-GS > UAS-*egfr*^{ACT}) was induced by mifepristone feeding for seven days (3.3). *Egfr*^{DN} or *egfr*^{ACT} expressing flies and uninduced control flies were compared in the experiment. For each replicate, five female flies were weighed and 1 ml 0.05% Tween-20 was added. Flies were homogenized in the BeadRuptor for 2 min at 3.25 m/s. Endogenous enzymes were heat-inactivated at 70 °C for 5 min. After centrifugation for 5 min at 3,000 × g, 500 µl of the supernatant were transferred into a new vial. The samples were warmed to 37 °C and vortexed. After

centrifugation for 3 min at 2,500 × g, 50 µl of the supernatant transferred to a 96-well microtiter plate and the absorbance (blank) was measured at 540 nm in a micro plate reader. 200 µl pre-warmed (37 °C) Infinity Triglyceride solution was added to each sample and incubated at 37 °C with mild shaking for 30–35 min. Total absorbance at 540 nm was measured and corrected by subtraction of blank and substrate absorbance. Subsequently, TAG equivalent content was calculated using 0–40 µg of triolein as triacylglycerol standard, which was treated like the samples. Statistical analysis was performed as described in 3.13.3.

3.12 Survival under Starved Conditions

Female and male flies with the genotype aFB-GS > UAS-*egfr*^{DN} or aFB-GS > UAS-*egfr*^{ACT} were transferred to mifepristone-containing standard food medium or the corresponding control medium (3.3), when they were 5–7 days old. After 24 h, groups of ten female or male flies were transferred to vials (16 mm) containing about 3 ml starvation medium with mifepristone or only with the corresponding amount of ethanol (3.3). Flies were kept at 25°C, and dead flies were counted daily. Survival curves were generated and compared as described in 3.13.4.

3.13 Statistical Analysis

For all statistical analysis the GraphPad Prism software was used and if multiple comparisons were done, Bonferroni correction was performed.

3.13.1 Learning Experiments

The learning index values and preference values are represented by box plots (with medians as middle line, 25% and 75% quantiles as box boundaries, and minimum and maximum as whiskers). For the comparison between two groups the Mann-Whitney test was used.

3.13.2 Locomotor Activity Assay, Sleep Analysis, and Geotaxis Assay

To compare daytime and nighttime activity or daytime and nighttime sleep or average pass rates, the unpaired t-test (parametric data) or the Mann-Whitney test (non-parametric data) was performed. The activity and sleep values are represented by box plots (with medians as middle line, 25% and 75% quantiles as box boundaries, and minimum and maximum as whiskers). To compare activity or sleep levels of flies expressing ligand^{RNAi} with control flies at each time in the course of the day, the Mann-Whitney test was applied.

3.13.3 Coupled colorimetric assay

Data generated with the coupled colorimetric assay were analysed using the unpaired t-test.

3.13.4 Survival Under Starved Conditions

For the analysis of the survival curves of the assay monitoring survival under starved conditions, statistical comparisons were performed with the log rank test.

4 RESULTS

4.1 ANALYSIS OF THE PROMOTER ACTIVITY PATTERNS OF EGFR PATHWAY COMPONENT GENES

To monitor the promoter activity patterns of different EGFR signaling pathway component genes, the presumptive promoter regions were used to generate *promoter-gal4* (*prom-gal4*) lines, which were mated to UAS-*gfp* responder lines. Fragments of about 3,000-4,000 bp upstream of the translation start of *egfr*, *spitz*, *keren, vein*, *gurken*, and *argos* were chosen, which also cover the region 5' of the transcription start site (Fig. 10). Thus, a region was selected, which comprises promoter and enhancer activity in most genes. For the most prominent EGFR ligand Spitz, an *enhancer-trap-gal4* line is publicly available from the DGRC. The insertion site of this enhancer-trap is located within the second exon (Fig. 10). The complex exon/intron architecture of *spitz* giving rise to five different transcripts is the major reason why this enhancer-trap does not cover the complete presumptive promoter/enhancer region. Therefore, two additional *prom-gal4* lines were generated, which are called *prom1-spitz-gal4* and *prom2-spitz-gal4* (Fig. 10). Regions chosen for the generation of these two lines are for the most part located downstream of the enhancer-trap insertion site.

To analyze promoter activities of EGFR pathway component genes on cellular level, the generated *prom-gal4* lines were crossed with a UAS-*gfp* reporter line. For visualization in the CNS and the retina, membrane-bound GFP (20XUAS-IVS-mCD8::GFP) turned out to be more suitable, whereas cytosolic GFP (UAS-GFP.S65T) was used for all other tissues. The F_1 generations of these crossings were screened for *gfp* expression.

Gfp expression driven by the *prom-gal4* lines was monitored in several tissues of larvae and adult flies. These were fat body, digestive tract, epidermis, salivary gland, trachea, body wall muscles, and brain in larvae as well as fat body, salivary gland, trachea, female and male reproductive tract, muscles, and brain in adult flies. No *gfp* expression was detectable in female reproductive tracts, adult muscles, and adult tracheae in any of the *prom-gal4* > UAS-*gfp* flies.

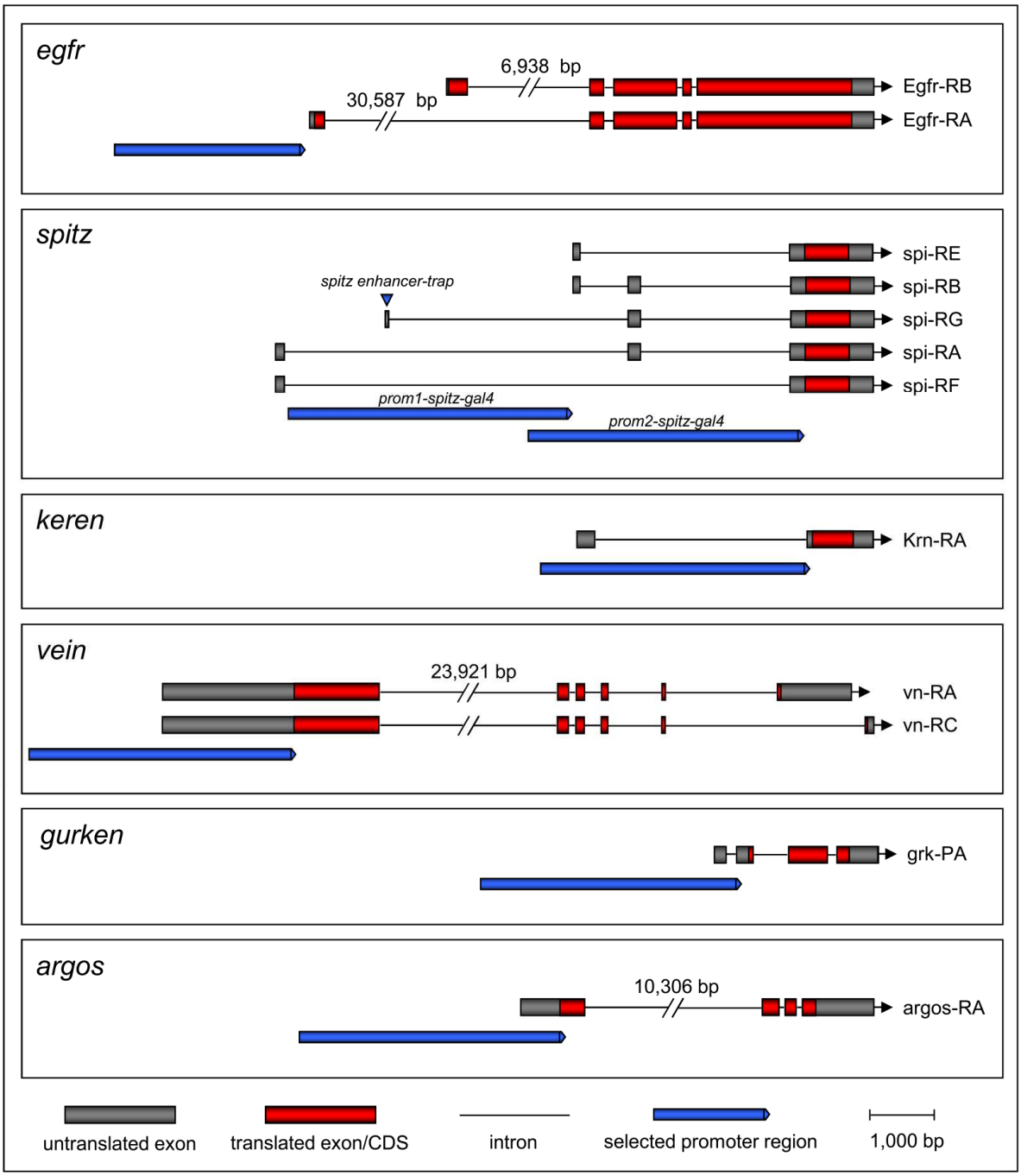

Fig. 10. Structure of EGFR pathway components' transcripts and selected promoter regions for the generation of the *promoter-gal4* lines. Modified from http://flybase.org/.

4.1.1 Spatial and Temporal Promoter Activity of *EGFR*

The gene coding for the EGFR is represented by the symbol Dmel\Egfr (annotation symbol CG10079) and has the FlyBase ID FBgn0003731. Oligonucleotides targeting a region of 4,078 bp were used to amplify the presumptive promoter region of the *egfr* gene.

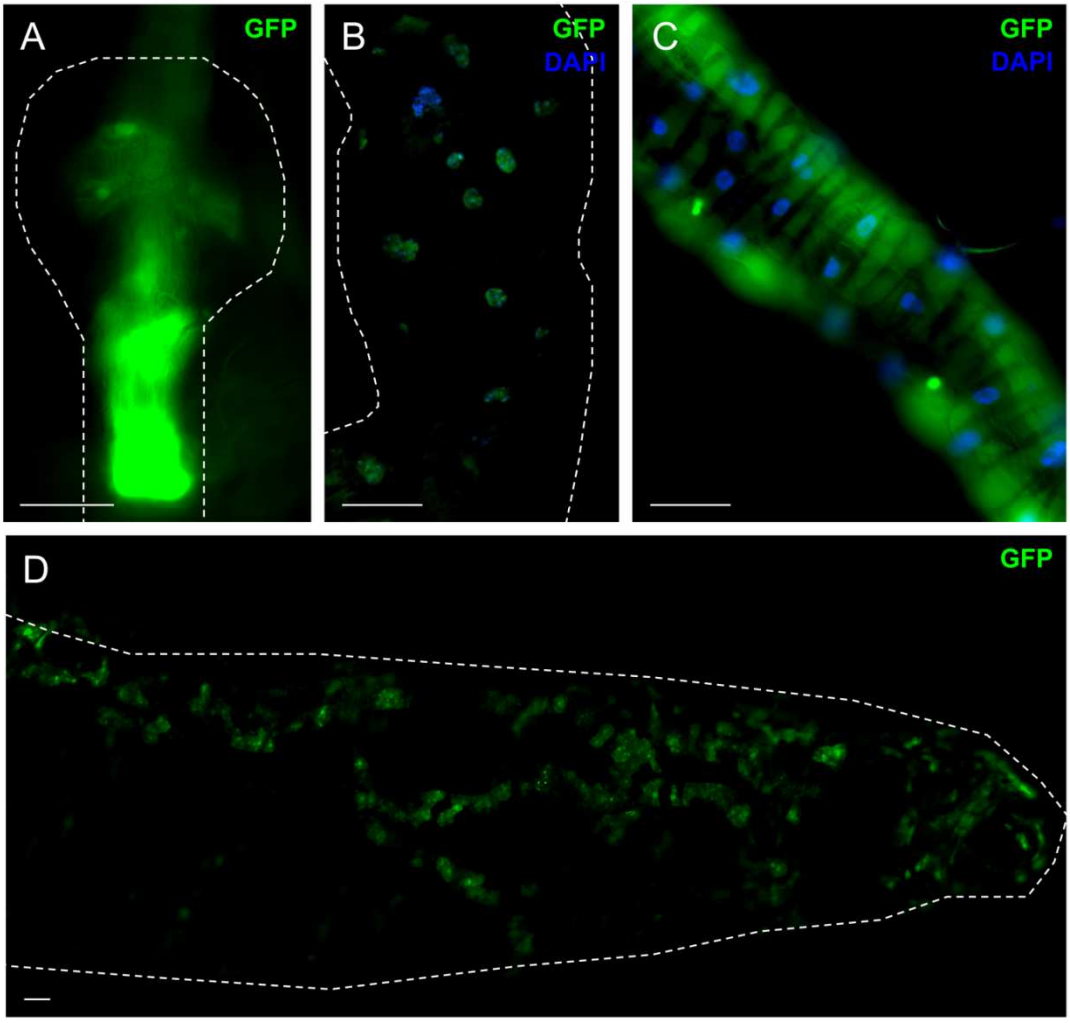

Fig. 11. *Egfr* promoter activity in larvae. *Gfp* expression indicating e*gfr* promoter activity was visualized in *prom-egfr-gal4* > UAS-*gfp* larvae using live imaging in (A) the proventriculus, (B) cells of the midgut, (C) cells of the hindgut, and (D) the fat body (ventral view on whole larva). Dashed lines represent the shape of the proventriculus, the midgut, or the whole larva visible in the differential interference contrast picture. DAPI was used to stain the nuclei. Scale bar = 50 µm.

In *prom-egfr-gal4* > UAS-*gfp* larvae, *gfp* was expressed in the inner part of the proventriculus and at the connection to the midgut (Fig. 11 A). Moreover, *prom-egfr-gal4* drove expression in clusters of midgut cells (Fig. 11 B), which showed the typical morphology of adult midgut progenitor cells, and in ECs of the hindgut (Fig. 11 C). The possibility that the GFP signal in the hindgut derives from the surrounding

muscle tissue was excluded by co-staining with phalloidin-TRITC (not shown). Whole larvae showed a GFP signal in single cells of the fat body (Fig. 11 D). This observation was further confirmed by microscopic analysis of the dissected organ (not shown).

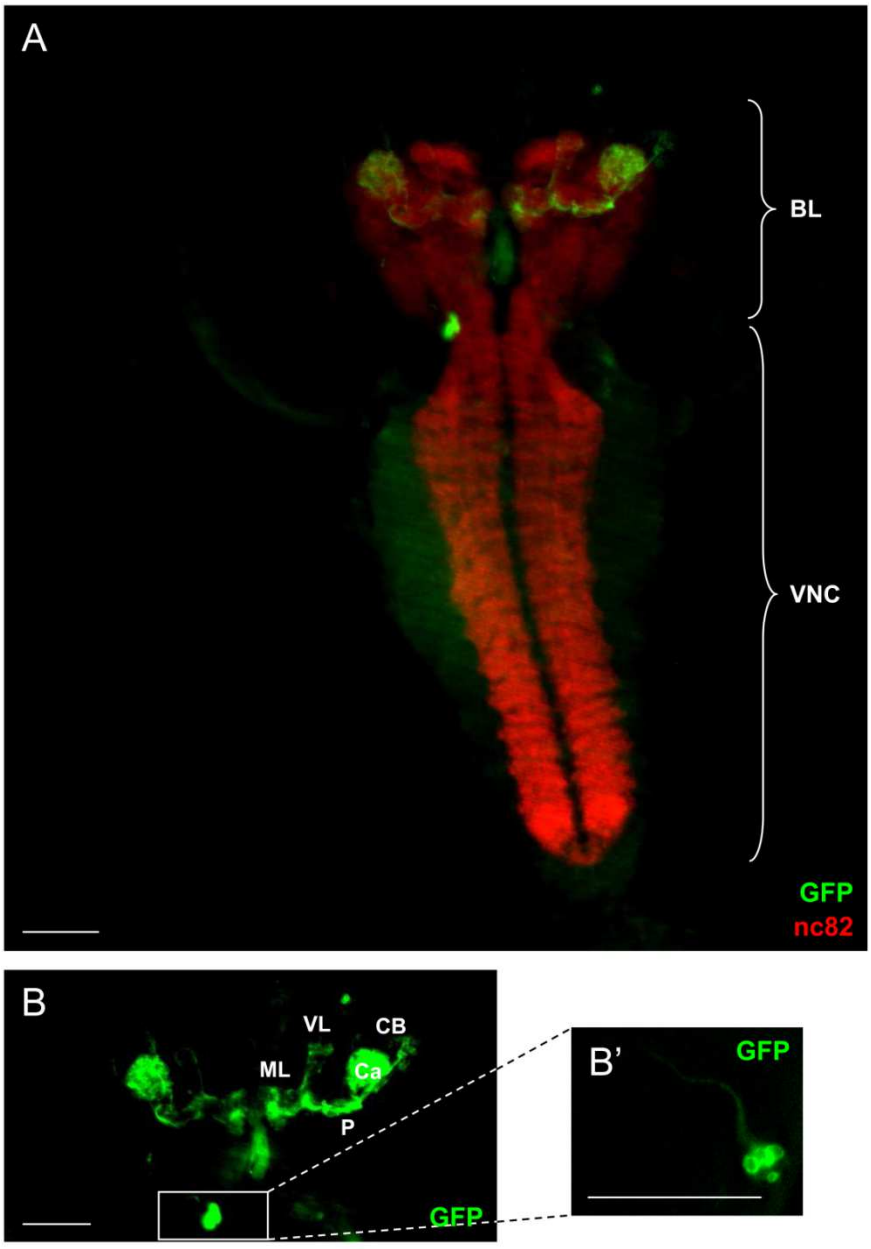

Fig. 12. ***Egfr* promoter activity in the larval brain.** GFP signals indicating *egfr* promoter activity were visualized in *prom-egfr-gal4* > UAS-*gfp* larval brains using an immunohisto-chemical staining with anti-GFP antibody. Co-staining with anti-nc82 antibody (neuropil marker, red) was used as a reference for brain morphology. (A) Overview. (B) Detailed view of brain lobes (BL) with the GFP-positive mushroom bodies. Cell bodies (CB), calyx (Ca), pedunculus (P), medial lobe (ML), vertical lobe (VL) of the larval mushroom bodies were visible. (B') Detailed view of GFP-positive cells in the BLs. VNC, ventral nerve cord. Scale bar = 50 µm

In larval brains of *prom-egfr-gal4* > UAS-*gfp* animals, expression of *gfp* was detectable in the MBs. All substructures were visible (Fig. 12 B). In each BL, a cluster of GFP-positive cells posterior of the MBs with a projection towards the MBs was observed (Fig. 12 B, box; detailed view C). No further neuronal *gfp* expression was seen.

In adult flies, *gfp* expression was found in the abdominal and in the head fat body (Fig. 13 A) as well as in the secondary cells of the accessory gland (Fig. 13 B).
No *gfp* expression was detected in adult brains using the *prom-egfr-gal4* > UAS-*gfp* flies.

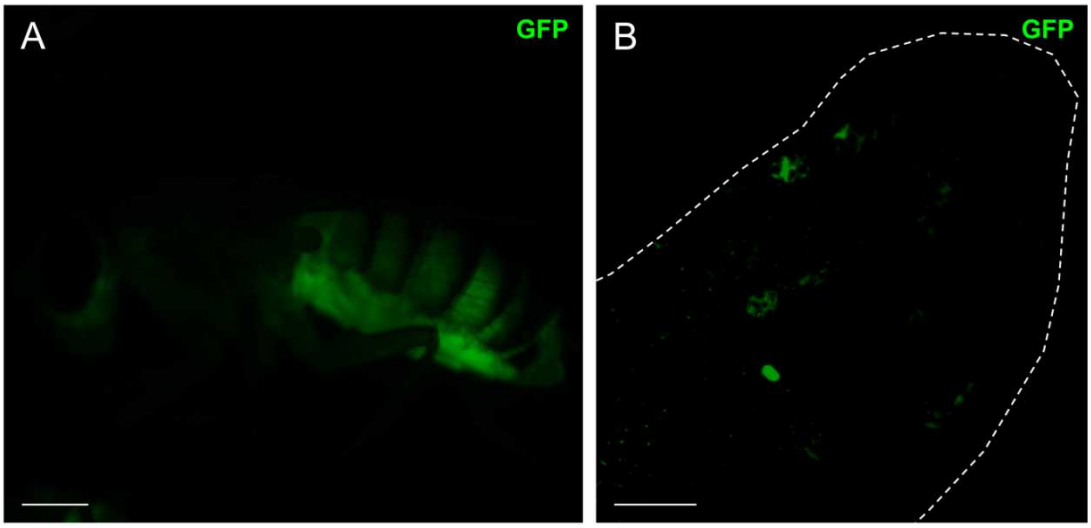

Fig. 13. *Egfr* promoter activity in adult flies. *Gfp* expression indicating e*gfr* promoter activity was visualized in *prom-egfr-gal4* > UAS-*gfp* flies using live imaging in (A) the abdominal fat body and weakly in the head fat body (lateral view whole fly) and (B) in the secondary cells of the accessory gland. Dashed lines represent the shape of the accessory gland visible in the differential interference contrast picture. Scale bar = 50 µm

4.1.2 Spatial and Temporal Promoter Activity of *SPITZ*

The gene coding for the most prominent ligand Spitz is represented by the symbol Dmel\spi (annotation symbol CG10334) and has the FlyBase ID FBgn0005672. *Prom1-spitz-gal4* was generated using oligonucleotides targeting 4,441 bp from the first to the third exon, whereas *prom2-spitz-gal4* was generated using oligonucleotides targeting a region of 4,300 bp from the third to the fifth exon of the *spitz* gene (Fig. 10). A commercially available *spitz-enhancer-trap-gal4* line was also used to screen for *spitz* promoter activity (Fig. 10).

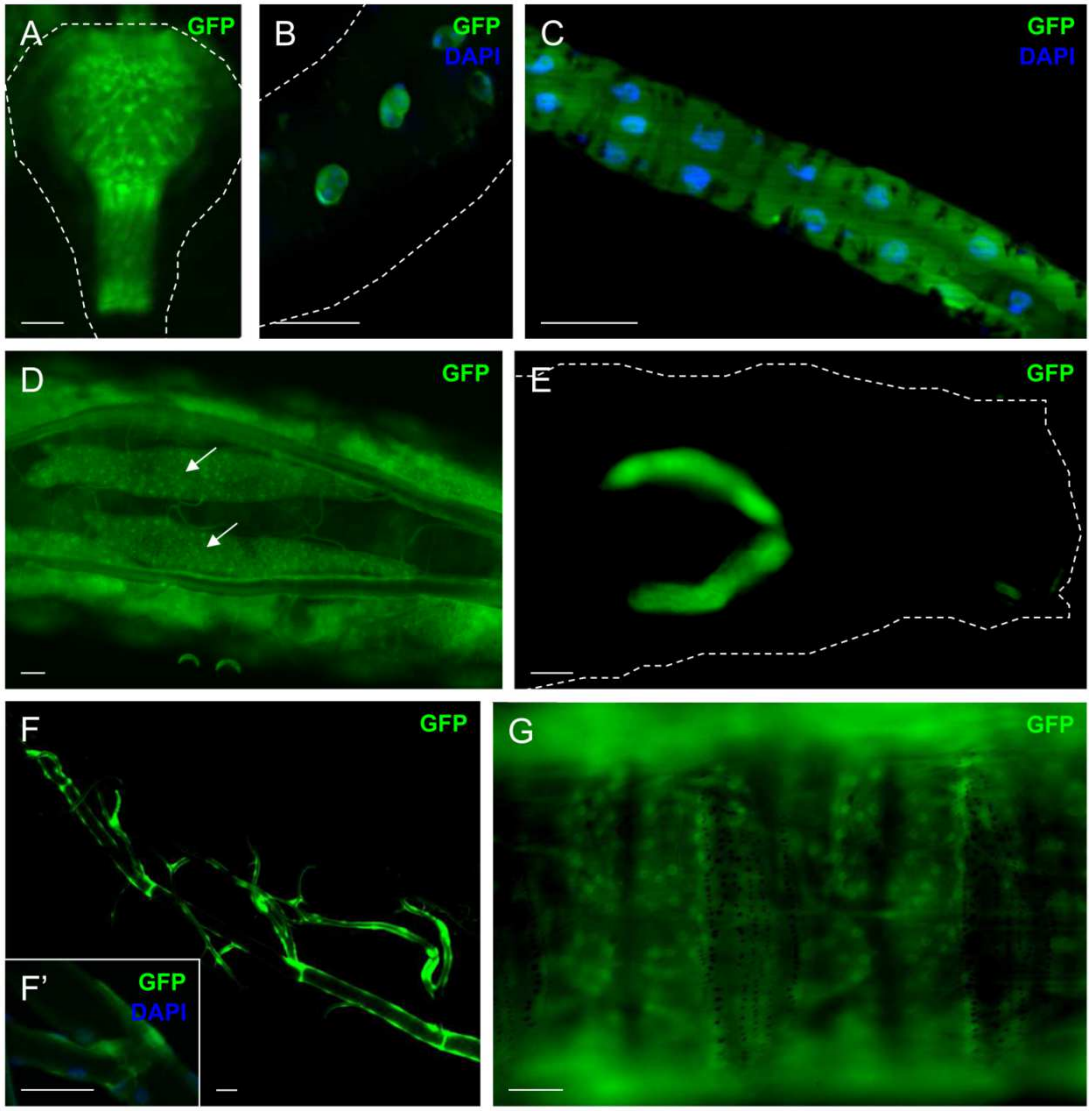

Fig. 14. ***Spitz* promoter activity in larvae.** *Gfp* expression indicating *spitz* promoter activity was visualized in *spitz-reporter-gal4* > UAS-*gfp* larvae using live imaging in (A) the proventriculus (*prom1-spitz-gal4* > UAS-*gfp*), (B) cell clusters in the midgut (*spitz-enhancer-trap-gal4* > UAS-*gfp)*, (C) cells in the hindgut (*prom1-spitz-gal4* > UAS-*gfp)*, (D) the fat body (arrows, dorsal view, *spitz-enhancer-trap-gal4* > UAS-*gfp*), (E) the salivary glands (dorsal view, *spitz enhancer-trap-gal4* > UAS-*gfp*), (F, F') the tracheae (*prom1-spitz-gal4* > UAS-*gfp)*, and (G) the epidermis (ventral view, *spitz-enhancer-trap-gal4* > UAS-*gfp*). Dashed lines represent the shape of the proventriculus, the midgut, or the whole larva visible in the differential interference contrast picture. DAPI was used to stain the nuclei. Scale bar = 50 µm.

Depending on the *reporter-gal4* line, *gfp* expression patterns differed slightly. This applies to larvae and adult flies. In larvae, *prom2-spitz-gal4* > UAS-*gfp* showed *gfp* expression only in the fat body and the brain, whereas *prom1-spitz-gal4* > UAS-*gfp* and the *spitz-enhancer-trap-gal4* > UAS-*gfp* showed additional expression in several tissues (Fig. 14).

Larval *gfp* expression in *spitz-reporter-gal4* > UAS-*gfp* animals was visible in the inner part of the proventriculus including the connection to the midgut (Fig. 14 A) and in cell clusters of the midgut, which were most likely identical with the adult midgut progenitors (Fig. 14 B). All three *spitz-reporter-gal4* lines drove a strong *gfp*

expression in the larval fat body (Fig. 14 D, arrows). In addition, expression was seen in the larval salivary glands, tracheae, and the epidermis (Fig. 14 E, F, G). Only *prom1-spitz-gal4* > UAS-*gfp* indicated *spitz* promoter activity in the hindgut (Fig. 14 C). Staining of the muscles around the hindgut using phalloidin-TRITC revealed no overlap of GFP fluorescence and TRITC fluorescence (Fig. 15). Thus, *gfp* was not expressed in muscles but in the main cell type of the hindgut, the ECs.

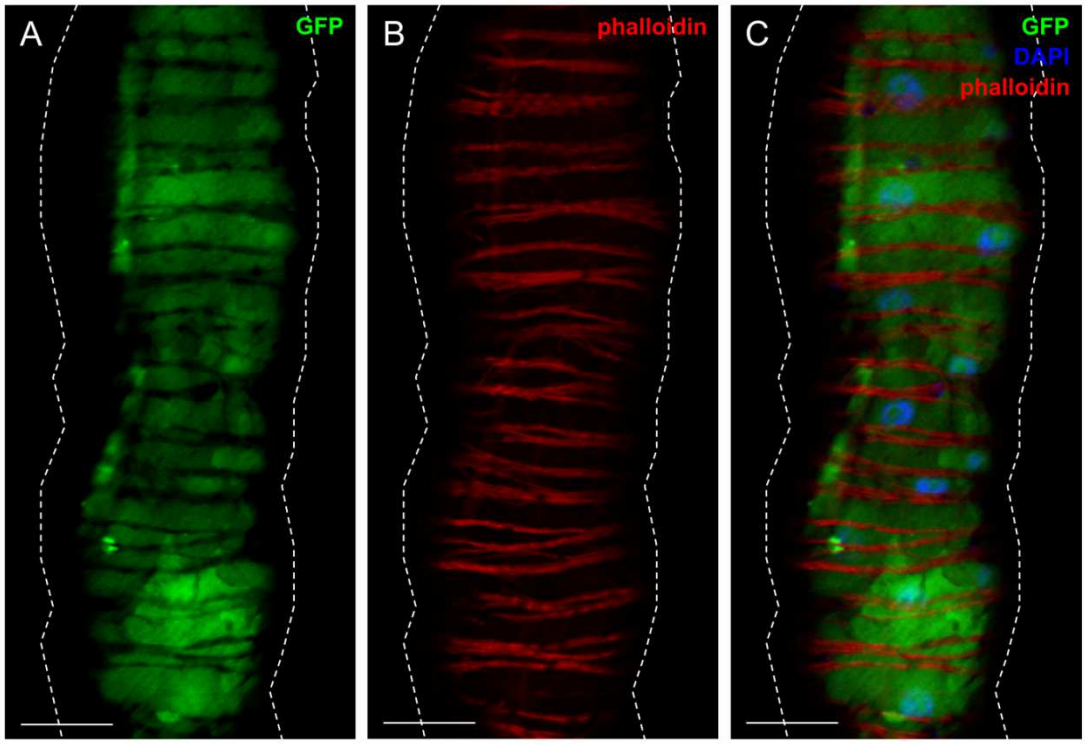

Fig. 15. *Spitz* promoter activity in enterocytes of the larval hindgut. Immunostaining of midguts of *prom1-spitz-gal4* > UAS-*gfp* larvae with (A) anti-GFP staining indicating promoter activity of *spitz* (green,) and (B) with phalloidin-TRITC staining of visceral muscles (red). (C) Merge of anti-GFP staining, phalloidin-TRITC staining, and DAPI staining labeling the nuclei. Dashed lines represent the shape of the gut visible in the differential interference contrast picture. Scale bar = 50 µm.

Gfp was also strongly expressed in larval brains of *spitz-reporter-gal4* > UAS-*gfp* animals (Fig. 16–Fig.18). A predominant expression in the larval MBs was observed in all three lines (Fig. 16–Fig. 18). The cell bodies, the calyx, the pedunculus, and the medial and vertical lobes were identified. In addition, *prom1-spitz-gal4* > UAS-*gfp* showed expression in the OLs of the BLs (Fig. 17 B).

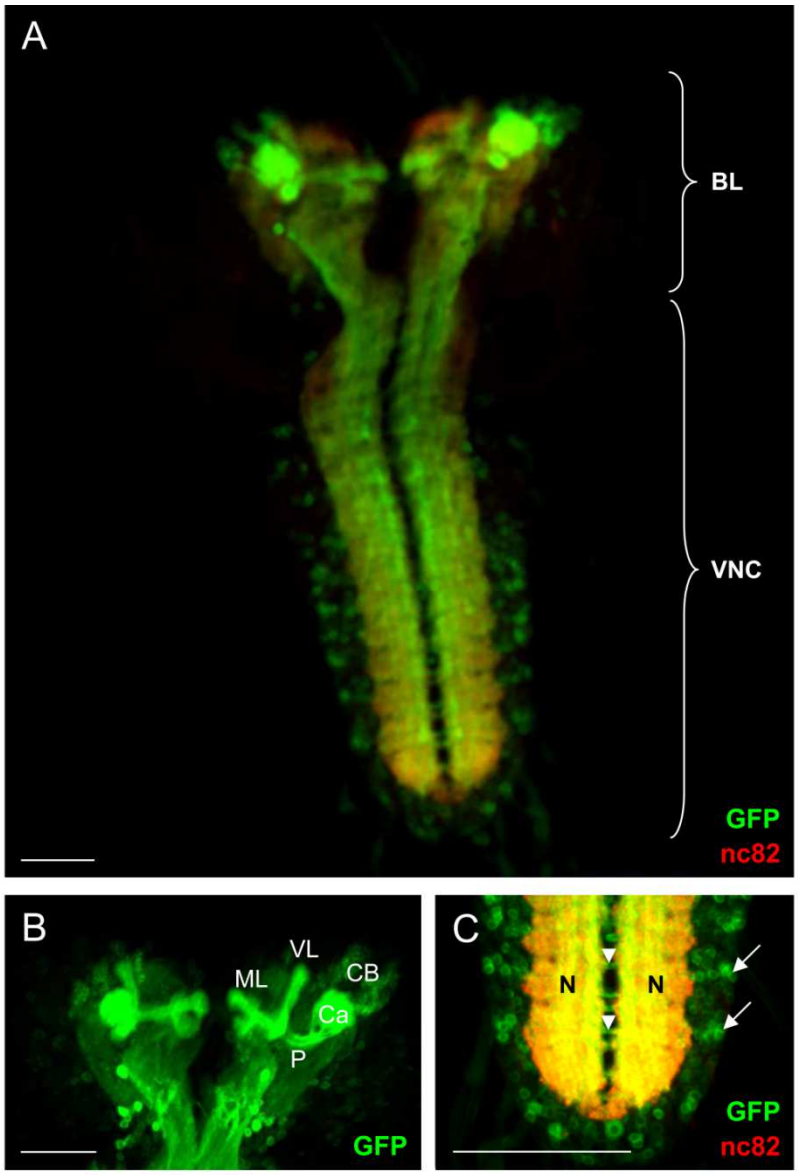

Fig. 16. *Spitz* promoter activity in the larval brain. GFP signals indicating *spitz* promoter activity were visualized in *spitz-enhancer-trap-gal4* > UAS-*gfp* larval brains using an immunohistochemical staining with anti-GFP antibody. Co-staining with anti-nc82 antibody (neuropil marker, red) was used as a reference for brain morphology. (A) Overview. (B) Detailed view of the brain lobes (BL) with detailed view on the GFP-positive mushroom bodies. Cell bodies (CB), calyx (Ca), pedunculus (P), and medial (ML) and vertical lobe (VL) were visible. (C) Detailed view of the ventral nerve cord (VNC) with GFP signals in cell bodies of neuronal cells (arrows) and in projections (arrow heads) between the two VNC neuropils (N). Scale bar = 50 µm.

All three *spitz-reporter-gal4* lines revealed expression of *gfp* in cells surrounding the VNC neuropil (Fig. 16–Fig. 18). Further expression was detected in projections between right and left side cells of the VNC (Fig. 16 C, arrow heads). Only *spitz-enhancer-trap-gal4* > UAS-*gfp* showed a staining of the entire neuropil (Fig. 16 A). *Prom2-spitz-gal4* > UAS-*gfp* demonstrated additional *gfp* expression in cells of the BLs around the MBs (Fig. 18 B). In the thoracic region of the VNC, cell bodies surrounding the VNC neuropil (Fig. 18 C, arrows) with connections between both VNC sides (Fig. 18 C, arrow heads) were visible.

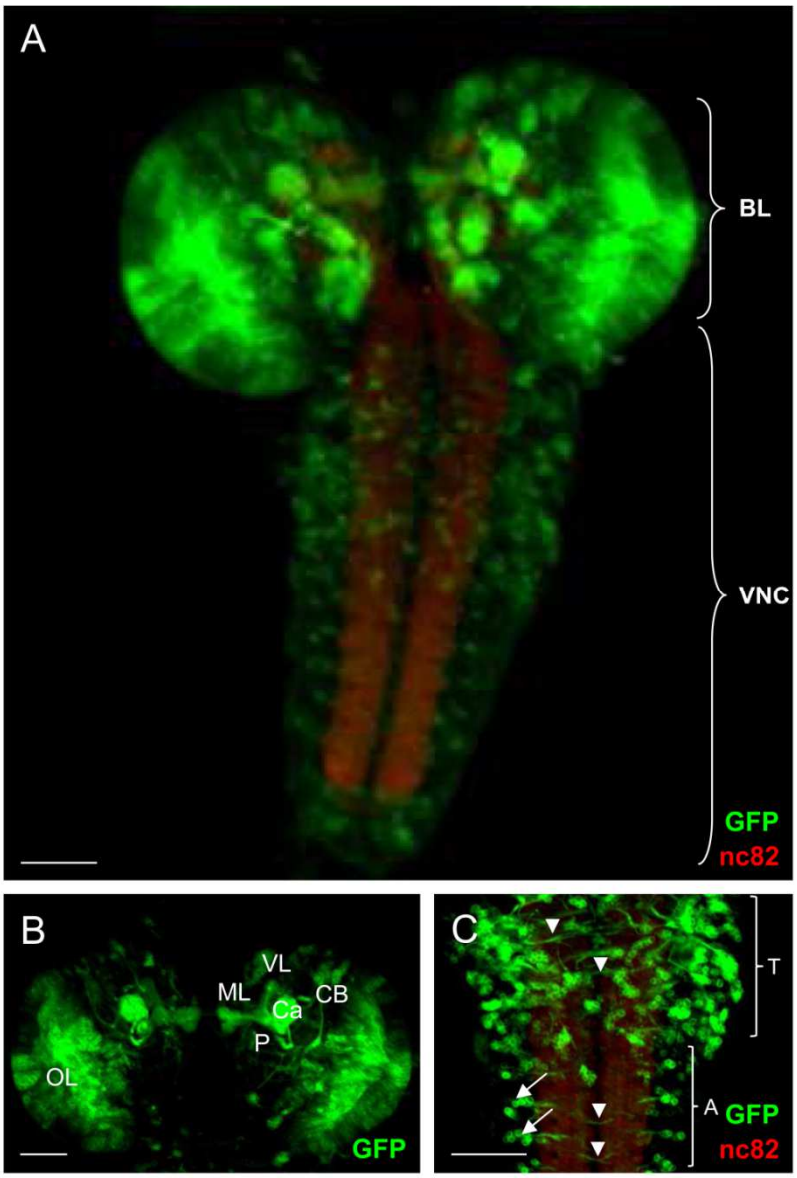

Fig. 17. *Spitz* promoter activity in the larval brain. GFP signals indicating *spitz* promoter activity were visualized in a *prom1-spitz-gal4* > UAS-*gfp* larval brains using an immunohistochemical staining with anti-GFP antibody. Co-staining with anti-nc82 antibody (neuropil marker, red) was used as a reference for brain morphology. (A) Overview. (B) Detailed view of the brain lobes (BL) with detailed view on the GFP-positive mushroom bodies. Cell bodies (CB), calyx (Ca), pedunculus (P), medial lobe (ML), vertical lobe (VL), and optic lobe (OL) were visible. (C) Detailed view of the thoracic (T) and abdominal (A) region of the ventral nerve cord (VNC) with GFP signals in cell bodies of neuronal cells (arrows) and in projections between the two VNC neuropils (arrow heads). Scale bar = 50 µm.

Interestingly, *prom1-spitz-gal4* > UAS-*gfp* (Fig. 17 A–C) showed the most various *gfp* expression in the larval brain, as it was also the case for the other larval tissues.

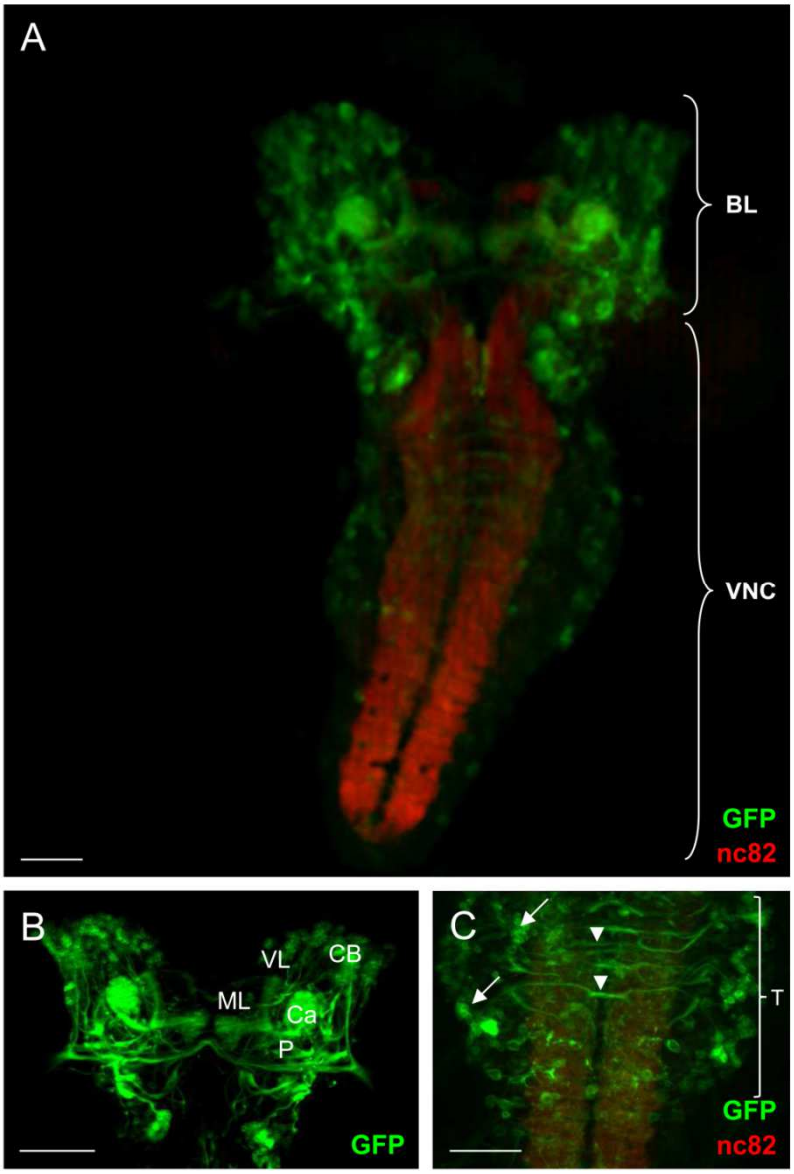

Fig. 18. *Spitz* promoter activity in the larval brain. *Gfp* expression indicating *spitz* promoter activity was visualized in a *prom2-spitz-gal4* > UAS-*gfp* larval brain using an immuno-histochemical staining with anti-GFP antibody. Co-staining with anti-nc82 antibody (neuropil marker, red) was used as a reference for brain morphology. (A) Overview. (B) Detailed view of the brain lobes (BL) with detailed view on the GFP-positive mushroom bodies. Cell bodies (CB), calyx (Ca), pedunculus (P), medial lobe (ML), and vertical lobe (VL) were visible. (C) Detailed view of the thoracic region (T) of the ventral nerve cord (VNC) with GFP signals in cell bodies of neuronal cells (arrows) and in projections (arrow heads) between the two VNC neuropils (N). Scale bar = 50 µm.

In accordance with the observation in larvae, *prom1-spitz-gal4* drove *gfp* expression in the majority of adult tissues, whereas expression detected with *prom2-spitz-gal4* > UAS-*gfp* and with *spitz-enhancer-trap-gal4* > UAS-*gfp* was much less prominent. However, all three *spitz-reporter-gal4* lines indicated promoter activity of *spitz* in the midgut, the male reproductive tract, and the brain (Fig. 19–Fig. 22). Additionally, in *prom1-spitz-gal4* > UAS-*gfp* and in the *spitz-enhancer-trap* > UAS-*gfp* flies, *gfp* expression was detectable in the salivary glands. Only *prom1-spitz-gal4* > UAS-*gfp* displayed a GFP signal in the hindgut and the fat body (Fig. 19).

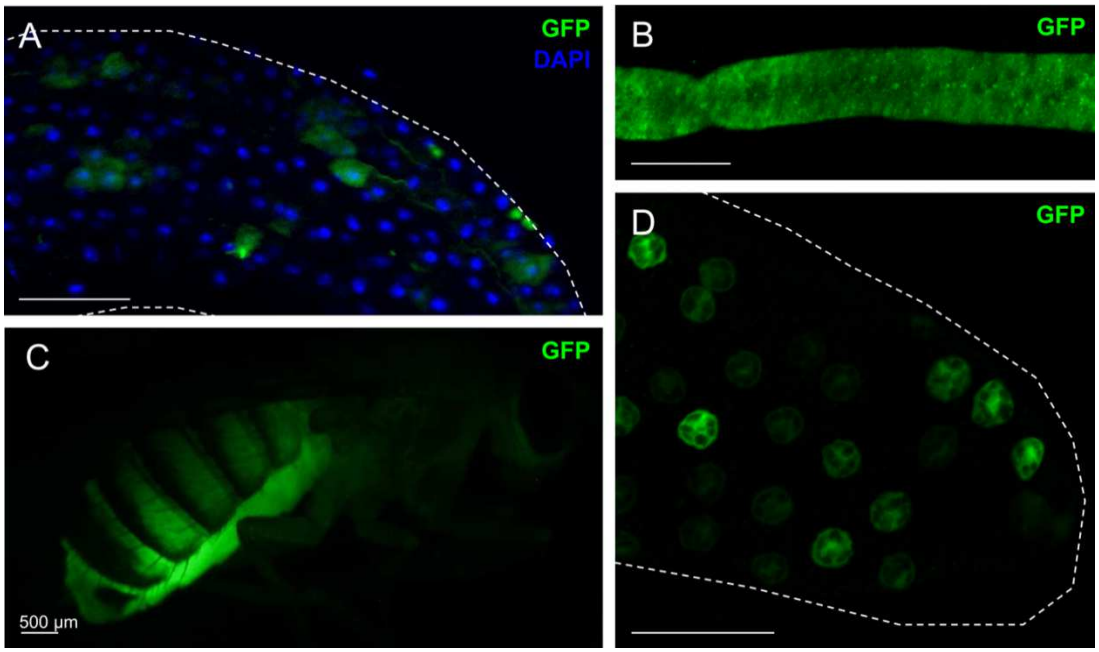

Fig. 19. *Spitz* promoter activity in adult flies. *Gfp* expression indicating *spitz* promoter activity was visualized in *spitz-reporter-gal4* > UAS-*gfp* adult flies using live imaging in (A) large cells of the hindgut (*prom1-spitz-gal4* > UAS-*gfp)*, (B) the salivary gland (*prom1-spitz-gal4* > UAS-*gfp*), (C) the fat body (lateral view, *prom1-spitz-gal4* > UAS-*gfp*), and (D) the secondary cells of the accessory gland (*prom2-spitz-gal4* > UAS-*gfp)*. Dashed lines represent the shape of the hindgut or the accessory gland visible in the differential interference contrast picture. DAPI was used to stain the nuclei. Scale bar = 50 µm.

Single ECs in the hindgut (Fig. 19 A), the whole salivary glands (Fig. 19 B), and the secondary cells of the accessory glands (Fig. 19 D) showed *gfp* expression. The GFP signal in the abdominal fat body was stronger than in the head fat body, where only a weak signal was detected (Fig. 19 C). *Gfp* expression in the fat body was further confirmed by microscopic analysis of the dissected organ (not shown).

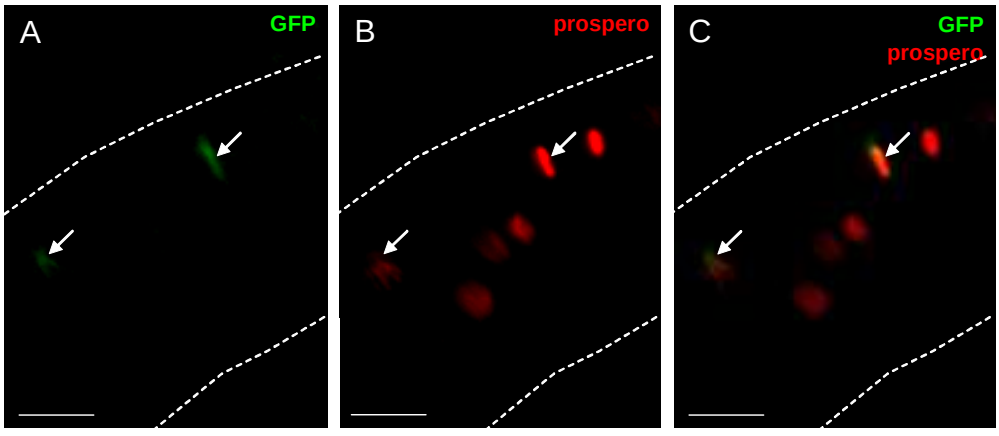

Fig. 20. Weak *spitz* promoter activity in enteroendocrine cells of the adult midgut. Immunostaining of midguts of *prom1-spitz-gal4* > UAS-*gfp* adult midguts with (A) anti-GFP staining indicating promoter activity of *spitz* (green) and (B) anti-prospero staining labeling enteroendocrine cells (red). (C) Merge of anti-GFP and anti-prospero staining. Dashed lines represent the shape of the gut visible in the differential interference contrast picture. Scale bar = 50 µm.

An immunohistochemical double-staining of dissected guts of *prom2-spitz-gal4* > UAS-*gfp* adult flies using anti-GFP antibody and anti-prospero antibody indicated a weak *spitz* promoter activity in EEs (Fig. 20).

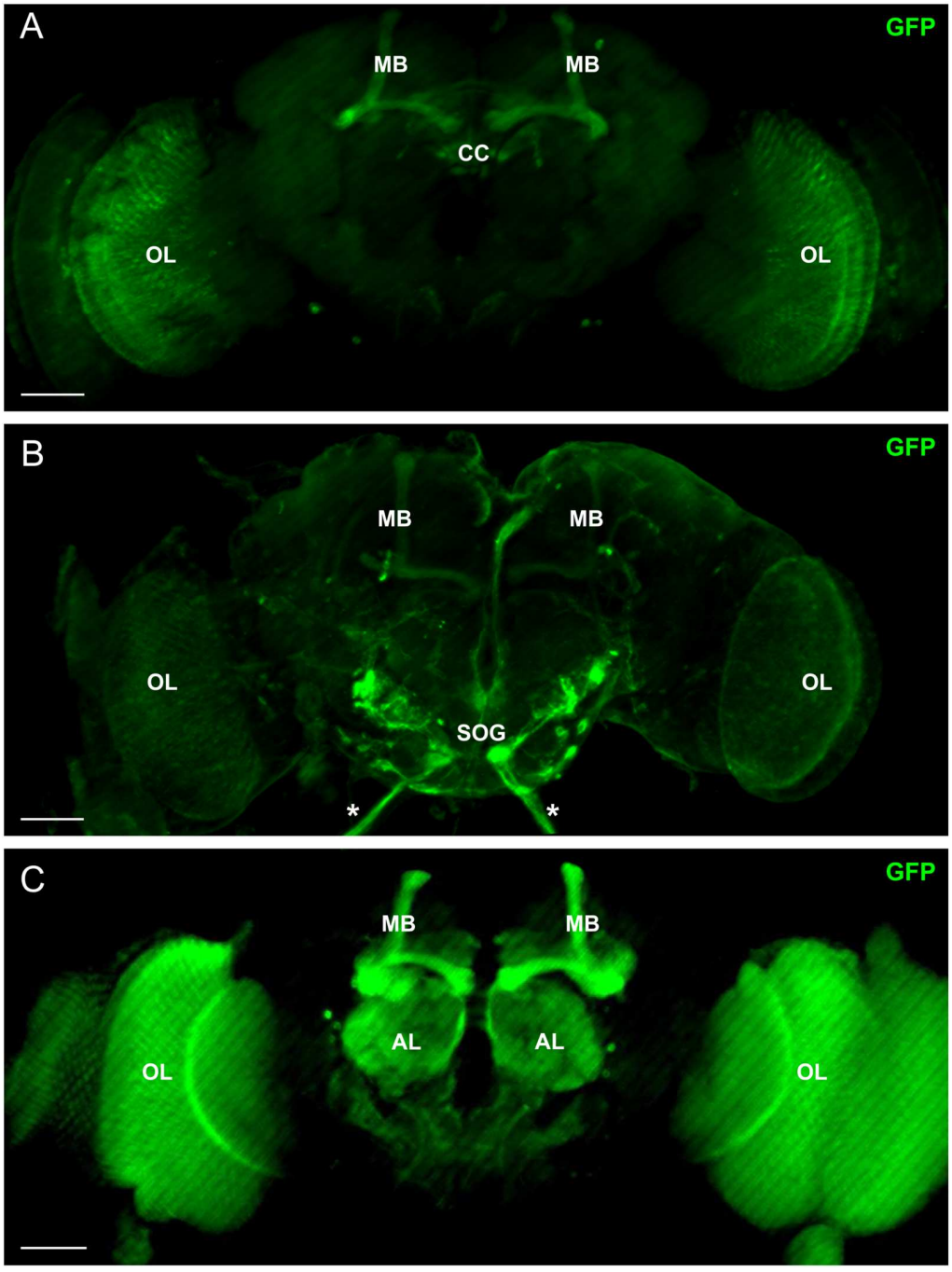

Fig. 21. *Spitz promoter activity* in the whole-mount adult brain. *Gfp* expression indicating *spitz* promoter activity was visualized in the three *spitz-reporter-gal4* > UAS-*gfp* lines using an immunohistochemical staining with anti-GFP antibody. (A) *Prom1-spitz-gal4* > UAS-*gfp* indicated *spitz* promoter activity in the optic lobes (OL), the mushroom bodies (MB), and the central complex (CC). (B) *Prom2-spitz-gal4* > UAS-*gfp* indicated *spitz* promoter activity in the MBs, in the subesophageal ganglion (SOG), and in two nerves exiting the SOG (asterisks). (C) *Spitz enhancer-trap-gal4* >UAS-*gfp* indicated *spitz* promoter activity in the OLs, the MBs, and in the antennal lobes (AL). Scale bar = 50 µm.

All three *spitz-reporter-gal4* lines drove *gfp* expression in the adult brain (Fig. 21).

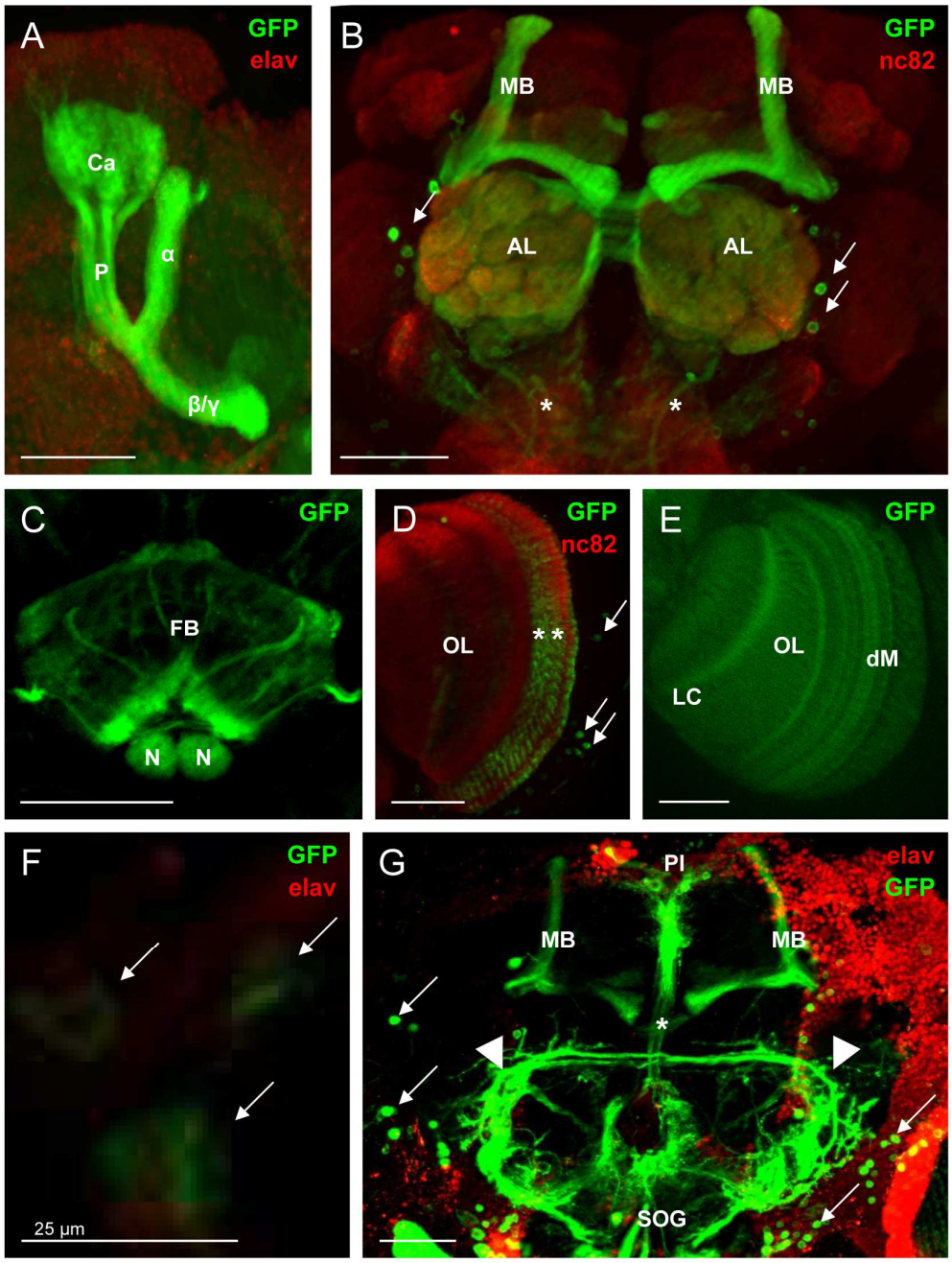

Fig. 22. Detailed view on *spitz* promoter activity in the adult brains. *Gfp* expression indicating *spitz* promoter activity was visualized in *spitz-reporter-gal4* > UAS-*gfp* adult brains using an immunohistochemical staining with anti-GFP antibody (green). Co-stainings with anti-nc82 antibody (neuropil marker, red) or anti-elav antibody (neuronal marker, red) were used as references for brain morphology. (A) The GFP-positive mushroom body complex with calyx (Ca), pedunculus (P), α lobe (α), and β/γ lobe (β/ γ) (*spitz-enhancer-trap-gal4* > UAS-*gfp)*. (B) GFP signals in antennal lobes (AL) with antennal nerves or labiomaxillary nerves (asterisks), and in single cells surrounding the ALs (arrows) as well as in the mushroom bodies (MB) (*spitz-enhancer-trap-gal4* > UAS-*gfp*). (C) GFP signals in the fan-shaped body (FB) and the noduli (N) of the central complex (*prom1-spitz-gal4* > UAS-*gfp*). (D) GFP signals in the endings of the R7 and R8 photoreceptor cells (asterisks) and in the cell bodies of transmedullary neurons (arrows) in the optic lobe (OL) (*prom1-spitz-gal4* > UAS-*gfp*,). (E) GFP signals in the entire OL including lobula complex (LC) and distal medulla (dM) (*spitz-enhancer-trap-gal4* > UAS-*gfp*). (F) GFP-positive cells of the pars intercerebralis (PI, arrows; *prom2-spitz-gal4* > UAS-*gfp*). (G) GFP signals in single cell bodies (arrows) and axons (arrow heads) in the region of the subesophageal ganglion (SOG), in the MBs, and in cells of the PI with axons along the midline (asterisk) (*prom2-spitz-gal4* > UAS-*gfp*). Scale bar = 50 µm, if not otherwise mentioned.

Expression in the MBs was visible in all of the lines. *Prom1-spitz-gal4* > UAS-*gfp* and the *spitz-enhancer-trap-gal4* > UAS-*gfp* demonstrated additional expression in the

OLs. Only *prom2-spitz-gal4* presented strong GFP signals in the SOG and in nerves that exit the central brain region (Fig. 21 B, asterisks). These nerves may be labial nerves that project their axons into the SOG and have their dendrites in the labellum. Moreover, *prom1-spitz-gal4* > UAS-*gfp* and *spitz-enhancer-trap-gal4* > UAS-*gfp* indicated *spitz* promoter activity in the CC (Fig. 21 A) and in the ALs, respectively (Fig. 21 C).

Detailed views on different structures of the adult brain revealed that *gfp* expression driven by the different *spitz-reporter-gal4* lines can be assigned to distinct neuronal structures and single cells (Fig. 22).

Spitz promoter activity was visualized in the MBs with the subdivisions α and β/γ lobes, pedunculus, and calyx (Fig. 22 A), as well as in the ALs (Fig. 22 B) with either the antennal nerves or the labiomaxillary nerves (Fig. 22 B, asterisks). Substructures of the CC revealed further *gfp* expression (Fig. 22 C). These substructures were the fan-shaped body and the noduli. No GFP signal was detected in the two other substructures, the ellipsoid body and the protocerebral bridge. Moreover, expression of *gfp* driven by *prom1-spitz-gal4* was observed in the OLs (Fig. 22 D) with single cell bodies visible distal of the medulla neuropil (arrows). The projections of the PR R7 and R8 end in the medulla (Fig. 22 D, asterisks). *Spitz-enhancer-trap-gal4* > UAS-*gfp* also revealed expression in the OL (Fig. 22 E). Notably, the expression pattern was different from that observed with the *spitz-prom1-gal4* line as a driver. This line drove *gfp* expression in a lot of axons reaching from the distal medulla to the proximal part of the lobula complex. No stained cell bodies were detected distal of the medulla. Additionally, expression was detected in single cell bodies (Fig. 22 G, arrows) and axons (Fig. 22 G, arrow heads) in the ventral central brain region. *Gfp* expression in the MBs and in large cells of the PI with axons passing along the midline into the tritocerebrum was driven by *prom2-spitz-gal4* (Fig. 22 G). GFP-positive nerves that innervate the SOG could also be seen (Fig. 22 G). These nerves might be mechanosensory neurons from both the antenna and the maxillary palps that project into the antenna mechanosensory motor center of the SOG (Fig. 22 G, arrow heads).

4.1.3 Spatial and Temporal Promoter Activity of *KEREN*

The gene coding for the membrane-bound ligand Keren is represented by the symbol Dmel\Krn (annotation symbol CG32179) and has the FlyBase ID FBgn0052179.

Oligonucleotides targeting a region of 4,210 bp were used to amplify the presumptive promoter region of the *keren* gene.

Prom-keren-gal4 > UAS-*gfp* larvae showed *gfp* expression in substructures of the anterior part of the proventriculus (Fig. 23 A). In the midgut and the hindgut, large *gfp* expressing cells were visible, which were identified as ECs due to cell shape and size of the nuclei (Fig. 23 B and C).

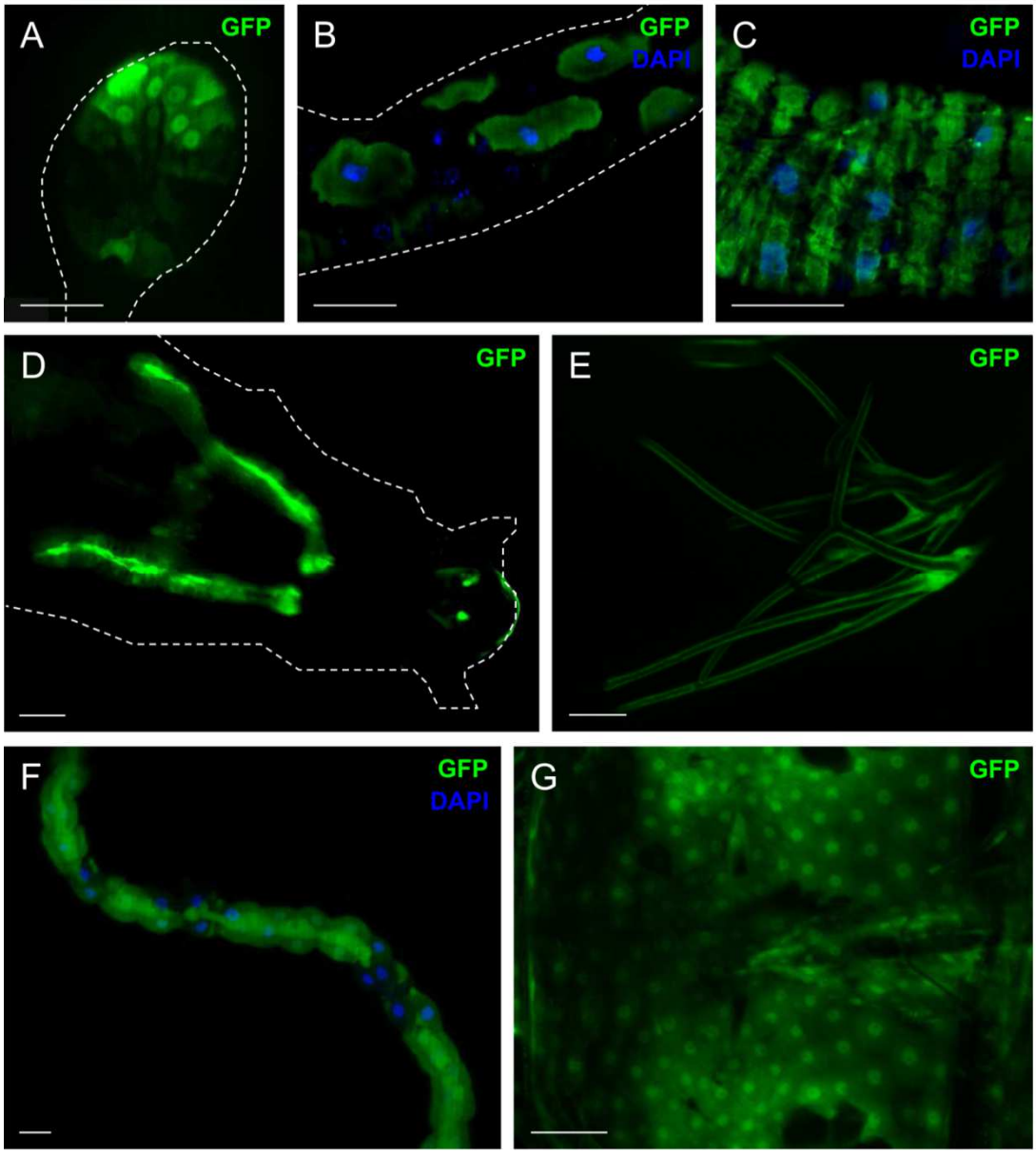

Fig. 23. *Keren* promoter activity in larvae. *Gfp* expression indicating *keren* promoter activity was visualized in *prom-keren-gal4* > UAS-*gfp* larvae using live imaging in (A) the proventriculus, (B) enterocytes of the midgut, (C)enterocytes of the hindgut, (D) the salivary glands (dorsal view), (E) the tracheae, (F) the Malpighian tubules, and (G) the epidermis (dorsal view). Dashed lines represent the shape of the proventriculus, the midgut, or the whole larva visible in the differential interference contrast picture. DAPI was used to stain the nuclei. Scale bar = 50 µm.

The possibility that the GFP signal in the hindgut derives from the surrounding muscle tissue was excluded by co-staining with phalloidin-TRITC (not shown).

Promoter activity in the salivary glands, the tracheae, the Malpighian tubules, and the epidermis of larvae was depicted by *prom-keren-gal4* > UAS-*gfp* (Fig. 23).

In the larval brain, *keren* promoter activity was indicated by *prom-keren-gal4* > UAS-*gfp* in the BLs as well as in the VNC (Fig. 24 A).

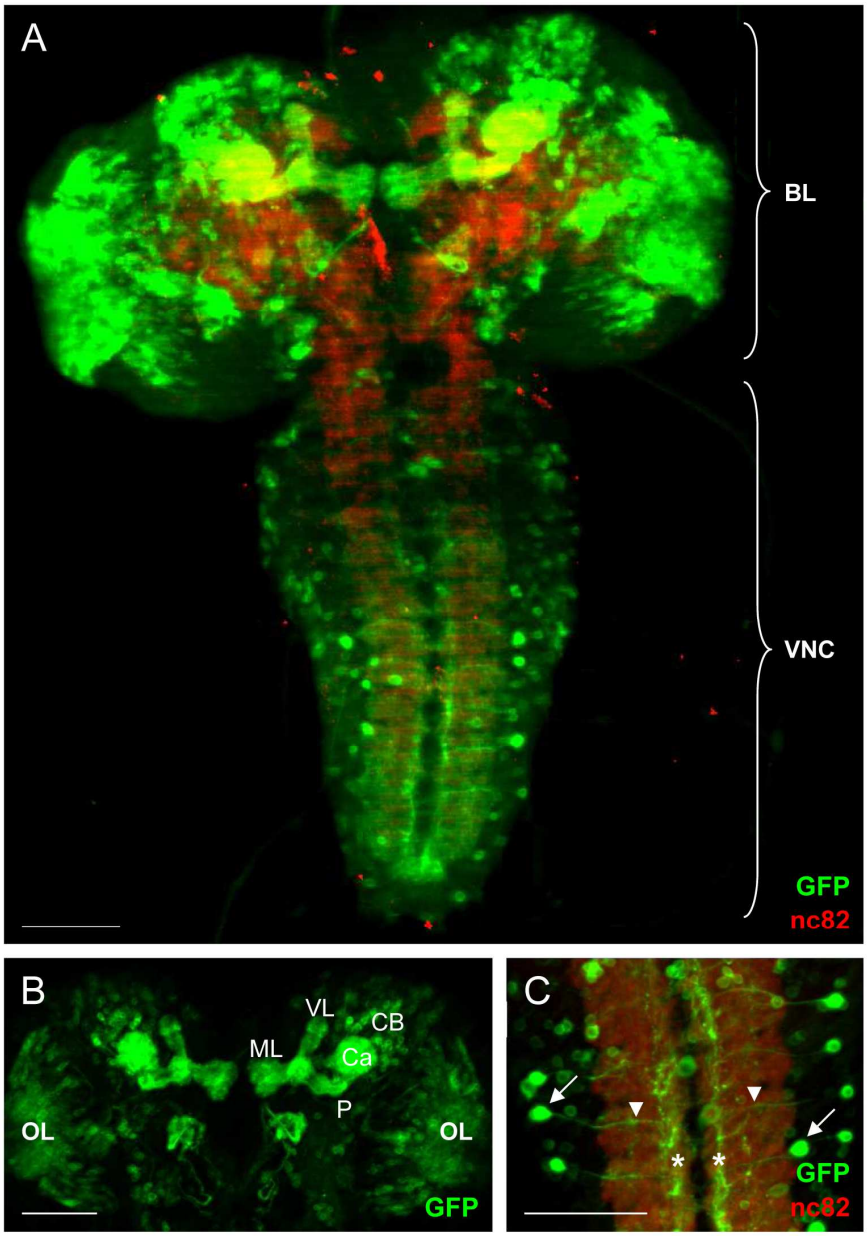

Fig. 24. *Keren* promoter activity in the larval brain. GFP signals indicating *keren* promoter activity were visualized in *prom-keren-gal4* > UAS-*gfp* larval brains using an immunohisto-chemical staining with anti-GFP antibody. Co-staining with anti-nc82 anti-body (neuropil marker, red) was used as a reference for brain morphology. (A) Overview. (B) Detailed view of the brain lobes (BL) with GFP-positive mushroom bodies. Cell bodies (CB), calyx (Ca), pedunculus (P), medial lobe (ML), vertical lobe (VL) and optic lobe (OL) were visible. (C) Detailed view of ventral nerve cord (VNC) with GFP signals in segmentally repeated lateral cells (arrows) with projection towards the midline (arrow heads) and in axons along the inner part of the ventral nerve cord (asterisks). Scale bar = 50 µm.

Distinct *gfp* expression was observed in the larval MBs (Fig. 24 B) and in the OLs (Fig. 24 A and B). Expression in the VNC was found in a lateral cluster of segmentally repeated cells (Fig. 24 C, arrows). In each abdominal hemisegment one lateral VNC neuron showed a particular strong signal (Fig. 24 C, arrows) and projections towards the midline (Fig. 24 C, arrow heads).

In adult flies, the *prom-keren-gal4* line drove *gfp* expression in ECs of the midgut and the hindgut (Fig. 25 A and B). ECs were identified due to cell shape and size of the

nuclei. In addition, immunohistochemistry was performed on dissected midguts using a co-staining with anti-GFP antibody and with anti-prospero antibody or anti-delta antibody. No overlay of the GFP signal with the prospero or delta signal was detectable with *keren* expressing cells (not shown). Thus, these cells were neither EEs nor stem cells. Phalloidin-TRITC co-staining was used to exclude *gfp* expression in the visceral muscles around the midgut and thus, to ascertain expression in ECs (Fig. 26).

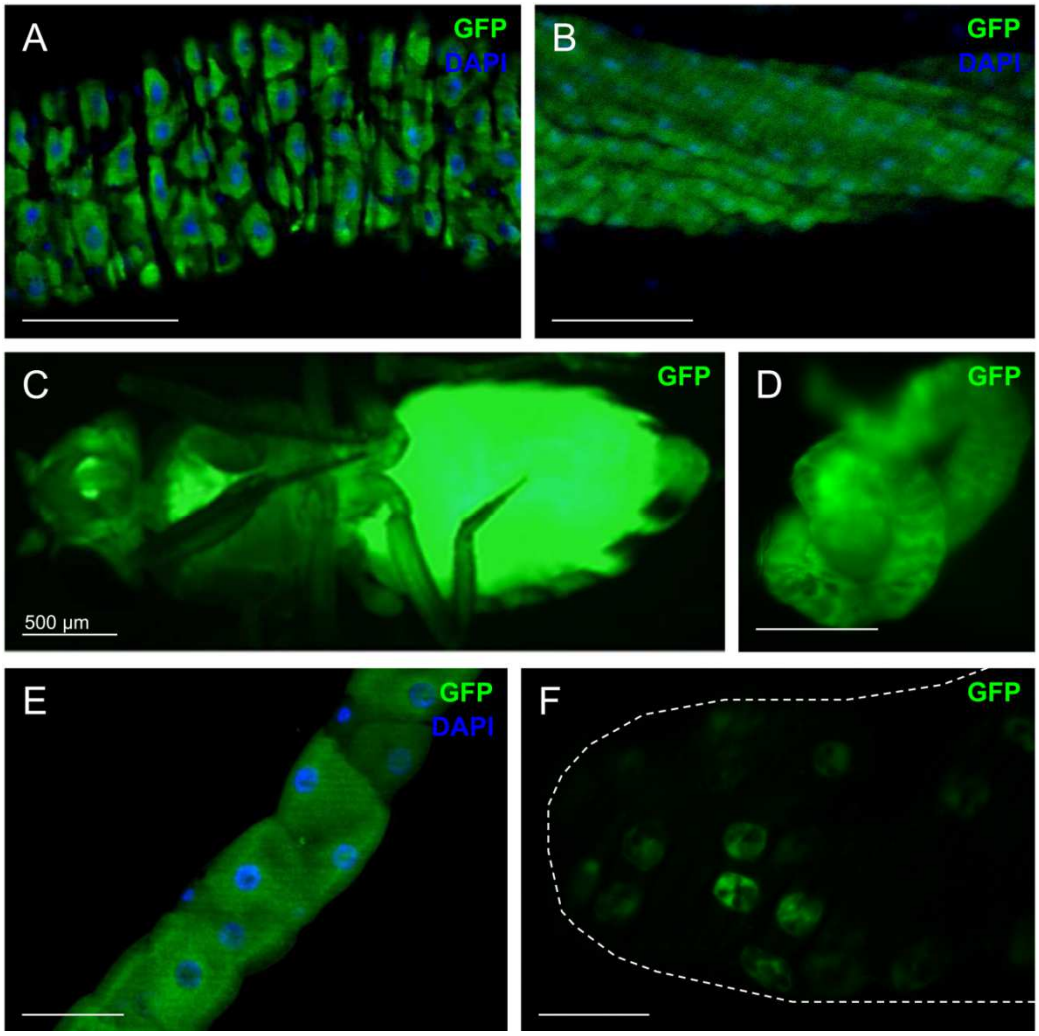

Fig. 25. *Keren* promoter activity in adult flies. *Gfp* expression indicating *keren* promoter activity was visualized in *prom-keren-gal4* > UAS-*gfp* flies using live imaging in (A) the enterocytes of the midgut and (B) the hindgut, (C) the fat body of the head and the abdomen (ventral view on whole fly), (D) the salivary gland, (E) the Malpighian tubules, and (F) the secondary cells of the accessory gland. Dashed lines represent the shape of the accessory gland visible in the differential interference contrast picture. DAPI was used to stain the nuclei. Scale bar = 50 µm, if not otherwise mentioned.

Gfp was also strongly expressed in the adult fat body. Promoter activity of *keren* was visualized in the head fat body and in the abdominal fat body (Fig. 25 C). This promoter activity was confirmed by analyzing the dissected fat body by microscopy

(not shown). Moreover, flies displayed *gfp* expression in the adult salivary glands (Fig. 25 D) and the Malpighian tubules (Fig. 25 E).

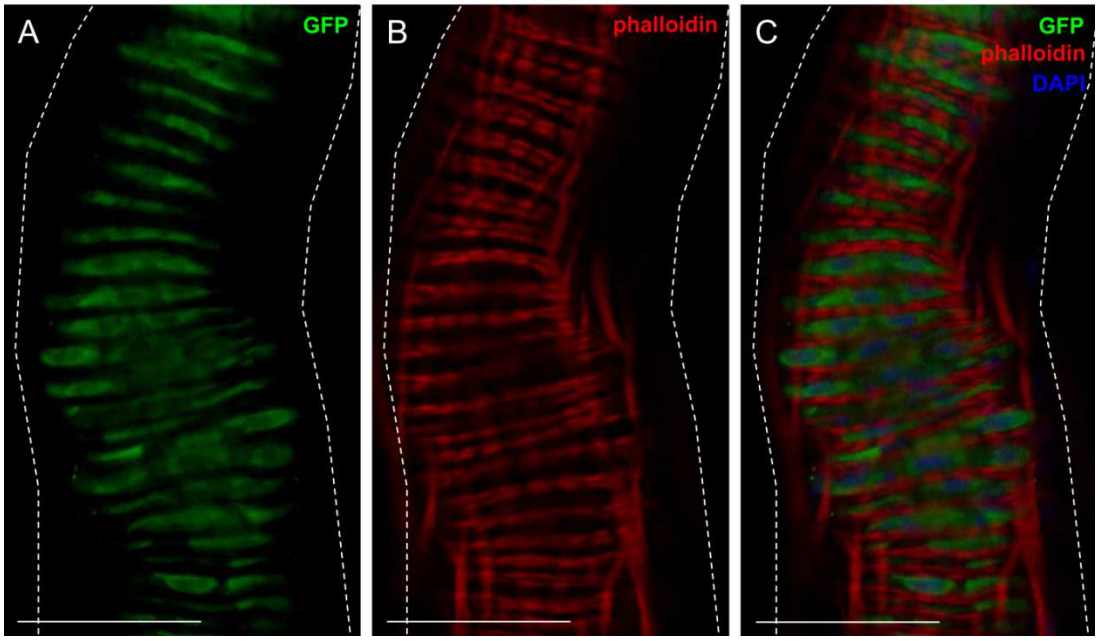

Fig. 26. *Keren* promoter activity in enterocytes of the adult midgut. Immunostaining of midguts of *prom-keren-gal4* > UAS-*gfp* adult midguts with (A) anti-GFP staining indicating promoter activity of *keren* (green) and (B) with phalloidin-TRITC staining of visceral muscles (red). (C) Merge of anti-GFP staining, phalloidin-TRITC staining, and DAPI staining labeling the nuclei. Dashed lines represent the shape of the midgut visible in the differential interference contrast picture. Scale bar = 50 µm.

In addition to *gfp* expression in the secondary cells of the accessory glands (Fig. 25 F), expression was also detectable in the seminal vesicle and the ejaculatory duct of the male reproductive tract (Fig. 27).

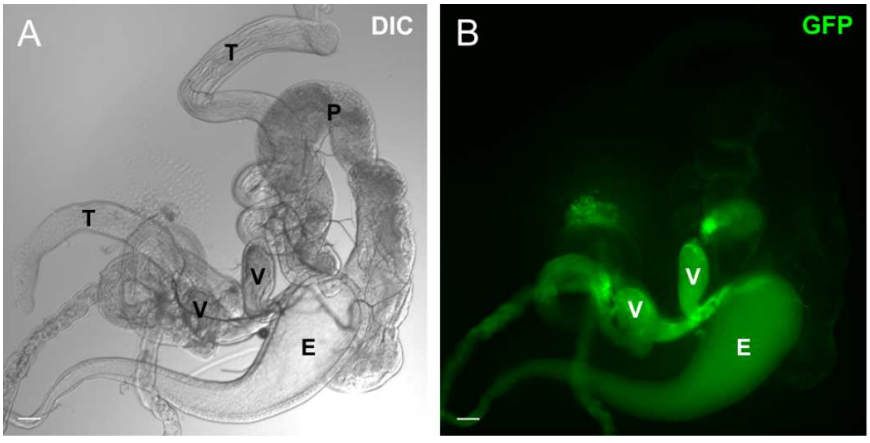

Fig. 27. *Keren* promoter activity in the seminal vesicle and the ejaculatory duct. (A) Differential interference contrast (DIC) picture of the male reproductive tract with testes (T), ejaculatory duct (E), paragonia/ accessory glands (P), and seminal vesicle (V). (B) *Gfp* expression indicating *keren* promoter activity was visualized in *prom-keren-gal4* > UAS-*gfp* flies using live imaging (green). Scale bar = 50 µm.

Keren promoter activity was visualized in adult brains (Fig. 28). Promoter activity of *keren* was not only found in MBs and ALs (Fig. 28 A and B) but also in two different types of nerves that innervate the ALs (Fig. 28 A). One pair of nerves (Fig. 28 A and B, asterisks) had the position of labiomaxillary nerves, whereas the other pair (Fig. 28 A, arrows) had the position ANs. Moreover, a symmetric structure in the

SOG was detected (Fig. 28 B, asterisks). This structure may be the antenna mechanosensory motor center, in which mechanosensory neurons from antenna and maxillary palp project into.

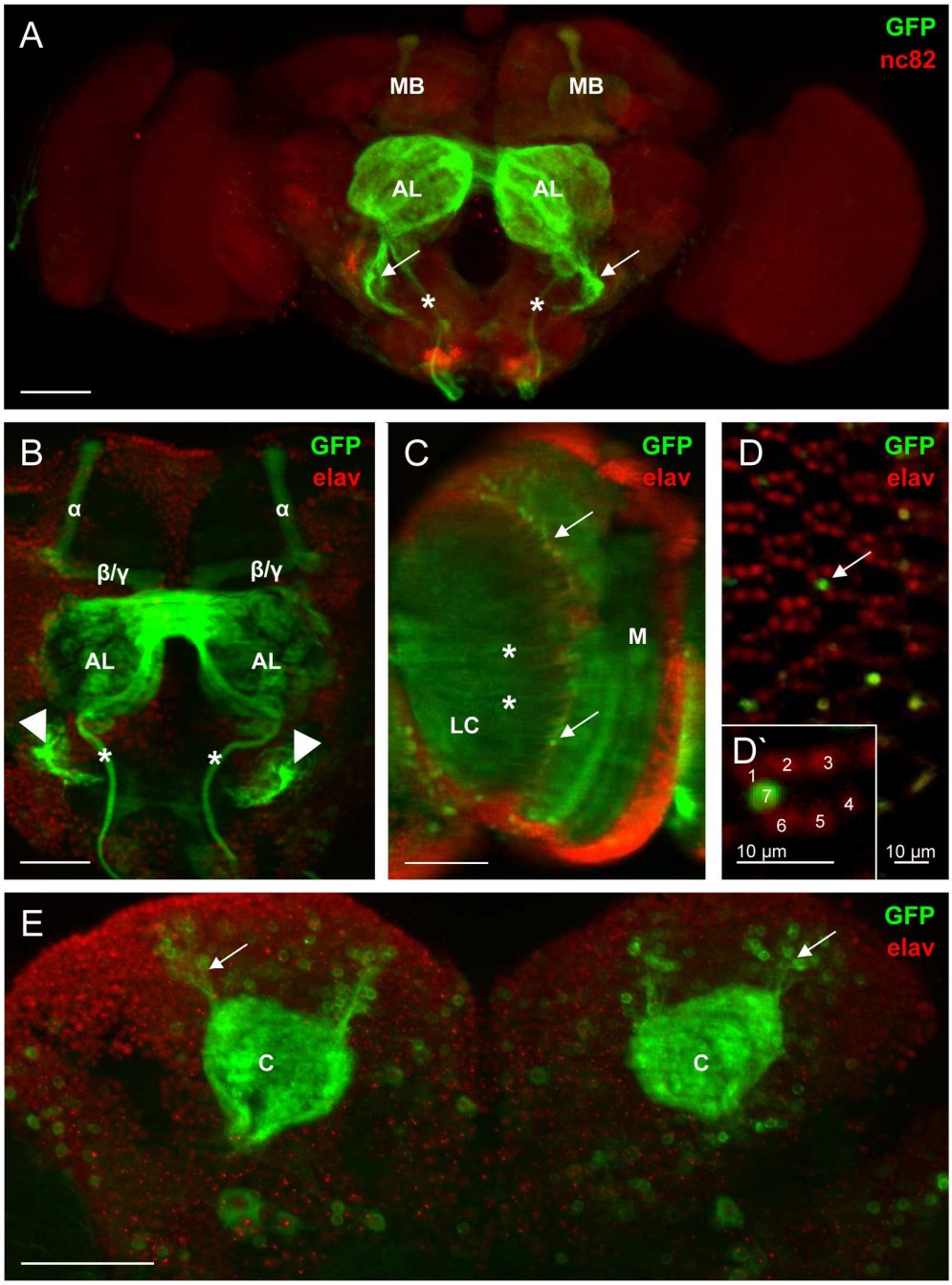

Fig. 28. *Keren* promoter activity in the adult brain. GFP signals indicating *keren* promoter activity were visualized in *prom-keren-gal4* > UAS-*gfp* adult brains using an immunohistochemical staining with anti-GFP antibody (green). Co-stainings with anti-nc82 antibody (neuropil marker, red) or anti-elav antibody (neuronal marker, red) were used as references for brain morphology. (A) Overview with GFP-positive mushroom bodies (MB), antennal lobes (AL), nerves innervating the ALs (asterisks and arrows). (B) Detailed view on the central brain region with GFP signals in the α lobes (α) and β/γ lobes (β/γ) of the MBs, in the ALs, in two nerves innervating the ALs (asterisks), and in two clubbed structures in the subesophageal ganglion (arrow heads). (C) GFP signals in single cells (arrows) in the cortex proximal of the medulla (M) with projections (asterisks) into the lobula complex (LC) of the optic lobe. (D) GFP signals in one photoreceptor cell (arrow) per ommatidium in the retina, 1-7 mark the single photoreceptor cells in one ommatidium (D'). (E) View from the posterior side to the supraesophageal ganglion with GFP signals in the calyx (C) of the MBs and in single surrounding cells with projections into the calyx (arrows). Scale bar = 50 µm, if not otherwise mentioned.

A GFP signal was also visible in the OLs (Fig. 28 C). GFP-positive axons in the entire OL but no cell bodies in the cortex of the medulla were seen. In the cortex between medulla and lobula complex, single cell bodies were detectable (Fig. 28 C, arrows), which had projections into the lobula complex (Fig. 28 C, asterisks). The retina was co-stained with anti-GFP antibody and anti-ELAV antibody to visualize PR neurons (Fig. 28 D). One single cell of each ommatidium was GFP-positive (Fig. 28 D, arrow). The detailed view of one ommatidium showed PRs R1-R6 (Fig. 28 D'). The GFP-positive cell was most likely the PR R7 due to its distal position.
The posterior view of the supraesophagial ganglion revealed distinct expression in the MBs. Kenyon cells and calyx were visible (Fig. 28 E).

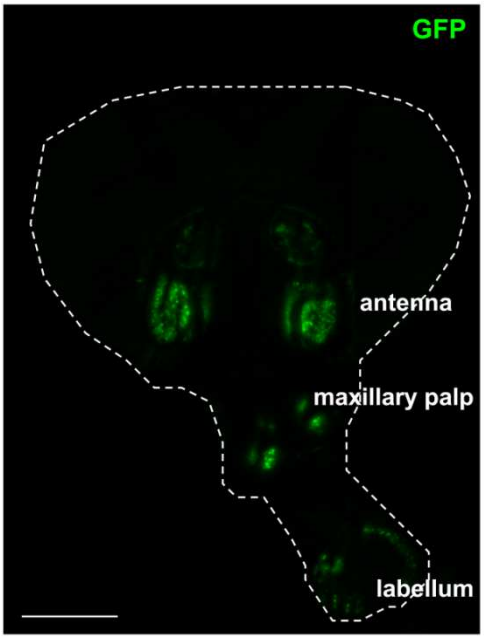

Fig. 29. *Keren* promoter activity in the adult antenna, maxillary palp, and labellum. *Gfp* expression indicating *keren* promoter activity was visualized in *prom-keren-gal4* > UAS-*gfp* adult heads using live imaging. Dashed lines represent the shape of the fly's head. Scale bar = 200 µm.

Furthermore, *gfp* was expressed in parts of the adult fly head (Fig. 29). A GFP signal was seen in two olfactory organs, the antennae and the maxillary palps, as well as in the main gustatory organ, the labellum. *Gfp* expression in these olfactory and gustatory organs supports the identification of the nerves that enter the SOG (Fig. 28 A and B) as ANs and labiomaxillary nerves, since these nerves have their dendrites in the antenna, maxillary palp, and in the labellum. They send their axons into the SOG and the ALs.

4.1.4 Spatial and Temporal Promoter Activity of *VEIN*

The gene coding for the secreted ligand Vein is represented by the symbol Dmel\vn (annotation symbol CG10491) and has the FlyBase ID FBgn0003984. Oligonucleotides targeting a region of 4,182 bp were used to amplify the presumptive promoter region upstream of the *vein* gene.

The proventriculus of *prom-vein-gal4* > UAS-*gfp* larvae showed *gfp* expressing structures in the inner part (Fig. 30 A). Expression was also detectable in some muscles of the larval body wall (Fig. 30 B). In particular, the four abdominal lateral transverse muscles of each segment displayed a strong GFP signal.

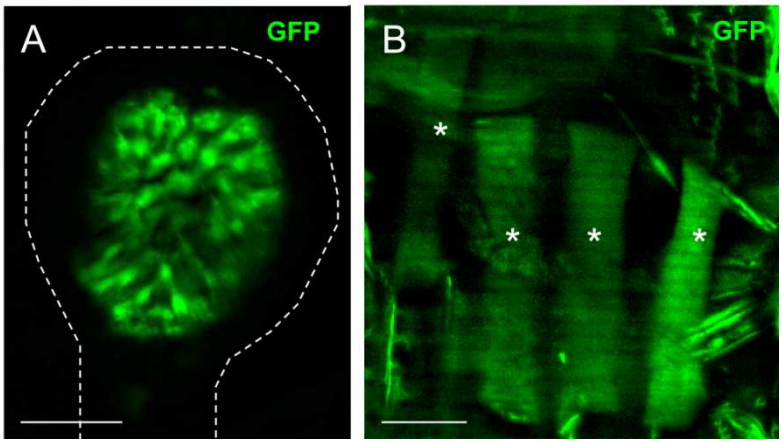

Fig. 30. *Vein* promoter activity in the proventriculus and parts of the body wall muscles of larvae. *Gfp* expression indicating *vein* promoter activity was visu-alized in *prom-vein-gal4* > UAS-*gfp* larvae using live imaging in (A) the inner part of the proventriculus and (B) the abdominal lateral transverse muscles of the larval body wall muscles (asterisks, lateral view, one segment shown). Dashed lines represent the shape of the proventriculus visible in the differential interference contrast picture. Scale bar = 50 µm.

Immunohistochemical co-staining of dissected larval midguts with anti-GFP antibody and anti-prospero antibody revealed that *gfp* was expressed in some EEs (Fig. 31, arrows). Another cell type of the gut, which showed a GFP signal, was not clearly identified (Fig. 31, arrow head) since no co-localization was seen with prospero staining. Due to shape and size, ECs were excluded.

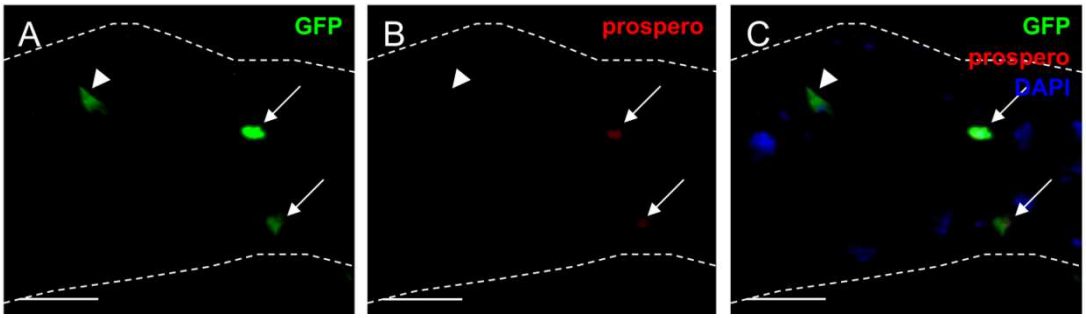

Fig. 31. *Vein* promoter activity in enteroendocrine cells of the larval midgut. Immunostaining of midguts of *prom-vein-gal4* > UAS-*gfp* larvae with (A) anti-GFP staining indicating promoter activity of *spitz* (green,) and (B) anti-prospero staining labeling enteroendocrine cells (red). (C) Merge of anti-GFP staining, anti-prospero staining, and DAPI staining labeling the nuclei. Dashed lines represent the shape of the gut visible in the differential interference contrast picture. Scale bar = 50 µm.

The larval CNS exhibited *gfp* expressing clusters of neurons in each BL (Fig. 32 A and B). The cell bodies, calyx, pedunculus, and medial and vertical lobes of the MBs could be seen (Fig. 32 B). In the VNC, expression was restricted to the thoracic region. A subset of lateral VNC cells with transverse projections was visible (Fig. 32 C, arrows). No *gfp* expression was detectable in the abdominal region of the VNC (Fig. 32 A).

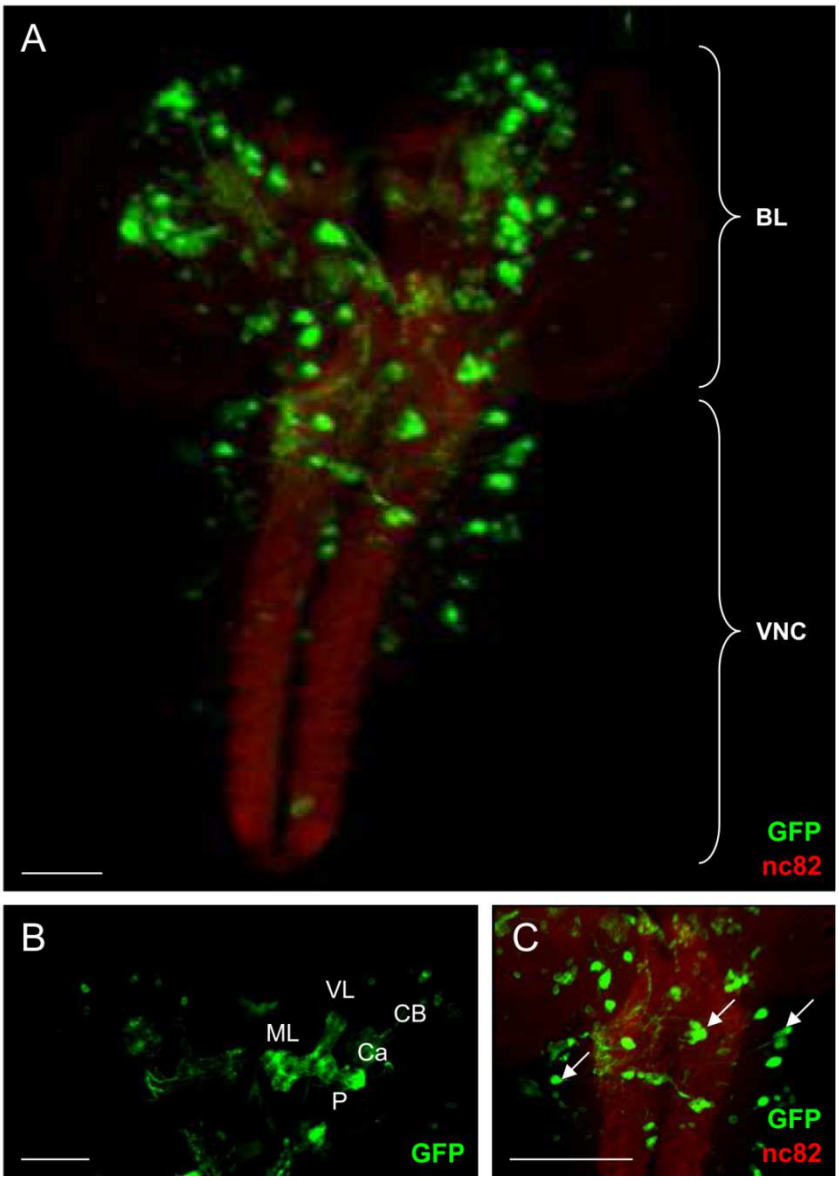

Fig. 32. *Vein* promoter activity in the larval brain. GFP signals indicating *vein* promoter activity were visualized in *prom-vein-gal4* > UAS-*gfp* larval brains using an immunohistochemical staining with anti-GFP antibody. Co-staining with anti-nc82 antibody (neuropil marker, red) was used as a reference for brain morpho-logy. (A) Overview. (B) Detailed view of the brain lobes (BL) with GFP-positive mush-room bodies. Cell bodies (CB), calyx (Ca), pedunculus (P), medial lobe (ML), and vertical lobe (VL) are visible. (C) Detailed view of the thoracic region of the ventral nerve cord (VNC) with GFP signals in lateral cells (arrows). Scale bar = 50 µm.

In the midguts of adult *prom-vein-gal4* > UAS-*gfp* flies, two different cell types revealed *vein* promoter activity in live imaging. Using immunohistochemistry, these cell types were identified as EEs and ECs (Fig. 33 and Fig. 34). An immunohistochemical double-staining using anti-GFP antibody and anti-prospero antibody showed that all small *gfp* expressing cells were EEs but not all EEs express

vein (Fig. 33). Thus, *vein* promoter activity was only observed in a subset of the EE population.

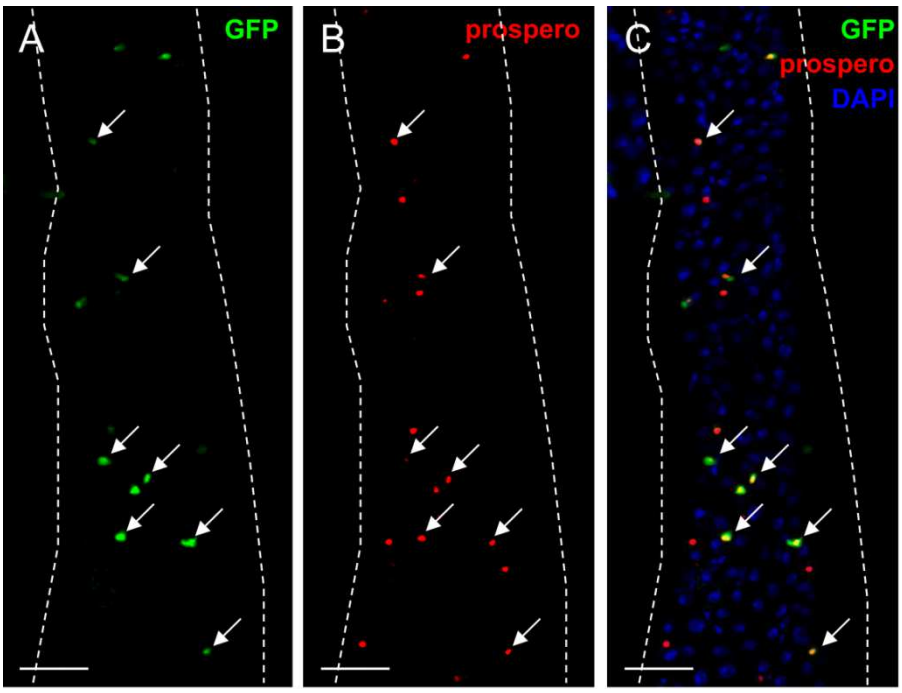

Fig. 33. *Vein* promoter activity in enteroendocrine cells of the adult midgut. Immunostaining of adult midguts of *prom-vein-gal4* > UAS-*gfp* flies with (A) anti-GFP staining indicating promoter activity of *vein* (green) and (B) anti-prospero staining labeling enteroendocrine cells (red). (C) Merge of anti-GFP staining, anti-prospero staining, and DAPI staining labeling the nuclei. Dashed lines represent the shape of the midgut visible in the differential interference contrast picture. Scale bar = 50 µm.

The other *gfp* expressing cells were identified as ECs, due to their shape and size of their nuclei and by excluding EEs or stem cells by an immunohistochemical double-staining with anti-GFP antibody and anti-prospero antibody (not shown) or anti-delta antibody (Fig. 34).

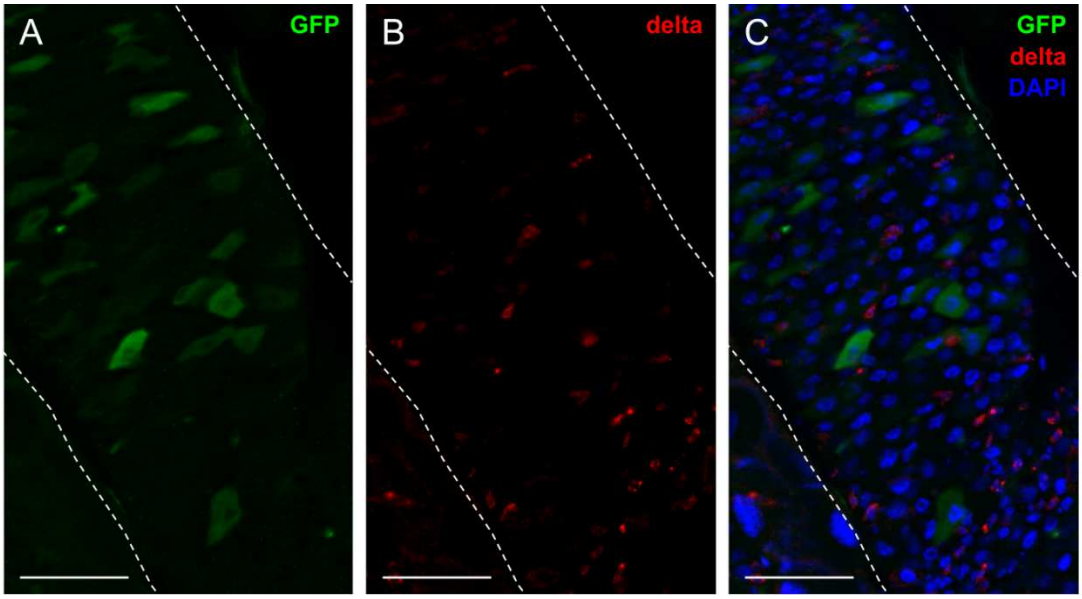

Fig. 34. *Vein* promoter activity in enterocytes of the adult midgut. Immunostaining of midguts of *prom-vein-gal4* > UAS-*gfp* flies with (A) anti-GFP staining indicating promoter activity of *vein* (green) and (B) anti-delta staining labeling stem cells (red). (C) Merge of anti-GFP staining, anti-delta staining, and DAPI staining labeling the nuclei. Dashed lines represent the shape of the gut visible in the differential interference contrast picture. Scale bar = 50 µm.

Strong *gfp* expression was detected in the secondary cells of the accessory glands of male flies by live imaging (Fig. 35).

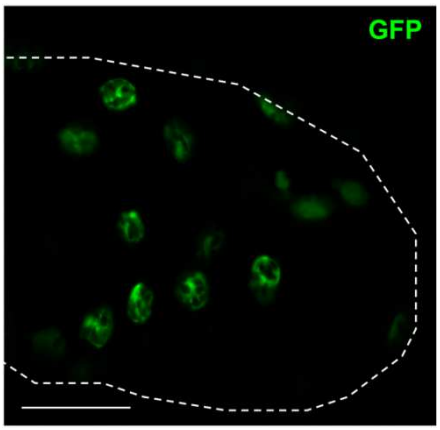

Fig. 35. *Vein* promoter activity in the secondary cells of the accessory gland. *Gfp* expression indicating *vein* promoter activity was visualized in *prom-vein-gal4* > UAS-*gfp* flies using live imaging in the male reproductive tract. Dashed lines represent the shape of the accessory gland visible in the differential interference contrast picture. Scale bar = 50 µm.

Brains of adult flies showed a complex *gfp* expression pattern. *Vein* promoter activity was visualized in the central brain region as well as in the OLs (Fig. 36 A). Large cells of the PI were seen that had axons along the midline (Fig. 36 A, asterisk).

Two structures that exit the SOG (Fig. 36 A) were identified as nerves by means of immunohistochemistry since they were surrounded by repo-positive glia cells (Fig. 36 E, arrows). These nerves may constitute the connection to the endocrine *glands corpora cardiaca* and *corpora allata*. It is also possible that these nerves are related to the olfactory or gustatory system and may have their dendrites in the antenna or proboscis. Furthermore, medulla columnar neurons showed *gfp* expression driven by *prom-vein-gal4* in the OL (Fig. 36 B). Their cell bodies were located distal to the medulla in the cortex of the OL (Fig. 36 B, arrows) and their axons reached through the entire OL, the neuropil of the medulla, and the lobula complex. Thus, these neurons were identified as Tm cells. The *gfp* expressing projections of the PR cells R7 and R8 end in the medulla (asterisks). Cells that indicate *vein* promoter activity were also present in the retinae of *prom-vein-gal4* > UAS-*gfp* flies (Fig. 36 D, arrows). Only one cell in the center of each ommatidium was GFP-positive. Based on the distal positions, this cell was most likely PR R7.

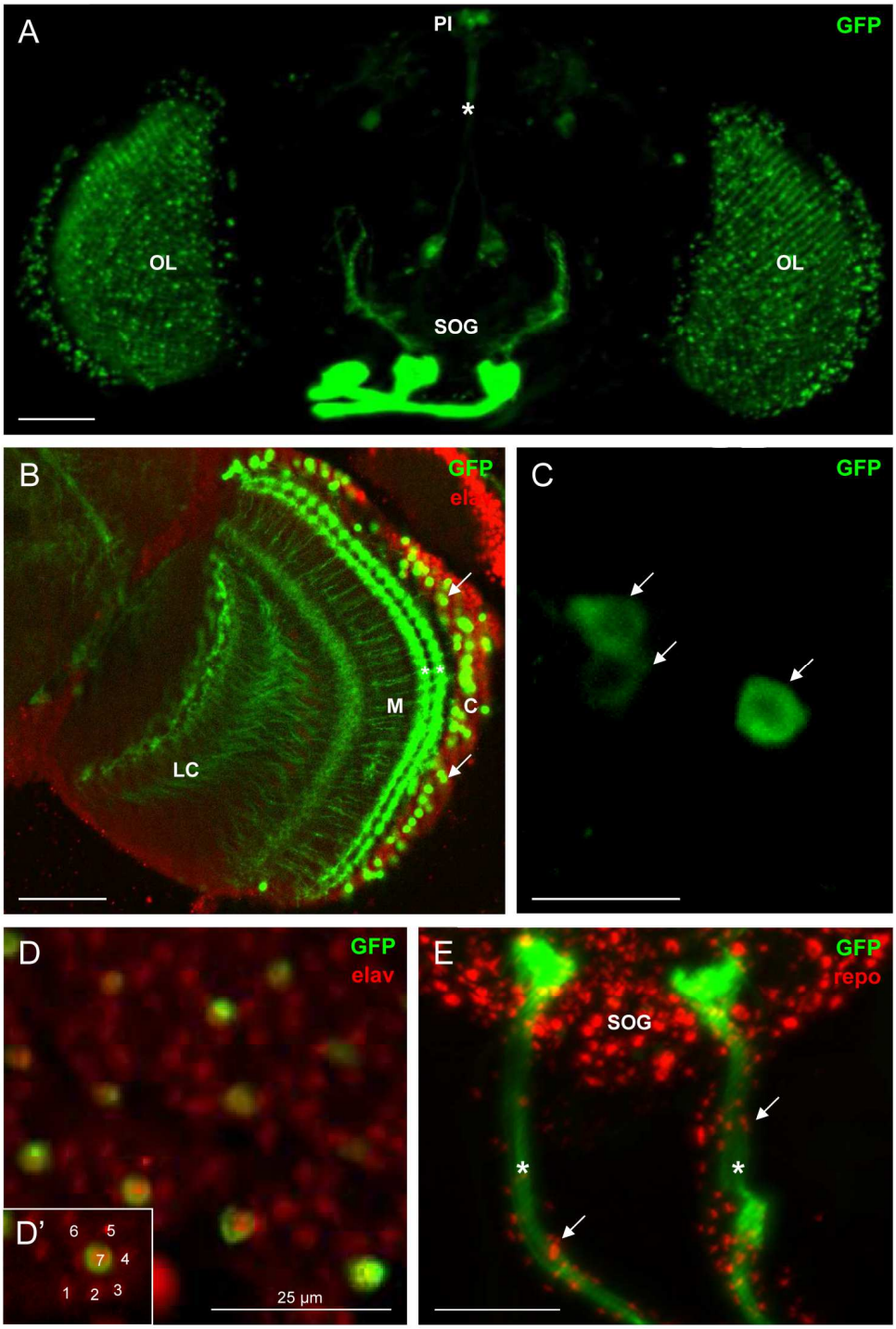

Fig. 36. *Vein* promoter activity in adult brains. GFP signals indicating *vein* promoter activity were visualized in *prom-vein-gal4* > UAS-*gfp* adult brains using an immunohistochemical staining with anti-GFP antibody (green). Co-stainings with anti-nc82 antibody (neuropil marker, red), anti-elav antibody (neuronal marker, red), or anti-repo antibody (glial marker, red) were used as references for brain morphology. (A) Overview with GFP signals in the optic lobes (OL), in the subesophageal ganglion (SOG), and in cells of the pars intercerebralis (PI) with axons along the midline (asterisk). (B) GFP signals in the lobula complex (LC), in the endings of the R7 and R8 photoreceptor cells (asterisks) in the medulla (M), and in cell bodies of the transmedullary neurons (arrows) in the cortex (C) of the OL. (C) GFP-positive cells of the PI (arrows). (D) GFP signals in the retina in one photoreceptor cell per ommatidium, 1-7 mark single photoreceptor cells in one ommatidium (D'). (E) GFP-positive nerves exiting the SOG (asterisks) surrounded by glia cells (arrows). Scale bar = 50 µm.

4.1.5 Spatial and Temporal Promoter Activity of *GURKEN*

The gene coding for the ligand Gurken is represented by the symbol Dmel\grk (annotation symbol CG17610) and has the FlyBase ID FBgn0001137. Oligonucleotides targeting a region of 2,946 bp were used to amplify the putative promoter region of the *gurken* gene.

In *prom-gurken-gal4* > UAS-*gfp* larvae, *gfp* was expressed in the body wall muscles of the head and the abdomen (Fig. 37). Abdominal dorsal oblique muscles (Fig. 37 B, asterisks) and abdominal dorsal acute muscles (Fig. 37 B, arrow heads) showed *gfp* expression in the dorsal view. The dorsolateral view also revealed *gfp* expression in the four abdominal lateral transverse muscle (Fig. 37 C, asterisks), two abdominal dorsal oblique muscle (Fig. 37 C, arrows), and the abdominal dorsal transverse muscle (Fig. 37 C, arrow head).

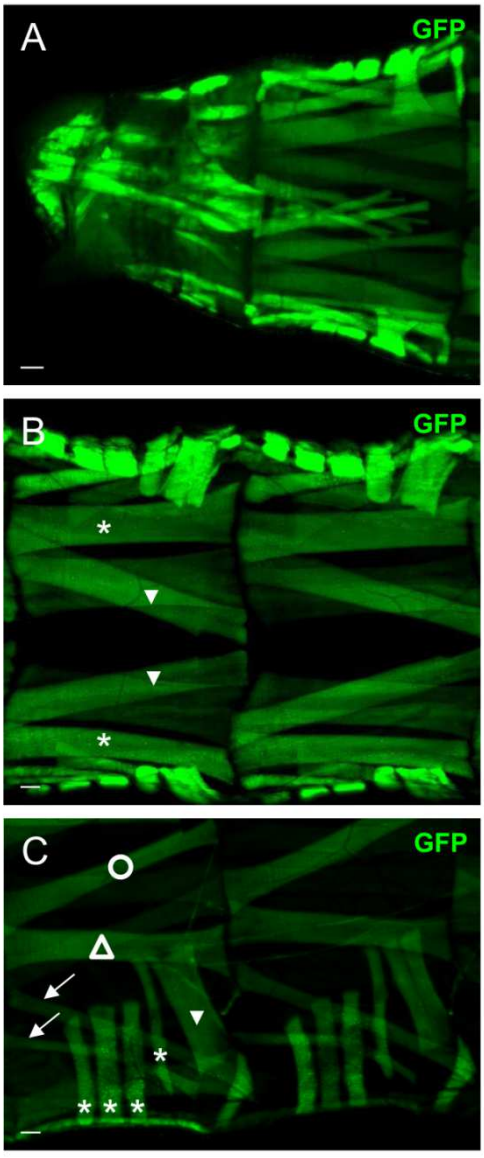

Fig. 37. *Gurken* promoter activity in larval body wall muscles. *Gfp* expression indicating *gurken* promoter activity was visualized in *prom-gurken-gal4* > UAS-*gfp* larvae using live imaging. (A) Dorsal view of the larval head region, (B) dorsal view of two segments of a larva with abdominal dorsal oblique muscles (asterisks) and abdominal dorsal acute muscles (arrow heads), and (C) dorsolateral view of two segments of a larva with GFP signals in four abdominal lateral transverse muscle (asterisks), in two abdominal dorsal oblique muscle (arrows), in the abdominal dorsal transverse muscle (arrow head), in the abdominal lateral longitudinal muscle (triangle), and the abdominal dorsal acute muscle (circle). Scale bar = 50 µm.

Moreover, *gurken* promoter activity was visualized in all substructures of the larval MBs (Fig. 38 B). In the thoracic region of the VNC, one single GFP signal was seen (Fig. 38 C, arrow).

Further *gfp* expression was neither detected in other larval tissues nor in adult flies of *prom-gurken-gal4* > UAS-*gfp* animals.

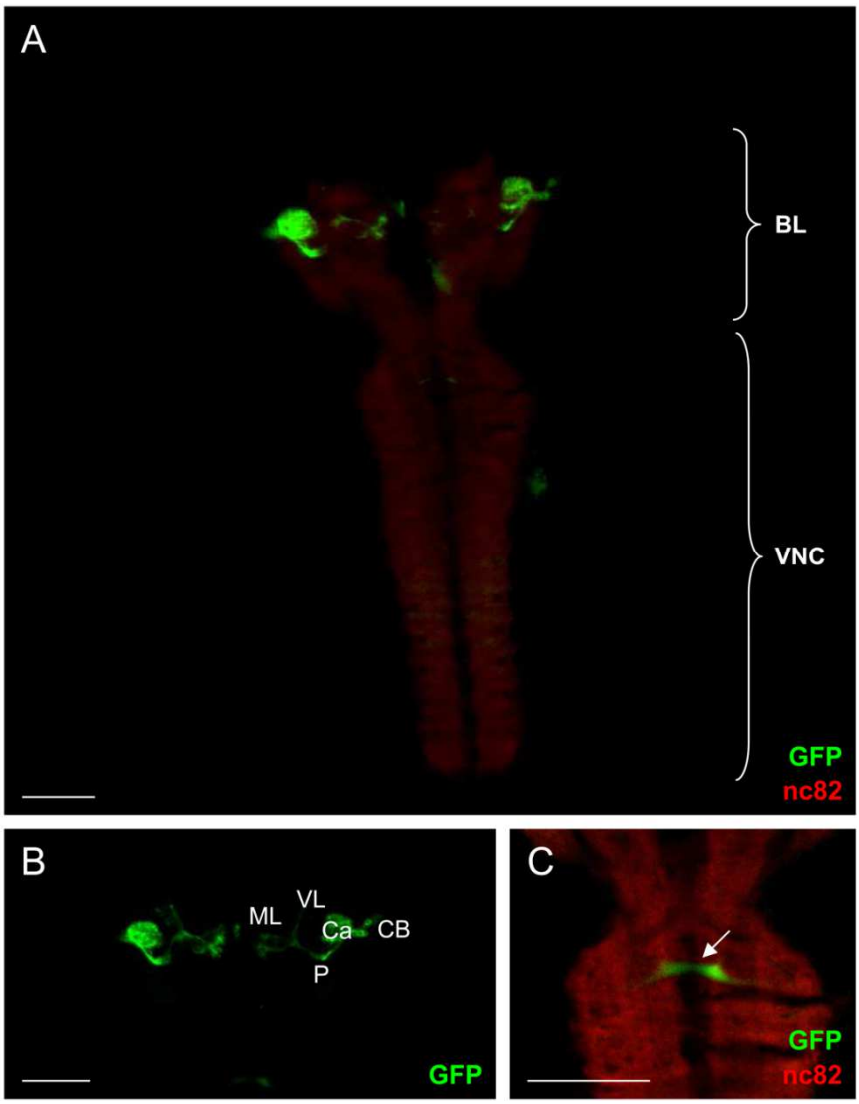

Fig. 38. *Gurken* promoter activity in the larval brain. GFP signals indicating *gurken* promoter activity were visualized in *prom-gurken-gal4* > UAS-*gfp* larval brain using an immunohistochemical staining with anti-GFP antibody. Co-staining with anti-nc82 antibody (neuropil marker, red) was used as a reference for brain morphology. (A) Overview. (B) Detailed view of brain lobes (BL) with GFP-positive mushroom bodies. Cell bodies (CB), the calyx (Ca), the pedunculus (P), the medial lobe (ML), and vertical lobes (VL) were visible. (C) Detailed view of the thoracic region of the ventral nerve cord (VNC) with a GFP signal in one distinct region (arrow). Scale bar = 50 µm.

4.1.6 Spatial and Temporal Promoter Activity of *argos*

The gene coding for the inhibitory ligand Argos is represented by the symbol Dmel\argos (annotation symbol CG4531) and has the FlyBase ID FBgn0004569. Oligonucleotides targeting a region of 4,150 bp were used to amplify the presumptive promoter region of the *argos* gene.

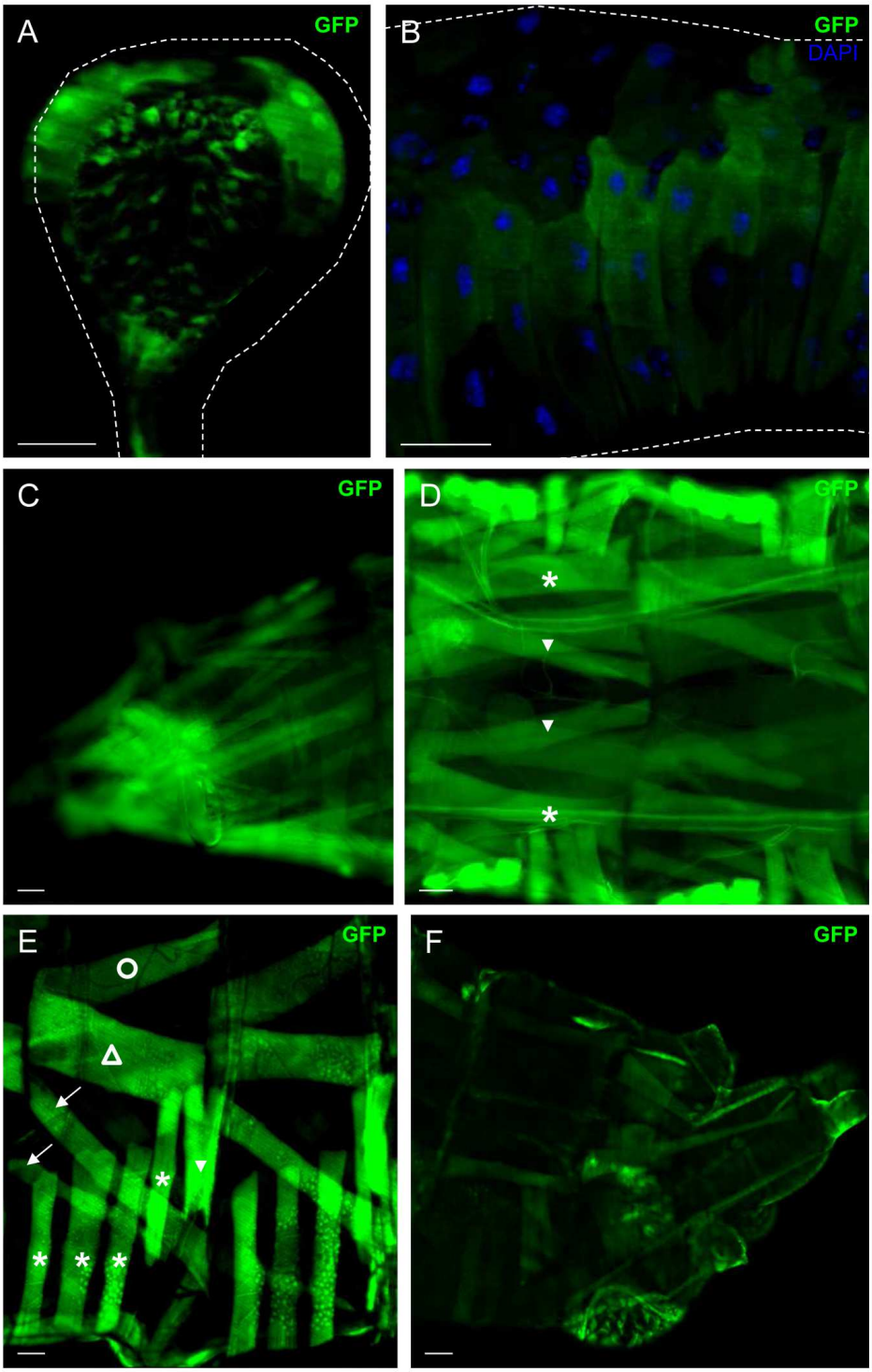

Fig. 39. *Argos* promoter activity in larvae. *Gfp* expression indicating *argos* promoter activity was visualized in *prom-argos-gal4* > UAS-*gfp* larvae using live imaging in (A) the proventriculus, (B) enterocytes in the midgut, and (C–F) body wall muscles. (C) Lateral view of the larval head region, (D) dorsal view of two segments with GFP signals in the abdominal dorsal oblique muscles (asterisks) and in the abdominal dorsal acute muscles (arrow heads). (E) Lateral view of two segments with GFP signals in the abdominal lateral transverse muscles (asterisks), in the abdominal dorsal oblique muscles (arrows), in the abdominal dorsal transverse muscle (arrow head), in the abdominal lateral longitudinal muscle (triangle), and in the abdominal dorsal acute muscle (circle). (F) Lateral view of the larval tail region with GFP signals in the muscles. Dashed lines represent the shape of the proventriculus or the midgut visible in the differential interference contrast picture. DAPI was used to stain the nuclei. Scale bar = 50 µm.

In larvae, *prom-argos-gal4* drove *gfp* expression in substructures of the inner and outer proventriculus including the connection to the midgut (Fig. 39 A). In the midgut, expression of *gfp* was detectable in large cells, which were identified as ECs due to cell shape and size of the nuclei (Fig. 39 B). *Argos* promoter activity was also observed in the body wall muscles of *prom-argos-gal4* > UAS-*gfp* larvae (Fig. 39 C-F). *Gfp* was expressed in muscles of the head, the abdomen, and the tail. Abdominal dorsal oblique and abdominal dorsal acute muscles expressed *gfp* (Fig. 39 D). Additionally, the lateral view revealed *gfp* expression in the four abdominal lateral transverse muscles, the abdominal dorsal transverse muscle, the two abdominal dorsal oblique muscles, the abdominal lateral longitudinal muscle, and the abdominal dorsal acute muscle (Fig. 39 E).

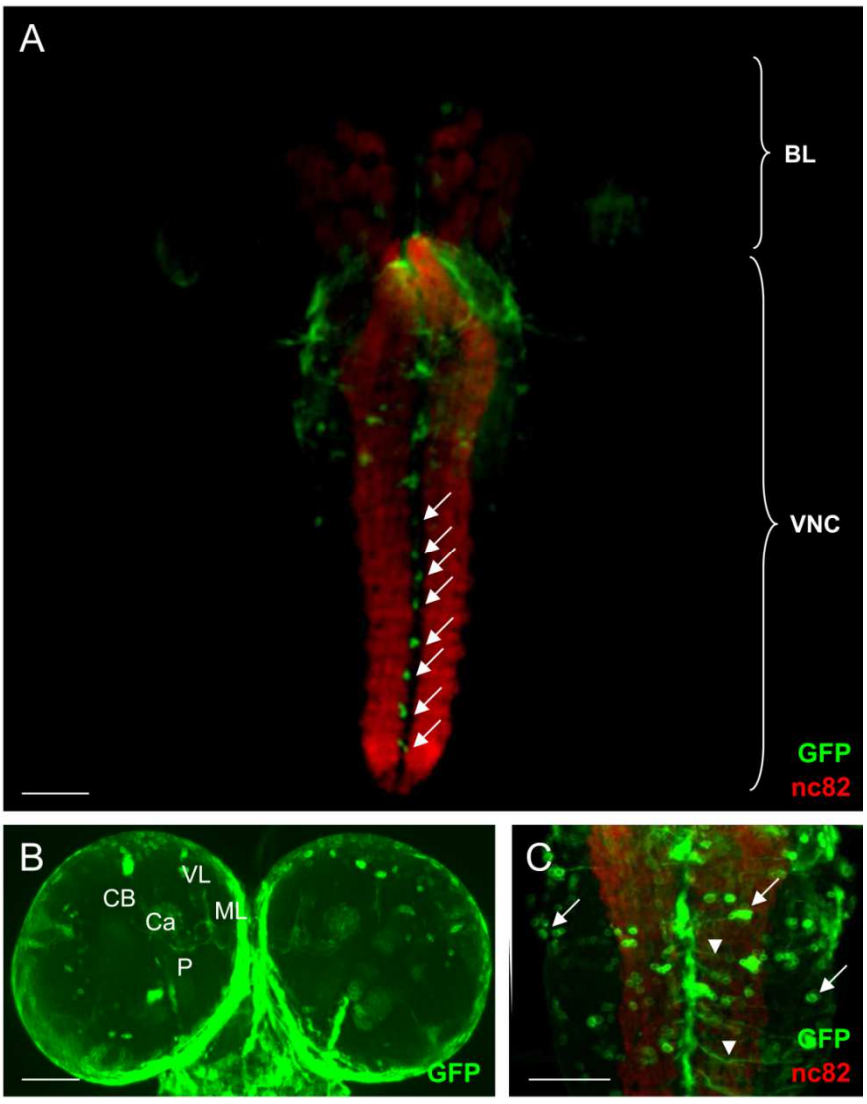

Fig. 40. *Argos* promoter activity in the larval brain. GFP signals indicating *argos* promoter activity were visualized in *prom-argos-gal4* > UAS-*gfp* larval brains using an immunohisto-chemical staining with anti-GFP antibody. Co-staining with anti-nc82 antibody (neuropil marker, red) was used as a reference for brain morphology (A) Overview with strong GFP signals in one cell per hemisegment of the ventral nerve cord (VNC; arrows). (B) Detailed view of the brain lobes (BL) with GFP-positive mushroom bodies. Cell bodies (CB), the calyx (Ca), the pedunculus (P), the medial lobe (ML), and vertical lobe (VL) were visible. (C) Detailed view of the thoracic region of the VNC with GFP signals in cell bodies of interneurons (arrows) with projections to the midline (arrow heads). Scale bar = 50 µm.

Furthermore, *argos* promoter activity was visualized in the brains of *prom-argos-gal4* > UAS-*gfp* larvae (Fig. 40). Single cells in the hemispheres of the larval BLs, in MBs, and parts of the VNC revealed *argos* promoter activity (Fig. 40). *Gfp* expression in the MBs was comparatively weak but all substructures could be identified (Fig. 40 B). The GFP signal surrounding the brain lobes (Fig. 40 B) points to an expression in glial cells. Along the midline of the VNC, one strong *gfp* expressing cell was observed in each hemisegment (Fig. 40 A, arrows). The staining correlates with the position of the neurohemal organs or midline glia cells that are localized in the middle of the VNC dorsal of the neuropils. In the thoracic part of the VNC, cell bodies of interneurons with projections to the midline were found (Fig. 40 C, arrows). No cell bodies around the neuropil were detectable in the abdominal part of the VNC.

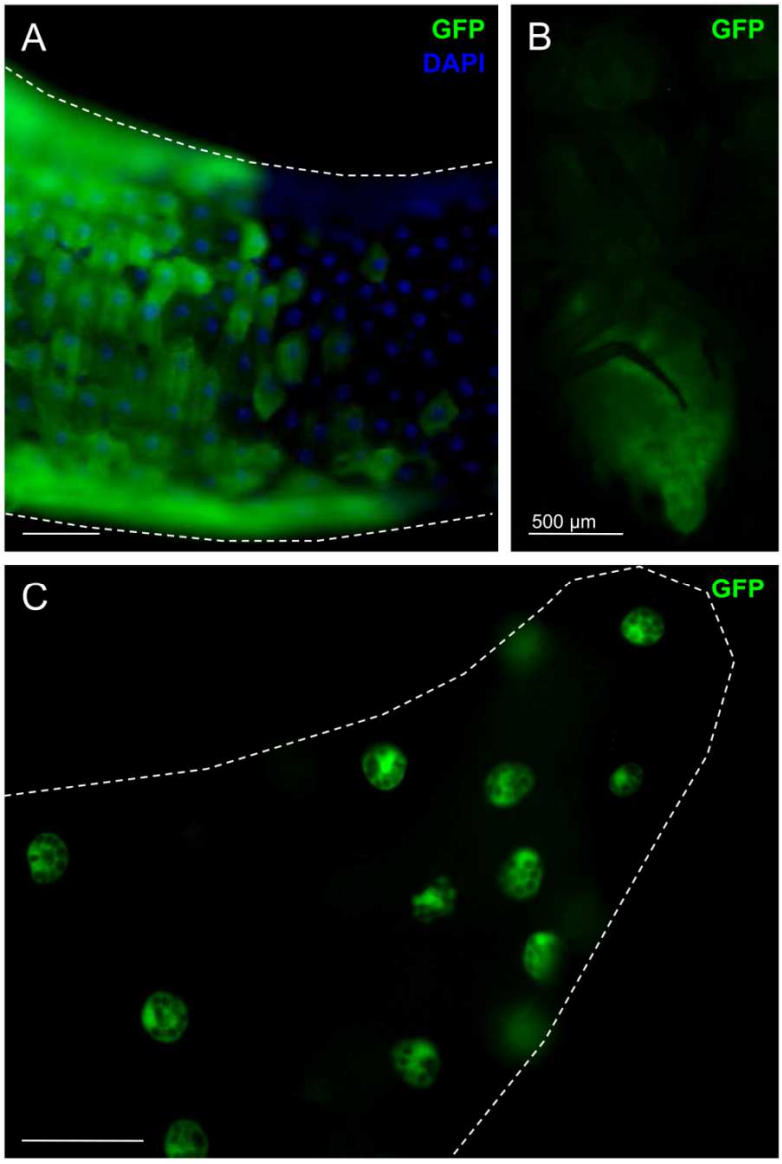

Fig. 41. *Argos* promoter activity in adult flies. *Gfp* expression indicating *argos* promoter activity was visualized in *prom-argos-gal4* > UAS-*gfp* flies using live imaging in (A) enterocytes of the midgut, (B) the abdominal fat body (ventral view on whole fly), and (C) the secondary cells of the accessory gland. Dashed lines represent the shape of the midgut or the accessory gland visible in the differential interference contrast picture. DAPI was used to stain the nuclei. Scale bar = 50 µm, if not otherwise mentioned.

In adult *prom-argos-gal4* > UAS-*gfp* flies, two different cell types in the midgut showed *gfp* expression. The large cells were identified as ECs due to cell shape and size as well as size of the nuclei (Fig. 41 A). A weak expression was detectable in the fat body of the abdomen but not in the fat body of the head (Fig. 41 B). Furthermore, the secondary cells of the accessory gland displayed a distinct GFP signal (Fig. 41 C).

The other *gfp* expressing cell type in the adult midgut was identified using an immunohistochemical double-staining with anti-GFP antibody and anti-delta antibody (Fig. 42). The staining of anti-delta co-localized with GFP-positive cells in *prom-argos-gal4* > UAS-*gfp* flies (Fig. 42 C-C'').

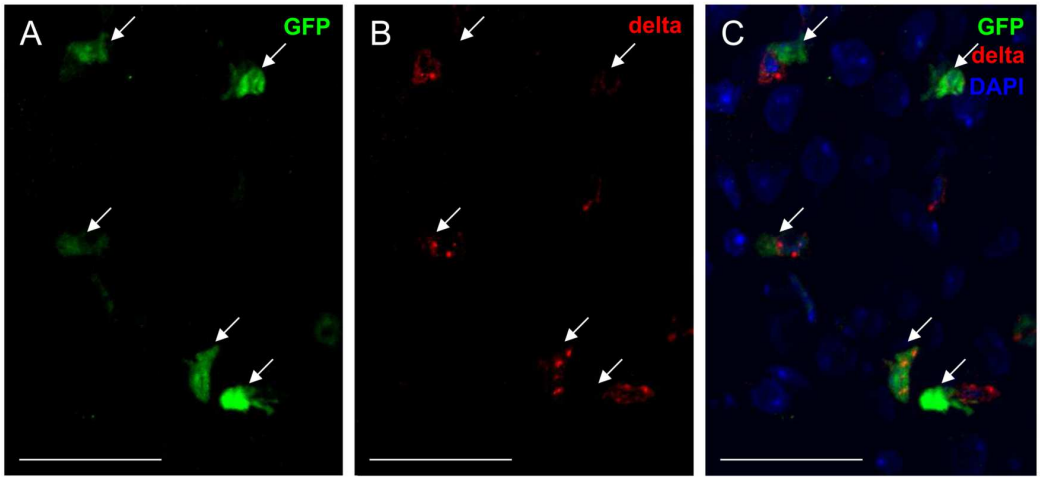

Fig. 42. ***Argos*** **promoter activity in intestinal stem cells.** Immunostaining of midguts of *prom-argos-gal4* > UAS-*gfp* flies with (A) anti-GFP staining indicating promoter activity of *argos* (green) and (B) anti-delta staining labeling stem cells (red). (C) Merge of anti-GFP staining, anti-delta staining, and DAPI staining labeling the nuclei. Scale bar = 50 µm.

4.2 Expression Analysis of EGFR Pathway Components

4.2.1 Expression Analysis of EGFR Pathway Component Genes in Larval and Adult Tissues

The expression of EGFR pathway component genes was analyzed in several tissues of larvae and adult flies. RT-PCR analyses with RNA isolated from larval guts, larval fat bodies, larval tracheae, larval Malpighian tubules, larval body walls, adult guts, adult fat bodies, adult Malpighian tubules, male or female reproductive tracts were performed (Fig. 43).

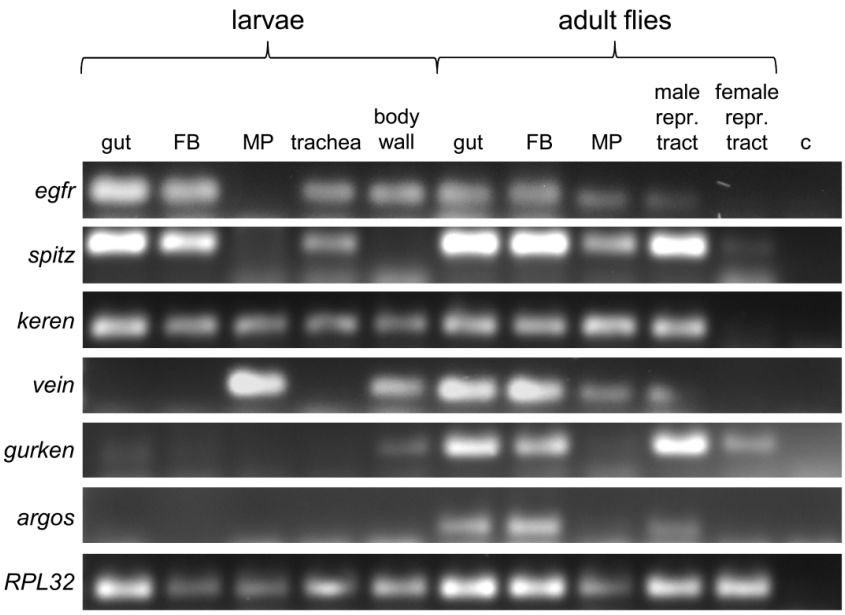

Fig. 43. EGFR pathway component gene ex-pression in larval and adult tissues. RT-PCR analysis with RNA isolated from guts, fat bodies (FBs), Malpighian tubules (MP), tracheae, or body walls of wild-type larvae as well as guts, fat bodies, Malpighian tubules, male or female reproductive tracts (male or female repr. tract) of wild-type adult flies. C, no template control; RPL32, house keeping gene (served as loading control).

Egfr transcript was found in all tissues with the exception of larval Malpighian tubules and female reproductive tracts (Fig. 43). Likewise, *spitz* was expressed in the majority of tissues but not in the larval body wall and larval Malpighian tubules (Fig. 43). Expression of *vein* was not detected in the larval gut, fat body, and tracheae, as well as in the female reproductive tract but in all other tissues (Fig. 43). *Keren* transcript was present in all samples with the exception of the female reproductive tract (Fig. 43). *Gurken* expression was limited to the larval body wall, adult gut, adult fat body, as well as male and female reproductive tracts (Fig. 43). *Argos* showed expression in the same tissues as *gurken* but not in the larval body wall and the female reproductive tract (Fig. 43).

4.2.2 EGFR Pathway Component Gene Expression in Larval and Adult Brains

EGFR pathway component gene expression was investigated in larval and adult brains as well as in retinae by RT-PCR analyses. In larval brains, expression of all EGFR pathway components was detectable in the BLs and the VNC with the exception of *egfr* that was only detectable in the BLs (Fig. 44).

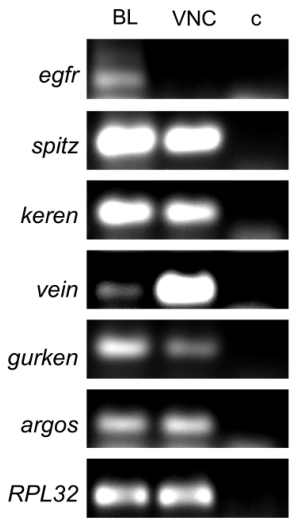

Fig. 44. EGFR pathway component gene expression in the larval brain. BL, brain lobes; VNC, ventral nerve cord; c, no template control.

In adult flies, all EGFR pathway component genes were found in the central brain region and in the retina (Fig. 45). In the OLs, only transcripts of *spitz* and *keren* were present.

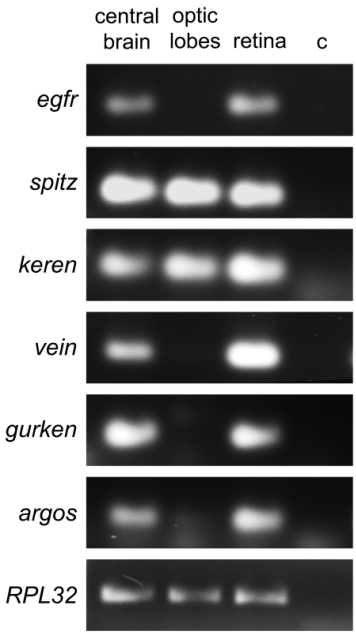

Fig. 45. EGFR pathway component gene expression in the adult brain and retina. C, no template control.

4.3 Olfactory Learning in Larvae

A predominant expression of *egfr* and the ligand genes was observed in the larval MBs that are known as centers for olfactory learning and memory. Thus, classical conditioning assays (Fig. 46 C) were performed to test the learning ability of larvae with impaired or enhanced EGFR signaling. To exclude general defects in the ability to taste or smell, experimentally naive, untrained larvae were compared in terms of their responses to the to-be-associated stimuli.

4.3.1 Impaired Olfactory Learning in Larvae Constitutively Expressing a Dominant-Negative EGFR

Olfactory learning ability was investigated in larvae constitutively and pan-neuronally expressing a gene coding for a dominant-negative form of EGFR (nsyb-*gal4* > UAS-$egfr^{DN}$) as well as in matching control animals (nsyb-*gal4* > w^{1118}) using an *en mass* olfactory learning assay. Larvae expressing $egfr^{DN}$ display a significantly lower learning index compared to controls (Fig. 46 A; $P = 0.0022$, $n_{\text{learning indices}} = 6$; $n_{\text{larvae}} > 170$). The median learning index of the experimental group (approximately 0.2) was reduced to 67% of that of the control group (approximately 0.3).

To exclude non-independent confounding interactions between individuals, larvae were also tested individually using an individual-animal version of the learning assay. In this assay, larvae expressing $egfr^{DN}$ also had a significantly reduced learning capability than control larvae (Fig. 46 B, $P < 0.0001$, $n_{\text{learning indices}} = 64$ each). The median learning index of the control larvae, approximately 0.4, clearly indicated olfactory learning, whereas the median learning index of larvae expressing $egfr^{DN}$ was reduced to approximately 0.

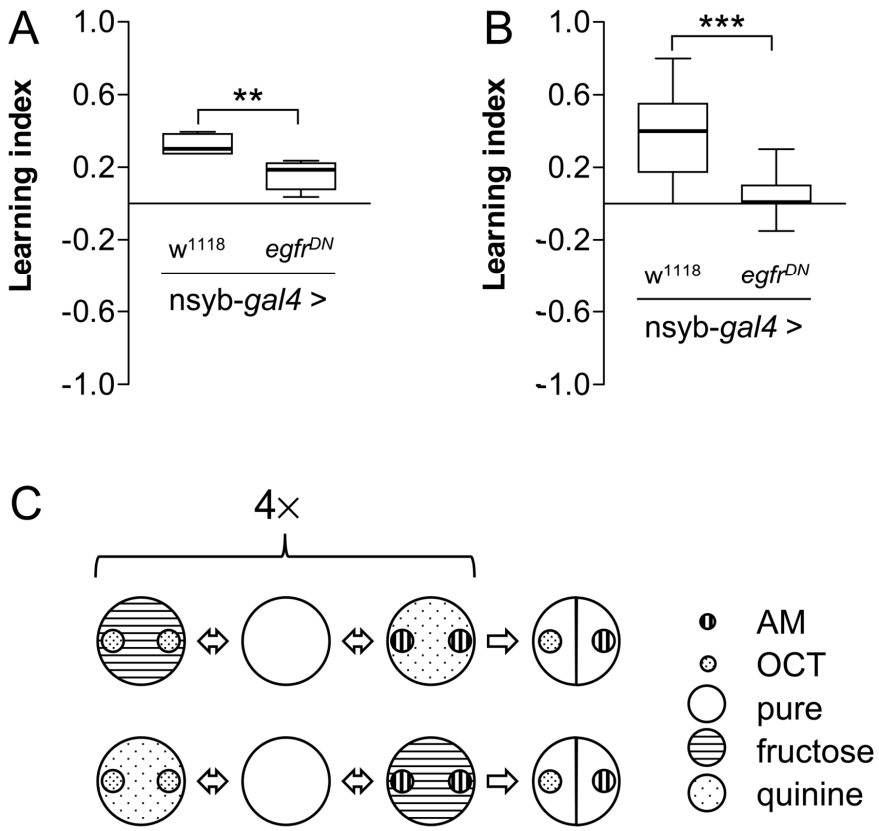

Fig. 46. Constitutive and pan-neuronal *egfr^{DN}* expression impaired larval learning. F_1 third instar control larvae (nsyb-*gal4* > w^{1118}) were compared with those with impaired pan-neuronal EGFR signaling (nsyb-*gal4* > UAS-*egfr^{DN}*) in an (A) en mass assay ($n_{learning\ indices}$ = 6 each; n_{larvae} > 170 each) and (B) in the individual-animal assay ($n_{learning\ indices}$ = 64 each). (C) Scheme of the olfactory learning assay. In the *en mass* assay groups of about 15 larvae were trained and tested together. After 3 min in an odor-choice situation between AM and OCT, the number of larvae on the different odor sides was counted. In the first training, OCT was paired with fructose, whereas AM was paired with quinine (upper row). For the second training, the tastes were swapped (lower row). In the individual-animal test groups of eight larvae were trained together but tested individually to exclude non-independent behavior. In the test situation, the position of the larvae was recorded every 30 sec for a period of 5 min. AM, amyl acetate; OCT, 1-octanol; **: $P < 0.01$, ***; $P < 0.00025$.

4.3.2 Constitutive and Pan-neuronal Expression of *EGFR^{DN}* Does Not Impair Taste or Smell

Olfactory learning deficits may result from general defects in the ability to taste or smell. To exclude this possibility, naive, untrained larvae were used to test their response to gustatory stimuli and to different odors.

The gustatory capability of larvae constitutively and pan-neuronally expressing *egfr^{DN}* and control larvae was investigated by offering fructose (attractive taste) or quinine (repellent taste) tested versus pure agarose (Fig. 47 C). Both, larvae constitutively and pan-neuronally expressing *egfr^{DN}* and control larvae showed significant preferences for fructose over pure agarose (Fig. 47 A) and for pure agarose over quinine (Fig. 47 B). Strikingly, no differences in the preferences were detected

between these groups of larvae (Fig. 47 A, fructose vs. pure: $P = 0.6450$; $n_{Pref} \geq 20$ and Fig. 47 B, quinine vs. pure: $P = 0.1026$; $n_{Pref} \geq 19$).

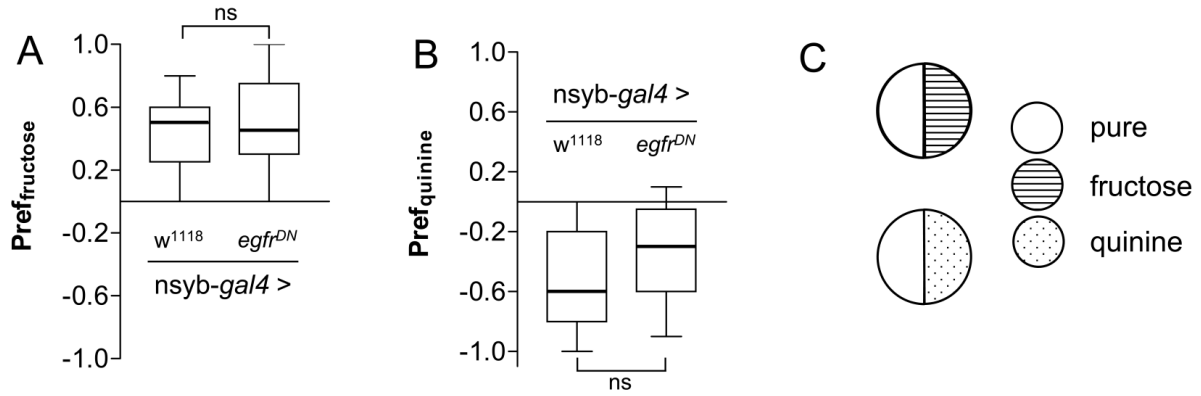

Fig. 47. Constitutive and pan-neuronal *egfr^{DN}* expression did not induce gustatory impairment. Control larvae (nsyb-gal4 > w1118) and those constitutively and pan-neuronally expressing *egfr^{DN}* (nsyb-*gal4* > UAS-*egfr^{DN}*) showed the same appetitive response to (A) fructose ($n_{Pref} \geq 20$ each) and aversive response to (B) quinine ($n_{Pref} \geq 19$). (C) Scheme of the gustatory test. The preference for the flavored side was tested by creating a pure agarose versus flavor choice situation. Ten larvae were placed in the middle of a Petri dish filled with pure agarose on one side and agarose containing a flavor (fructose or quinine) on the other side. The position of the larvae was noted after 15 min, and the preference (Pref) for the flavor was calculated by subtracting the number of larvae on the pure side from the number of larvae on the flavored side and dividing the difference by the total number of larvae. Ns, not significant ($P > 0.05$).

To test the olfactory abilities of larvae expressing *egfr^{DN}* and control larvae, an odor (banana) versus no-odor setup was applied (Fig. 48 B). Both groups showed significant attraction by this odor (Fig. 48 A). Importantly, the two genotypes did not reveal any significant difference regarding the preference for the odor of banana (Fig. 48 A, $P = 0.4022$; $n_{Pref} = 50$ each).

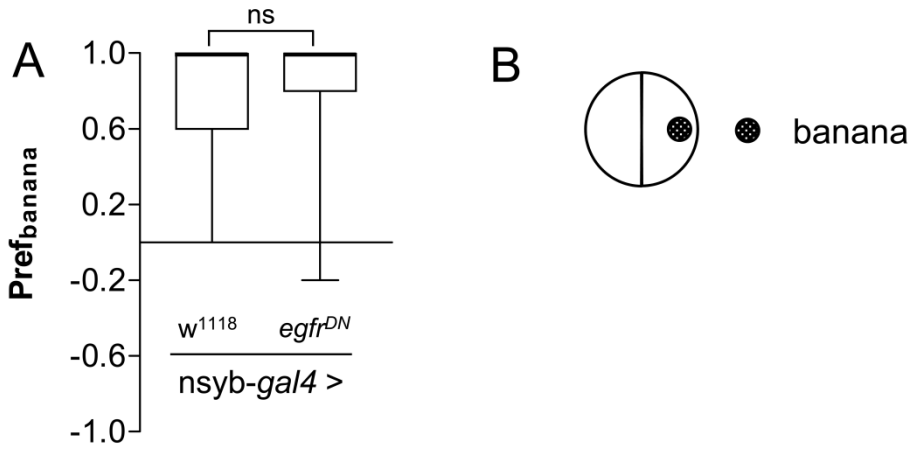

Fig. 48. Constitutive and pan-neuronal expression of *egfr^{DN}* did not cause olfactory impairment: banana. (A) Control larvae (nsyb-*gal4* > w^{1118} and those constitutively and pan-neuronally expressing *egfr^{DN}* (nsyb-*gal4* > UAS-*egfr^{DN}*) did not demonstrate any difference in their response to the attractive odor of smashed banana (n_{Pref} = 50 each). (B) Odor sensing of banana. The preference (Pref) for an attractive odor was tested by placing a single larva in the middle of a Petri dish filled with pure agarose. Smashed banana was placed on one side of the plate, whereas the other side was empty. The position of the larvae was noted every 30 sec for a period of 5 min as “banana” or “empty”. The preference for the banana side was calculated by subtracting the number of counts on the empty side from the counts on the banana side and dividing the difference by the total number of counts. Ns, not significant ($P > 0.05$).

To test the abilities of larvae expressing *egfr*^{DN} and control larvae in detecting the odors used in the olfactory learning experiment (AM and OCT), these odors were also presented in an odor versus no-odor setup (Fig. 49 C). Both groups showed no significant difference in the attraction by the odors (Fig. 49 A, AM: P = 0.8821; n_{Pref} = 50 and Fig. 49 B, OCT: P = 0.5978; n_{Pref} = 50).

Thus, I could show that the *egfr*^{DN} expressing larvae are neither impaired in smelling nor in tasting. Accordingly, the decreased learning ability of larvae constitutively and pan-neuronally expressing *egfr*^{DN} can be attributed to a genuine learning defect.

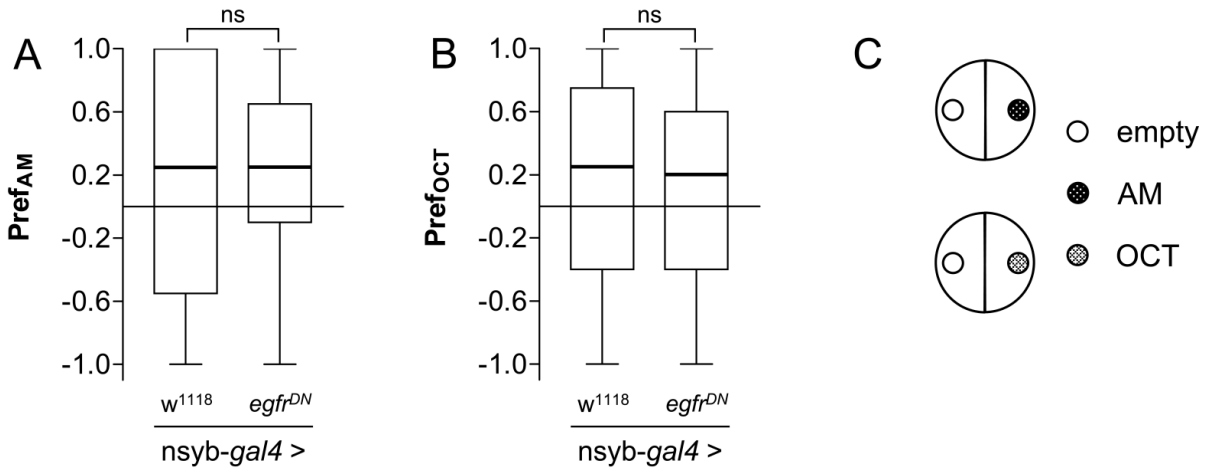

Fig. 49. Constitutive and pan-neuronal expression of *egfr*^{DN} did not cause olfactory impairment: AM and OCT. Control larvae (nsyb-*gal4* > w^{1118}) and those constitutively and pan-neuronally expressing EGFR^{DN} (nsyb-*gal4* > UAS-*egfr*^{DN}) did not demonstrate any difference in their response to the odor of (A) AM (n_{Pref} = 50 each) or (B) OCT (n_{Pref} = 50 each). (C) Odor sensing of AM or OCT. The preferences (Pref) for the odors were tested by placing a single larva in the middle of a Petri dish filled with pure agarose. AM or OCT was presented in a bin on one side of the plate, whereas an empty bin was placed on the other side. The position of the larvae was noted every 30 sec for a period of 5 min as "AM", „OCT", or "empty". The preference for the odor side was calculated by subtracting the number of counts on the empty side from the counts on the odor side and dividing the difference by the total number of counts. AM, amyl acetate;.ns, not significant (P > 0.05); OCT, 1-octanol.

4.3.3 Pan-neuronal Induction of EGFR^{DN} for 24 h during Late Larval Stages Impaired Olfactory Learning

To exclude developmental effects, we used the mifepristone-inducible pan-neuronal elav-GeneSwitch line (elav-GS) to reduce EGFR signaling for 24 h during late larval stages. Larvae treated with mifepristone and control larvae were tested in the individual-animal assay. Notably, the short induction of *egfr*^{DN} expression led to a significantly reduced olfactory learning ability (Fig. 50 A, P < 0.0001; $n_{learning\ indices}$ = 64 each). The control clearly showed olfactory learning with a median of the learning index of approximately 0.4, whereas that of the treated larvae was reduced to 0.

The effect of the mifepristone feeding for 24 h on learning skills was analyzed in control larvae (elav-GS > w^{1118}). No significant difference in the olfactory learning capability was detectable in larvae fed with mifepristone-containing food medium or with the corresponding control food medium (Fig. 50 B, $P = 0.2737$; $n_{learning\ indices} = 64$ each).

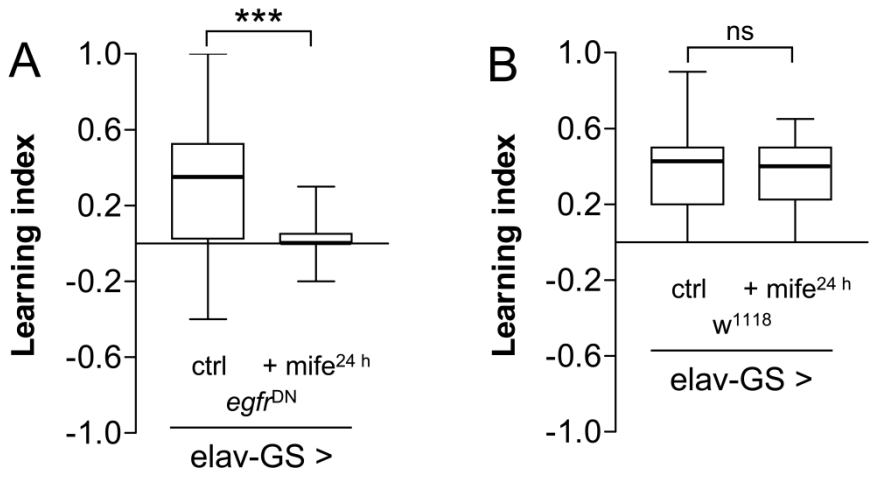

Fig. 50. After 24 h of pan-neuronal EGFR^{DN} expression, olfactory learning is significantly impaired. (A) After pan-neuronal *egfr*^{DN} expression for 24 h, olfactory learning ability was significantly reduced in the individual-animal assay ($n_{learning\ indices} = 64$ each). (B) Feeding the respective mifepristone-containing food to control larvae (elav-GS > w^{1118}) did not impair the olfactory learning capability ($n_{learning\ indices} = 64$ each). Ctrl, control; GS, GeneSwitch; mife, mifepristone; ns, not significant ($P > 0.05$); ***, $P < 0.001$.

4.3.4 Single EGFR Ligands are Necessary for Olfactory Learning

As not only expression of the *egfr* but also of its activating ligands was detected in MBs of the larval brain, we investigated the influence of these upstream components on olfactory learning. For this purpose, the individual-animal assay was performed using larvae with constitutive and pan-neuronal expression of *spitz*^{RNAi}, *keren*^{RNAi}, or *vein*^{RNAi}. All three genotypes showed strongly impaired olfactory learning compared to the nsyb-*gal4* > w^{1118} control (Fig. 51, *spitz*^{RNAi}: $P < 0.0001$; *keren*^{RNAi}: $P < 0.0001$; *vein*^{RNAi}: $P < 0.0001$; $n_{learning\ indices} = 64$ each).

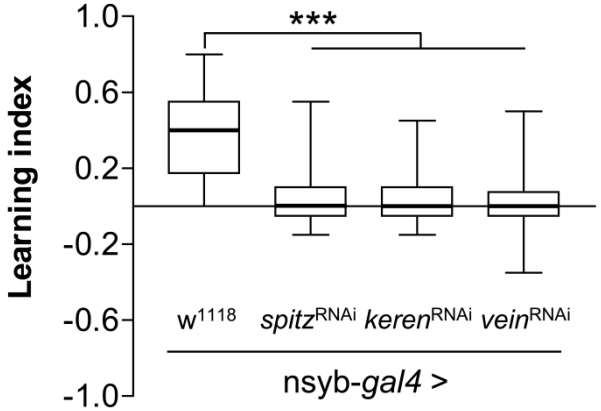

Fig. 51. Constitutive and pan-neuronal RNAi-mediated silencing of a single EGFR ligand gene significantly impaired olfactory learning ability. In the individual-animal test, olfactory learning ability was clearly decreased in larvae constitutively and pan-neuronally expressing *spitz*^{RNAi}, *keren*^{RNAi}, or *vein*^{RNAi} (nsyb-*gal4* > ligand^{RNAi}), if compared to the control (nsyb-*gal4* > w^{1118}; $n_{learning\ indices} = 64$ each). ***, $P < 0.00025$.

The median learning index of each of the genotypes was 0, whereas the median learning index of the control was 0.4.

In addition, the mifepristone-inducible elav-GS system was applied for RNAi-mediated gene silencing. In contrast to the induction of *egfr*^{DN} expression, which was performed for only 24 h, the expression of ligand^{RNAi} started right after hatching until experiments were performed with third instar larvae.

Comparing the ligand^{RNAi} induced animals and the uninduced controls in the individual-animal assay again revealed a significant difference in olfactory learning. RNAi directed against each of the three ligands led to impaired memory formation (Fig. 52, *spitz*^{RNAi}: $P < 0.0001$; *keren*^{RNAi}: $P < 0.0001$; *vein*^{RNAi}: $P < 0.0001$; $n_{\text{learning indices}} = 64$ each). Uninduced control larvae of all three ligand^{RNAi} experiments had a median learning index of approximately 0.4 and, thus, were clearly capable of olfactory learning. The induced ligand^{RNAi} larvae (*spitz*^{RNAi}, *keren*^{RNAi}, and *vein*^{RNAi}) were apparently affected in their ability to learn, exhibiting a median learning index of 0. These experiments clearly demonstrate that silencing of a single EGFR ligand gene during postembryonic stages is sufficient to reduce learning ability of *Drosophila* larvae.

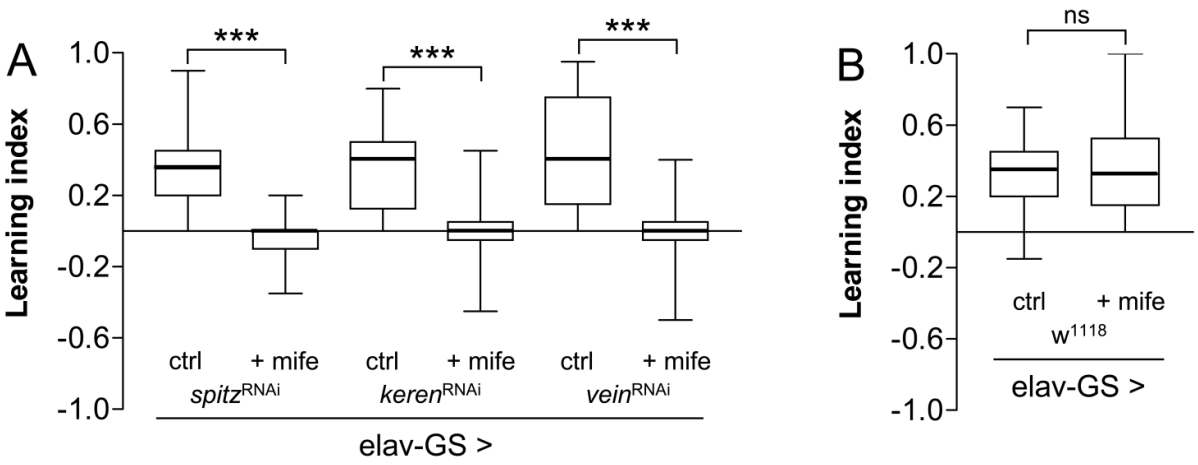

Fig. 52. Induction of pan-neuronal RNAi-mediated silencing of a single EGFR ligand gene after hatching leads to decreased olfactory learning ability. (A) In the individual-animal assay, olfactory learning capability was decreased in larvae after induction of pan-neuronal RNAi-mediated gene silencing of the ligands *spitz*, *keren*, or *vein* immediately after hatching ($n_{\text{learning indices}} = 64$ each). (B) Mifepristone feeding starting after hatching did not affect olfactory learning in control larvae (elav-GS > w^{1118}; $n_{\text{learning indices}} = 64$ each). Ctrl, control (uninduced); GS, GeneSwitch; mife, mifepristone; ns, not significant ($P > 0.05$); ***, $P < 0.001$.

To exclude an effect of mifepristone feeding starting after hatching on olfactory learning, control larvae (elav-GS > w^{1118}) were treated as the corresponding experimental larvae. No significant difference in the olfactory learning ability was detected (Fig. 52 B, $P = 0.6455$; $n_{\text{learning indices}} = 64$ each).

To verify normal taste and smell in the induced ligand^{RNAi} larvae compared to uninduced control larvae, gustatory choice assays and odor sensing experiments were performed with the corresponding larvae. No differences in the preference for fructose (Fig. 53 A, *spitz*^{RNAi}: $P = 0.8280$; *keren*^{RNAi}: $P = 0.9351$; *vein*^{RNAi}: $P = 0.1469$; $n_{Pref} = 20$ each) or for quinine (Fig. 53 B, *spitz*^{RNAi}: $P = 0.7656$; *keren*^{RNAi}: $P = 0.8071$; *vein*^{RNAi}: $P = 0.7551$; $n_{Pref} = 20$ each) between induced and uninduced ligand^{RNAi} larvae was found.

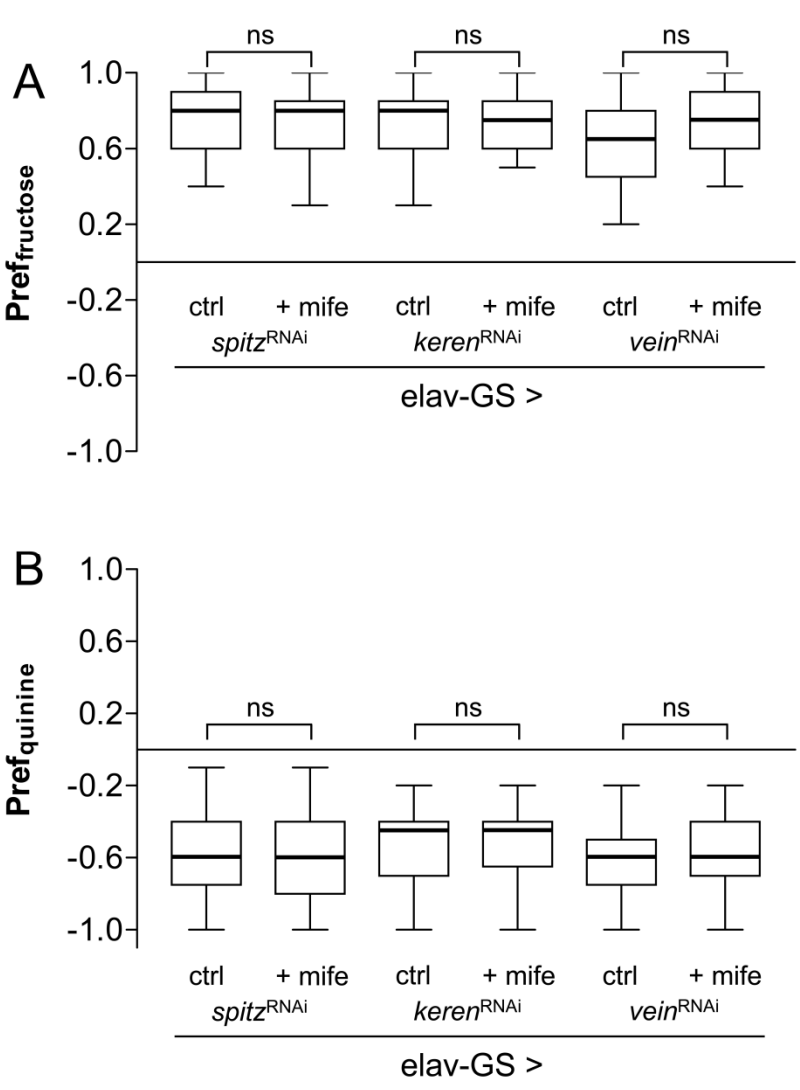

Fig. 53. Induction of pan-neuronal RNAi-mediated silencing of EGFR ligand genes after hatching did not cause gustatory impairment. Uninduced control larvae (ctrl) and induced ligand^{RNAi} larvae did not demonstrate any difference in their preference (Pref) for (A) fructose ($n_{Pref} = 20$ each) or (B) quinine ($n_{Pref} = 20$ each). Ctrl, control (un-induced); GS, GeneSwitch; ns, not significant ($P > 0.05$).

Induced ligand^{RNAi} larvae and uninduced control larvae also showed the same responses to the odors AM (Fig. 54 A, *spitz*^{RNAi}: $P = 0.4939$; *keren*^{RNAi}: $P = 0.2768$; *vein*^{RNAi}: $P = 0.8601$; $n_{Pref} = 50$ each) or OCT (Fig. 54 B, *spitz*^{RNAi}: $P = 0.3040$; *keren*^{RNAi}: $P = 0.4988$; *vein*^{RNAi}: $P = 0.7746$; $n_{Pref} = 50$ each).

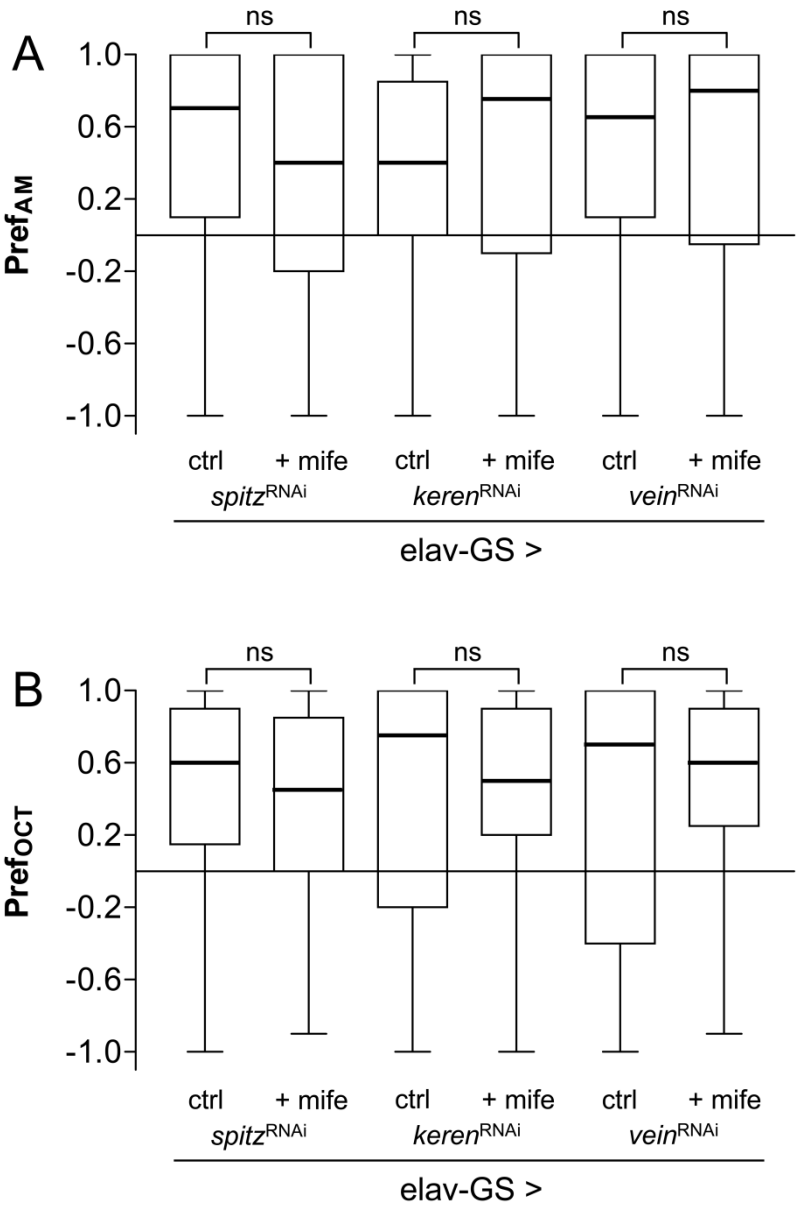

Fig. 54. Induction of pan-neuronal RNAi-mediated silencing of EGFR ligand genes after hatching did not cause olfactory impairment: AM and OCT. Uninduced control larvae (ctrl) and induced ligand^{RNAi} larvae did not demonstrate any difference in their preference (Pref) for the odors of (A) AM (n_{Pref} = 50 each) or (B) OCT (n_{Pref} = 50 each). AM, amyl acetate; GS, GeneSwitch; ns, not significant (P > 0.05); OCT, 1-octanol.

4.3.5 EGFR Signaling Balance is Important for Olfactory Learning

Next, it was assessed whether memory formation is modified by enhanced EGFR signaling. To address this question, larvae were investigated in the individual-animal assay that pan-neuronally expressed *secreted-spitz* (*s-spitz*) induced for 24 h. These larvae exhibited a clearly reduced olfactory learning ability compared to the uninduced control. (Fig. 55, P < 0.0001; $n_{learning\ indices}$ = 64 each). The median learning index of the control was the same as in former experiments (0.4), whereas the *s-spitz* overexpressing mutant showed only minor learning with a median learning index of approximately 0.1.

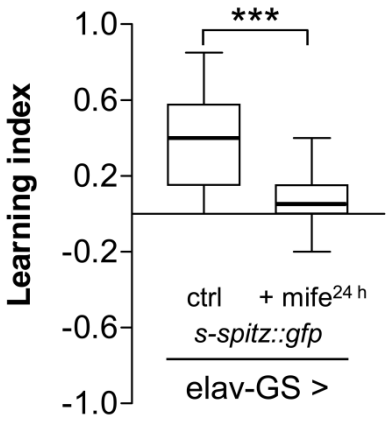

Fig. 55. Pan-neuronal activation of EGFR signaling via secreted-Spitz (s-Spitz) significantly impairs olfactory learning ability. In the individual-animal assay, olfactory learning capability decreased in those larvae expressing *s-spitz* for 24 h ($n_{learning\ indices}$ = 64 each). Ctrl, control (uninduced); GFP, green fluorescent protein; GS, GeneSwitch; mife, mifepristone; ***, $P < 0.001$.

To exclude an effect of pan-neuronal *s-spitz* expression for 24 h on taste or smell, the gustatory and olfactory preferences of *s-spitz* expressing larvae and uninduced control larvae were tested. Both groups showed the same attraction by fructose (Fig. 56 A, fructose: $P = 0.6776$; $n_{learning\ indices}$ = 64 each) and the same repulsion by quinine (Fig. 56 B, $P = 0.8284$; $n_{learning\ indices}$ = 64 each).

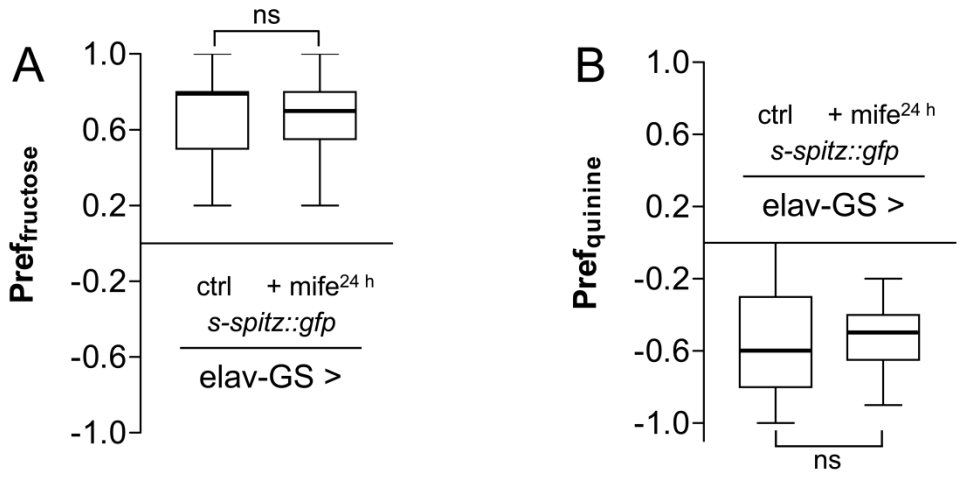

Fig. 56. Induction of pan-neuronal secreted Spitz (sSpitz) for 24 h did not cause gustatory impairment. Uninduced control larvae (ctrl) and those larvae expressing *s-spitz* for 24 h did not demonstrate any difference in their preference (Pref) for (A) fructose (n_{Pref} = 20 each) or (B) quinine (n_{Pref} = 20 each). GS, GeneSwitch; ns, not significant ($P > 0.05$).

No difference was detected in the preferences for the odors AM (Fig. 57 A, $P = 0.9945$; $n_{learning\ indices}$ = 64 each) or OCT (Fig. 57 B, $P = 0.4855$; $n_{learning\ indices}$ = 64 each) between *s-spitz* expressing larvae and uninduced control larvae.

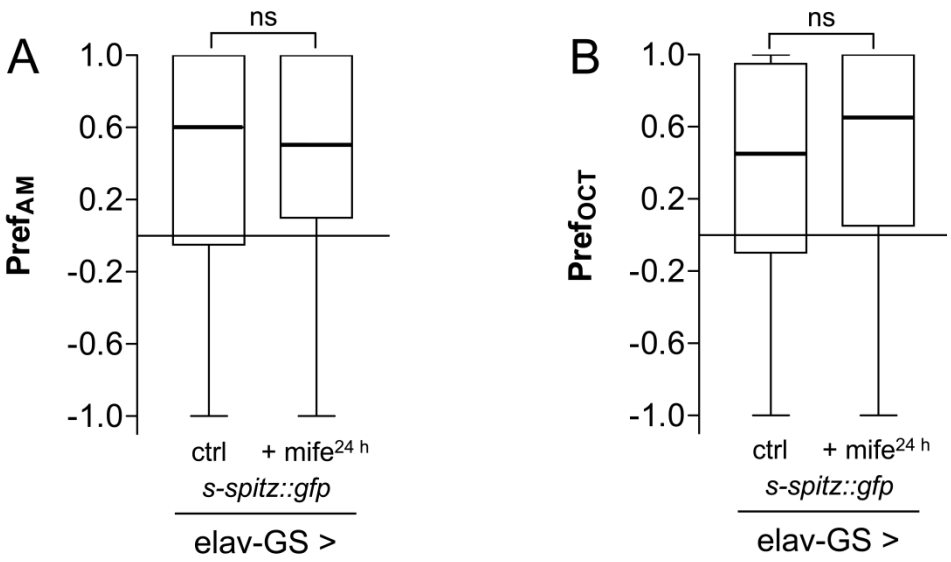

Fig. 57. Induction of pan-neuronal secreted-Spitz (s-Spitz) for 24 h did not cause olfactory impairment. Uninduced control larvae (ctrl) and those larvae expressing *s-spitz* for 24 h did not demonstrate any difference in their preference (Pref) for the odors of (A) AM (n_{Pref} = 50 each) or (B) OCT (n_{Pref} = 50 each). AM, amyl acetate; ctrl, control (uninduced); GS, GeneSwitch; ns, not significant ($P > 0.05$); OCT, 1-octanol.

4.4 EGFR Signaling in the Central Nervous System of Adult Flies

The analysis of *prom-gal4* > UAS-*gfp* of single EGFR pathway components revealed promoter activity of the ligands *spitz*, *keren*, and *vein* in the adult *Drosophila* brain. Ligand expression was found in the adult MBs and in the CC, which both are known to influence locomotor activity and circadian rhythms. To test the neural role of single EGFR ligands in behavioral activity and the regulation of sleep levels, locomotor activity assays were applied. The assays were performed with flies, in which the genes coding for the ligands *spitz*, *keren*, and *vein* were constitutively and pan-neuronally silenced using RNA interference.

4.4.1 Analysis of Locomotor Activity and Sleep Rhythm

The phenotypes of control flies (nsyb-*gal4* > w^{1118}) and those constitutively and pan-neuronally expressing *spitz*^{RNAi}, *vein*^{RNAi}, or *keren*^{RNAi} were analyzed (Fig. 58). Some of the flies expressing *spitz*^{RNAi} had crippled wings (Fig. 58 B). This phenotype was not observed in flies expressing *vein*^{RNAi} or *keren*^{RNAi}, which did not display any morphological defects (Fig. 58 C and D).

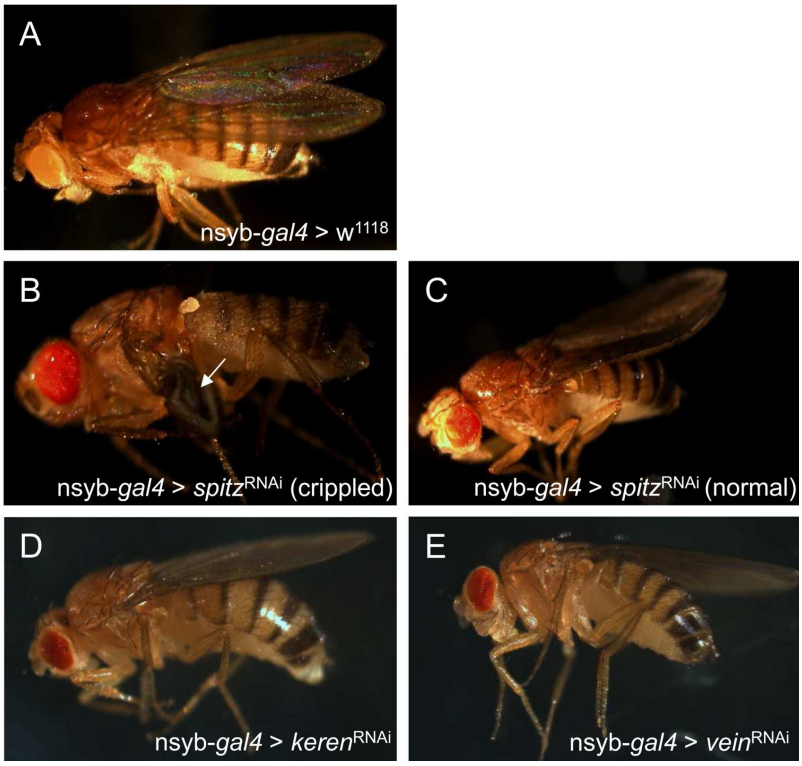

Fig. 58. Phenotypes of control flies and flies with reduced EGFR signaling in the brain. Wings of (A) control flies compared to wings of flies with (B and C) constitutive and pan-neuronal *spitz*^{RNAi} expression, (D) *keren*^{RNAi} expression, and (E) *vein*^{RNAi} expression. (B) Some of the flies with constitutive and pan-neuronal *spitz*^{RNAi} expression had crippled wings.

Locomotor activity assays were used to monitor both activity and sleep in adult flies. Therefore, single flies were investigated in horizontal glass vials and their confined motion was detected and counted by infrared light beams in an incubator with a 12-h light and dark cycle.

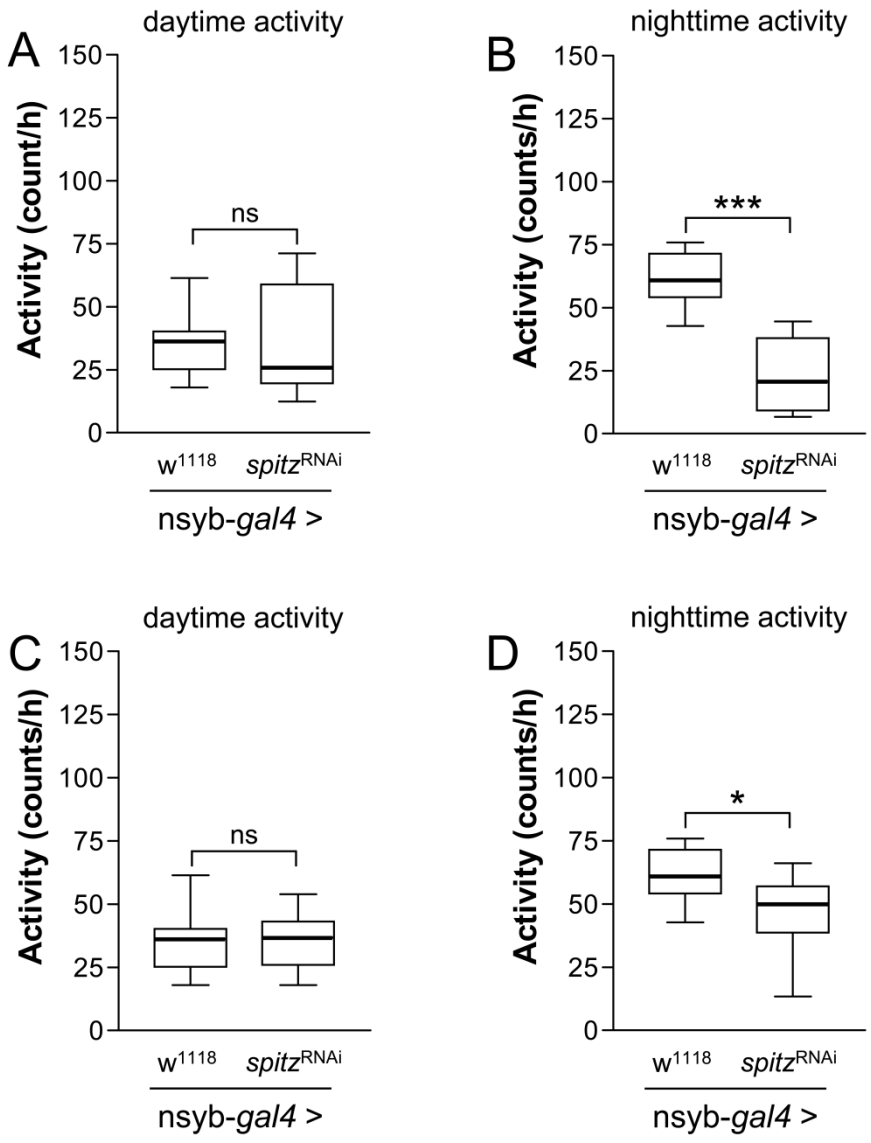

Fig. 59. Daytime and nighttime activity of flies constitutively and pan-neuronally expressing *spitz*^{RNAi} with crippled wings or normal wings. (A) Flies expressing *spitz*^{RNAi} with crippled wings and (C) flies expressing *spitz*^{RNAi} with normal wings (C) showed no significantly different activity levels during daytime compared to control flies (nsyb-*gal4* > w^{1118}). During nighttime, (B) flies with crippled wings and (D) flies with normal wings had a significantly lower activity level compared to control flies. Ns, not significant (P > 0.05); *, P < 0.025; ***, P < 0.0005.

For the analysis of flies constitutively and pan-neuronally expressing *spitz*^{RNAi}, flies with crippled wings and flies with normal wings were investigated separately. *Spitz*^{RNAi} expressing flies with crippled wings had no significantly different daytime activity (Fig. 59 A, P = 0.5433; $n_{control}$ = 16, $n_{spitzRNAi}$ = 7) but a significantly lower nighttime activity (Fig. 59 B, P < 0.0001; $n_{control}$ = 16, $n_{spitzRNAi}$ = 7) compared to control flies. Likewise, flies expressing *spitz*^{RNAi} with normal wings and control flies did not differ in daytime activity (Fig. 59 C, P = 0.8585; $n_{control}$ = 16, $n_{spitzRNAi}$ = 8) but

in nighttime activity (Fig. 59 D, $P = 0.0140$; $n_{control} = 16$, $n_{spitzRNAi} = 8$). Again, *spitz*^{RNAi} flies showed lower activity levels.

Flies expressing *keren*^{RNAi} were significantly more active during daytime (Fig. 60 A, $P = 0.0177$; $n_{control} = 15$, $n_{kerenRNAi} = 12$), whereas activities during nighttime did not differ significantly (Fig. 60 B, $P = 0.2516$; $n_{control} = 15$, $n_{kerenRNAi} = 12$) from control flies.

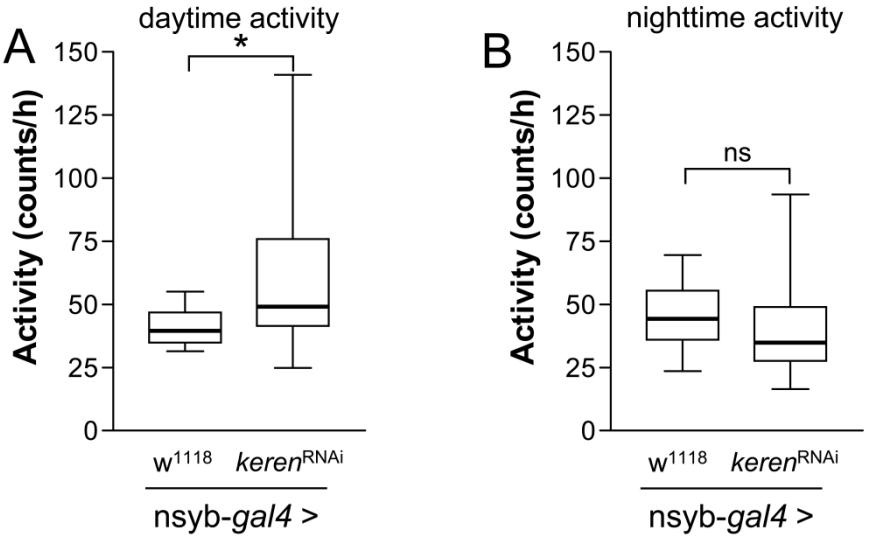

Fig. 60. Daytime and nighttime activity of flies constitutively and pan-neuronally expressing *keren*^{RNAi}. Flies expressing *keren*^{RNAi} showed (A) significantly higher daytime activity but (B) no significantly different nighttime activity compared to nsyb-*gal4* > w^{1118} control flies. *, $P < 0.05$; ns, not significant ($P > 0.05$).

Daytime activity (Fig. 61 A, $P = 0.0647$; $n_{control} = 14$, $n_{veinRNAi} = 15$) and nighttime activity (Fig. 61 B, $P = 0.4514$; $n_{control} = 14$, $n_{veinRNAi} = 15$) did not differ significantly between flies expressing *vein*^{RNAi} and control flies.

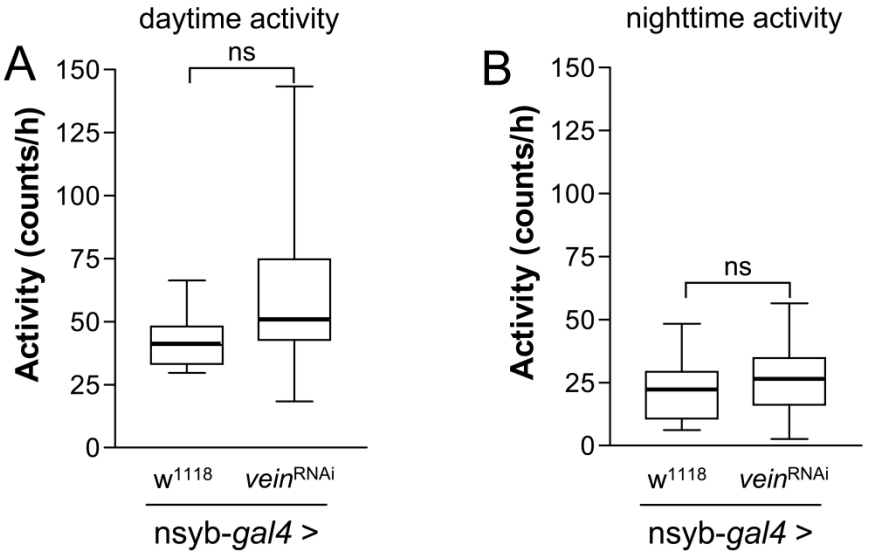

Fig. 61. Daytime and nighttime activity of flies constitutively and pan-neuronally expressing *vein*^{RNAi}. Flies expressing *vein*^{RNAi} showed no significant difference in (A) daytime activity or (B) nighttime activity compared to nsyb-*gal4* > w^{1118} control flies. Ns, not significant ($P > 0.05$).

Sleep was also monitored using the locomotor activity assays, whereby sleep was defined as one minute without activity and the minutes of sleep per hour were counted.

Monitoring of sleep revealed significantly higher levels of sleep during daytime (Fig. 62 A, $P = 0.0212$; $n_{control} = 16$, $n_{spitzRNAi} = 7$) and nighttime (Fig. 62 B, $P < 0.0001$; $n_{control} = 16$, $n_{spitzRNAi} = 7$) in *spitz*^{RNAi} expressing flies with crippled wings compared to control flies. *Spitz*^{RNAi} expressing flies with normal wings and control flies did not differ significantly in their sleep behavior during daytime (Fig. 62 C, $P = 0.2053$; $n_{control} = 16$, $n_{spitzRNAi} = 8$) but at nighttime. Here, the amount of sleep was significantly higher in *spitz*^{RNAi} expressing flies (Fig. 62 D, $P = 0.0068$; $n_{control} = 16$, $n_{spitzRNAi} = 8$).

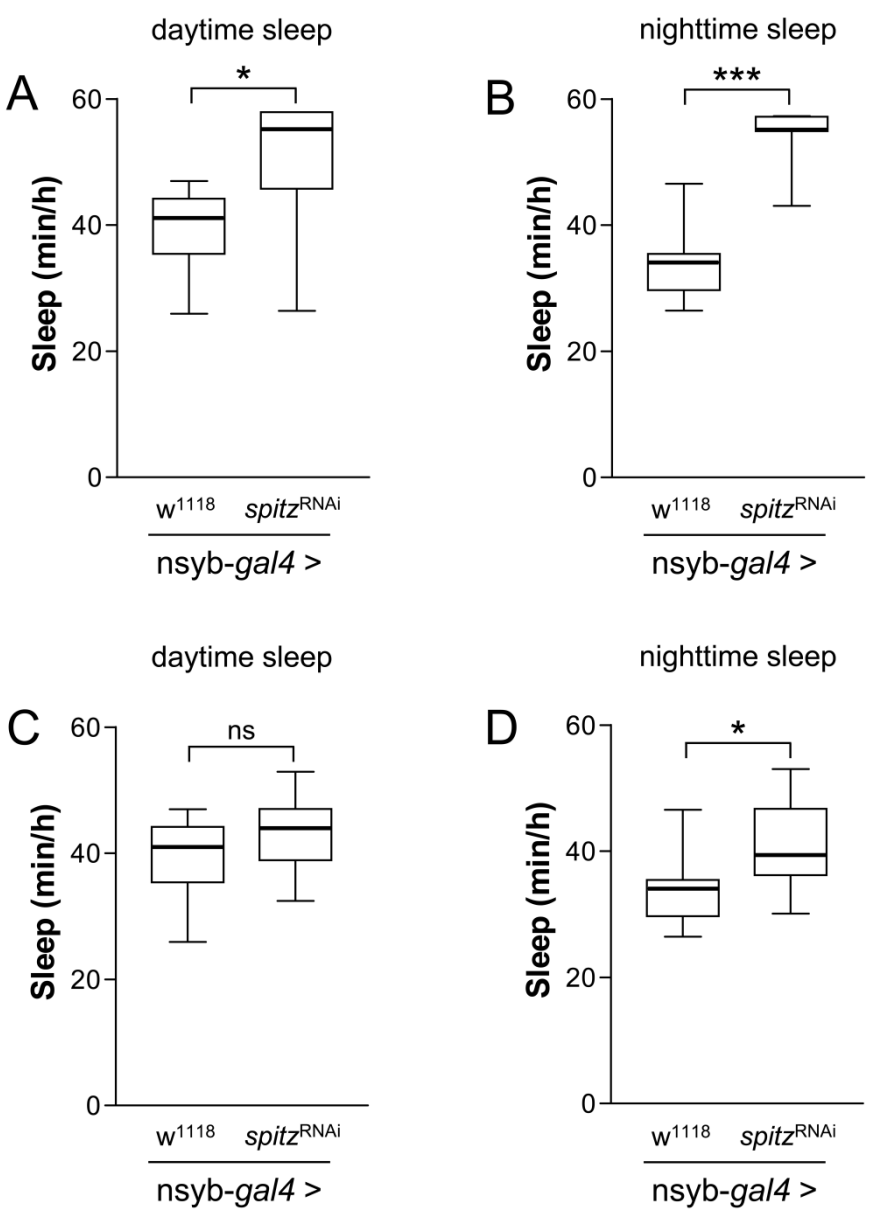

Fig. 62. Daytime and nighttime sleep of flies constitutively and pan-neuronally expressing *spitz*^{RNAi} with crippled or normal wings. (A and B) Flies expressing *spitz*^{RNAi} with crippled wings showed a significantly higher amount of sleep during daytime and nighttime compared control flies (nsyb-*gal4* > w^{1118}). (C) Flies expressing *spitz*^{RNAi} with normal wings did not significantly differ from control flies in daytime sleep but (D) had a higher amount of nighttime sleep compared to control flies. *, $P < 0.025$; ***, $P < 0.0005$; ns, not significant ($P > 0.05$).

Expression of *keren*^{RNAi} resulted in significantly lower levels of sleep during daytime (Fig. 63 A, P = 0.0091; $n_{control}$ = 15, $n_{kerenRNAi}$ = 12) compared to control flies. At nighttime, no significant differences in sleep levels were observed between the genotypes (Fig. 63 B, P = 0.3172; $n_{control}$ = 15, $n_{kerenRNAi}$ = 12).

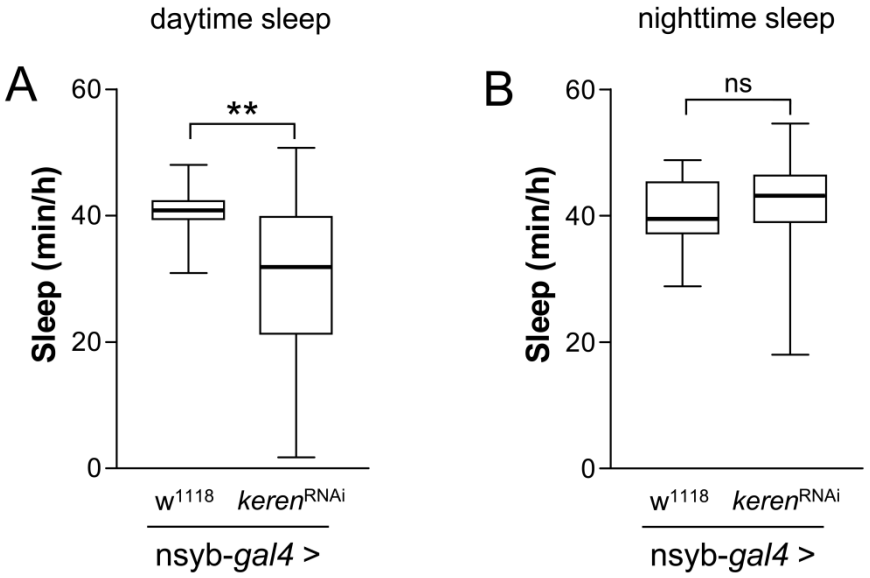

Fig. 63. Daytime and nighttime sleep of flies constitutively and pan-neuronally expressing *keren*^{RNAi}. Flies expressing *keren*^{RNAi} showed (A) a significantly lower amount of sleep during daytime compared to control flies (nsyb-*gal4* > w^{1118}). (B) No significant difference between the genotypes in the amounts of nighttime sleep was observed. **, P > 0.01; ns, not significant (P > 0.05).

Flies expressing *vein*^{RNAi} showed a significantly lower amount of sleep during daytime (Fig. 64 A, P = 0.0023, $n_{control}$ = 15, $n_{veinRNAi}$ = 15) compared to control flies. On the contrary, no significant difference in the levels of sleep during nighttime (Fig. 64 B, P = 0.6896, $n_{control}$ = 15, $n_{veinRNAi}$ = 15) were observed.

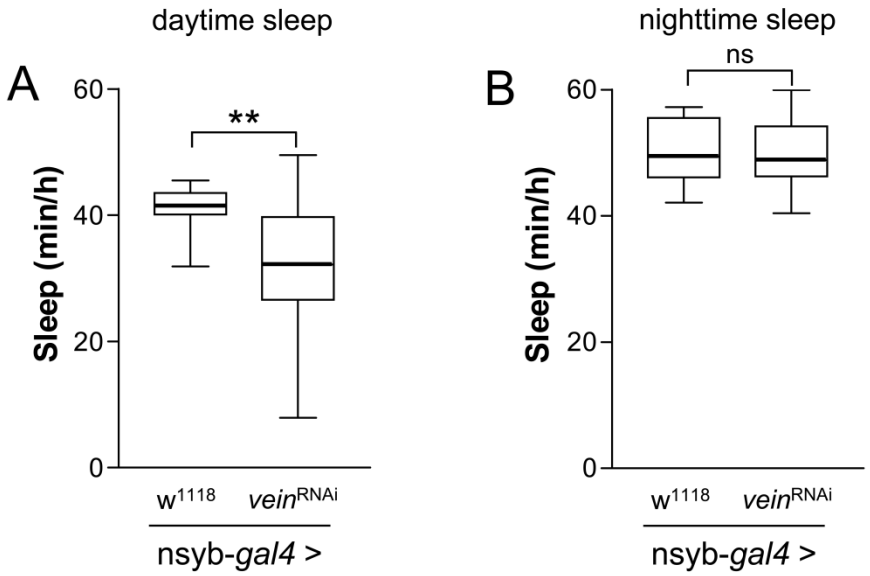

Fig. 64. Daytime and nighttime sleep of flies expressing constitutively and pan-neuronally *vein*^{RNAi}. Flies ex-pressing *vein*^{RNAi} showed (A) a significantly lower amount of sleep during daytime but (B) no significantly different amount of sleep during nighttime compared to nsyb-*gal4* > w^{1118} control flies. **, P < 0.01; ns, not significant (P > 0.05).

For the analysis of the influence of single EGFR ligands on circadian rhythms, activity levels and the amount of sleep were monitored in the course of the day.

Activity patterns of *spitz*^{RNAi} expressing flies with crippled wings and control flies differed to a large extent (Fig. 65). The control flies reacted to the light switch in the morning (8.00 h) and in the evening (20.00 h) with higher activity levels, whereas *spitz*^{RNAi} expressing flies did not show this reaction.

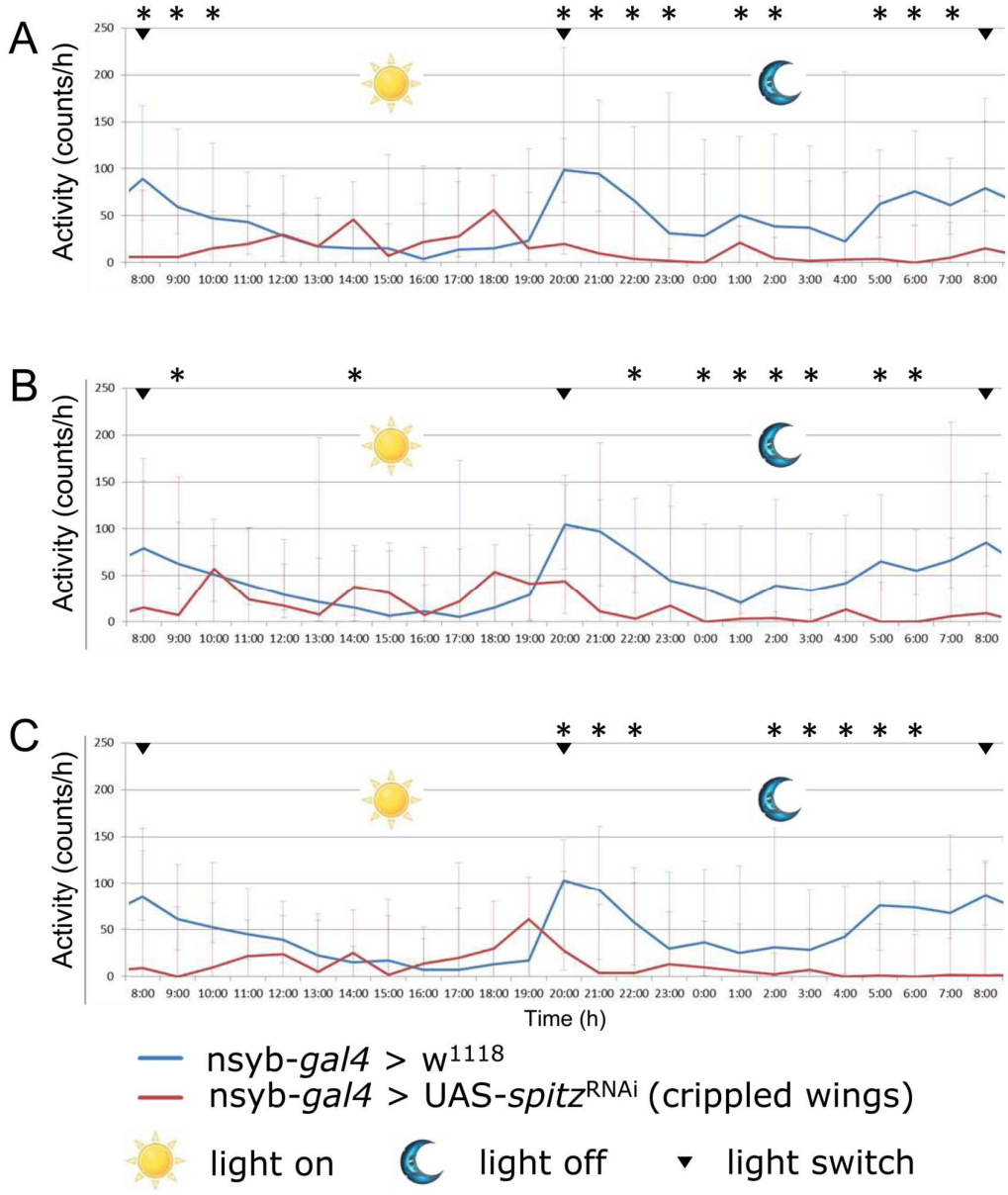

Fig. 65. Activity during day of flies expressing constitutively and pan-neuronally *spitz*^{RNAi} with crippled wings. Median activity traces of flies constitutively and pan-neuronally expressing *spitz*^{RNAi} (nsyb-*gal4* > *spitz*^{RNAi}) with crippled wings and control traces (nsyb-*gal4* > w^{1118}) are shown. A, B, and C show the activity traces of one day, each. *, $P > 0.025$, $n_{control} = 16$; $n_{spitzRNAi} = 7$.

During the entire night (20.00 h to 8.00 h), *spitz*^{RNAi} expressing flies had a lower median activity level compared to control flies (Fig. 65).

By contrast, the phenotype of a lower nighttime activity was less dramatic in *spitz*^{RNAi} expressing flies with normal wings (Fig. 66).

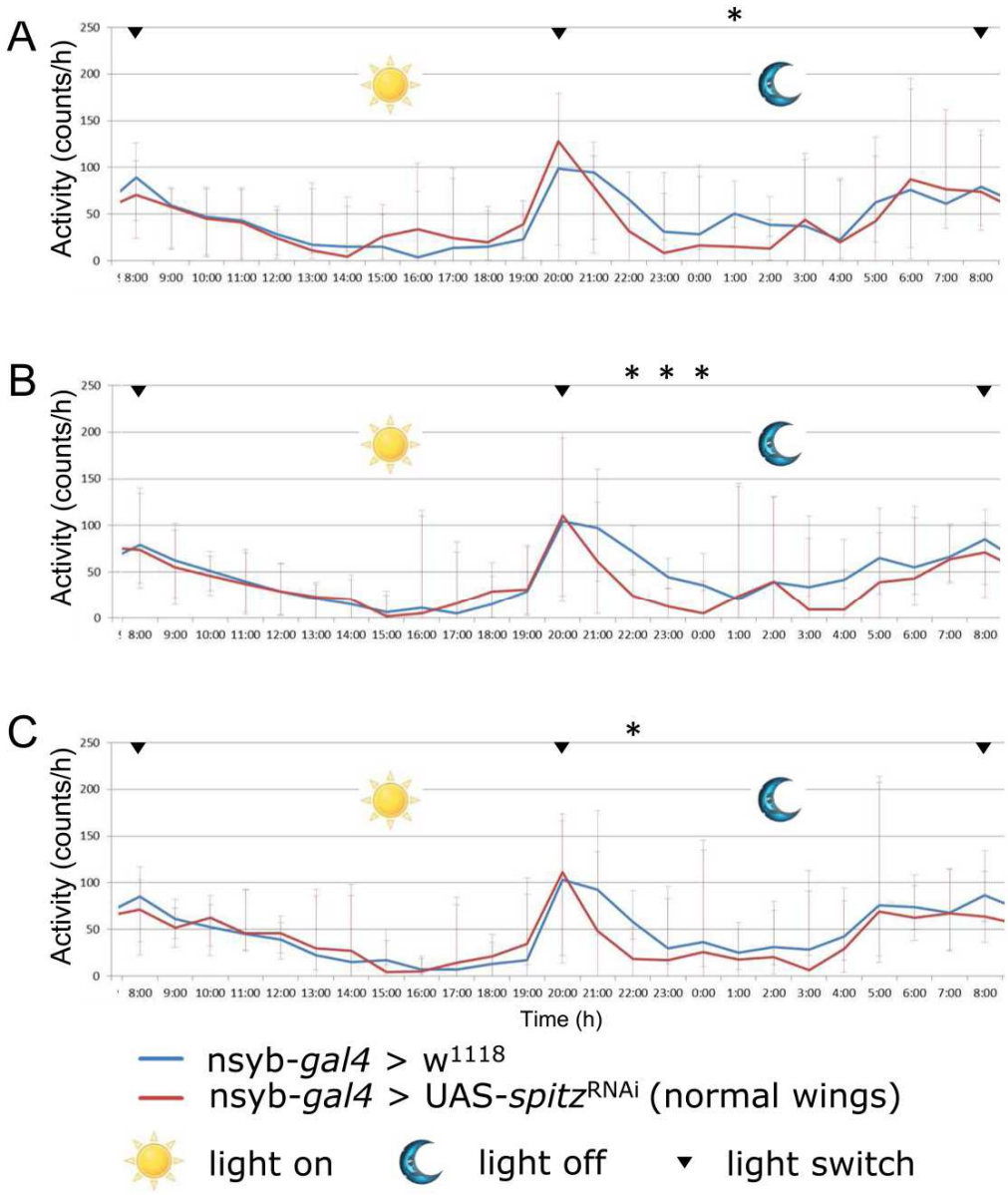

Fig. 66. Activity during the day of flies expressing constitutively and pan-neuronally *spitz*^{RNAi} with normal wings. Median activity traces of flies constitutively and pan-neuronally expressing *spitz*^{RNAi} (nsyb-*gal4* > *spitz*^{RNAi} with normal wings and control traces (nsyb-*gal4* > w^{1118}) are shown. A, B, and C show the activity traces of one day, each.*, $P > 0.025$, $n_{control} = 16$; $n_{spitzRNAi} = 8$.

Nevertheless, also *spitz*^{RNAi} expressing flies with normal wings had significantly lower activity levels after the evening light switch (Fig. 66).

Keren^{RNAi} expressing flies had significantly higher activity levels during daytime but significantly lower activity levels before the morning light switch compared to control flies (Fig. 67). No significant differences in the activities were detectable in response to the evening light switch and during nighttime.

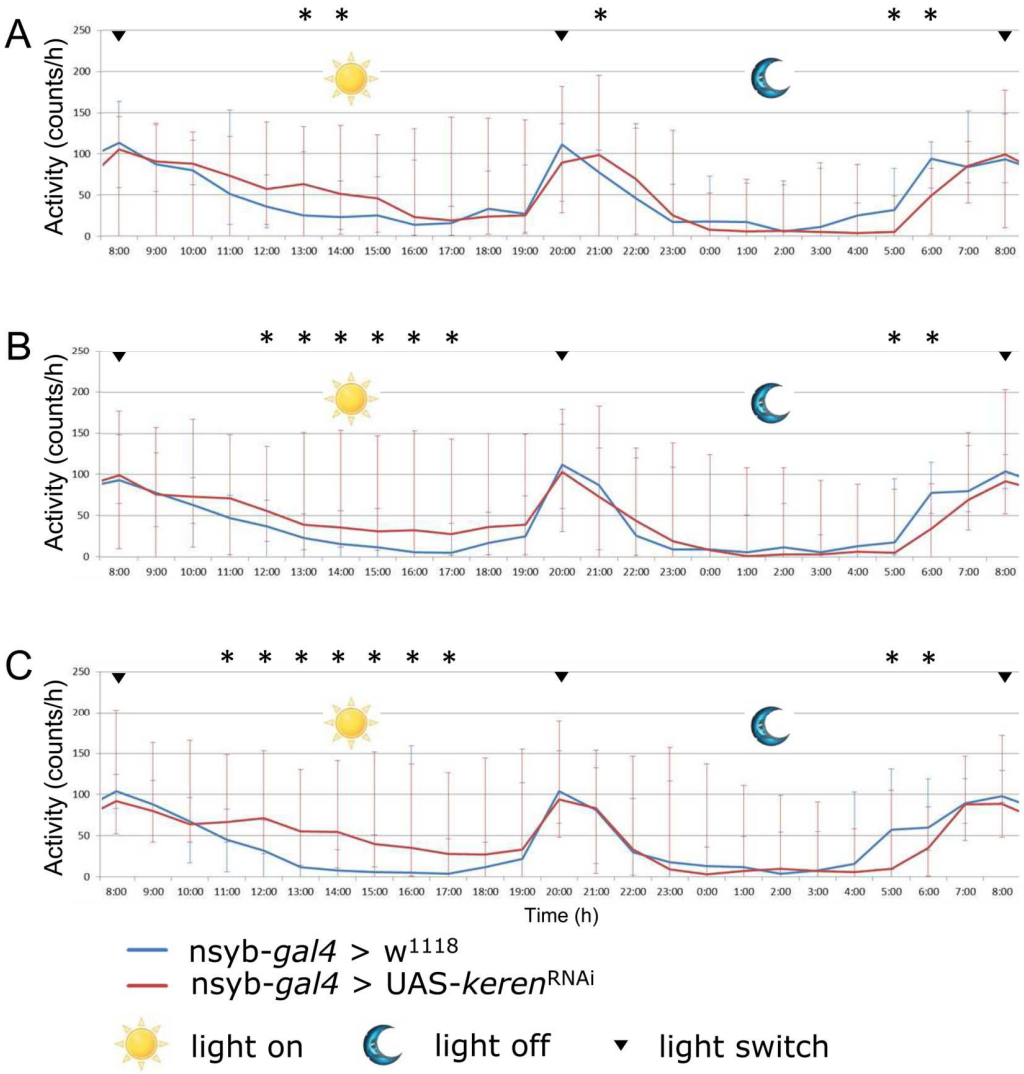

Fig. 67. Activity during the day of flies expressing constitutively and pan-neuronally *keren*^{RNAi}. Median activity traces of flies constitutively and pan-neuronally expressing *keren*^{RNAi} (nsyb-*gal4* > *keren*^{RNAi}) and control traces (nsyb-*gal4* > w^{1118}) are shown. A, B, and C show the activity traces of one day, each. *, *P* > 0.05, $n_{control}$ = 15; $n_{kerenRNAi}$ = 12.

Flies expressing *vein*^{RNAi} also showed higher activity levels during daytime and lower activity levels before the morning light switch compared to control flies (Fig. 68). Furthermore, their median activity at evening light switch was higher than the median activity of control flies.

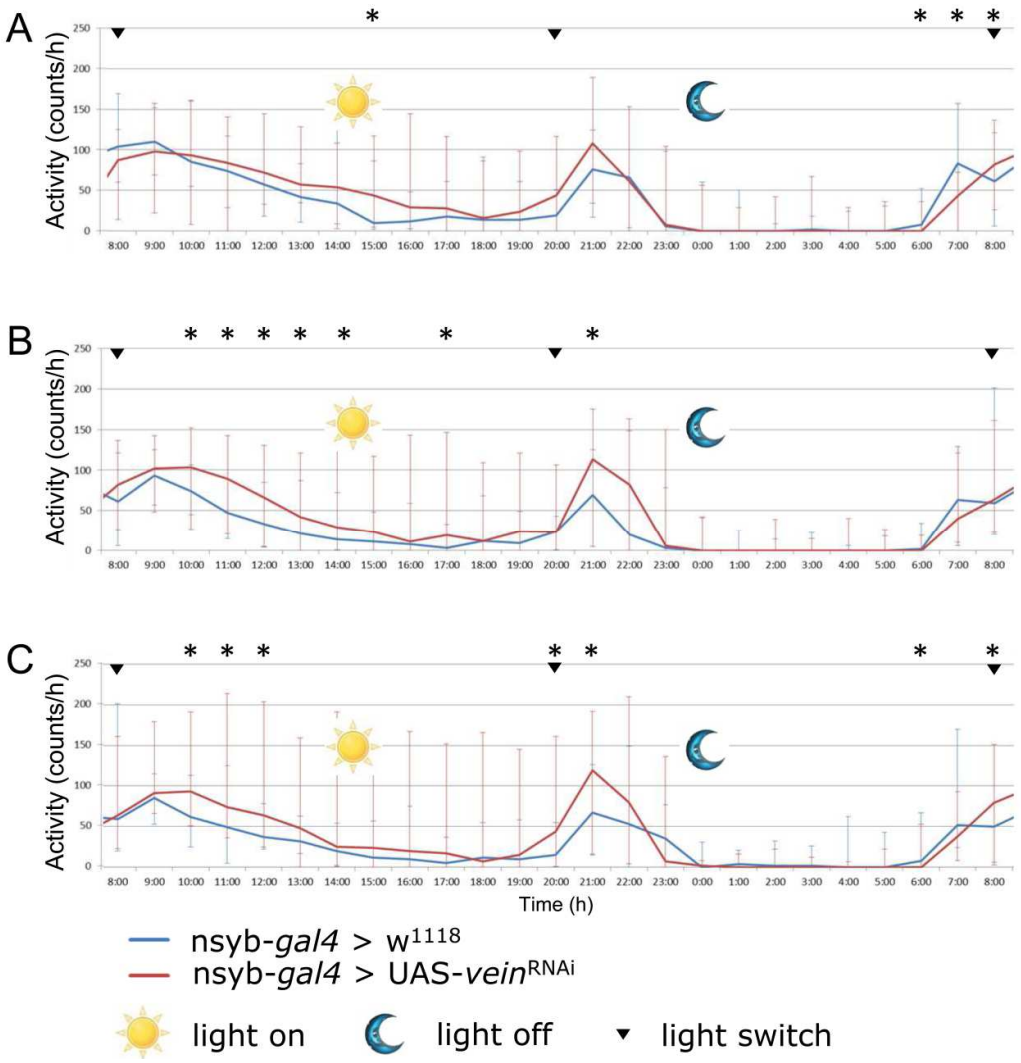

Fig. 68. Activity during the day of flies expressing constitutively and pan-neuronally *vein*^{RNAi}. Median activity traces of flies constitutively and pan-neuronally expressing *vein*^{RNAi} (nsyb-*gal4* > *vein*^{RNAi}) and control traces (nsyb-*gal4* > w^{1118}) are shown. A, B, and C show the activity traces of one day, each. *, $P > 0.05$, $n_{control} = 15$; $n_{veinRNAi} = 15$.

The analysis of sleep levels in the course of the day revealed that *spitz*^{RNAi} expressing flies with crippled wings had significantly higher sleep levels during both daytime and nighttime compared to control flies (Fig. 69). The sleep pattern of control flies showed low sleep levels at light switches, which were not detectable in *spitz*^{RNAi} flies.

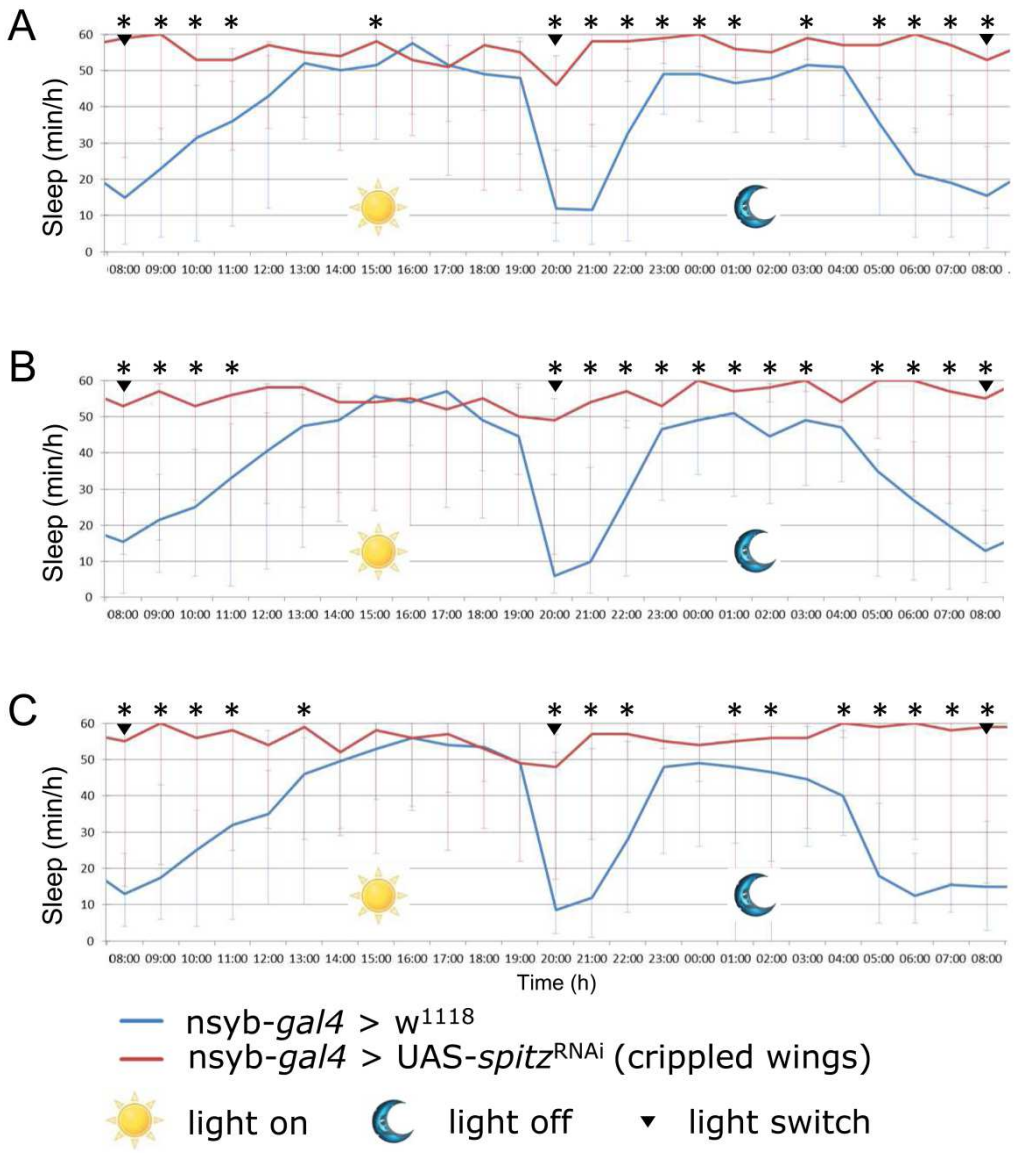

Fig. 69. Sleep levels during the day of flies expressing constitutively and pan-neuronally *spitz*^{RNAi} with crippled wings. Median sleep traces of flies constitutively and pan-neuronally expressing *spitz*^{RNAi} (nsyb-*gal4* > *spitz*^{RNAi}) with crippled wings and control traces (nsyb-*gal4* > w^{1118}) are shown. A, B, and C show the sleep traces of one day, each. *, $P > 0.025$, $n_{control} = 16$; $n_{spitzRNAi} = 7$.

In contrast to *spitz*^{RNAi} expressing flies with crippled wings, *spitz*^{RNAi} expressing flies with normal wings had a sleep pattern more similar to control flies (Fig. 70). Low sleep levels were visible for both *spitz*^{RNAi} flies and control flies at light switches but median sleep levels of *spitz*^{RNAi} flies after light switches were higher.

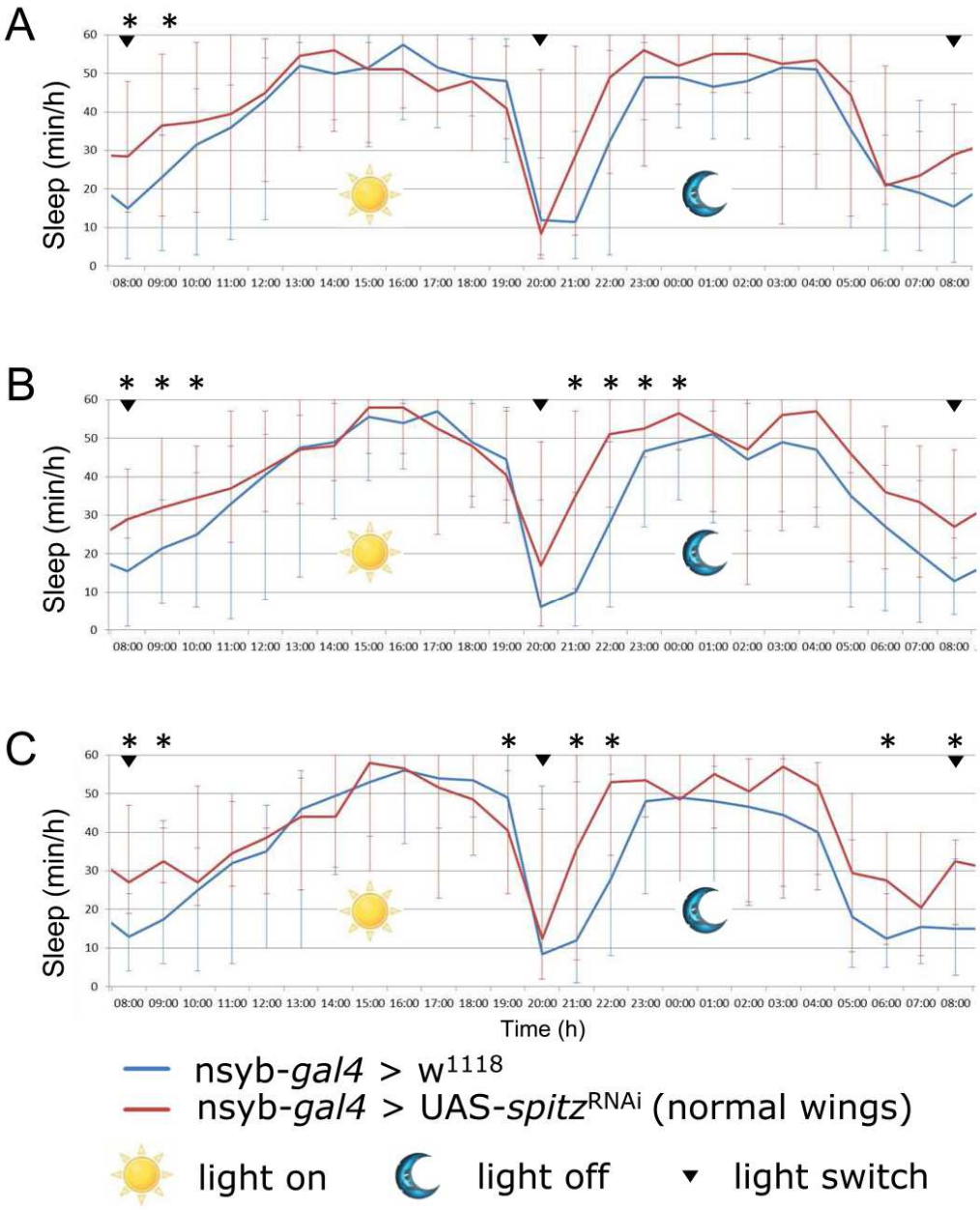

Fig. 70. Sleep levels during the day of flies expressing constitutively and pan-neuronally *spitz*^{RNAi} with normal wings. Median sleep traces of flies constitutively and pan-neuronally expressing *spitz*^{RNAi} (nsyb-*gal4* > *spitz*^{RNAi}) with normal wings and control traces (nsyb-*gal4* > w^{1118}) are shown. A, B, and C show the sleep traces of one day, each. *, $P > 0.025$, $n_{control} = 16$; $n_{spitzRNAi} = 8$.

Keren^{RNAi} expressing flies had lower sleep level during daytime but higher sleep levels before morning light switch compared to control flies (Fig. 71).

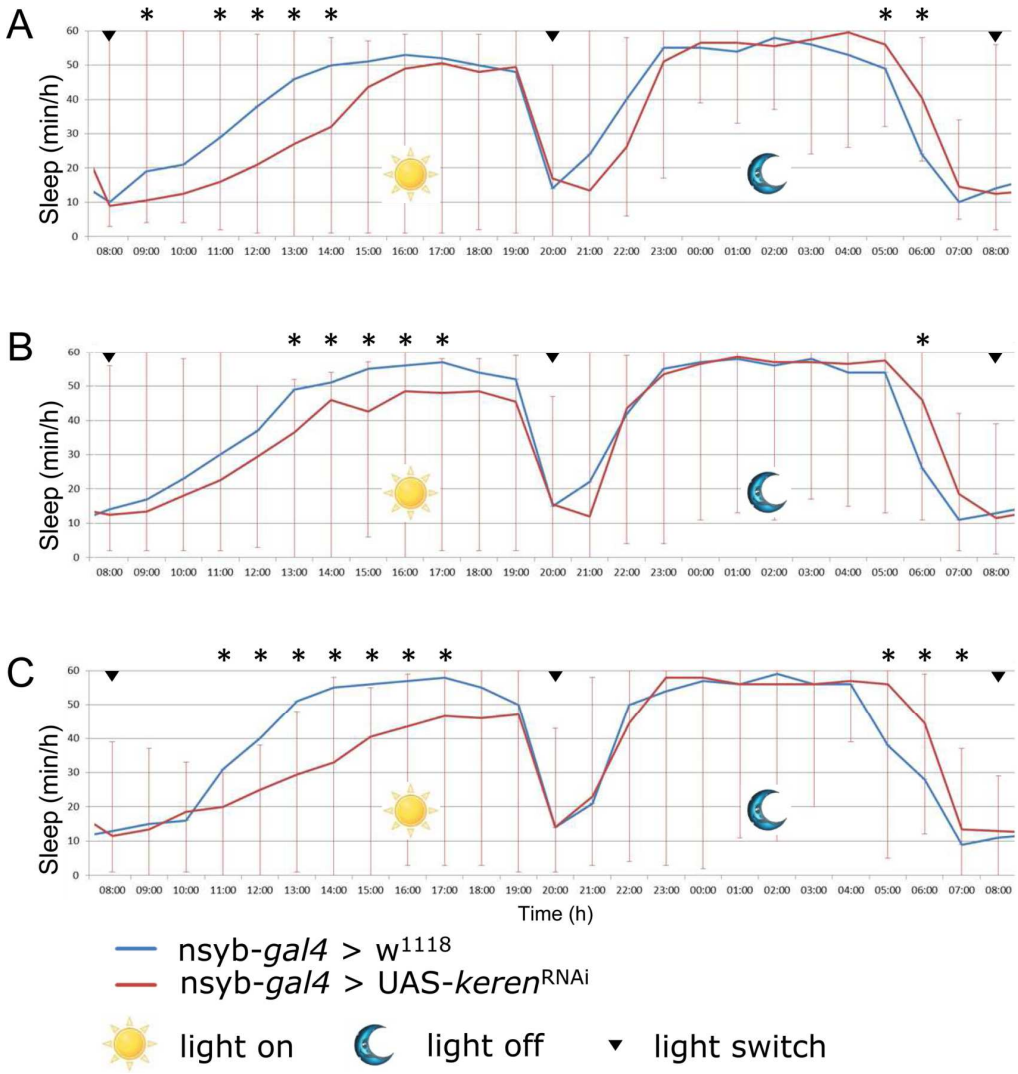

Fig. 71. Sleep levesl during the day of flies expressing constitutively and pan-neuronally *keren*^{RNAi}. Median sleep traces of flies constitutively and pan-neuronally expressing *keren*^{RNAi} (nsyb-*gal4* > *keren*^{RNAi}) and control traces (nsyb-*gal4* > w^{1118}) are shown. A, B, and C show the sleep traces of one day, each. *, *P* > 0.05, $n_{control}$ = 15; $n_{kerenRNAi}$ = 12.

Sleep levels of flies expressing *vein*^{RNAi} were significantly lower after morning light switch and at evening light switch (Fig. 72). However, the median sleep levels of *vein*^{RNAi} flies were higher before morning light switch.

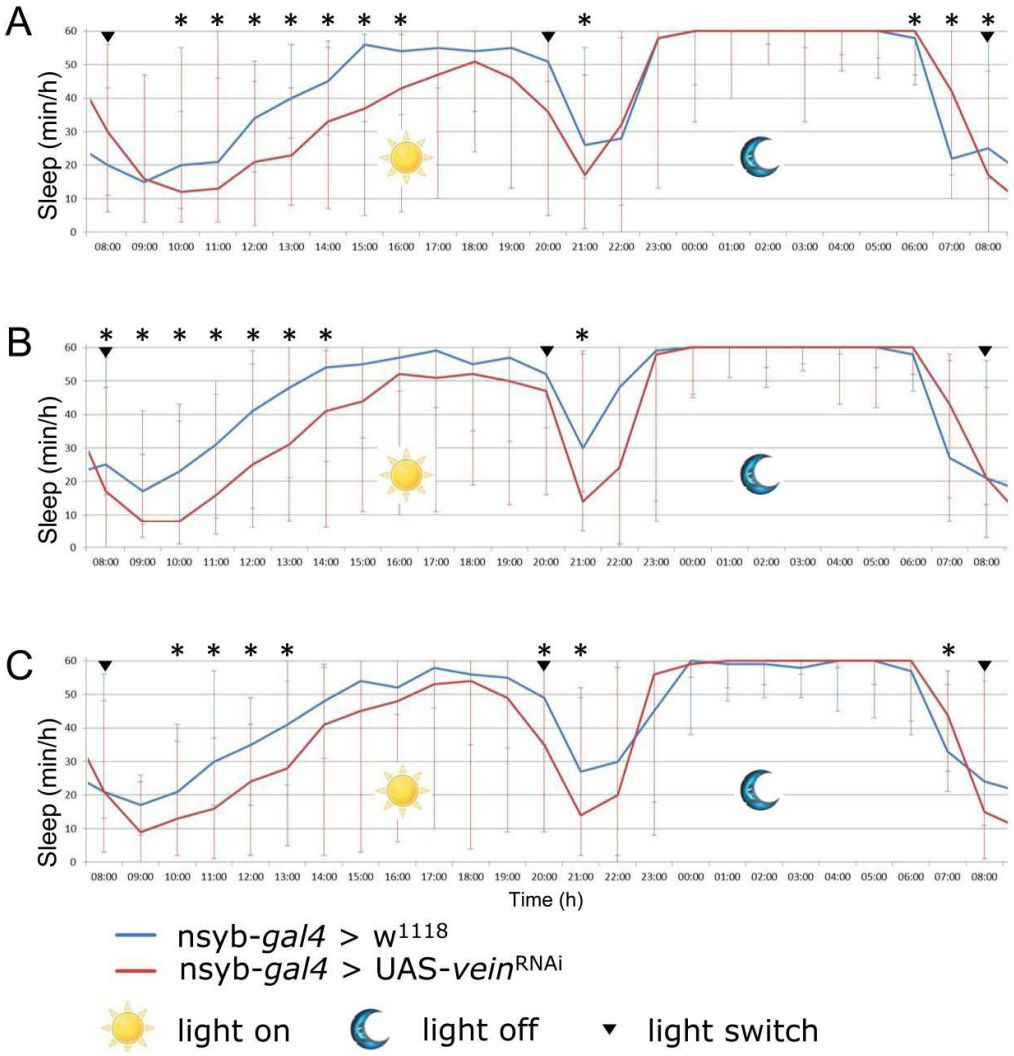

Fig. 72. Sleep levels during the day of flies expressing constitutively and pan-neuronally *vein*^{RNAi}. Median sleep traces of the effect of flies constitutively and pan-neuronally expressing *vein*^{RNAi} (nsyb-*gal4* > *vein*^{RNAi}) and control traces (nsyb-*gal4* > w^{1118}) are shown. A, B, and C show the sleep traces of one day, each. *, $P > 0.05$, $n_{control} = 15$; $n_{veinRNAi} = 15$.

4.4.2 Analysis of Geotaxis

The geotaxis assay is applied to analyze the natural tendency of *Drosophila* to move against gravity when agitated and, hereby, find genetic manipulations or conditions that hinder locomotor capacity.

Here, flies with pan-neuronal and constitutive expression of *spitz*^{RNAi}, *keren*^{RNAi}, and *vein*^{RNAi} were monitored, whereby *spitz*^{RNAi} expressing flies with crippled wings and with normal wings were investigated separately.

Notably, only *spitz*^{RNAi} expressing flies with crippled wings showed a significantly lower average pass rate (Fig. 73; $P < 0.0001$, n = 15) compared to control flies (nsyb-*gal4* > w^{1118}; n = 16) and, hence, had a clear defect in the ability for locomotor

activity. Flies expressing *spitz*^{RNAi} with normal wings and flies expressing *keren*^{RNAi} or *vein*^{RNAi} did not differ significantly in their average pass rate compared to control flies (*spitz*^{RNAi}: $P = 0.2554$, n = 10; *keren*^{RNAi}: $P = 0.0739$, n = 14; *vein*^{RNAi}: $P = 0.9827$, n = 15) and, thus, showed no impaired movement behaviour.

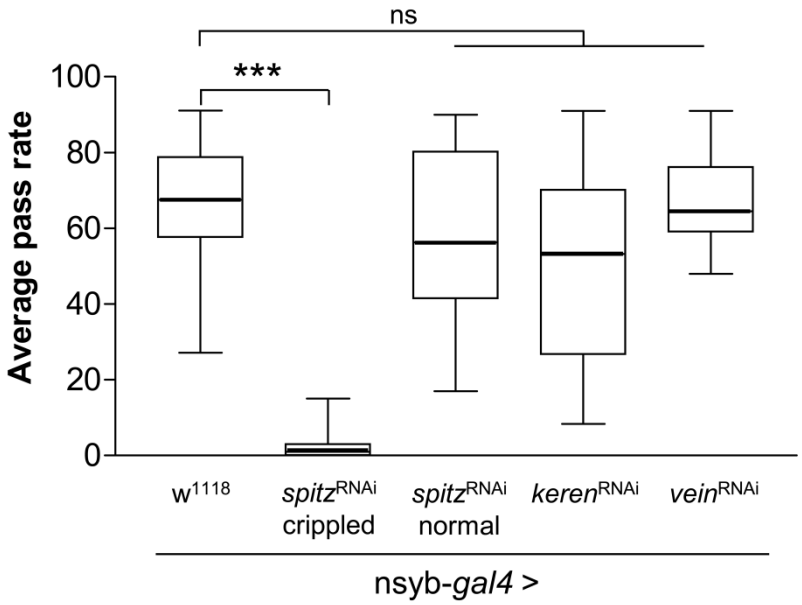

Fig. 73. Analysis of geotaxis. Flies expressing pan-neuronally and constitutively (nsyb-*gal4*) *spitz*^{RNAi} (with crippled wings), *spitz*^{RNAi} (with normal wings), *keren*^{RNAi}, or *vein*^{RNA} were analyzed in the geotaxis assay to investigate defects in movement. Only flies expressing *spitz*^{RNAi} with crippled wings showed a significantly lower average pass rate compared to control flies (nsyb-*gal4* > w^{1118}). ***, $P < 0.0002$; ns, not significant ($P > 0.01$). $n_{w1118} = 16$; $n_{spitz\ RNAi\ crippled} = 15$; $n_{spitz\ RNAi\ normal} = 10$; $n_{keren\ RNAi} = 14$; $n_{vein\ RNAi} = 15$.

4.5 EGFR Signaling in the Adult Fat Body

On transcriptional level, EGFR and all of the ligands were present in the adult fat body. In addition, promoter activity of *egfr*, *spitz*, *keren*, and *argos* was found in this tissue. Constitutive expression of *egfr*^{DN} or *egfr*^{ACT} in the fat body using the driver line RKF 125 was lethal by no later than pupal stage. Hence, the inducible GeneSwitch system was used to induce impaired EGFR signaling in this tissue for 24 h. Afterwards, the gene expression pattern was investigated as a foundation for further analysis. Based on the gene expression pattern, the influence of EGFR signaling on the two main functions of the tissue, immune response and fat storage, were analyzed.

4.5.1 Gene Expression Profiling in the Fat Body

To investigate the functions of EGFR signaling in the adult fat body, *egfr*^{DN} was expressed in this tissue for 24 h using the GeneSwitch system and, subsequently, fat body RNA was isolated to perform microarray analyses. To exclude genes whose expression was influenced by the inducing agent mifepristone, control flies (aFB-GS > w^{1118}) were treated as the experimental flies and their fat body RNA was also used for microarray analysis.

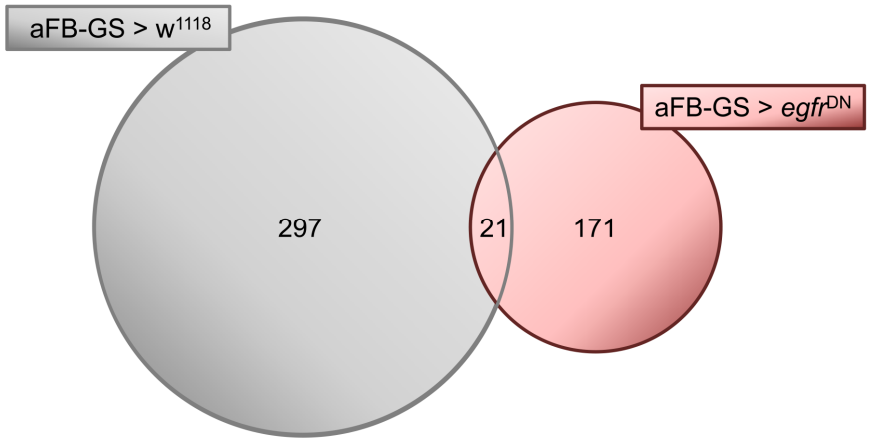

Fig. 74. Venn diagram: upregulated genes. Comparison of genes, which were at least 1.5-fold upregulated in flies fed with mifepristone, in the control (aFB-GS > w^{1118}, grey) and in flies with reduced EGFR signaling in the fat body (aFB-GS > *egfr*^{DN}, red). The number in the intersection displays, the number of genes upregulated in both control and aFB-GS > *egfr*^{DN}. One biological replicate was performed for the control, whereas three were done for aFB-GS > *egfr*^{DN} flies.

In the fat bodies of aFB-GeneSwitch > UAS-*egfr*^{DN} flies, which were induced for 24 h, 192 genes were upregulated and 279 genes were downregulated at least 1.5-fold in two of three microarrays. In the fat bodies of induced control flies (aFB-GS > w^{1118}), which were treated with mifepristone, 318 genes were upregulated and 259 genes were downregulated at least 1.5 fold. A group of upregulated 21 genes (Fig. 74) and a group of 47 downregulated genes (Fig. 75) was found in both induced control flies (aFB-GS > w^{1118}) and in induced *egfr*^{DN} expressing experimental flies (aFB-GS > UAS-*egfr*^{DN}). These genes were excluded for further analysis because their regulation may be caused by the mifepristone feeding and not by the EGFR pathway manipulation.

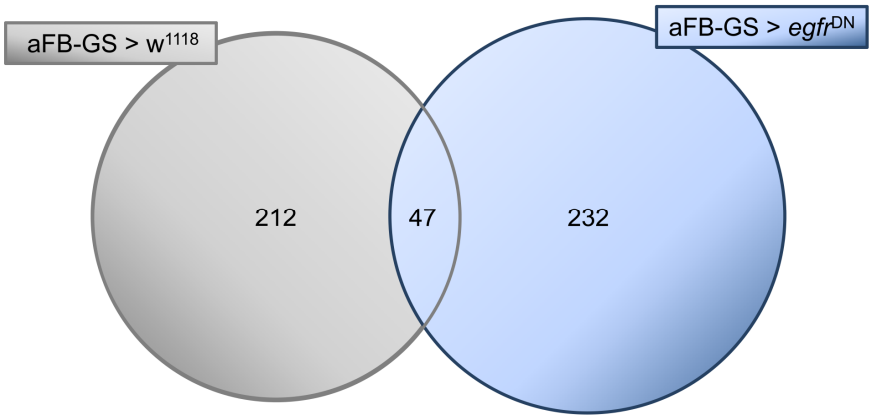

Fig. 75. Venn diagram: downregulated genes. Comparison of genes, which were at least 1.5-fold downregulated in flies fed with mifepristone, in the control (aFB-GS > w^{1118}) and in flies with reduced EGFR signaling in the fat body (aFB-GS > $egfr^{DN}$). The number in the intersection displays, the number of genes downregulated in both control and aFB-GS > $egfr^{DN}$. One biological replicate was performed for the control, whereas three were done for aFB-GS > $egfr^{DN}$ flies.

The web-accessible program DAVID was used to identify enriched biological themes and discover enriched functional-related gene groups. Among the downregulated gene, four were connected to the glycerophospholipid metabolism (Fig. 76, blue, violett, and black stars). These four genes were *glycerophosphate oxidase-1*, Dmel CG9459, Dmel CG6660, and Dmel CG4825. Glycerophosphate oxidase-1 has a glycerol-3-phosphate dehydrogenase activity that catalyzes the reduction of dihydroxyacetone phosphate to glycerin-3-phosphate. Dmel CG9459 and Dmel CG 6660 are GNS1/SUR4 membrane proteins, whereas Dmel CG4825 has a cytidine diphosphate-diacylglycerol-serine O-phosphatidyltransferase activity and participates in glycine, serine, threonine and glycerophospholipide metabolism.

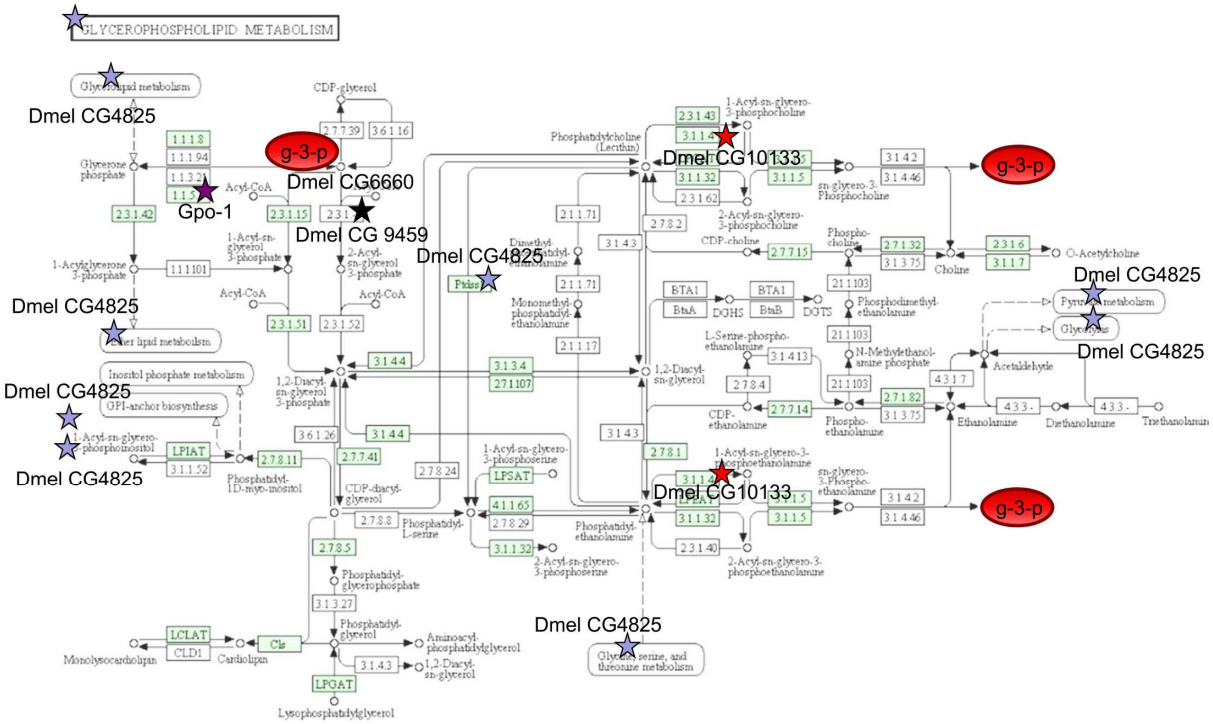

Fig. 76. Glycerophospholipid metabolism. Red stars mark genes upregulated at least 1.5-fold in induced aFB-GS > *egfr*^{DN} flies, whereas different-colored stars mark genes downregulated at least 1.5fold in induced aFB-GS > *egfr*^{DN} flies. AFB-GS, abdominal fat body-GeneSwitch; Gpo-1, glycerophosphate oxidase-1; g-3-p, glycerin-3-phosphate.

Among the upregulated genes, one additional gene was connected to the glycerophospholipid metabolism: Dmel CG101333 (Fig. 76, red stars). Dmel CG101333 has a phospholipase A2 activity to dissociate fatty acids from phosphoglycerides.

Tab. 10. Selected genes involved in energy metabolism and upregulated or downregulated (at least 1.5-fold) in induced abdominal fat body-GeneSwitch > *egfr*^{DN} flies. Note: Flybase-predicted activities.

upregulated gene	note	downregulated gene	note
CG3942	glycerophosphodiester phosphodiesterase activity; phospholipase C activity	CG18258	catalytic activity, protein feature: lipase
CG32444	aldose 1-epimerase	glycerophosphate oxidase-1 (CG8256)	glycerol-3-phosphate dehydrogenase activity
		trehalose transporter 1-2 (CG8234)	fructose transmembrane transporter activity
		CG6145	NAD+ kinase activity

In Tab. 10, selected genes are displayed that are involved in energy and were upregulated or downregulated in induced aFB-GS > UAS-*egfr*^{DN} flies.

Among the upregulated and downregulated genes, some genes were also connected to defense responses to bacteria (Tab. 11).

Tab. 11. Selected genes involved in bacterial defense and upregulated or downregulated (at least 1.5-fold) in induced abdominal fat body-GeneSwitch > *egfr*^{DN} flies. . Note: FlyBase-predicted activities and functions.

upregulated genes	note	downregulated genes	note
rac2 (CG8556)	GTPase activity; defense response to bacterium; phagocytosis triggered by activation of immune response cell surface activating receptor	sickie (CG10662)	nucleoside-triphosphatase activity; ATP binding; defense response to Gram-negative bacterium
		immune induced molecule 1 (CG18108)	defense response
		nimrod B4 (CG33115)	bacterial cell surface binding;
		gram-positive Specific Serine protease (CG5896)	serine-type endopeptidase activity; defense response to Gram-positive bacterium
		nimrod B1 (CG33119)	bacterial cell surface binding; defense response to bacterium

4.5.2 Transcriptional Analysis of Antimicrobial Peptide Genes after EGFR Signaling Manipulation in the Fat Body

One of the main functions of the fat body is the mediation of the immune response, including the production and secretion of antimicrobial peptides (AMPs). Several genes involved in bacterial defense were regulated in the microarray analysis as a result of reduced EGFR signaling (aFB-GS > *egfr*^{DN}; Tab. 11). The influence of reduced and enhanced EGFR signaling for 24 h on AMP production was investigated on transcriptional level by qRT-PCR.

As a control, aFB-GS was mated to wild type flies (w^{1118}). These aFB-GS > w^{1118} flies were fed with the respective mifepristone-containing food medium and the effect of the mifepristone treatment on AMP expression was investigated.

Strikingly, mifepristone feeding biased AMP expression in aFB-GS > w^{1118} control flies (Fig. 77). Metchnikovin transcription was upregulated up to a 144 fold change in one replicate of the control flies and also expression of *attacin A, cecropin C, defensin, diptericin, drosocin*, and *drosomycin* was regulated in controls. In general, expression of the tested AMP genes was highly variable among the biological

replicates in control flies (aFB-GS > w^{1118}) and in induced flies that express a gene coding for a dominant-negative (aFB-GS > UAS-*egfr*^{DN}) or a constitutively active form of EGFR (aFB-GS > UAS-*egfr*^{ACT}).

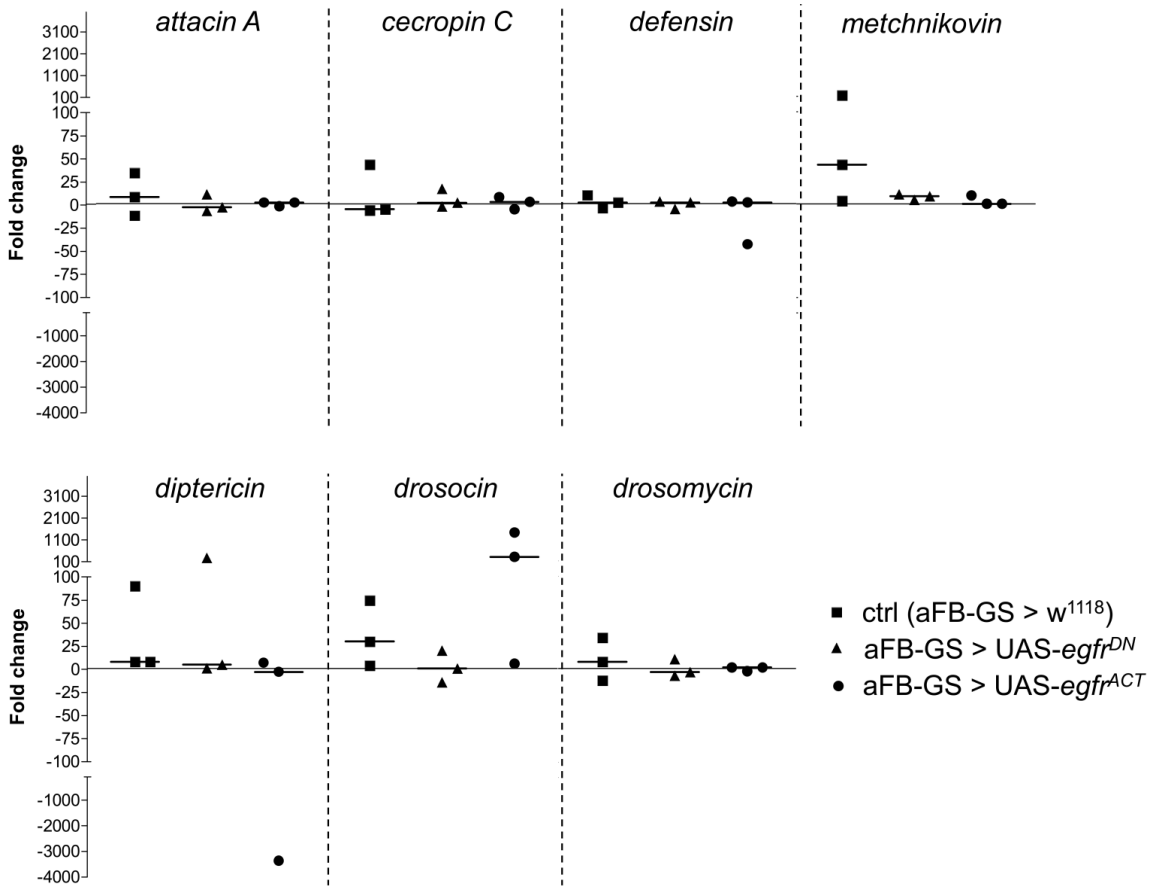

Fig. 77. Regulation of antimicrobial peptide genes after EGFR signaling manipulation in the fat body. Fold change of expression of the antimicrobial peptides *attacin A, cecropin C, defensin, metchnikovin, diptericin, drosocin*, and *drosomycin* in control flies (ctrl, aFB-GS > w^{1118}), and in flies expressing a gene coding for a dominant-negative form (UAS-*egfr*^{DN}) or a constitutively active form of EGFR (UAS-*egfr*^{ACT}) in the adult abdominal fat body (aFB) induced by mifepristone feeding for 24 h. Three biological replicates are displayed for each genotype. GS, GeneSwitch.

4.5.3 Influence of EGFR Signaling Manipulation in the Fat Body on Fat Content

The second main function of the fat body is the storage and release of fat. To test whether EGFR signaling influences the fat content, a BODIPY (493/503) staining was performed with flies expressing *egfr*^{DN} or *egfr*^{ACT} for one week in the abdominal fat body. The lipophilic fluorescent dye BODIPY (493/503) emits bright green fluorescence and specifically stains neutral lipid, e.g. cholesteryl esters, TAGs, and fatty acids, which accumulate in cellular lipid droplets. Hence, this dye is suitable to detect changes in the content of stored fat.

Flies expressing a gene coding for a dominant-negative form of EGFR (UAS-*egfr*^{DN}) in the abdominal fat body using the GeneSwitch system for seven days showed no difference in the fat content compared to control flies visualized with BODIPY (493/503) under the fluorescence stereomicroscope (Fig. 78).

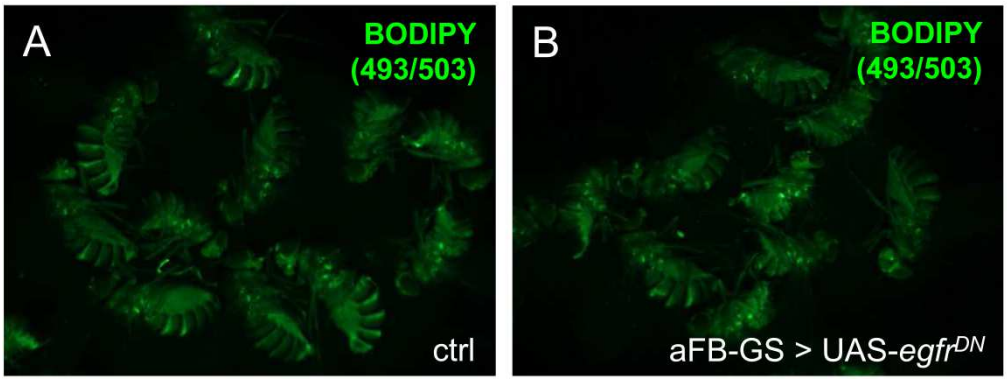

Fig. 78: Fat content of flies with reduced EGFR signaling in the fat body for one week. (A) Uninduced control flies and (B) induced aFB-*gal4* > UAS-*egfr*^{DN}, which expressed a gene coding for the dominant-negative form of EGFR for seven days did not show a detectable difference in the fat content visualized by BODIPY (493/503) staining. GS, GeneSwitch.

Expression of a gene coding for a constitutively active form of EGFR in the abdominal fat body (aFB-GS > UAS-*egfr*^{ACT}) for seven days resulted in a tendentially lower fat content compared to control flies (Fig. 79) visualized by BODIPY (493/503) staining. This effect was visible in female (Fig. 79 A) and male (Fig. 79 B) flies.

To varify the results of the BODIPY (493/503) staining, the coupled colorimetric assay (CCA) was performed in female flies to measure the TAG content quantitatively. No significant difference was detected comparing the TAG content of induced aFB-GS > UAS-*egfr*^{DN} flies and uninduced control flies (P = 0.9392; n = 7). However, induced aFB-GS > UAS-*egfr*^{ACT} had a significantly lower TAG content compared to control flies (P = 0.0208; n = 7). These results confirm the results of the BODIPY (493/503) staining.

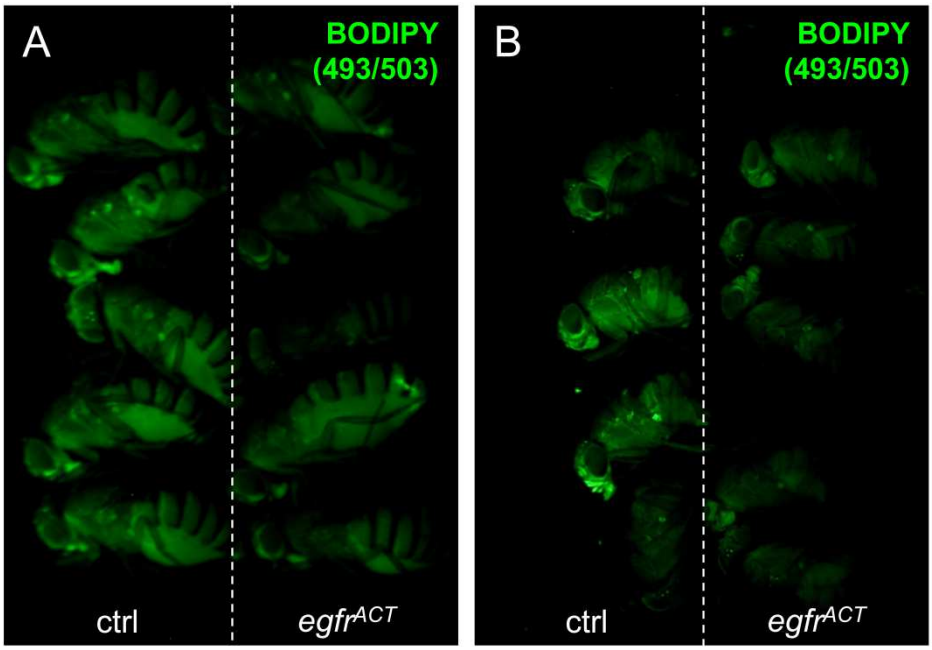

Fig. 79. Fat content of flies with enhanced EGFR signaling in the fat body for one week. (A) Female and (B) male flies with induced expression of a gene coding for a constitutively active form of EGFR (UAS-*egfr*^{ACT}, right side of A and B) in the abdominal fat body for seven days showed the tendency for a lower fat content compared to control flies (ctrl, left side A and B) visualized by BODIPY (493/503) staining.

4.5.4 Survival of Starving Flies

Since differences in the fat metabolism can influence the survival under starved conditions, the effect of reduced and enhanced EGFR signaling in the abdominal fat body using the GeneSwitch system was investigated.

Reduction of EGFR signaling in the abdominal fat body by induced expression of *egfr*^{DN} did not significantly reduce the median survival of females (Fig. 80 A, $P = 0.0848$; $n \geq 50$) or males (Fig. 80 B, $P = 0.5212$; $n = 50$) compared to uninduced controls.

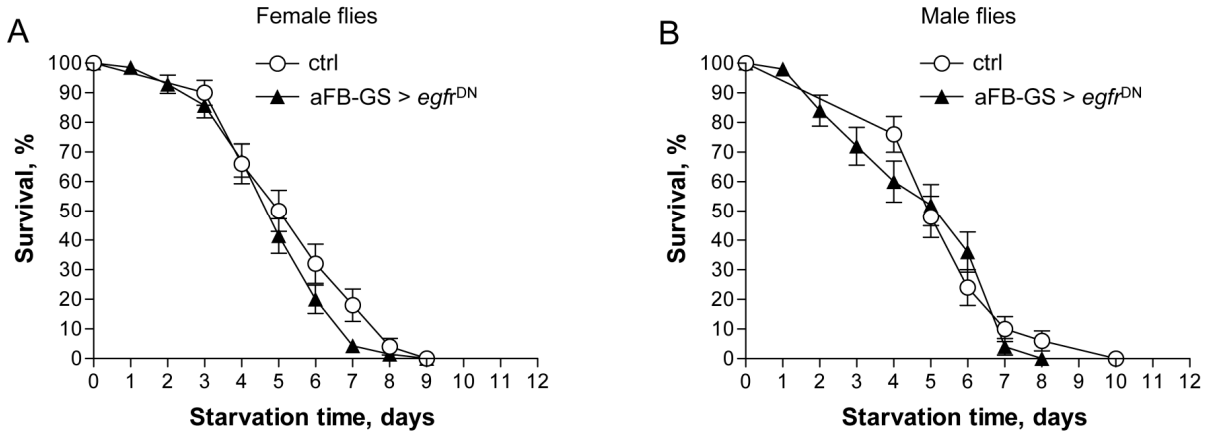

Fig. 80. Survival under starved conditions of flies with reduced EGFR signaling in the fat body. (A) Female and (B) male flies expressing a gene coding for a dominant-negative form of EGFR in the abdominal fat body (aFB-GeneSwitch > UAS-*egfr*^{DN}) did not differ in their median survival from their controls (ctrl). $N_{female} \geq 50$, $n_{male} = 50$.

However, enhanced EGFR signaling in the abdominal fat body by induced expression of *egfr*^{ACT} decreased median survival under starving conditions in females (Fig. 81 A, $P = 0.0009$; n = 160) but not in males (Fig. 81 B, $P = 0.6514$; n ≥ 110) compared to uninduced control flies.

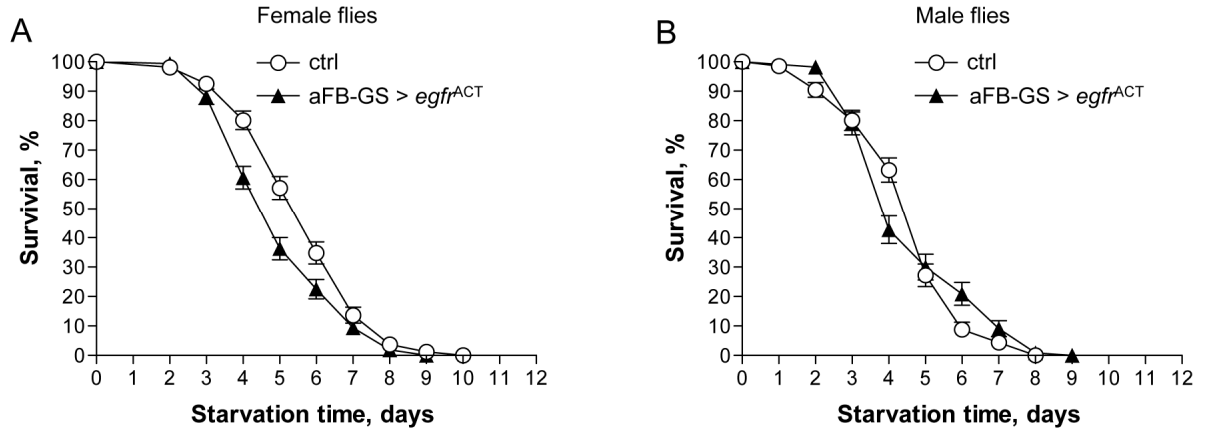

Fig. 81. **Survival under starved conditions of flies with enhanced EGFR signaling in the fat body.** (A) Female flies expressing a constitutively-active form of *egfr* in the abdominal fat body using the GeneSwitch system (aFB-GeneSwitch > UAS-*egfr*^{ACT}) showed a lifespan extension under starved conditions, whereas (B) male flies with the same enhanced EGFR signaling did not differ in their survival compared to their uninduced controls (ctrl). $N_{female} = 160$, $n_{male} \geq 110$.

5 DISCUSSION

EGFR is a long known, versatile signal transducer that has been well conserved during evolution. The homology of human EGFR and *Drosophila* EGFR was revealed already in 1985 (Wadsworth *et al.*, 1985) and, only one year later, possible functions in fly's development were assumed (Shilo *et al.*, 1986). Since that time, the number of developmental processes in *Drosophila*, for which EGFR signaling is known to be necessary, is increasing. On the contrary, little is known about non-developmental processes. So far, only the involvement of EGFR signaling in maintenance of gut homeostasis (Buchon *et al.*, 2010; Jiang and Edgar, 2009; Jiang *et al.*, 2011) and in some neuronal functions have been shown (Corl *et al.*, 2009; Foltenyi *et al.*, 2007). Notably, in humans, dysregulation of EGFR signaling in both of these organs has been connected to several severe diseases including cancer of the digestive system (Dragovich and Campen, 2009; Enrique *et al.*, 2012) and neurological disorders, like Parkinson's disease (Chen-Plotkin *et al.*, 2011) and Alzheimer's disease (Fleck *et al.*, 2011). As *Drosophila* has not only organs that perform the equivalent functions of several mammalian organs, including gut and brain, but also shares many key systems on molecular level, larvae and adult flies are well suited to study the basis of human diseases in a comparatively simple model organism.

Using promoter-reporter lines, I screened larvae and adult flies for EGFR pathway component promoter activity. The localization of promoter activity to mostly even single cells pointed at the physiological importance of EGFR signaling in several so far not discussed tissues and processes.

Based on the promoter activity in cells dedicated to learning, locomotor activity, sleep rhythms, immune response, and fat storage, the influence of a disturbed EGFR signaling homeostasis on these processes was analyzed using EGFR signaling mutants.

5.1 EXPRESSION OF EGFR PATHWAY COMPONENTS

The elucidation of promoter activity patterns of *egfr*, *spitz*, *keren*, *vein*, *gurken*, and *argos* was the basis for further functional analyses. Promoter activity was detected via *gfp* expression using *promoter-gal4* lines mated to UAS-*gfp* in live imaging or

immunohistochemistry. These results give strong hints for expression of the gene, whose promoter region was selected for the generation of the reporter line.

In general, promoters are located immediately upstream from the start site of transcription and are typically about 100 bp in length (Maniatis *et al.*, 1987). In contrast to the conserved position of these basal promoter sequences, enhancer elements often function distant from the promoter and may be located 5' or 3' of the transcription start site (Hess *et al.*, 2007). Therefore, fragments of about 3,000–4,000 bp directly upstream of the translation start, which also cover the region 5' of the transcription start site were chosen for the generation of the *promoter-gal4* lines (Fig. 10). Thus, I expected to determine promoter and enhancer activity in the most common regions. Nevertheless, it must be taken in consideration that the promoter activity pattern revealed with this technique does not show the complete picture of EGFR pathway component genes expression. Strikingly, this was demonstrated for the gene coding for the ligand *spitz*.

So far, only an enhancer-trap line is publicly available from the DGRC. The insertion site of this enhancer-trap is located within the second exon. The complex exon/intron architecture giving rise to five different transcripts is the major reason why this enhancer-trap does not cover the complete presumptive promoter/enhancer region. Thus, two additional *promoter-gal4* lines were generated. For the generation of these lines, regions mainly located downstream of the enhancer-trap insertion site were used.

Notably, the three *spitz*-reporter lines showed different but overlapping promoter activity patterns. *Prom1-spitz-gal4* > UAS-*gfp* showed the most various GFP signals in larvae and in adult flies suggesting that most promoter and enhancer elements of *spitz* are located between the first and the third exon. The results of screening the *promoter-gal4* > UAS-*gfp* animals revealed new sites of *spitz* gene expression even in tissues, in which the *spitz enhancer-trap-gal4* > UAS-*gfp* has been previously analyzed. Furthermore, this stated the importance of the genomic region close to the translation start for promoter and enhancer analyses.

Promoter activity of EGFR pathway components was localized to several larval and adult tissues, often even to single cells, using microscopic techniques. These tissues were in particular larval and adult brains, larval and adult digestive tracts, larval and adult fat bodies, larval and adult Malpighian tubules, larval and adult salivary glands, as well as larval tracheae, larval epidermis, larval muscles, and male reproductive

tracts. Previously, mostly developmental roles of EGFR signaling have been reported in these tissues, which were investigated predominantly in *Drosophila* embryos. For instance, defects in EGFR signaling affected Malpighian tubules' development (Baumann and Skaer, 1993) and the involvement in maintaining the epithelial integrity during tracheal development has been shown (Cela and Llimargas, 2006). Furthermore, Geiger *et al.* (2011) have recently shown that EGFR signaling is necessary for wound repair in embryos. In the male reproductive system, the necessity in restriction of germline stem cell proliferation was reported (Kiger *et al.*, 2000).

Solely for the brain and the digestive tract non-developmental roles that have been investigated in larvae and adult flies have been shown (Buchon *et al.*, 2010; Corl *et al.*, 2009; Foltenyi *et al.*, 2007). No functions of EGFR signaling have been reported in the fat body, neither of larvae nor of adult flies. Notably, I found promoter activity of several EGFR pathway components in these tissues in larvae and adult flies and performed functional analyses with mutant flies with altered EGFR signaling in these tissues. The results of these investigations are discussed below.

In addition to the analyses of promoter activity patterns using the promoter-reporter lines, RT-PCR analyses were applied to confirm expression of the EGFR pathway component gene on tissue level.

In the majority of tissues, both methods produced consistent results. In some of the tissues, an EGFR pathway component was found on transcriptional level but no signal was detectable via the reporter line. An explanation for this may be that the specific promoter elements necessary for expression in a particular tissue are missing in the selected promoter regions used for generation of the *promoter-gal4* lines. These promoter elements might be further upstream of the selected region or downstream of the coding sequence of the gene of interest. Moreover, introns might contain further promoter sequences.

Merely in very few cases, no gene-specific RNA was detectable via RT-PCR in a certain tissue, although a signal was present there in the corresponding promoter-reporter line. Strikingly, this was only the case for *vein* and for *argos*. Both ligands are not produced as membrane-bound precursors but as secreted proteins. Thus, they will only be expressed, when they are physiologically needed. This is particularly true for *argos*, which is part of a negative feedback loop, and is only expressed when EGFR signaling is activated at high levels. However, also *vein* is part of a feedback

loop but for positive reinforcement of initial EGFR activation by other ligands (Shilo, 2003). Hence, expression of *argos* and *vein* is tightly regulated and only activated in certain physiologically states. Furthermore, GFP accumulates in cells, whereas RNA is degraded very fast. Thus, a GFP signal in the *prom-gal4* > UAS-*gfp* animals may be visible, even if the gene was transcribed at an earlier time point.

5.2 EGFR Signaling in the Central Nervous System

Reporter lines of EGFR pathway components showed expression in larval and adult brains. Strikingly, all *prom-gal4* > UAS-*gfp* larvae revealed expression of the corresponding genes in the larval CNS, whereas only reporter lines of *spitz*, *keren*, and *vein* drove *gfp* expression also in the adult brain. In larvae, the most prominent promoter activity of all pathway components was detected in the MBs, a higher brain center, which is known to be necessary for olfactory learning (Dubnau, 2012).
In adult flies, promoter activity was not only observed in the MBs but also in regions, which are dedicated to visual and olfactory perception, hormone production, and locomotor activity. These findings point at diverse functions of EGFR signaling in differentiated larval and adult brains beyond developmental processes and provided a good starting point to investigate further roles of the pathway. In addition, single ligands had overlapping promoter activity patterns but nevertheless, the three promoter-reporter lines also showed GFP signals in different parts of the brain. This supports the assumption of specific functions of different ligands.

5.2.1 Larval Olfactory Learning

Promoter activity of *egfr* and its activating ligands *spitz*, *keren*, *vein,* and *gurken,* as well as promoter activity of the EGFR signaling inhibitor *argos* is most apparent in the larval MBs. Thus, EGFR signaling is assumed to be of high physiological relevance in the differentiated larval brain. Since Heisenberg *et al.* (1985) have shown that the MBs are involved in learning and memory, this is the major task the MBs are known for. Moreover, *Drosophila* larvae have been used for learning experiments already for more than thirty years (Aceves-Pina and Quinn, 1979). Since the beginning of this century, a great deal of work has been invested in the improvement of larval learning

experiments. One simple and reliable method is the individual-animal olfactory learning assay (Scherer *et al.*, 2003). Here, larvae are trained together but tested individually to exclude non-independent behavior between individuals. To enhance learning, an inter-trial phase was inserted between the odor/taste presentations during the training (Hendel *et al.*, 2005), the training cycle was repeated four times (Neuser *et al.*, 2005), and quinine was used as a negative reinforcer for aversive learning (Scherer *et al.*, 2003). Although enhancement by a negative reinforcer was controversially discussed by Scherer *et al.* (2003) and Hendel *et al.* (2005), it has been shown that it, at least, does not lower the learning effect (Hendel *et al.*, 2005).

This olfactory learning regime revealed that constitutive and pan-neuronal expression of a gene coding for a dominant-negative form of EGFR strongly reduces olfactory learning in larvae. To exclude that this reduction of EGFR signaling impaired not just the larval abilities to taste or smell, behavioral control experiments were performed. These control experiments clearly showed normal responses to the to-be-associated stimuli. This indicates that the observed learning phenotype depends on central rather than sensory defects. Moreover, using the inducible, mifepristone-dependent GeneSwitch system, it could be demonstrated that this learning phenotype resulted from impaired EGFR signaling in the functional brain and not from developmental defects caused by impaired signaling during embryogenesis. Interestingly, silencing of each of the EGFR ligand genes *spitz*, *keren*, and *vein* at larval stages as well as enhanced EGFR signaling via expression of *secreted-spitz* led to a dramatic decrease of olfactory learning ability but did not influence the responses to the used tastes or smells. By performing learning experiments with induced and uninduced control larvae, it was excluded that mifepristone feeding itself affected larval learning skills.

The most important result of these learning experiments is the finding that proper EGFR signaling is essential for olfactory learning in *Drosophila*, particularly with regard to a limited number of known non-developmental functions of EGFR signaling in the larval brain.

A link between EGFR and signaling systems associated with learning was also recently established. Notably, Hannan *et al.* (2006) connected EGFR signaling to a novel adenylyl cyclase (AC) neurofibromin 1 (NF1)/Ras-dependent pathway in the *Drosophila* brain. In their *ex vivo* experiments, AC activity was stimulated by rodent growth factors in dissected larval brains. In hypomorphic EGFR mutant larvae, AC

activity was not stimulated by growth factors. They assume binding of the growth factors to EGFR to activate an as yet unidentified AC (Fig. 82).

Furthermore, the pathway is assumed to constitute an alternative to the Rutabaga AC-mediated pathway in the brain, with both leading to cAMP/PKA signaling, which is in turn a major component associated with short-term memory formation (Blum *et al.*, 2009).

These findings imply that EGFR signaling acts upstream of cAMP/PKA and thus regulates olfactory learning via an alternative AC. Moreover, attenuated as well as enhanced PKA signaling has been reported to reduce learning ability in flies (Drain *et al.*, 1991), which is consistent with the observation that the correct balance of EGFR signaling in the brain is important for memory formation. My results support the hypothesis of Hannan *et al.* (2006) *in vivo*. Moreover, I revealed that the ligands Spitz, Keren, and Vein are necessary to trigger EGFR signaling.

Why all three EGFR ligands are essential for proper olfactory learning is not yet understood. One possible explanation is that signaling via all ligands is necessary to maintain the proper signaling balance essential for olfactory learning. Alternatively, the system may not be organized in such a manner that different ligands can be functionally exchanged.

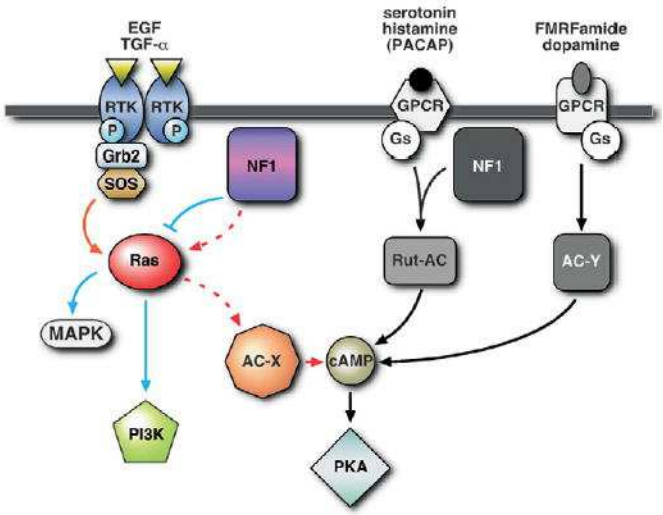

Fig. 82. *Drosophila* pathways involved in learning. Activation of cyclic adenosine monophosphate (cAMP)/protein kinase A (PKA) signaling by three different pathways. (1) Growth factors like transforming growth factor α (TGF-α) or epidermal growth factor (EGF) bind a receptor tyrosine kinase (RTK) and cAMP/PKA signaling via an unidentified adenylyl cyclase X (AC-X). (2) Pituitary AC activating polypeptide neuropeptides (PACAP) like serotonin and histamine or (3) Phe-Met-Arg-Phe-amide (FMRFamide) and dopamine bind G protein-coupled receptors (GPCR) and activate cAMP/PKA signaling via (2) Rutabaga-AC (Rut-AC) or (3) an unidentified AC (AC-Y). Gs, G protein subunit α_s; Grb2, growth factor receptor binding protein 2; MAPK, mitogen-activated protein kinase; PI3K, phosphatidylinositol 3-kinase; Ras, rat sarcoma; SOS, son of sevenless. Modified from Hannan *et al.* (2006).

Based on the promoter activity patterns observed for *egfr* and all ligand genes, different modes of signaling are possible. During *Drosophila* brain development, axonal structures are thought to release Spitz to activate the EGFR pathway in glial cells to promote cell survival (Bergmann *et al.*, 2002). Another EGFR ligand, Vein, is produced by pioneer neurons and is required for the survival of longitudinal glia (Hidalgo *et al.*, 2001). My observations further suggest an alternative signaling system. Because all components of the EGFR signaling system are present in the MBs, autocrine or paracrine modes of signaling are possible. Autocrine EGFR signaling is relevant to various systems ranging from epithelial mechanotransduction (Kojic *et al.*, 2010) to brain tumor development (Tang *et al.*, 1997). Expression of a gene coding for a dominant-negative EGFR in neurons impaired learning. Furthermore, *argos* promoter activity was detected in the MBs. *Argos* is a gene, which is known to be a transcriptional target of EGFR signaling and is part of a negative feedback loop (Golembo *et al.*, 1996). These findings suggest that EGFR signaling directly in the MB neurons is needed for proper learning. But nevertheless, EGFR ligands are secreted and silencing or overexpression of them in neurons might affect not only signaling in these cells. Thus, proper autocrine and paracrine EGFR signaling within the Kenyon cells of the MBs may be required to maintain a cellular homeostasis, necessary for olfactory learning.

The present findings suggest that holding a fine tuned homeostatic balance in the cells of the MBs is critical for proper learning. Furthermore, signaling systems such as the EGFR pathway that may not be directly involved in transmitting learning related content may nevertheless be essential to enable learning.

In vertebrates, dysregulation of EGFR signaling has been linked to neurodegenerative diseases. In several cases, reduced EGFR signaling was connected to worsening effects. In Parkinson patients, low levels of plasma EGF correlated with poor cognitive abilities. Inhibition of EGFR signaling via leucine-rich repeat and Ig domain containing 1 (LINGO-1) is involved in the inhibition of axonal growth, disturbance of oligodendrocyte differentiation and myelination, as well as the survival of neuron (Inoue *et al.*, 2007; Zhou *et al.*, 2012). In rodent brains, signaling via the ligand neuregulin-1 inhibits motor neurons from apoptosis (Ricart *et al.*, 2006) and induces the survival of spiral ganglion neurons (Stankovic *et al.*, 2004). Also after ischemia, EGFR signaling has exhibited neuroprotective functions (Li *et al.*, 2007; Shyu *et al.*, 2004). Aguirre *et al.* (2007) demonstrated that overexpression of human

EGFR in mice has a beneficial influence on remyelination, a process important in multiple sclerosis. Furthermore, the results of Scalabrino *et al.* (2010) indicated that decreased EGF levels in the cerebrospinal fluid of multiple sclerosis patients may be one factor impending regeneration of nerve's myelin sheath. Moreover, chronic activation of MAPK, which is part of the downstream signaling cascade of EGFR, plays a role in the mechanisms that trigger neurodegeneration (Colucci-D'Amato *et al.*, 2003).

Recently, Woo *et al.* (2011) have found higher immunoreactivities of ErbB4 and phospho-ErbB4 in the brains of Alzheimer patients compared to age-matched controls. They suggest that upregulation of ErbB4 immunoreactivity may be involved in the progression of Alzheimer's pathology but also debate neuroprotective functions of EGFR signaling. This study clearly demonstrates that the advantageous or disadvantageous function of EGFR signaling has to be discussed on a case-by-case basis.

Impairments in learning and memory are the initial symptoms of Alzheimer's disease (Arshavsky, 2010) but also known manifestations of Parkinson's disease (Poletti *et al.*, 2012) and multiple sclerosis (Gunduz *et al.*, 2012). Thus, investigation of learning defects and their triggers in *Drosophila* may serve as a good model for the study of human neurodegenerative diseases.

The results of the olfactory learning experiments with *Drosophila* larvae showed that reduced EGFR signaling in the CNS leads to impairment in learning. This observation is in line with the above mentioned findings that decreased EGFR signaling in mammals has negative effects on cognition and on the maintenance of CNS integrity. Moreover, enhanced EGFR signaling reduced learning abilities in *Drosophila*. This finding fits into the concept of Colucci-D'Amato *et al.* (2003), who postulated negative effects of chronically activated MAPK, and to the suggestion of Woo *et al.* (2011) that increased ErbB4 immunoreactivity leads to Alzheimer-pathology progression.

The outcomes of this study support the assumptions that a specific level of EGFR signaling is necessary for the maintenance of normal CNS functions but also clearly demonstrate that enhanced signaling disturbs regular brain physiology.

5.2.2 Activity and Sleep Rhythms

Foltenyi *et al.* (2007) have shown that EGFR signaling is involved in the regulation of sleep in adult *Drosophila*. Heat-shock induced expression of *rhomboid-1* and *star* resulted in increased sleep levels, whereas constitutive and pan-neuronal expression of a gene coding for a dominant-negative form of Rhomboid resulted in decreased sleep levels and low locomotor activity.

My study included the investigation of promoter activity patterns of genes coding for the ligands Spitz, Keren, and Vein in adult brains. The *spitz*-reporter lines indicated promoter activity in three distinct regions of the adult *Drosophila* brain that are related to locomotor activity and sleep rhythms. In particular, these regions were the CC (Strauss and Heisenberg, 1993) and the cells of the PI (Belgacem and Martin, 2002), which are either associated with locomotor activity as well as the MBs, which are dedicated to both locomotor activity (Helfrich-Forster *et al.*, 2002) and sleep rhythms (Joiner *et al.*, 2006; Pitman *et al.*, 2006). Furthermore, *Keren* and *vein* promoter activity was detectable in the MBs and in cells of the PI, respectively.

Locomotor activity and sleep levels were analyzed in flies constitutively and pan-neuronally expressing *spitz*^{RNAi}, *keren*^{RNAi}, or *vein*^{RNAi}. Because some of the *spitz*^{RNAi} expressing flies had crippled wings, the influence of the silencing of *spitz* was investigated in two groups separating flies with crippled wings and flies with normal wings. Possibly, that there is a simple yes-or-no situation for proper development of the wings at a certain point of development, at which a certain minimum level of *spitz* expression is needed. In some of the *spitz*^{RNAi} expressing flies, *spitz* expression levels might still be sufficient for normal wing development and in the others not. The latter flies then would have the crippled-wing phenotype. Maybe this point of separation also influences circadian rhythms in these flies.

Notably, both *spitz*^{RNAi} expressing flies with crippled wings and *spitz*^{RNAi} expressing flies with normal wings did not differ in their total daytime activity from the controls. This shows that the crippled wings phenotype does not generally affect the locomotor activity measured in this assay. However, during nighttime, the activity levels of both *spitz*^{RNAi} expressing phenotypes were lower compared to control flies. Considering the unchanged activity level during the day, decreased activity levels during the night point at defects in circadian rhythm rather than in locomotor defects. Moreover, the analysis of activity in the course of the day revealed that only *spitz*^{RNAi} expressing

flies with crippled wings lack the activity peak at evening light switch, whereas flies with normal wings show the typical increase in activity at that time.

Keren^{RNAi} expressing flies had a higher daytime activity but did not differ from their control in nighttime activity. In the course of the day, significantly lower activity levels before the morning light switch were revealed.

Vein^{RNAi} expressing flies did neither differ in daytime nor in nighttime activity from their controls. Nevertheless, they showed higher activity levels after the morning light switch and at evening light switch.

Analyzing sleep levels at daytime and nighttime revealed even greater differences between ligand^{RNAi} expressing flies and controls. Flies expressing *spitz*^{RNAi} with crippled wings had higher sleep levels during the day and during the night, whereas *spitz*^{RNAi} expressing flies with normal wings did not differ significantly in daytime sleep from their controls but also had higher sleep levels during nighttime. Notably, *spitz*^{RNAi} expressing flies with crippled wings had a normal daytime activity but higher daytime sleep. Again, this points at defects beyond impairment in locomotor activity. The altered sleep levels of *spitz*^{RNAi} flies with normal wings support this assumption as they lack the disability of crippled wings and are not affected by morphological changes.

Monitoring of sleep in the course of the day revealed a totally different sleep pattern of *spitz*^{RNAi} flies with crippled wings compared to controls. The typical decrease in sleep levels was neither detectable at morning light switch nor at evening light switch. Hence, the sleep levels of *spitz*^{RNAi} flies with crippled wings did not show a circadian rhythm at all. This was different in *spitz*^{RNAi} flies with normal wings. They had a sleep pattern in the course of the day comparable to control flies but with higher sleep levels after morning and evening light switch.

Both *keren*^{RNAi} and *vein*^{RNAi} expressing flies showed lower daytime sleep but unchanged sleep levels during the night. Despite unaltered nighttime sleep, analyses of sleep in the course of the day depicted higher sleep levels before morning light switches in both genotypes compared to control flies.

The analyses of daytime and nighttime activity as wells as daytime and nighttime sleep revealed that *spitz*^{RNAi} expressing flies with crippled and with normal wings showed the same tendencies in activity and sleep levels, whereas *vein*^{RNAi} and *keren*^{RNAi} expressing flies showed mostly the opposite behaviors. These results demonstrate that silencing of different ligands leads to diverse activity and sleep

phenotypes. Furthermore, the ligands Keren and Vein seem to be necessary for similar or even the same physiological process.

Moreover, the vertical locomotor capacity of *spitz*^{RNAi} expressing flies with crippled wings and with normal wings as well as of flies expressing *keren*^{RNAi} or *vein*^{RNAi} was monitored in the geotaxis assay. This experiment revealed that only flies expressing *spitz*^{RNAi} with crippled wings had significant defects in their vertical movement abilities. The crippled wings obviously impaired the skills for moving against gravity. This finding supports the assumption that silencing of the ligand controls rather circadian rhythms than merely locomotor skills since *spitz*^{RNAi} expressing flies with normal wings as well as *keren*^{RNAi} or *vein*^{RNAi} expressing flies had no vertical locomotor defects.

Strikingly, the results of sleep analysis with *rhomboid*^{DN} expressing flies of Foltenyi *et al.* (2007) are in line with the sleep phenotypes of *keren*^{RNAi} or *vein*^{RNAi} expressing flies. On the contrary, Foltenyi *et al.* (2007) reported an abnormally low locomotor activity what fits to the activity phenotypes of *spitz*^{RNAi} expressing flies. Notably, reduction of EGFR signaling via expression of *rhomboid*^{DN} only targets the availability of Spitz and Keren that have to be proteolytically cleaved by Rhomboid, whereas Vein is produced as a secreted protein. Thus, the phenotype of *rhomboid*^{DN} expressing flies possibly displays the sum of the phenotypes of *spitz*^{RNAi} and *keren*^{RNAi} expressing flies.

My results also suggest that a balance between different ligands is important to maintain circadian rhythms because silencing of each one of them resulted in reduced or enhanced activity or sleep levels.

Foltenyi *et al.* (2007) tried to elute the location of EGFR signaling in the fly's brain. For that they used immunohistochemical staining of phosphorylated MAPK in flies overexpressing *rhomboid* and *star* (Fig. 83 h). Staining was detected in an axonal tract that projects through the dorsal protocerebrum and median bundle into the tritocerebrum.

Expression of *rhomboid* was investigated using *rhomboid in situ* hybridization and anti-Rhomboid antibody (Fig. 83 d–g). Furthermore, they used different *gal4*-lines to drive *rhomboid*^{DN} expression and compared the expression patterns of the *gal4*-lines, which altered sleep patterns, when crossed to UAS-*rhomboid*^{DN}. All of these lines drove expression in cells of the PI, which project into the tritocerebrum (Fig. 83 a–c and h). They suggest that EGFR ligands are proteolytically processed in the PI by

Rhomboid and Star. Subsequently, the secreted ligands activate EGFR in the tritocerebrum, leading to the phosphorylation of MAPK in this region. Thus, the PI and the tritocerebrum are predicted to be involved in the regulation of sleep. Previously, only the MBs have been correlated with this process (Joiner *et al.*, 2006; Pitman *et al.*, 2006), whereas the PI has been linked to differences in locomotor activity between female and male flies (Belgacem and Martin, 2002).

Notably, all these results are in line with the promoter activity patterns observed in the reporter lines used in my study. *Spitz* promoter activity was detected in the MBs, cells of the PI, and neurons of the tritocerebrum, whereas *keren* and *vein* promoter activity was detected in the MBs and the PI, respectively. Promoter activity of *spitz* and *vein* in the PI and the influence of silencing of these ligands on sleep rhythm support the proposition that this region is actually involved in sleep regulation.

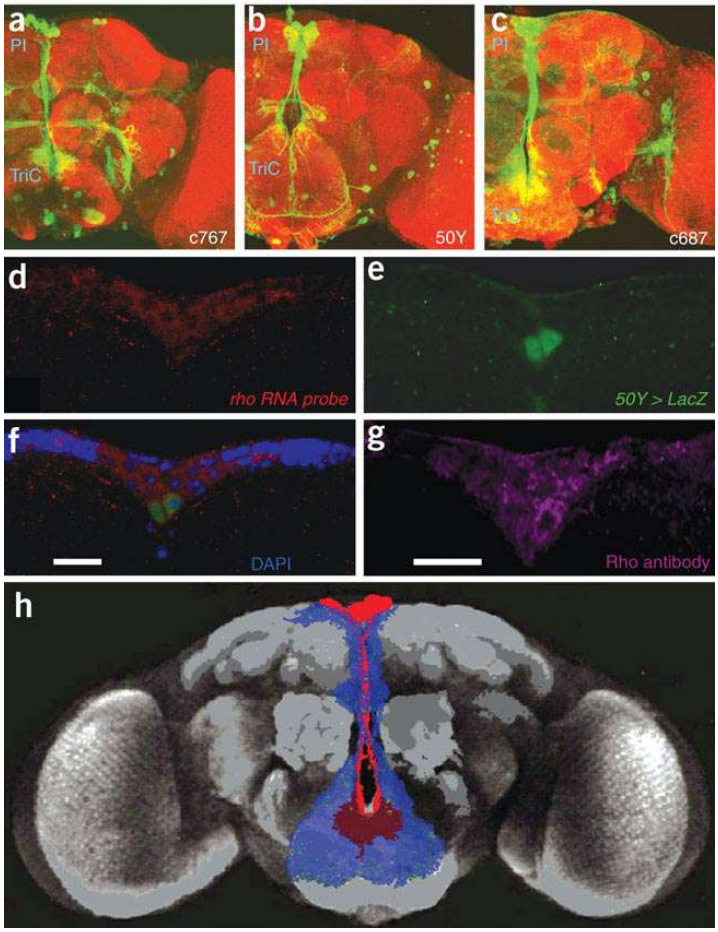

Fig. 83. *Rhomboid* expression in the pars intercerebralis (PI). (a-c) Expression patterns of the Gal4-lines c767-*gal4*, 50Y-*gal4*, and c687-*gal4* visualized using UAS-mCD8::GFP (membrane-bound GFP; green). All three lines drive expression in cells of the pars intercerebralis (PI) with axons innervating the tritocerebrum (TriC). Staining with the anti-nc82 antibody (red) was used as a reference for brain morphology. (d-f) PI of a 50Y-*gal4* > UAS-LacZ fly co-stained with (d) rhomboid (rho) antisense RNA probe (red) and (e) β galactosidase immunohistochemistry (green). (f) Merge of (d) and (e) with DAPI staining of the nuclei. (g) PI of w^{1118} fly's brain stained with anti-rhomboid antibody (violet). (h) Composite false-colored assembled image of the expression pattern of c767-*gal4* > UAS- mCD8::GFP (red) and staining of dually phosphorylated MAPK in response to *rhomboid* and *star* overexpression (blue) overlaid onto an image of a whole mount *Drosophila* brain. Scale bar = 20 µm. Modified from Foltenyi *et al.* (2007).

Interestingly, the PI is the developmental equivalent to the mammalian hypothalamic-pituitary axis (de Velasco *et al.*, 2007), whereby the hypothalamus is a major center for the control of sleep and wakefulness (Saper *et al.*, 2001). In particular, a small region of the hypothalamus, the suprachiasmatic nucleus (SCN) is known for regulation of circadian rhythms. Kramer *et al.* (2003) showed that EGFR signaling in the SCN of mice regulates circadian rhythms. Furthermore, the ligand TGF α has been revealed as an SCN locomotor inhibitor factor and a hypomorphic EGFR mutation exhibited excessive daytime locomotor activity. Notably, these results from mice with reduced EGFR signaling do not fit to the findings in flies of Foltenyi *et al.* (2007), in which reduced EGFR signaling led to lower locomotor activity. However, in my studies, *keren*^{RNAi} expressing flies had higher daytime locomotor activity. Hence, Keren is not only a structural but also a functional TGF α homologue that shares the role of an inhibitor of locomotion.

On the contrary, Kushikata *et al.* (1998) found that exogenous EGF enhanced spontaneous sleep in rabbits. In turn, this result is in line with increased sleep in flies with enhanced EGFR signaling in flies (Foltenyi *et al.*, 2007). Furthermore, this effect is *vice versa* comparable to the decreased daytime sleep in flies with reduced EGFR signaling via silencing of *keren* or *vein*.

Compared to mammals, flies do not only have morphologically similar brains, they also exhibit many of the behavioral characteristic of sleep (Cirelli, 2009). They have a peak of activity in the morning, when the lights are switched on, and in the evening, when the lights are switched off. In the afternoon and during the night they are relatively inactive. In addition, the effects of caffeine (Andretic *et al.*, 2008) and of sleep-inducing drugs (Pandey and Nichols, 2011) are the same as in mammals. Since sleep disturbances are a widespread problem and also a symptom of many neurological diseases like Parkinson's disease and Alzheimer's disease (Aritake *et al.*, 2007), studying the basis of sleep regulation is of fundamental importance. Notably, *Drosophila* has already served as a model for the investigation of sleep disturbances in Huntington's disease (Gonzales and Yin, 2010). The results of the activity and sleep monitoring with silencing of three different EGFR ligands may point at diverse functions of single EGFR ligands in the regulation of circadian rhythms in general.

5.3 EGFR Signaling in the Adult Fat Body

Promoter activity of *egfr*, *spitz*, *keren*, and *argos* and RNA of all tested EGFR pathway components was detected in the adult abdominal fat body organ. Fat body RNA was isolated after reduction of EGFR signaling in this organ. This RNA was used for the investigation of the transcriptome via microarray analysis that revealed a possible involvement of the pathway in immune response, energy metabolism, and biomembrane synthesis.

In further analyses, the influence of reduced and enhanced EGFR signaling in the fat body on AMP production and on energy storage was investigated.

For all fat body-specific experiments, the GeneSwitch system was applied to induce reduction or enhancement of EGFR signaling in adult flies because constitutive expression of $egfr^{DN}$ or $egfr^{ACT}$ were lethal at latest during pupal stage. For the transcriptional analysis, expression of a gene coding for a dominant-negative EGFR was induced for 24 h. Upregulated or downregulated genes in experimental flies, which were also regulated in mifepristone-fed control flies, were excluded from further analysis. The high number of regulated genes in the controls was based on the fact that the results were generated using one microarray. Three experiments have been performed with RNA of fat bodies from experimental flies and only genes that were upregulated or downregulated in two of three experiments were included in the analysis.

Among the regulated genes, several ones were connected to the defense against bacteria. To investigate this further, AMP expression was analyzed in flies with reduced or enhanced EGFR signaling in the fat body using qRT-PCR. To monitor the effect of the inducing agent on AMP expression, control flies were also fed with mifepristone.

Notably, expression of AMPs was strongly regulated in control flies fed with mifepristone. Furthermore, no distinct upregulation or downregulation of one of the AMPs was detected in the flies with reduced or enhanced EGFR signaling.

The effect of mifepristone feeding on AMP expression in control flies and the high variability between the biological replicates did not allow the drawing of a conclusion about the influence of EGFR signaling on AMP expression.

However, several of the regulated genes after reduction of EGFR signaling are related to the glycerophospholipid metabolism. Since glycerophospholipid is the major component of biological membranes, this may point at an involvement of

EGFR signaling in biomembrane synthesis. Strikingly, the glycerophosphatase oxidase-1 has a glycerol-3-phosphate dehydrogenase activity that catalyzes the reduction of dihydroxyacetone phosphate to glycerin-3-phosphate. Furthermore, Dmel CG10133 is also related to glycerin-3-phosphate production. Glycerin-3-phosphate is the substrate for glycerophospholipid synthesis and also the base material for the synthesis of TAGs. Moreover, several genes connected to energy metabolism were regulated (Tab. 10). Thus, a role of EGFR signaling in the synthesis of biological membranes and/or in the energy homeostasis is possible. The latter was investigated using two different fat content determination methods. The lipophilic fluorescent dye BODIPY (493/503) specifically stains neutral lipids, which includes TAGs, cholesteryl esters, and fatty acids, whereas the CCA is used to measure only the TAG content (Hildebrandt *et al.*, 2011).

Semi-quantitative analysis using BODIPY (493/503) revealed a tendency for a lower fat content of female and male flies with enhanced EGFR signaling in the fat body for seven days compared to control flies. The fat content of female and male flies with reduced EGFR signaling in the fat body for seven days did not differ from that of control flies.

Quantitative measurement using CCA was applied to confirm the results of the BODIPY (493/503) staining in females. No significant difference was found in $egfr^{DN}$ expressing flies but $egfr^{ACT}$ expressing females had significantly lower TAG contents. These results were consistent with the findings of the BODIPY (493/503) staining.

TAGs are the major energy reserve and the main component of cellular lipid droplets. They are accumulated in periods of food abundance and are used as reserves, when no food is available (Arrese and Soulages, 2010). Mobilization of TAGs is regulated by the adipokinetic hormone, which is produced by the *corpora cardiaca* (Gade and Auerswald, 2003). This mobilization occurs for example during starvation. The lower fat contents observed in flies with enhanced EGFR signaling in the fat body may lead to problems during starvation. Hence, survival assays under starved conditions with these mutants were performed and actually revealed an impaired starvation resistance in female flies expressing $egfr^{ACT}$ compared to control flies, whereas starvation resistance of male flies expressing $egfr^{ACT}$ and of both female and male flies expressing $egfr^{DN}$ did not differ significantly from control flies. The gender-specific difference between female and male flies expressing $egfr^{ACT}$ may result from

higher energy storage needs of females due to egg production (Parisi *et al.*, 2011). Thus, starvation phenotypes might be easier detectable in females.

Changes in the starving resistance may have different reasons (Rion and Kawecki, 2007). The most common strategy is the presence of greater or lower energy reserves, in particular lipid stores, already at the starting point of the starvation. Another but equivocal mechanism for enhanced starvation resistance is a greater efficiency of using metabolic reserves.

Both fat content determination methods showed reduced fat stores in female flies with enhanced EGFR signaling in the fat body after seven days. As expression of *egfr*^{ACT} was induced 24 h before the start of the survival assay under starved conditions, this might already cause lower fat contents at the starting point of starvation. Thus, lower fat contents at the beginning of starvation might be the reason for the reduced starvation resistance. Therefore, the results of the fat content determination and the survival assay under starved condition are in line.

Fat content determination was analyzed after seven days of enhanced EGFR signaling and at that timepoint a decrease in fat stores was detectable. A continuous reduction of fat was expected to occur during the starvation. Strikingly, this reduction of fat does not make energy reserves available for the flies to survive the time of starvation. This leads to the suggestion that enhanced EGFR signaling decreases the amount of fat but is not involved in the mobilization and utilization process, in a way that makes energy more accessible for the fly.

5.4 Promoter Activity Patterns of EGFR Pathway Component Genes in the Digestive System

The promoter activity patterns of EGFR signaling pathway components in larval and adult digestive systems were investigated in detail. Compared to the expression analyses of Jiang and Edgar (2009), Buchon *et al.* (2010), and Jiang *et al.* (2011), I found several new expression sites of EGFR pathway components in the larval and adult digestive tract (Tab. 12).

Tab. 12. Comparison of promoter activity patterns of EGFR pathway components detected with the *promoter-reporter* lines and published expression data.

gene	larvae		adult flies	
	promoter activity	expression	promoter activity	expression
egfr	AMPs[1] ECs[2]			
spitz	AMPs[1] ECs[2]	AMPs[3]	EEs[1] ECs[2]	precursor cells[6,7] ECs[8]
keren	ECs[1,2]	AMPs[4]	ECs[1,2]	precursor cells[9] ECs[10]
vein	EEs[1]	VM[5]	EEs[1] ECs[1]	VM[11,12] ECs[13]
argos	ECs[1]		ISCs[1] ECs[1]	

[1], in the midgut; [2], in the hindgut; [3], Jiang and Edgar (2009): microscopic analysis of *spitz-enhancer-trap-gal4* > UAS-*gfp* and *spitz in situ* hybridization; [4], Jiang and Edgar (2009): *keren in situ* hybridization; [5], Jiang and Edgar (2009): microscopic analysis of *vein-lacz*; [6], Buchon *et al.* (2010): microscopic analysis of *spitz-enhancer-trap-gal4* > UAS-*gfp* and silencing of *spitz* in precursor cells blocked infection-induced proliferation; [7], Jiang *et al.* (2011): microscopic analysis of *spitz-enhancer-trap-gal4* > UAS-*gfp*; [8], Jiang *et al.* (2011): microscopic analysis of *spitz-enhancer-trap-gal4* > UAS-*gfp*; [9], Buchon *et al.* (2010): silencing of *keren* in precursor cells blocked infection-induced proliferation; [10], Jiang *et al.* (2011): *keren in situ* hybridization; [11], Buchon *et al.* (2010): microscopic analysis of *vein-lacz* (after bacterial infection); [12], Jiang *et al.* (2011): *vein in situ* hybridization (in uninfected controls and after bacterial infection in regenerating posterior midguts); [13], Jiang *et al.* (2011): *vein-lacz* (after ectopic activation of JNK signaling). AMPs, adult midgut progenitor cells; ECs, enterocytes; EEs, enteroendocrine cells; ISC, intestinal stem cells; precursor cells, stem cells and enteroblasts; VM, visceral muscle.

No expression data have been published for *egfr* since no reporter line has been available. Analyses of *prom-egfr-gal4* > UAS-*gfp* showed promoter activity of *egfr* in larval adult midgut progenitor cells. This finding confirmed the results of Jiang and Edgar (2009), who detected phosphorylated MAPK via immunostaining in these cells. As MAPK is a downstream component of EGFR and is phosphorylated upon activation of EGFR, phosphorylated MAPK points at EGFR signaling activity in adult midgut progenitor cells. But nevertheless, expression or promoter activity of *egfr* has not been shown in these cells.

Promoter activity of *keren* and *egfr* was detected in ECs in the larval midgut. In adult flies, Buchon *et al.* (2010) have shown that reduced or enhanced EGFR signaling via expression of a mutated receptor or via expression of secreted *keren* in ECs influenced EC shape and EC delamination. Promoter activity of *egfr* and *keren* in larval ECs might point at the fact that EGFR signaling has the same roles in larvae that it has in adult flies, i.e. EC shaping and EC delamination.

Jiang and Edgar (2009) have published that *vein* promotes adult midgut progenitor cell proliferation although it is produced in the visceral muscle of larval midguts. In this study, *vein* promoter activity was detected in larval EEs. I surmise that expression of this ligand in these cells also serves as a paracrine enhancer of adult

midgut progenitor proliferation but an additional function of EGFR signaling in the larval midgut is conceivable.

Jiang *et al.* (2011) have demonstrated that induced expression of *s-spitz* or *vein* in adult visceral muscles, ECs, or precursor cells promotes proliferation of ISCs. Here, I found promoter activity of *spitz* and *vein* in another adult cell type, the EEs. As EGFR signaling has not been manipulated in these cells (Buchon *et al.*, 2010; Jiang *et al.*, 2011), the functions of *spitz* and *vein* expression in adult EEs are unknown. Possibly, it may also serve as paracrine enhancement of ISC proliferation but, as speculated for larvae, expression in EEs might have other roles.

Notably, I could verify the expression of *keren* in adult ECs reported by Jiang *et al.* (2011) using the respective generated promoter-reporter line. As Buchon *et al.* (2010) have reported, EGFR signaling in these cells is involved in EC shaping and EC delamination.

Furthermore, no expression data have been published for the inhibitory ligand *argos* because no reporter line has been available. Analyses of *prom-argos-gal4* > UAS-*gfp* indicated promoter activity in adult ECs and adult stem cells. As *argos* expression is a hint for high levels of EGFR activation (Golembo *et al.*, 1996), these results support the hypothesis of Buchon *et al.* (2010) that EGFR signaling happens in adult ECs and ISCs.

Notably, promoter activity of *spitz*, and *keren* was detected in ECs of the larval and adult hindgut. In addition, *egfr* promoter activity was found in the ECs of the hindguts of larvae. These locations of EGFR signaling have not been reporter and its functions in larval and adult hindguts have not been investigated. Possibly, EGFR signaling in this part of the digestive system is also involved in shaping, delamination, and anoikis of damaged ECs.

6 SUMMARY / ZUSAMMENFASSUNG

6.1 SUMMARY

The aim of this study was to reveal so-far unknown, non-developmental functions of epidermal growth factor receptor (EGFR) signaling in *Drosophila melanogaster*. As a basis for further functional analyses, I generated *promoter-gal4* lines for *egfr* and the ligands *spitz*, *keren*, *vein*, *gurken*, and *argos*. Using these lines, a mapping of promoter activity of EGFR pathway component genes was performed in in all main tissues of larvae and adult flies. Most interestingly, promoter activity was detected in larval and adult brains in neurons dedicated to visual and olfactory perception, learning, hormone production, locomotor activity, and sleep rhythms. Furthermore, fat bodies of adult flies showed promoter activity of several EGFR pathway component genes. Based on these findings, the functions of EGFR signaling in the larval and adult brain as well as in the adult fat body were investigated further.

Promoter activity of the *egfr* and all ligand genes was found in the larval mushroom bodies, which are known to be a higher brain center required for olfactory learning. I investigated the role of the EGFR pathway in this process by using different mutant larvae with reduced pan-neuronal EGFR signaling. Expression of a gene coding for a dominant-negative form of EGFR as well as silencing of the ligand genes via RNA interference were applied and resulted in significantly impaired olfactory learning performances. General defects in the ability to taste or smell as well as impaired EGFR signaling during embryonic development could be excluded as major reasons for this learning phenotype. In addition, expression of a gene coding for a constitutively active form of the ligand Spitz during larval stages also led to a significantly reduced learning ability. Thus, very low levels as well as very high levels of EGFR signaling in the larval brain are deleterious for olfactory learning and memory formation. I hypothesize that EGFR signaling in a certain range maintains a functioning homeostatic system in the mushroom bodies that is necessary for proper learning and memory. Notably, dysregulation of EGFR signaling has been controversially discussed in the context of human neurological disorders like Alzheimer’s disease and Parkinson’s disease that also have defects in learning as common manifestations. The results of this study may serve as new starting points for the in-depth investigation of EGFR signaling in neurological diseases.

In addition, I could show that constitutive silencing of single activating EGFR ligand genes (*spitz*, *keren*, or *vein*) in the brain resulted in differentially altered locomotor activity patterns and sleep rhythms of adult flies, pointing at an involvement of all three main ligands in circadian rhythms with specific functions of each one. A homeostasis between the different ligands seems essential for the maintenance of normal sleep and locomotor behavior in the course of the day.

Furthermore, an influence of EGFR signaling on the fat metabolism in adult flies was revealed. Enhanced pathway activity in the adult fat body resulted in lower fat contents in female flies and also reduced their starvation resistance. These results point at a role of EGFR signaling in fat storage and in particular fat mobilization.

In summary, I could show that EGFR signaling homeostasis in the larval brain is necessary for olfactory learning in *Drosophila* larvae and that a balance between the activating ligands is important for maintaining circadian rhythms in adult flies. Furthermore, a critical physiological function of EGFR signaling was shown in fat storage and starvation resistance.

6.2 ZUSAMMENFASSUNG

Das Ziel dieser Arbeit war es, bisher unbekannte und nicht-entwicklungsspezifische Funktionen des Epidermal Growth Factor Receptor (EGFR) Signalweges in *Drosophila melanogaster* aufzudecken. Als Ausgangspunkt für weiterführende funktionelle Analysen generierte ich *promotor-gal4*-Linien für das EGFR-Gen und die Ligandengene *spitz*, *keren*, *vein*, *gurken* und *argos.* Anschließend führte ich eine Kartierung der Promotoraktivität dieser Gene in larvalen und adulten Geweben durch, wobei insbesondere die Promotoraktivität in verschiedenen Neuronen von larvalen und adulten Gehirnen auffiel. Diese Neuronen sind unter anderem für ihre Rolle in Lernprozessen, bei der Wahrnehmung von visuellen und olfaktorischen Reizen, in der Hormonproduktion sowie bei der Steuerung von Bewegungsaktivität und Schlafrhythmus bekannt. Darüber hinaus wurde Promotoraktivität von verschiedenen Genen des EGFR-Signalweges im Fettkörper von adulten Fliegen gefunden. Basierend auf diesen Ergebnissen wurden die Funktionen des EGFR-Signalweges in larvalen und adulten Gehirnen sowie im adulten Fettkörper untersucht.

Besonders auffällig waren die Promotoraktivitäten des EGFR-Gens und allen Ligandengenen im larvalen Gehirnzentrum für olfaktorisches Lernen, den sogenannten Pilzkörpern. Daher analysierte ich das Lernverhalten von verschiedenen *Drosophila*-Mutanten mit verminderter pan-neuronaler Aktivität des EGFR-Signalweges. Sowohl die Expression eines Gens, das für eine dominant-negative Form des EGFR kodiert, als auch das *Silencing* der Ligandengene mittels RNA-Interferenz führten zu einer signifikant verringerten Lernfähigkeit der Larven. Eine direkte Beeinträchtigung der Fähigkeit zu schmecken oder zu riechen und entwicklungsbiologische Defekte, die möglicherweise durch eine verminderte Aktivität des EGFR-Signalweges während der Embryonalentwicklung hervorgerufen werden, konnten als Ursache für die beobachteten Effekte ausgeschlossen werden. Des Weiteren konnte gezeigt werden, dass auch die Aktivierung des EGFR-Signalweges mittels pan-neuronaler Expression eines Gens, das für eine konstitutiv aktive Form des Liganden Spitz kodiert, zu einer signifikant reduzierten Lernfähigkeit führt. Somit verringert sowohl eine sehr niedrige als auch eine sehr hohe Aktivität des EGFR-Signalweges im larvalen Gehirn die Lernkapazität dramatisch. Daher vermute ich, dass ein exaktes Maß an EGFR-Signalweg-Aktivierung für die Erhaltung eines funktionierenden Gleichgewichtssystems in den larvalen Pilzkörpern für effektives

Lernen notwendig ist. Bemerkenswerterweise wurde eine fehlgesteuerte Regulierung dieses Signalweges im Zusammenhang mit neurologischen Krankheiten wie Alzheimer und Parkinson, bei denen Lernprobleme als ein häufiges Symptom auftreten, bisher kontrovers diskutiert. Die Ergebnisse dieser Arbeit könnten einen neuen Ansatzpunkt für eine intensive Untersuchung des EGFR-Signalweges in Hinblick auf diese Krankheiten bieten.

Außerdem konnte ich zeigen, dass das konstitutive *Silencing* einzelner Ligandengene (*spitz*, *keren* oder *vein*) mittels RNA-Interferenz im Gehirn zu einer veränderten Bewegungsaktivität und zu einem gestörten Schlafrhythmus in adulten Fliegen führt. Dies deutet auf einen Einfluss der aktivierenden Liganden auf den circadianen Rhythmus hin, wobei jeder einzelne Ligand eine spezifische Funktion hat. Die richtige Balance der drei Liganden scheint essentiell für die Aufrechterhaltung des normalen Aktivitäts- und Schlafverhaltens zu sein.

In einem weiteren Projekt wurde in dieser Arbeit die Rolle des EGFR-Signalweges im Fettmetabolismus untersucht. Gesteigerte Aktivität des Signalweges im adulten Fettkörper führte sowohl zu einem reduzierten Fettgehalt in weiblichen Fliegen als auch zu einer verminderten Hungerresistenz. Diese Ergebnisse deuten auf eine Funktion des EGFR-Signalweges in der Regulierung von Fettspeicherung und Fettmobilisierung hin.

Zusammenfassend konnte ich zeigen, dass der EGFR-Signalweg eine wichtige Rolle bei der Erhaltung der Lernfähigkeit von Larven sowie bei der Fettspeicherung und Hungerresistenz von adulten Fliegen spielt. Außerdem muss ein Gleichgewicht zwischen einzelnen aktivierenden EGFR-Liganden im Gehirn bestehen, um den natürlichen circadianen Rhythmus bei adulten Fliegen beizubehalten.

7 REFERENCES

Aceves-Pina EO, Quinn WG (1979) Learning in normal and mutant *Drosophila* larvae. *Science* **206:** 93-96

Adams MD, Celniker SE, Holt RA, Evans CA, Gocayne JD, Amanatides PG, Scherer SE, Li PW, Hoskins RA, Galle RF, George RA, Lewis SE, Richards S, Ashburner M, Henderson SN, Sutton GG, Wortman JR, Yandell MD, Zhang Q, Chen LX, Brandon RC, Rogers YH, Blazej RG, Champe M, Pfeiffer BD, Wan KH, Doyle C, Baxter EG, Helt G, Nelson CR, Gabor GL, Abril JF, Agbayani A, An HJ, Andrews-Pfannkoch C, Baldwin D, Ballew RM, Basu A, Baxendale J, Bayraktaroglu L, Beasley EM, Beeson KY, Benos PV, Berman BP, Bhandari D, Bolshakov S, Borkova D, Botchan MR, Bouck J, Brokstein P, Brottier P, Burtis KC, Busam DA, Butler H, Cadieu E, Center A, Chandra I, Cherry JM, Cawley S, Dahlke C, Davenport LB, Davies P, de Pablos B, Delcher A, Deng Z, Mays AD, Dew I, Dietz SM, Dodson K, Doup LE, Downes M, Dugan-Rocha S, Dunkov BC, Dunn P, Durbin KJ, Evangelista CC, Ferraz C, Ferriera S, Fleischmann W, Fosler C, Gabrielian AE, Garg NS, Gelbart WM, Glasser K, Glodek A, Gong F, Gorrell JH, Gu Z, Guan P, Harris M, Harris NL, Harvey D, Heiman TJ, Hernandez JR, Houck J, Hostin D, Houston KA, Howland TJ, Wei MH, Ibegwam C, Jalali M, Kalush F, Karpen GH, Ke Z, Kennison JA, Ketchum KA, Kimmel BE, Kodira CD, Kraft C, Kravitz S, Kulp D, Lai Z, Lasko P, Lei Y, Levitsky AA, Li J, Li Z, Liang Y, Lin X, Liu X, Mattei B, McIntosh TC, McLeod MP, McPherson D, Merkulov G, Milshina NV, Mobarry C, Morris J, Moshrefi A, Mount SM, Moy M, Murphy B, Murphy L, Muzny DM, Nelson DL, Nelson DR, Nelson KA, Nixon K, Nusskern DR, Pacleb JM, Palazzolo M, Pittman GS, Pan S, Pollard J, Puri V, Reese MG, Reinert K, Remington K, Saunders RD, Scheeler F, Shen H, Shue BC, Siden-Kiamos I, Simpson M, Skupski MP, Smith T, Spier E, Spradling AC, Stapleton M, Strong R, Sun E, Svirskas R, Tector C, Turner R, Venter E, Wang AH, Wang X, Wang ZY, Wassarman DA, Weinstock GM, Weissenbach J, Williams SM, WoodageT, Worley KC, Wu D, Yang S, Yao QA, Ye J, Yeh RF, Zaveri JS, Zhan M, Zhang G, Zhao Q, Zheng L, Zheng XH, Zhong FN, Zhong W, Zhou X, Zhu S, Zhu X, Smith HO, Gibbs RA, Myers EW, Rubin GM, Venter JC (2000) The genome sequence of *Drosophila melanogaster*. *Science* **287:** 2185-2195

Aguirre A, Dupree JL, Mangin JM, Gallo V (2007) A functional role for EGFR signaling in myelination and remyelination. *Nat Neurosci* **10:** 990-1002

Akalal DB, Yu D, Davis RL (2010) A late-phase, long-term memory trace forms in the gamma neurons of *Drosophila* mushroom bodies after olfactory classical conditioning. *J Neurosci* **30:** 16699-16708

Andretic R, Kim YC, Jones FS, Han KA, Greenspan RJ (2008) *Drosophila* D1 dopamine receptor mediates caffeine-induced arousal. *Proc Natl Acad Sci U S A* **105:** 20392-20397

Aritake S, Enomoto M, Matsuura M (2007) Neurological diseases and sleep disturbances. *Nihon Yakurigaku Zasshi* **129:** 418-421

Arnulf I, Leu S, Oudiette D (2008a) Abnormal sleep and sleepiness in Parkinson's disease. *Curr Opin Neurol* **21:** 472-477

Arnulf I, Nielsen J, Lohmann E, Schiefer J, Wild E, Jennum P, Konofal E, Walker M, Oudiette D, Tabrizi S, Durr A (2008b) Rapid eye movement sleep disturbances in Huntington disease. *Arch Neurol* **65:** 482-488

Arrese EL, Soulages JL (2010) Insect fat body: energy, metabolism, and regulation. *Annu Rev Entomol* **55:** 207-225

Arshavsky YI (2010) Why Alzheimer's disease starts with a memory impairment: neurophysiological insight. *J Alzheimers Dis* **20:** 5-16

Bachmann A, Knust E (2008) The use of P-element transposons to generate transgenic flies. *Methods Mol Biol* **420:** 61-77

Baumann P, Skaer H (1993) The *Drosophila* EGF receptor homologue (DER) is required for Malpighian tubule development. *Dev Suppl***:** 65-75

Belgacem YH, Martin JR (2002) Neuroendocrine control of a sexually dimorphic behavior by a few neurons of the pars intercerebralis in *Drosophila*. *Proc Natl Acad Sci U S A* **99:** 15154-15158

Bender W, Spierer P, Hogness D (1979) Gene isolation by chromosomal walking. *J Supra Mol Struct* **8:** 32

Bergmann A, Tugentman M, Shilo BZ, Steller H (2002) Regulation of cell number by MAPK-dependent control of apoptosis: a mechanism for trophic survival signaling. *Dev Cell* **2:** 159-170

Blagburn JM, Bacon JP (2004) Control of central synaptic specificity in insect sensory neurons. *Annu Rev Neurosci* **27:** 29-51

Bloch Qazi MC, Heifetz Y, Wolfner MF (2003) The developments between gametogenesis and fertilization: ovulation and female sperm storage in *Drosophila melanogaster*. *Dev Biol* **256:** 195-211

Blum AL, Li W, Cressy M, Dubnau J (2009) Short- and long-term memory in *Drosophila* require cAMP signaling in distinct neuron types. *Curr Biol* **19:** 1341-1350

Bogdan S, Klämbt C (2001) Epidermal growth factor receptor signaling. *Curr Biol* **11:** R292-295

Brand AH, Perrimon N (1993) Targeted gene expression as a means of altering cell fates and generating dominant phenotypes. *Development* **118:** 401-415

Bridges CB (1914) Direct proof through non-disjunction that the sex-linked genes of *Drosophila* are borne by the X-chromosome. *Science* **40:** 107-109

Brown KE, Kerr M, Freeman M (2007) The EGFR ligands Spitz and Keren act cooperatively in the *Drosophila* eye. *Dev Biol* **307:** 105-113

Bublil EM, Yarden Y (2007) The EGF receptor family: spearheading a merger of signaling and therapeutics. *Curr Opin Cell Biol* **19:** 124-134

Buchon N, Broderick NA, Kuraishi T, Lemaitre B (2010) *Drosophila* EGFR pathway coordinates stem cell proliferation and gut remodeling following infection. *BMC Biol* **8:** 152

Buff E, Carmena A, Gisselbrecht S, Jimenez F, Michelson AM (1998) Signalling by the *Drosophila* epidermal growth factor receptor is required for the specification and diversification of embryonic muscle progenitors. *Development* **125:** 2075-2086

Busto GU, Cervantes-Sandoval I, Davis RL (2010) Olfactory learning in *Drosophila*. *Physiology (Bethesda)* **25:** 338-346

Cela C, Llimargas M (2006) Egfr is essential for maintaining epithelial integrity during tracheal remodelling in *Drosophila*. *Development* **133:** 3115-3125

Chen-Plotkin AS, Hu WT, Siderowf A, Weintraub D, Goldmann Gross R, Hurtig HI, Xie SX, Arnold SE, Grossman M, Clark CM, Shaw LM, McCluskey L, Elman L, Van Deerlin VM, Lee VM, Soares H, Trojanowski JQ (2011) Plasma epidermal growth factor levels predict cognitive decline in Parkinson disease. *Ann Neurol* **69:** 655-663

Ciardiello F, Tortora G (2008) EGFR antagonists in cancer treatment. *N Engl J Med* **358:** 1160-1174

Cirelli C (2009) The genetic and molecular regulation of sleep: from fruit flies to humans. *Nature Reviews Neuroscience* **10:** 549-560

Colucci-D'Amato L, Perrone-Capano C, di Porzio U (2003) Chronic activation of ERK and neurodegenerative diseases. *Bioessays* **25:** 1085-1095

Corl AB, Berger KH, Ophir-Shohat G, Gesch J, Simms JA, Bartlett SE, Heberlein U (2009) Happyhour, a Ste20 family kinase, implicates EGFR signaling in ethanol-induced behaviors. *Cell* **137:** 949-960

Das A, Sen S, Lichtneckert R, Okada R, Ito K, Rodrigues V, Reichert H (2008) *Drosophila* olfactory local interneurons and projection neurons derive from a common neuroblast lineage specified by the empty spiracles gene. *Neural Dev* **3:** 33

Davis RL (2004) Olfactory learning. *Neuron* **44:** 31-48

de Bruyne M, Clyne PJ, Carlson JR (1999) Odor coding in a model olfactory organ: the *Drosophila* maxillary palp. *J Neurosci* **19:** 4520-4532

de Velasco B, Erclik T, Shy D, Sclafani J, Lipshitz H, McInnes R, Hartenstein V (2007) Specification and development of the pars intercerebralis and pars lateralis, neuroendocrine command centers in the *Drosophila* brain. *Dev Biol* **302:** 309-323

Dhomen NS, Mariadason J, Tebbutt N, Scott AM (2012) Therapeutic targeting of the epidermal growth factor receptor in human cancer. *Crit Rev Oncog* **17:** 31-50

Dietzl G, Chen D, Schnorrer F, Su KC, Barinova Y, Fellner M, Gasser B, Kinsey K, Oppel S, Scheiblauer S, Couto A, Marra V, Keleman K, Dickson BJ (2007) A genome-wide transgenic RNAi library for conditional gene inactivation in *Drosophila*. *Nature* **448:** 151-156

Dragovich T, Campen C (2009) Anti-EGFR-targeted therapy for esophageal and gastric cancers: an evolving concept. *J Oncol* **2009:** 804108

Drain P, Folkers E, Quinn WG (1991) cAMP-dependent protein kinase and the disruption of learning in transgenic flies. *Neuron* **6:** 71-82

Dubnau J (2003) Neurogenetic dissection of conditioned behavior: evolution by analogy or homology? *J Neurogenet* **17:** 295-326

Dubnau J (2012) Neuroscience. Ode to the mushroom bodies. *Science* **335:** 664-665

Duchek P, Somogyi K, Jekely G, Beccari S, Rørth P (2001) Guidance of cell migration by the *Drosophila* PDGF/VEGF receptor. *Cell* **107:** 17-26

Dumstrei K, Nassif C, Abboud G, Aryai A, Aryai A, Hartenstein V (1998) EGFR signaling is required for the differentiation and maintenance of neural progenitors along the dorsal midline of the *Drosophila* embryonic head. *Development* **125:** 3417-3426

Enrique AA, Gema PC, Jeronimo JC, Auxiliadora GE (2012) Role of anti-EGFR target therapy in colorectal carcinoma. *Front Biosci (Elite Ed)* **4:** 12-22

Finelli A, Kelkar A, Song HJ, Yang H, Konsolaki M (2004) A model for studying Alzheimer's Abeta42-induced toxicity in *Drosophila melanogaster*. *Mol Cell Neurosci* **26:** 365-375

Fishilevich E, Domingos AI, Asahina K, Naef F, Vosshall LB, Louis M (2005) Chemotaxis behavior mediated by single larval olfactory neurons in *Drosophila*. *Curr Biol* **15:** 2086-2096

Fleck D, Garratt AN, Haass C, Willem M (2011) BACE1 dependent neuregulin proteolysis. *Curr Alzheimer Res*

Foltenyi K, Greenspan RJ, Newport JW (2007) Activation of EGFR and ERK by rhomboid signaling regulates the consolidation and maintenance of sleep in *Drosophila*. *Nat Neurosci* **10:** 1160-1167

Freeman M (1996) Reiterative use of the EGF receptor triggers differentiation of all cell types in the *Drosophila* eye. *Cell* **87:** 651-660

Gabay L, Scholz H, Golembo M, Klaes A, Shilo BZ, Klambt C (1996) EGF receptor signaling induces pointed P1 transcription and inactivates Yan protein in the *Drosophila* embryonic ventral ectoderm. *Development* **122:** 3355-3362

Gade G, Auerswald L (2003) Mode of action of neuropeptides from the adipokinetic hormone family. *Gen Comp Endocrinol* **132:** 10-20

Gagnon JF, Petit D, Latreille V, Montplaisir J (2008) Neurobiology of sleep disturbances in neurodegenerative disorders. *Current Pharmaceutical Design* **14:** 3430-3445

Gao S, Takemura SY, Ting CY, Huang S, Lu Z, Luan H, Rister J, Thum AS, Yang M, Hong ST, Wang JW, Odenwald WF, White BH, Meinertzhagen IA, Lee CH (2008) The neural substrate of spectral preference in *Drosophila*. *Neuron* **60:** 328-342

Geiger JA, Carvalho L, Campos I, Santos AC, Jacinto A (2011) Hole-in-one mutant phenotypes link EGFR/ERK signaling to epithelial tissue repair in *Drosophila*. *PLoS One* **6:** e28349

Geminard C, Rulifson EJ, Leopold P (2009) Remote control of insulin secretion by fat cells in *Drosophila*. *Cell Metab* **10:** 199-207

Gervasi N, Tchenio P, Preat T (2010) PKA dynamics in a *Drosophila* learning center: coincidence detection by rutabaga adenylyl cyclase and spatial regulation by dunce phosphodiesterase. *Neuron* **65:** 516-529

Golembo M, Schweitzer R, Freeman M, Shilo BZ (1996) Argos transcription is induced by the *Drosophila* EGF receptor pathway to form an inhibitory feedback loop. *Development* **122:** 223-230

Gonzales E, Yin J (2010) *Drosophila* models of Huntington's disease exhibit sleep abnormalities. *PLoS Curr* **2**

Gordon MD, Scott K (2009) Motor control in a *Drosophila* taste circuit. *Neuron* **61:** 373-384

Gunduz T, Emir O, Kurtuncu M, Mutlu M, Tumac A, Akca S, Coban O, Bahar S, Oktem-Tanor O, Tuzun E, Eraksoy M, Gurvit H, Akman-Demir G (2012) Cognitive impairment in Neuro-Behcet's disease and Multiple Sclerosis: a comparative study. *Int J Neurosci*

Gutierrez E, Wiggins D, Fielding B, Gould AP (2007) Specialized hepatocyte-like cells regulate *Drosophila* lipid metabolism. *Nature* **445:** 275-280

Hanesch U, Fischbach KF, Heisenberg M (1989) Neuronal architecture of the central complex in *Drosophila melanogaster*. *Cell Tissue Res* **257:** 343-366

Hannan F, Ho I, Tong JJ, Zhu Y, Nurnberg P, Zhong Y (2006) Effect of neurofibromatosis type I mutations on a novel pathway for adenylyl cyclase activation requiring neurofibromin and Ras. *Hum Mol Genet* **15:** 1087-1098

Harrison PJ, Law AJ (2006) Neuregulin 1 and schizophrenia: genetics, gene expression, and neurobiology. *Biol Psychiatry* **60:** 132-140

Hartenstein V (1993) *Atlas of Drosophila development*: Cold Spring Harbor Laboratory Press.

Heisenberg M, Borst A, Wagner S, Byers D (1985) *Drosophila* mushroom body mutants are deficient in olfactory learning. *J Neurogenet* **2:** 1-30

Helfrich-Forster C, Wulf J, de Belle JS (2002) Mushroom body influence on locomotor activity and circadian rhythms in *Drosophila melanogaster*. *J Neurogenet* **16:** 73-109

Hendel T, Michels B, Neuser K, Schipanski A, Kaun K, Sokolowski MB, Marohn F, Michel R, Heisenberg M, Gerber B (2005) The carrot, not the stick: appetitive rather than aversive gustatory stimuli support associative olfactory learning in individually assayed *Drosophila* larvae. *J Comp Physiol A Neuroethol Sens Neural Behav Physiol* **191:** 265-279

Hess NK, Singer PA, Trinh K, Nikkhoy M, Bernstein SI (2007) Transcriptional regulation of the *Drosophila melanogaster* muscle myosin heavy-chain gene. *Gene Expr Patterns* **7:** 413-422

Hidalgo A, Kinrade EF, Georgiou M (2001) The *Drosophila* neuregulin vein maintains glial survival during axon guidance in the CNS. *Dev Cell* **1:** 679-690

Hildebrandt A, Bickmeyer I, Kuhnlein RP (2011) Reliable *Drosophila* body fat quantification by a coupled colorimetric assay. *PLoS One* **6:** e23796

Hochstrasser T, Ehrlich D, Marksteiner J, Sperner-Unterweger B, Humpel C (2011) Matrix Metalloproteinase-2 and Epidermal Growth Factor are Decreased in Platelets of Alzheimer Patients. *Curr Alzheimer Res* **[Epub ahead of print]**

Holbro T, Hynes NE (2004) ErbB receptors: directing key signaling networks throughout life. *Annu Rev Pharmacol Toxicol* **44:** 195-217

Huang Z, Shilo BZ, Kunes S (1998) A retinal axon fascicle uses spitz, an EGF receptor ligand, to construct a synaptic cartridge in the brain of *Drosophila*. *Cell* **95:** 693-703

Hummel T, Vasconcelos ML, Clemens JC, Fishilevich Y, Vosshall LB, Zipursky SL (2003) Axonal targeting of olfactory receptor neurons in *Drosophila* is controlled by Dscam. *Neuron* **37:** 221-231

Imler JL, Bulet P (2005) Antimicrobial peptides in *Drosophila*: structures, activities and gene regulation. *Chem Immunol Allergy* **86:** 1-21

Inoue H, Lin L, Lee X, Shao Z, Mendes S, Snodgrass-Belt P, Sweigard H, Engber T, Pepinsky B, Yang L, Beal MF, Mi S, Isacson O (2007) Inhibition of the leucine-rich repeat protein LINGO-1 enhances survival, structure, and function of dopaminergic neurons in Parkinson's disease models. *Proc Natl Acad Sci U S A* **104:** 14430-14435

Jiang H, Edgar BA (2009) EGFR signaling regulates the proliferation of *Drosophila* adult midgut progenitors. *Development* **136:** 483-493

Jiang H, Grenley MO, Bravo MJ, Blumhagen RZ, Edgar BA (2011) EGFR/Ras/MAPK signaling mediates adult midgut epithelial homeostasis and regeneration in *Drosophila*. *Cell Stem Cell* **8:** 84-95

Joiner WJ, Crocker A, White BH, Sehgal A (2006) Sleep in *Drosophila* is regulated by adult mushroom bodies. *Nature* **441:** 757-760

Katzel JA, Fanucchi MP, Li Z (2009) Recent advances of novel targeted therapy in non-small cell lung cancer. *J Hematol Oncol* **2:** 2

Keene AC, Waddell S (2007) *Drosophila* olfactory memory: single genes to complex neural circuits. *Nat Rev Neurosci* **8:** 341-354

Kiger AA, White-Cooper H, Fuller MT (2000) Somatic support cells restrict germline stem cell self-renewal and promote differentiation. *Nature* **407:** 750-754

Klein DE, Nappi VM, Reeves GT, Shvartsman SY, Lemmon MA (2004) Argos inhibits epidermal growth factor receptor signalling by ligand sequestration. *Nature* **430:** 1040-1044

Kojic N, Chung E, Kho AT, Park JA, Huang A, So PT, Tschumperlin DJ (2010) An EGFR autocrine loop encodes a slow-reacting but dominant mode of mechanotransduction in a polarized epithelium. *FASEB J* **24:** 1604-1615

Kramer A, Yang FC, Snodgrass P, Li X, Scammell TE, Davis FC, Weitz CJ (2003) Regulation of daily locomotor activity and sleep by hypothalamic EGF receptor signalling. *Novartis Found Symp* **253:** 250-262; discussion 102-259, 263-256, 281-254

Kushikata T, Fang J, Chen Z, Wang Y, Krueger JM (1998) Epidermal growth factor enhances spontaneous sleep in rabbits. *Am J Physiol* **275:** R509-514

LaJeunesse DR, Johnson B, Presnell JS, Catignas KK, Zapotoczny G (2010) Peristalsis in the junction region of the *Drosophila* larval midgut is modulated by DH31 expressing enteroendocrine cells. *BMC Physiol* **10:** 14

Law JH, Wells MA (1989) Insects as biochemical models. *J Biol Chem* **264:** 16335-16338

Lee T, Lee A, Luo L (1999) Development of the *Drosophila* mushroom bodies: sequential generation of three distinct types of neurons from a neuroblast. *Development* **126:** 4065-4076

Lehane MJ (1997) Peritrophic matrix structure and function. *Annu Rev Entomol* **42:** 525-550

Lessing D, Bonini NM (2009) Maintaining the brain: insight into human neurodegeneration from *Drosophila melanogaster* mutants. *Nat Rev Genet* **10:** 359-370

Li Y, Xu Z, Ford GD, Croslan DR, Cairobe T, Li Z, Ford BD (2007) Neuroprotection by neuregulin-1 in a rat model of permanent focal cerebral ischemia. *Brain Res* **1184:** 277-283

Lindsley DL, Sandler L, Baker BS, Carpenter AT, Denell RE, Hall JC, Jacobs PA, Miklos GL, Davis BK, Gethmann RC, Hardy RW, Steven AH, Miller M, Nozawa H, Parry DM, Gould-Somero M, Gould-Somero M (1972) Segmental aneuploidy and the genetic gross structure of the *Drosophila* genome. *Genetics* **71:** 157-184

Maniatis T, Goodbourn S, Fischer JA (1987) Regulation of inducible and tissue-specific gene expression. *Science* **236:** 1237-1245

Marella S, Fischler W, Kong P, Asgarian S, Rueckert E, Scott K (2006) Imaging taste responses in the fly brain reveals a functional map of taste category and behavior. *Neuron* **49:** 285-295

McDonald JA, Pinheiro EM, Kadlec L, Schupbach T, Montell DJ (2006) Multiple EGFR ligands participate in guiding migrating border cells. *Dev Biol* **296:** 94-103

McGuire SE, Mao Z, Davis RL (2004) Spatiotemporal gene expression targeting with the TARGET and gene-switch systems in *Drosophila*. *Sci STKE* **2004:** pl6

Michels B, Diegelmann S, Tanimoto H, Schwenkert I, Buchner E, Gerber B (2005) A role for Synapsin in associative learning: the *Drosophila* larva as a study case. *Learn Mem* **12:** 224-231

Middleton CA, Nongthomba U, Parry K, Sweeney ST, Sparrow JC, Elliott CJ (2006) Neuromuscular organization and aminergic modulation of contractions in the *Drosophila* ovary. *BMC Biol* **4:** 17

Miller A (1950) *The internal anatomy and histology of the imago of Drosophila melanogaster*: Biology of Drosophila.

Misra JR, Horner MA, Lam G, Thummel CS (2011) Transcriptional regulation of xenobiotic detoxification in *Drosophila*. *Genes Dev* **25:** 1796-1806

Montell C (2005) Drosophila TRP channels. *Pflugers Arch* **451:** 19-28

Morante J, Desplan C (2004) Building a projection map for photoreceptor neurons in the *Drosophila* optic lobes. *Semin Cell Dev Biol* **15:** 137-143

Mullis KB (1990) The unusual origin of the polymerase chain reaction. *Sci Am* **262:** 56-61, 64-55

Muqit MM, Feany MB (2002) Modelling neurodegenerative diseases in *Drosophila*: a fruitful approach? *Nat Rev Neurosci* **3:** 237-243

Nagaraj R, Banerjee U (2004) The little R cell that could. *Int J Dev Biol* **48:** 755-760

Neuman-Silberberg FS, Schüpbach T (1993) The *Drosophila* dorsoventral patterning gene gurken produces a dorsally localized RNA and encodes a TGF alpha-like protein. *Cell* **75:** 165-174

Neuser K, Husse J, Stock P, Gerber B (2005) Appetitive olfactory learning in larvae: effects of repetition, reward strength, age, gender, assay type and memory span. *Animal Behaviour* **69:** 891-898

Nicholson L, Singh GK, Osterwalder T, Roman GW, Davis RL, Keshishian H (2008) Spatial and temporal control of gene expression in *Drosophila* using the inducible GeneSwitch GAL4 system. I. Screen for larval nervous system drivers. *Genetics* **178:** 215-234

Nusslein-Volhard C, Wieschaus E (1980) Mutations affecting segment number and polarity in *Drosophila*. *Nature* **287:** 795-801

O'Keefe L, Dougan ST, Gabay L, Raz E, Shilo BZ, DiNardo S (1997) Spitz and Wingless, emanating from distinct borders, cooperate to establish cell fate across the Engrailed domain in the *Drosophila* epidermis. *Development* **124:** 4837-4845

Ohlstein B, Spradling A (2007) Multipotent *Drosophila* intestinal stem cells specify daughter cell fates by differential notch signaling. *Science* **315:** 988-992

Osterwalder T, Yoon KS, White BH, Keshishian H (2001) A conditional tissue-specific transgene expression system using inducible GAL4. *Proc Natl Acad Sci U S A* **98:** 12596-12601

Pandey UB, Nichols CD (2011) Human disease models in *Drosophila melanogaster* and the role of the fly in therapeutic drug discovery. *Pharmacol Rev* **63:** 411-436

Parisi M, Li R, Oliver B (2011) Lipid profiles of female and male *Drosophila*. *BMC Res Notes* **4:** 198

Patterson JT (1943) Studies in the genetics of *Drosophila*. III. The Drosophilidae of the Southwest. *University of Texas Publications* **4313:** 7-216

Pauls D, Selcho M, Gendre N, Stocker RF, Thum AS (2010) *Drosophila* larvae establish appetitive olfactory memories via mushroom body neurons of embryonic origin. *J Neurosci* **30:** 10655-10666

Pavlov IP (1927) *Conditioned reflexes: An investigation of the physiological activity of the cerebral cortex*: London: Oxford University Press.

Pfaffl MW (2001) A new mathematical model for relative quantification in real-time RT-PCR. *Nucleic Acids Res* **29:** e45

Pitman JL, McGill JJ, Keegan KP, Allada R (2006) A dynamic role for the mushroom bodies in promoting sleep in *Drosophila*. *Nature* **441:** 753-756

Poletti M, Frosini D, Pagni C, Baldacci F, Nicoletti V, Tognoni G, Lucetti C, Del Dotto P, Ceravolo R, Bonuccelli U (2012) Mild cognitive impairment and cognitive-motor relationships in newly diagnosed drug-naive patients with Parkinson's disease. *J Neurol Neurosurg Psychiatry* **83:** 601-606

Ravi Ram K, Wolfner MF (2007) Seminal influences: *Drosophila* Acps and the molecular interplay between males and females during reproduction. *Integr Comp Biol* **47:** 427-445

Reich A, Shilo BZ (2002) Keren, a new ligand of the *Drosophila* epidermal growth factor receptor, undergoes two modes of cleavage. *EMBO J* **21:** 4287-4296

Reiter LT, Potocki L, Chien S, Gribskov M, Bier E (2001) A systematic analysis of human disease-associated gene sequences in *Drosophila melanogaster*. *Genome Res* **11:** 1114-1125

Ricart K, J. Pearson R J, Viera L, Cassina P, Kamaid A, Carroll SL, Estevez AG (2006) Interactions between beta-neuregulin and neurotrophins in motor neuron apoptosis. *J Neurochem* **97:** 222-233

Rion S, Kawecki TJ (2007) Evolutionary biology of starvation resistance: what we have learned from *Drosophila*. *J Evol Biol* **20:** 1655-1664

Rohrbough J, Broadie K (2002) Electrophysiological analysis of synaptic transmission in central neurons of *Drosophila* larvae. *J Neurophysiol* **88:** 847-860

Rubin GM, Lewis EB (2000) A brief history of *Drosophila'*s contributions to genome research. *Science* **287:** 2216-2218

Rutledge BJ, Zhang K, Bier E, Jan YN, Perrimon N (1992) The *Drosophila* spitz gene encodes a putative EGF-like growth factor involved in dorsal-ventral axis formation and neurogenesis. *Genes Dev* **6:** 1503-1517

Saper CB, Chou TC, Scammell TE (2001) The sleep switch: hypothalamic control of sleep and wakefulness. *Trends Neurosci* **24:** 726-731

Scalabrino G, Galimberti D, Mutti E, Scalabrini D, Veber D, De Riz M, Bamonti F, Capello E, Mancardi GL, Scarpini E (2010) Loss of epidermal growth factor regulation by cobalamin in multiple sclerosis. *Brain Res* **1333:** 64-71

Schejter ED, Segal D, Glazer L, Shilo BZ (1986) Alternative 5' exons and tissue-specific expression of the *Drosophila* EGF receptor homolog transcripts. *Cell* **46:** 1091-1101

Scherer S, Stocker RF, Gerber B (2003) Olfactory learning in individually assayed *Drosophila* larvae. *Learn Mem* **10:** 217-225

Schnepp B, Grumbling G, Donaldson T, Simcox A (1996) Vein is a novel component in the *Drosophila* epidermal growth factor receptor pathway with similarity to the neuregulins. *Genes Dev* **10:** 2302-2313

Schramm G, Bruchhaus I, Roeder T (2000) A simple and reliable 5'-RACE approach. *Nucleic Acids Res* **28:** E96

Schweitzer R, Shaharabany M, Seger R, Shilo BZ (1995) Secreted Spitz triggers the DER signaling pathway and is a limiting component in embryonic ventral ectoderm determination. *Genes Dev* **9:** 1518-1529

Scott K, Brady R, Jr., Cravchik A, Morozov P, Rzhetsky A, Zuker C, Axel R (2001) A chemosensory gene family encoding candidate gustatory and olfactory receptors in *Drosophila*. *Cell* **104**

Selcho M, Pauls D, Han KA, Stocker RF, Thum AS (2009) The role of dopamine in *Drosophila* larval classical olfactory conditioning. *PLoS One* **4:** e5897

Shilo BZ (2003) Signaling by the *Drosophila* epidermal growth factor receptor pathway during development. *Exp Cell Res* **284:** 140-149

Shilo BZ (2005) Regulating the dynamics of EGF receptor signaling in space and time. *Development* **132:** 4017-4027

Shilo BZ, Schejter ED, Segal D, Ginsberg DS, Glazer L (1986) The *Drosophila* epidermal growth factor receptor homolog: structure, evolution, and possible functions. *Symp Fundam Cancer Res* **39:** 87-97

Shyu WC, Lin SZ, Chiang MF, Yang HI, Thajeb P, Li H (2004) Neuregulin-1 reduces ischemia-induced brain damage in rats. *Neurobiol Aging* **25:** 935-944

Singh SR, Liu W, Hou SX (2007) The adult *Drosophila* malpighian tubules are maintained by multipotent stem cells. *Cell Stem Cell* **1:** 191-203

Søndergaard L (1993) Homology between the mammalian liver and the *Drosophila* fat body. *Trends Genet* **9:** 193

Spradling AC, Rubin GM (1982) Transposition of cloned P elements into *Drosophila* germ line chromosomes. *Science* **218:** 341-347

Stankovic K, Rio C, Xia A, Sugawara M, Adams JC, Liberman MC, Corfas G (2004) Survival of adult spiral ganglion neurons requires erbB receptor signaling in the inner ear. *J Neurosci* **24:** 8651-8661

Stein RA, Staros JV (2000) Evolutionary analysis of the ErbB receptor and ligand families. *J Mol Evol* **50:** 397-412

Stein RA, Staros JV (2006) Insights into the evolution of the ErbB receptor family and their ligands from sequence analysis. *BMC Evol Biol* **6**

Strauss R, Heisenberg M (1993) A higher control center of locomotor behavior in the *Drosophila* brain. *J Neurosci* **13:** 1852-1861

Sturtevant AH (1913) The linear arrangement of six sex-linked
factors in Drosophila, as shown by their mode of association. *J. Exp. Zool.* **14**

Sturtevant MA, Roark M, Bier E (1993) The *Drosophila* rhomboid gene mediates the localized formation of wing veins and interacts genetically with components of the EGF-R signaling pathway. *Genes Dev* **7:** 961-973

Sudarsan V, Pasalodos-Sanchez S, Wan S, Gampel A, Skaer H (2002) A genetic hierarchy establishes mitogenic signalling and mitotic competence in the renal tubules of *Drosophila*. *Development* **129:** 935-944

Sung TI, Wang YJ, Chen CY, Hung TL, Guo HR (2012) Increased serum level of epidermal growth factor receptor in liver cancer patients and its association with exposure to arsenic. *Sci Total Environ* **424:** 74-78

Tang P, Steck PA, Yung WK (1997) The autocrine loop of TGF-alpha/EGFR and brain tumors. *J Neurooncol* **35:** 303-314

Tomchik SM, Davis RL (2009) Dynamics of learning-related cAMP signaling and stimulus integration in the *Drosophila* olfactory pathway. *Neuron* **64:** 510-521

Urban S, Lee JR, Freeman M (2002) A family of Rhomboid intramembrane proteases activates all *Drosophila* membrane-tethered EGF ligands. *EMBO J* **21:** 4277-4286

Venken KJ, Bellen HJ (2012) Genome-wide manipulations of *Drosophila melanogaster* with transposons, Flp recombinase, and PhiC31 integrase. *Methods Mol Biol* **859:** 203-228

Vivekanand P, Rebay I (2006) Intersection of signal transduction pathways and development. *Annu Rev Genet* **40:** 139-157

Wadsworth SC, Vincent WS, 3rd, Bilodeau-Wentworth D (1985) A *Drosophila* genomic sequence with homology to human epidermal growth factor receptor. *Nature* **314:** 178-180

Wang W, Liu W, Wang Y, Zhou L, Tang X, Luo H (2011) Notch signaling regulates neuroepithelial stem cell maintenance and neuroblast formation in *Drosophila* optic lobe development. *Dev Biol* **350:** 414-428

Weiss KR, Kimura Y, Lee WC, Littleton JT (2012) Huntingtin aggregation kinetics and their pathological role in a *Drosophila* Huntington's disease model. *Genetics* **190:** 581-600

Whitworth AJ (2011) *Drosophila* models of Parkinson's disease. *Adv Genet* **73:** 1-50

Wieduwilt MJ, Moasser MM (2008) The epidermal growth factor receptor family: biology driving targeted therapeutics. *Cell Mol Life Sci* **65:** 1566-1584

Woo RS, Lee JH, Yu HN, Song DY, Baik TK (2011) Expression of ErbB4 in the neurons of Alzheimer's disease brain and APP/PS1 mice, a model of Alzheimer's disease. *Anat Cell Biol* **44:** 116-127

Yarden Y, Schlessinger J (1987) Epidermal growth factor induces rapid, reversible aggregation of the purified epidermal growth factor receptor. *Biochemistry* **26:** 1443-1451

Yarden Y, Ullrich A (1988) Growth factor receptor tyrosine kinases. *Annu Rev Biochem* **57:** 443-478

Zhou Z, Sathiyamoorthy S, Tan E (2012) LINGO-1 and neurodegeneration: pathophysiologic clues for essential tremor? *Tremor Other Hyperkinet Mov (N Y)*

Zhu H, Acquaviva J, Ramachandran P, Boskovitz A, Woolfenden S, Pfannl R, Bronson RT, Chen JW, Weissleder R, Housman DE, Charest A (2009) Oncogenic EGFR signaling cooperates with loss of tumor suppressor gene functions in gliomagenesis. *Proc Natl Acad Sci U S A* **106:** 2712-2716

8 ACKNOWLEDGEMENTS

First of all, I would like to cordially thank my doctoral adviser Prof. Dr. Matthias Leippe for the opportunity to work on my dissertation, his scientific support, and personal guidance from the beginning to the end of my thesis. His constructive criticism helped a lot to improve my skills as a researcher and competencies in writing scientific manuscripts

Furthermore, I am thankful for the scientific fly expertise, encouragement, and positive motivation of Prof. Dr. Thomas Roeder and also for agreeing to act as second examiner.

I owe special thanks to Dr. Henning Fedders for his enduring scientific advice. Rarely, you find an advisor and colleague, who always finds the time to listen to greater or minor problems in the course of performing research. His help in technical and editorial questions was essential for the completion of this dissertation.

The financial support of the Inflammation at Interfaces Cluster of Excellence is gratefully acknowledged.

My sincere thanks also goes to the Departments of Zoophysiology I and II for the very good working environment. It was a pleasure to work with you! I enjoyed the friendly relations and the supportive atmosphere.

I am deeply indebted to my husband for his ongoing patience, personal support, and love especially in challenging times. It is wonderful to have you beside me, in the past, present, and future. It is still true what I wrote in the acknowledgements of my Diploma thesis: You make my life better – every day!

Besides, I am grateful for the promotion and love of my mother.

I would like to give my special thanks my friends, who have not tired to listen to the issues of my researcher’s life and helped me by offering some distraction. I hope that I can provide the same for you, whenever you will need it!

9 CURRICULUM VITAE

PERSONAL INFORMATION	
First name	Tasja
Surname	Rahn
Date of birth	27. August 1984
Place of birth	Heide
Nationality	German
PRIMARY EDUCATION	
Dates	1991 – 1995
Name and type of organisation providing education and training	Grundschule Tellingstedt, primary school, Tellingstedt
SECONDARY EDUCATION	
Dates	1995 – 2004
Title of qualification awarded	Abitur
Principal subjects	Intensive courses: Biology and English Examination subjects: History (P3) and Mathematics (P4)
Name and type of organisation providing education and training	Gymnasium Heide-Ost, grammar school, Heide
UNIVERSITY EDUCATION	
Dates	2004 – 2009
Title of qualification awarded	Diploma in Biology
Principal subjects/occupational skills covered	Cell Biology (major subject), Zoology, and Toxicology (minor subjects) Diploma thesis: ‘Molecular analysis of the innate immune system of *Hydra’*
Name and type of organisation providing education and training	Christian-Albrechts-Universität, university, Kiel

DOCTORAL DISSERTATION	
Dates	Since January 2010
Thesis title	Molecular Characterization of EGFR signaling in *Drosophila melanogaster*
Name and type of organisation providing education and training	Zoological Institute, Zoophysiology Christian-Albrechts-Universität, university, Kiel
WORK EXPERIENCE	
Dates	March – July 2009
Main activities and responsibilities	Research assistant, working on the project: 'METAGUT: Development, prevention and early diagnostic detection of *Clostridium difficile* associated colitis – an interdisciplinary network'
Name and address of employer	Prof. Stefan Schreiber, Institute of Clinical Molecular Biology, Schittenhelmstraße 12, 24105 Kiel

10 DECLARATION

I hereby declare that this thesis is my own original work and that I have not used other than the acknowledged resources and aids. This dissertation has not been submitted for the award of any other degree or diploma in any other tertiary institution. Throughout this thesis, I followed the guidelines of “Good Scientific Practice” of the Deutsche Forschungsgemeinschaft.

Parts of this thesis are submitted for publication in the following article:

Tasja Rahn, Matthias Leippe, Thomas Roeder, Henning Fedders (2012). EGFR signaling is necessary for olfactory learning in *Drosophila melanogaster* larvae. Learning & Memory, in revision.

Kiel, 12. September 2012

Tasja Rahn

11 SUPPLEMENTAL MATERIAL

Tab. S 1. List of genes, which were (A) upregulated or (B) downregulated after expression of *egfr*^{DN} in the abdominal fat body for 24 h. The fold-change of expression for the three replicates is displayed (Microarray 1–3).

A	Microarray 1	Microarray 2	Microarray 3
CG10133	3.253	2.016	<no data>
CG10175	3.259	2.063	<no data>
CG10339	1.519	0.907	2.247
CG10393	2.082	1.650	1.393
CG10414	1.735	1.072	1.573
CG10604	1.762	1.311	2.114
CG10641	2.261	0.841	1.759
CG10798	0.868	1.576	2.115
CG10834	1.219	1.626	1.501
CG10855	5.799	<no data>	4.479
CG10874	0.339	2.769	3.312
CG10901	4.839	1.505	0.266
CG10917	1.791	0.666	1.579
CG10952	1.220	1.701	1.523
CG11060	1.615	0.732	1.505
CG11238	1.377	1.922	1.573
CG11247	1.628	<no data>	1.764
CG11317	1.224	1.821	2.173
CG11320	1.154	1.940	1.705
CG114731	2.408	1.626	<no data>
CG11489	1.570	0.961	1.663
CG11590	1.512	<no data>	1.720
CG11621	1.532	0.666	2.377
CG11859	2.172	1.099	2.029
CG12311	4.827	0.392	2.036
CG12408	1.934	<no data>	6.943
CG12659	0.720	1.599	1.631
CG12964	1.840	0.846	2.541
CG1308	0.676	1.888	1.766
CG13210	0.854	1.532	1.519
CG13214	1.844	1.847	0.779
CG13229	1.882	2.362	0.382
CG13337	4.218	<no data>	2.358
CG13373	1.536	1.424	1.547
CG13391	1.726	0.841	2.446
CG13424	1.143	1.866	2.003
CG13494	1.768	<no data>	2.473
CG13723	1.548	<no data>	2.111
CG13893	2.089	0.683	1.789

B	Microarray 1	Microarray 2	Microarray 3
CG10080	0.242	<no data>	0.655
CG101182	0.627	0.462	1.385
CG10145	0.631	0.650	<no data>
CG10237	0.641	0.833	0.382
CG10281	0.620	0.401	0.405
CG10365	0.602	0.847	0.395
CG10528	0.501	0.637	1.958
CG10553	0.552	0.741	0.296
CG10646	0.469	1.194	0.628
CG10662	0.597	0.940	0.500
CG10753	0.403	0.582	2.688
CG10788	0.372	0.588	2.789
CG10843	0.440	0.499	1.565
CG10992	0.400	0.400	0.863
CG11019	0.488	<no data>	0.503
CG110270	0.371	0.147	1.488
CG11091	0.929	0.257	0.566
CG11120	0.218	<no data>	0.279
CG11142	0.301	<no data>	0.391
CG11159	0.619	0.781	0.651
CG11175	0.309	1.078	0.405
CG11191	0.282	0.929	0.389
CG11227	0.361	0.426	0.589
CG11248	0.255	0.910	0.398
CG11259	0.403	0.947	0.540
CG11405	0.619	0.475	2.533
CG11458	0.652	0.652	1.963
CG11594	0.557	1.462	0.607
CG11614	0.626	0.998	0.313
CG11624	0.603	0.805	0.548
CG11686	0.555	0.775	0.575
CG11760	0.254	0.231	1.612
CG11814	0.251	0.214	1.659
CG11847	0.545	0.565	1.065
CG11857	0.562	0.513	0.993
CG11895	0.634	0.632	1.136
CG12192	0.963	0.665	0.595
CG12325	0.609	0.574	1.016
CG12341	0.636	0.546	1.091

CG1404	1.539	<no data>	1.814
CG14059	2.515	0.512	1.681
CG14149	1.683	0.866	1.548
CG14307	1.574	2.138	1.391
CG14438	1.646	0.511	1.628
CG14469	2.152	0.915	1.525
CG14593	1.240	2.250	2.316
CG14617	3.118	2.240	1.181
CG14655	1.535	1.750	0.761
CG1490	2.768	0.802	1.617
CG15097	2.387	4.743	1.026
CG15107	2.641	4.600	1.034
CG1519	2.089	5.189	3.389
CG15811	1.952	<no data>	2.015
CG15844	1.668	0.444	1.728
CG15883	1.722	0.646	1.513
CG15894	1.582	0.490	2.448
CG17108	1.496	2.159	4.754
CG17218	3.283	0.789	1.524
CG17290	1.559	0.960	2.226
CG17328	1.533	0.630	1.970
CG17742	1.530	1.927	<no data>
CG17820	0.455	6.562	2.583
CG17903	1.513	2.293	0.659
CG1794	3.537	<no data>	2.930
CG18188	5.594	<no data>	22.518
CG18193	1.936	0.477	2.752
CG1835	1.741	4.977	1.857
CG18367	1.567	1.091	2.079
CG1856	1.639	<no data>	1.769
CG2014	1.537	1.570	0.985
CG2021	2.367	0.829	1.530
CG2104	0.889	1.711	1.726
CG2503	1.273	1.608	1.678
CG2670	1.298	1.917	2.049
CG2794	1.926	1.524	1.030
CG300020	0.865	2.934	2.595
CG30019	1.654	1.491	2.332
CG30028	1.211	1.688	2.534
CG30101	1.965	0.585	1.920
CG30143	1.825	0.605	2.170
CG30183	2.032	1.031	1.800
CG31158	0.713	1.758	1.595
CG31196	2.077	17.563	3.690
CG31249	2.059	1.913	<no data>
CG31257	1.888	1.153	1.671

CG12374	0.317	<no data>	0.258
CG12385	0.322	<no data>	0.106
CG12442	0.489	0.613	1.466
CG12720	0.467	0.574	1.638
CG12796	0.656	0.505	1.140
CG12896	0.563	0.563	2.049
CG13126	0.519	0.943	0.661
CG13260	0.607	0.544	1.981
CG13280	0.666	0.501	1.692
CG13364	0.303	0.665	1.306
CG13810	0.608	0.362	1.587
CG13826	0.579	0.548	2.026
CG14228	0.376	0.947	0.453
CG14314	0.360	0.544	0.478
CG14646	0.159	<no data>	0.181
CG14680	0.253	<no data>	0.242
CG14715	0.576	1.100	0.540
CG14763	0.573	2.340	0.575
CG14780	0.892	0.522	0.395
CG14997	0.241	0.503	0.852
CG15007	0.322	0.460	1.211
CG15010	0.530	1.196	0.654
CG15093	0.488	0.362	1.525
CG1512	0.611	1.082	0.522
CG15347	0.458	0.640	1.603
CG15464	0.422	0.649	1.537
CG15538	0.552	0.621	0.804
CG15633	0.642	0.535	0.478
CG15661	0.657	0.511	0.516
CG15740	0.579	0.603	1.193
CG15829	0.285	0.604	0.448
CG158488	0.594	0.562	0.366
CG15871	0.412	0.601	1.090
CG15899	0.485	0.615	0.371
CG15914	0.353	0.617	0.336
CG1602	0.219	0.661	0.366
CG1666	0.664	<no data>	0.591
CG16749	0.371	0.769	0.378
CG16827	0.487	0.541	1.138
CG1683	0.122	0.193	0.850
CG16837	0.369	0.470	1.083
CG16848	0.537	0.630	1.162
CG1685	0.630	0.629	0.911
CG16899	0.606	0.604	1.140
CG16947	0.556	0.842	0.553
CG16988	0.411	1.182	0.348

CG31345	0.958	1.577	1.858
CG31389	1.106	1.687	1.874
CG31451	1.810	0.762	2.280
CG31508	4.659	4.950	8.164
CG31509	2.735	3.461	10.895
CG31546	2.207	15.648	7.993
CG31557	1.370	5.592	3.438
CG31618	7.064	0.879	2.612
CG32041	1.657	1.675	1.390
CG32070	1.554	0.887	2.073
CG32267	1.881	1.031	2.056
CG32278	1.736	1.599	1.189
CG32368	2.505	0.871	33.420
CG32393	1.517	1.001	1.564
CG32444	1.241	2.322	1.525
CG32491	1.833	0.927	1.551
CG3259	1.680	<no data>	1.657
CG32670	1.066	1.537	2.880
CG32856	1.929	0.690	2.748
CG32859	1.587	1.018	2.138
CG32950	2.096	0.818	2.020
CG33056	0.874	1.996	2.164
CG33088	2.165	<no data>	1.500
CG33090	0.820	2.056	2.072
CG33169	1.569	1.502	0.867
CG3322	2.355	0.372	1.679
CG33338	1.631	1.047	1.883
CG3413	1.609	1.927	0.636
CG3446	1.551	2.505	0.647
CG3528	2.292	0.668	1.543
CG3536	1.710	0.666	1.605
CG3604	1.772	1.009	1.865
CG3700	1.039	2.871	2.460
CG3717	1.799	1.670	0.629
CG3736	1.558	0.722	1.798
CG3905	0.916	2.314	1.675
CG3942	0.678	2.306	1.879
CG40044	1.527	0.931	2.436
CG40085	3.068	1.098	2.843
CG4015	1.193	2.016	1.612
CG40178	1.744	1.706	1.181
CG4180	6.170	<no data>	3.520
CG4205	1.136	1.518	1.947
CG4238	1.823	1.690	0.722
CG4329	5.666	2.400	1.558
CG4349	1.135	1.878	1.984

CG17034	0.536	1.009	0.660
CG17045	0.634	1.247	0.354
CG17119	0.258	<no data>	0.357
CG17167	0.404	0.570	1.678
CG17341	0.625	1.179	0.582
CG17549	0.655	0.602	1.260
CG17559	0.276	0.342	1.692
CG17564	0.582	1.161	0.235
CG17566	0.503	1.076	0.396
CG17610	0.572	1.227	0.246
CG17636	0.612	2.073	0.563
CG1774	1.971	0.628	0.469
CG17746	0.624	1.149	0.489
CG17970	1.498	0.576	0.665
CG18108	0.636	0.495	2.499
CG18212	0.238	1.751	0.226
CG18258	0.193	<no data>	0.055
CG18341	0.341	0.765	0.129
CG18437	0.504	0.592	0.342
CG1844	0.313	<no data>	0.072
CG18444	0.498	0.525	1.090
CG18519	0.639	0.959	0.495
CG18584	0.657	0.907	0.546
CG1869	0.281	<no data>	0.392
CG2046	0.593	0.613	0.643
CG2053	0.432	1.075	0.517
CG2069	0.494	0.991	0.456
CG2079	0.566	0.637	0.801
CG2157	0.321	0.385	0.485
CG2198	0.152	1.332	0.427
CG2336	0.561	0.803	0.495
CG2471	0.478	0.798	0.498
CG27742	0.503	1.106	0.587
CG30033	0.232	<no data>	0.194
CG30045	0.240	0.322	1.783
CG30076	0.258	0.371	1.889
CG30194	0.378	0.953	0.427
CG30280	0.160	0.275	1.066
CG30401	0.293	0.083	1.898
CG3126	0.238	0.148	1.308
CG31326	0.274	0.523	0.779
CG31373	0.186	0.917	0.109
CG31415	0.160	<no data>	0.089
CG315232	0.481	1.621	0.453
CG3164	0.454	1.236	0.552
CG31705	0.470	0.634	<no data>

CG4648	1.749	1.181	2.019
CG4869	2.577	0.503	1.563
CG5300	3.008	0.683	1.661
CG5330	2.300	0.612	1.651
CG5474	1.670	1.618	0.378
CG5618	1.534	2.059	0.665
CG5675	1.519	2.036	0.961
CG5727	1.698	0.680	1.866
CG5809	1.500	1.557	0.523
CG5810	1.980	1.544	0.854
CG6187	1.992	4.666	0.808
CG6198	1.575	1.707	<no data>
CG6238	2.356	1.520	0.390
CG6251	3.034	0.747	1.734
CG6343	2.935	3.367	0.745
CG67657	2.092	1.708	1.057
CG6808	0.518	2.043	1.919
CG6817	2.255	2.045	1.469
CG6852	1.644	0.916	1.723
CG6854	1.502	0.909	2.294
CG6860	1.672	<no data>	1.680
CG6912	1.648	2.735	0.581
CG7051	1.695	0.548	1.577
CG7324	1.327	1.894	1.584
CG7509	1.789	0.753	1.509
CG7530	1.403	2.452	1.841
CG7595	1.746	0.480	15.762
CG7749	2.013	1.840	0.604
CG7759	1.222	2.406	1.633
CG7935	1.756	0.735	1.557
CG8345	2.170	3.626	0.577
CG8358	2.615	<no data>	2.670
CG8396	2.094	0.523	1.538
CG8420	1.949	1.718	1.066
CG8556	2.287	1.787	0.622
CG8892	2.085	1.008	1.666
CG9000	1.971	0.573	1.580
CG9012	2.111	0.828	1.550
CG9077	2.577	1.131	1.524
CG9242	1.732	1.168	1.752
CG9295	2.007	0.860	1.714
CG9302	2.098	1.003	1.705
CG9354	2.922	0.572	2.409
CG9512	1.352	1.791	1.796
CG9539	1.728	1.725	0.367
CG9553	1.595	1.289	1.628

CG31763	0.605	0.374	1.623
CG31776	0.619	0.375	0.232
CG31807	0.486	0.368	0.814
CG31832	0.486	0.399	0.852
CG31839	0.288	0.324	0.583
CG31955	0.278	0.427	1.679
CG31997	0.567	0.567	1.547
CG32032	0.584	0.567	0.971
CG3210	0.596	0.633	1.145
CG32207	0.759	0.611	0.586
CG32280	0.535	0.527	0.806
CG32304	0.554	0.536	0.671
CG32399	0.612	0.618	1.599
CG32523	0.440	0.610	0.702
CG3264	0.556	<no data>	0.556
CG32666	1.517	0.625	0.442
CG32677	0.337	0.367	1.651
CG32688	0.665	0.622	1.265
CG32696	0.521	<no data>	0.394
CG32700	0.468	0.618	1.396
CG33109	0.178	0.094	1.045
CG33113	0.557	0.640	0.726
CG33115	0.329	0.662	<no data>
CG331262	0.666	0.203	0.572
CG33193	0.920	0.550	0.445
CG3342	0.579	0.488	<no data>
CG3373	0.467	0.816	0.342
CG3403	2.109	0.530	0.258
CG3436	0.642	0.824	0.597
CG3669	0.609	0.991	0.536
CG3707	0.615	0.428	0.553
CG3724	0.453	0.441	2.030
CG3870	0.131	<no data>	0.140
CG39152	0.628	1.016	0.245
CG3979	0.664	1.136	0.594
CG3989	0.531	0.418	0.503
CG40131	0.359	0.948	0.367
CG40177	0.369	0.976	0.374
CG40225	0.484	0.327	0.525
CG4036	0.520	0.907	0.407
CG4363	0.325	0.142	1.055
CG4669	0.308	0.638	0.367
CG4696	0.262	0.534	0.364
CG4709	0.514	0.568	1.490
CG4713	0.564	1.440	0.453
CG4784	0.568	0.558	1.819

CG9672	2.215	1.045	1.543
CG9682	1.949	1.952	1.069
CG9695	1.571	1.886	1.258
CR31621	1.746	<no data>	3.910
CR31853	1.845	2.415	0.423
CR32910	2.885	0.630	1.582
Q9LJQ4	0.915	2.148	1.535
CG11910	<no data>	4.317	4.015
CG13454	<no data>	2.268	1.938
CG17436	<no data>	1.536	5.436
CG18374	<no data>	4.168	1.759
CG3151	<no data>	11.293	6.962
CG33054	<no data>	1.861	1.574
CG6871	<no data>	1.696	1.949
CG7186	<no data>	2.239	1.548

192

CG4785	0.137	<no data>	0.165
CG4803	0.675	0.623	0.529
CG4825	0.543	1.601	0.665
CG4877	0.235	0.373	0.607
CG4891	0.215	0.310	0.649
CG4955	0.586	0.545	2.620
CG4969	0.480	0.630	1.849
CG5178	0.565	0.604	1.825
CG5479	1.562	0.527	0.616
CG5482	0.747	0.511	0.525
CG5604	0.645	0.527	0.688
CG5730	0.639	0.659	0.823
CG5738	0.642	0.458	1.519
CG5741	0.602	0.480	1.591
CG5787	0.345	0.218	0.894
CG5813	0.435	0.219	0.842
CG5830	0.262	0.226	0.869
CG5853	0.656	1.068	0.583
CG5896	0.472	0.551	0.886
CG5897	0.430	1.113	0.389
CG5938	0.521	1.105	0.555
CG5949	0.271	0.784	0.540
CG6007	0.424	1.818	0.478
CG6012	0.607	0.503	1.534
CG6034	0.589	0.532	1.759
CG6116	0.545	0.517	2.922
CG6145	0.656	1.182	0.373
CG6167	0.355	0.516	2.848
CG6222	0.434	0.615	1.570
CG6265	0.423	0.605	1.282
CG6283	0.305	0.646	1.397
CG6362	0.385	0.424	1.855
CG6485	0.591	1.281	0.597
CG6522	0.635	0.618	1.047
CG6660	0.457	1.012	0.390
CG6687	0.459	0.378	3.315
CG6726	0.291	<no data>	0.206
CG6757	0.388	0.593	2.677
CG6798	0.268	0.580	0.351
CG6874	0.461	1.538	0.573
CG6888	0.347	1.900	0.531
CG6901	0.629	0.369	0.895
CG6983	0.488	1.108	0.614
CG7053	0.615	0.618	1.746
CG7189	0.584	0.629	0.681
CG7199	0.329	0.819	0.084

CG7231	0.589	0.666	0.682
CG7246	0.494	<no data>	0.105
CG7274	0.360	0.633	0.810
CG7402	0.399	1.056	0.528
CG7439	0.463	1.196	0.400
CG7620	0.669	0.529	0.597
CG77520	0.532	1.328	0.659
CG7769	0.393	0.619	0.934
CG78755	0.380	<no data>	0.165
CG7910	0.365	<no data>	0.111
CG7911	0.561	0.859	0.316
CG7920	0.592	1.281	0.237
CG7926	0.474	1.057	0.580
CG7936	0.523	1.032	0.558
CG7971	0.552	0.890	0.536
CG8013	0.604	0.443	1.728
CG8190	0.499	0.785	0.416
CG8200	0.392	1.020	0.495
CG8234	0.391	0.588	2.830
CG8245	0.259	0.794	0.528
CG8256	0.371	0.781	0.338
CG8282	0.530	0.506	0.838
CG8336	0.558	0.947	0.575
CG8386	0.615	0.664	1.703
CG8424	0.240	0.829	0.397
CG8526	0.664	0.206	1.153
CG8611	0.651	0.575	1.709
CG8630	0.506	0.558	0.449
CG8664	0.219	0.241	1.476
CG86761	0.511	0.568	0.223
CG8790	0.509	0.396	0.806
CG8874	0.428	<no data>	0.218
CG8931	0.406	0.586	0.573
CG9044	0.612	1.621	0.639
CG9081	0.574	0.678	0.453
CG9132	0.827	0.655	0.649
CG9391	0.597	0.516	1.252
CG9394	0.390	1.359	0.399
CG9459	0.514	1.333	0.571
CG9476	0.768	0.430	0.593
CG9507	0.457	0.651	1.071
CG9509	0.517	1.636	0.146
CG9528	0.399	0.822	0.655
CG9580	0.421	0.191	0.863
CG9676	0.458	0.489	0.643
CG9738	0.547	0.534	1.403

CG9746	2.720	0.594	0.573
CG9839	0.503	0.489	0.724
CG9865	0.106	0.096	0.146
CR318086	0.601	1.081	0.194
CG10981	<no data>	0.438	0.471
CG114277	<no data>	0.248	0.148
CG18467	<no data>	0.545	0.340
CG30413	<no data>	0.485	0.623
CG33119	<no data>	0.477	0.295
CG9496	<no data>	0.174	0.106

Tab. S 2. List of genes, which were (A) upregulated or (B) downregulated in aFB-GS > w^{1118} flies after mifepristone-feeding for 24 h. The fold-change of expression for one replicates is displayed (Microarray 1).

A	Microarray 1
CG10036	1.609
CG10080	3.226
CG10121	1.970
CG10219	2.809
CG10307	2.376
CG10326	1.878
CG10414	1.568
CG10428	1.799
CG10477	2.114
CG10653	2.110
CG10734	1.603
CG10806	2.887
CG10811	2.163
CG10909	1.943
CG10944	1.722
CG10952	2.843
CG1112	3.511
CG11133	1.567
CG11142	3.600
CG11143	1.741
CG11153	2.607
CG11284	1.885
CG11421	1.630
CG11462	1.570
CG11523	2.292
CG11843	1.572
CG11902	1.822
CG11985	1.660
CG12016	1.896
CG12123	2.514
CG12126	2.081

B	Microarray 1
CG10034	0.651
CG10041	0.525
CG10073	0.589
CG10113	0.469
CG10168	0.525
CG10209	0.554
CG1021	0.568
CG10243	0.579
CG10361	0.531
CG10375	0.632
CG10528	0.524
CG10560	0.188
CG10575	0.529
CG10843	0.495
CG10972	0.628
CG11015	0.450
CG11156	0.551
CG11317	0.565
CG11391	0.609
CG11447	0.600
CG11458	0.603
CG11502	0.472
CG11621	0.474
CG11785	0.559
CG11899	0.600
CG11963	0.518
CG12014	0.520
CG12042	0.552
CG1213	0.574
CG12234	0.622
CG12286	0.602

CG12192	1.877	**CG12384**	0.626
CG12263	2.141	**CG12391**	0.654
CG12268	1.620	**CG12442**	0.403
CG12284	2.088	**CG12781**	0.536
CG12292	1.509	**CG12796**	0.096
CG12323	2.625	**CG12846**	0.572
CG12436	1.502	**CG12950**	0.526
CG12659	2.071	**CG12959**	0.484
CG12780	2.424	**CG1330**	0.169
CG1298	1.520	**CG13308**	0.631
CG13000	2.141	**CG13625**	0.618
CG13062	1.966	**CG13717**	0.524
CG13202	1.548	**CG13802**	0.437
CG13285	1.642	**CG13809**	0.618
CG13290	1.655	**CG13869**	0.458
CG13311	2.074	**CG13954**	0.583
CG13317	1.701	**CG14029**	0.624
CG13390	1.651	**CG14184**	0.654
CG13397	1.566	**CG14234**	0.433
CG13410	2.096	**CG14312**	0.259
CG13610	1.686	**CG14417**	0.504
CG13699	2.658	**CG14570**	0.625
CG14028	2.474	**CG14678**	0.606
CG14218	2.056	**CG1472**	0.584
CG14228	2.155	**CG14760**	0.602
CG14450	2.081	**CG14788**	0.607
CG14483	2.428	**CG14960**	0.628
CG14488	1.956	**CG14979**	0.478
CG14528	1.675	**CG14997**	0.470
CG14581	2.954	**CG15013**	0.609
CG1462	1.840	**CG15020**	0.592
CG14690	1.560	**CG15033**	0.640
CG14701	1.752	**CG15085**	0.622
CG14792	4.592	**CG15153**	0.095
CG14794	4.569	**CG15189**	0.413
CG14888	2.366	**CG1532**	0.389
CG148895	2.836	**CG15438**	0.639
CG15097	1.753	**CG15443**	0.611
CG15125	1.553	**CG15730**	0.484
CG1524	2.060	**CG15740**	0.487
CG15280	1.741	**CG15881**	0.610
CG15368	1.841	**CG16827**	0.136
CG15398	1.752	**CG1683**	0.127
CG1569	2.363	**CG16899**	0.171
CG15699	1.583	**CG169830**	0.443
CG15828	1.893	**CG16988**	0.613

CG1634	1.571	**CG17030**	0.633
CG1651	1.627	**CG17136**	0.628
CG16704	1.501	**CG17142**	0.570
CG16713	1.759	**CG17264**	0.415
CG16742	1.860	**CG17347**	0.432
CG16758	1.693	**CG17470**	0.579
CG16905	1.618	**CG17510**	0.580
CG17108	2.081	**CG17559**	0.621
CG17239	2.034	**CG17631**	0.616
CG17241	1.670	**CG176973**	0.511
CG1742	1.881	**CG17737**	0.658
CG17482	2.244	**CG17763**	0.210
CG17489	2.140	**CG17777**	0.648
CG17494	2.355	**CG17782**	0.531
CG17498	2.376	**CG17820**	0.362
CG17522	1.668	**CG17930**	0.621
CG17540	1.660	**CG18111**	0.606
CG17564	2.204	**CG18335**	0.202
CG17566	2.365	**CG18437**	0.483
CG17610	2.461	**CG18444**	0.563
CG17636	2.074	**CG1927**	0.285
CG17726	2.136	**CG2038**	0.551
CG17991	2.095	**CG2061**	0.532
CG18110	1.611	**CG2062**	0.393
CG18212	8.647	**CG2145**	0.562
CG18234	1.555	**CG2675**	0.444
CG18304	1.858	**CG2718**	0.269
CG1835	1.949	**CG2830**	0.455
CG1844	3.540	**CG2863**	0.592
CG18536	1.785	**CG2934**	0.565
CG1854	1.585	**CG2937**	0.425
CG18581	1.661	**CG2952**	0.572
CG18586	1.837	**CG30010**	0.557
CG18743	1.696	**CG30127**	0.617
CG18765	1.751	**CG30267**	0.202
CG1964	1.801	**CG3029**	0.605
CG2005	1.719	**CG30360**	0.550
CG2054	1.764	**CG31326**	0.558
CG20827	1.759	**CG31679**	0.441
CG2146	1.579	**CG31747**	0.592
CG2157	2.288	**CG31763**	0.614
CG2336	1.646	**CG31779**	0.400
CG2816	1.937	**CG31839**	0.568
CG2819	2.085	**CG32031**	0.099
CG2998	1.792	**CG320589**	0.598
CG2999	3.413	**CG32114**	0.414

CG30028	2.659	**CG32151**	0.588
CG30095	1.526	**CG32230**	0.637
CG30152	1.582	**CG32240**	0.614
CG30153	1.501	**CG32280**	0.642
CG30158	1.730	**CG32677**	0.406
CG30181	1.779	**CG32714**	0.481
CG30196	1.805	**CG32856**	0.644
CG30383	2.557	**CG32986**	0.228
CG30457	2.228	**CG33002**	0.366
CG30460	1.937	**CG3309**	0.603
CG30463	2.357	**CG33090**	0.610
CG3048	1.530	**CG331262**	0.277
CG30485	2.895	**CG33149**	0.599
CG3051	2.189	**CG33220**	0.488
CG3052	1.646	**CG3338**	0.522
CG31093	1.733	**CG33467**	0.658
CG31196	5.320	**CG3382**	0.552
CG31453	4.348	**CG3527**	0.439
CG31508	2.851	**CG3597**	0.504
CG31509	2.535	**CG3688**	0.580
CG31613	2.765	**CG3762**	0.595
CG31618	2.141	**CG3927**	0.581
CG31692	1.645	**CG40044**	0.583
CG31778	1.605	**CG40049**	0.643
CG3186	1.572	**CG40128**	0.551
CG32026	2.631	**CG40157**	0.616
CG32095	2.555	**CG40198**	0.617
CG3210	1.607	**CG4027**	0.592
CG32171	1.775	**CG4095**	0.661
CG32304	1.895	**CG41090**	0.573
CG32429	2.696	**CG4173**	0.228
CG32580	2.003	**CG4312**	0.599
CG32592	1.889	**CG4600**	0.565
CG32954	1.637	**CG4602**	0.650
CG33114	1.516	**CG4785**	0.107
CG3314	2.082	**CG4803**	0.609
CG33151	3.287	**CG4877**	0.602
CG33256	2.526	**CG4891**	0.543
CG33280	2.522	**CG4988**	0.603
CG33332	2.133	**CG5023**	0.552
CG33459	2.025	**CG5057**	0.639
CG3347	2.056	**CG5059**	0.661
CG33494	1.655	**CG5073**	0.407
CG3350	2.218	**CG50780**	0.477
CG3397	2.958	**CG5171**	0.476
CG3427	1.649	**CG5192**	0.518

CG3664	1.715	**CG5258**	0.550
CG3679	1.601	**CG5300**	0.426
CG3725	1.766	**CG5428**	0.517
CG3803	1.583	**CG5482**	0.655
CG3822	1.826	**CG5625**	0.569
CG3905	1.524	**CG5671**	0.635
CG3924	1.587	**CG5730**	0.570
CG3971	2.003	**CG5738**	0.577
CG3972	1.737	**CG5864**	0.614
CG3979	1.722	**CG5915**	0.620
CG40131	1.986	**CG5972**	0.642
CG40177	1.885	**CG6034**	0.666
CG40470	1.555	**CG6105**	0.451
CG41120	1.746	**CG6116**	0.548
CG4185	4.373	**CG6142**	0.378
CG4226	2.446	**CG61511**	0.653
CG4265	1.807	**CG6214**	0.598
CG4268	1.707	**CG6234**	0.513
CG4326	1.619	**CG6283**	0.626
CG4558	1.624	**CG6362**	0.594
CG4586	1.589	**CG6394**	0.503
CG4654	1.884	**CG6464**	0.502
CG4800	2.025	**CG6522**	0.483
CG4863	2.011	**CG6530**	0.587
CG4896	1.542	**CG6543**	0.440
CG4898	2.293	**CG6683**	0.517
CG4900	2.441	**CG6692**	0.532
CG4910	1.727	**CG6726**	0.278
CG4928	2.657	**CG6854**	0.539
CG49340	3.020	**CG6958**	0.576
CG4935	2.332	**CG7049**	0.137
CG4996	2.147	**CG7051**	0.392
CG5001	2.084	**CG7053**	0.456
CG5092	2.141	**CG7062**	0.648
CG5154	1.757	**CG7081**	0.484
CG5163	2.581	**CG71847**	0.576
CG5167	2.400	**CG7245**	0.617
CG5188	1.592	**CG7381**	0.626
CG5247	3.542	**CG7408**	0.639
CG5271	1.859	**CG7582**	0.396
CG5277	1.788	**CG7604**	0.476
CG5452	1.502	**CG7638**	0.343
CG5474	1.741	**CG7713**	0.631
CG5502	2.496	**CG7872**	0.587
CG5547	2.337	**CG78755**	0.152
CG5651	1.570	**CG7910**	0.288

CG5707	1.796
CG5711	2.211
CG5778	1.541
CG5779	1.587
CG5804	2.569
CG5827	1.756
CG5840	1.574
CG5878	1.725
CG5885	1.775
CG5897	2.062
CG5920	1.635
CG5973	1.651
CG6046	1.773
CG6147	1.742
CG6187	1.853
CG6198	1.629
CG6220	1.566
CG6253	1.545
CG6289	1.793
CG6343	1.575
CG6428	1.667
CG6472	2.640
CG6519	1.666
CG6660	1.630
CG6672	1.682
CG6687	1.768
CG6724	1.618
CG6734	1.529
CG6802	1.801
CG6833	1.804
CG6874	1.686
CG6932	1.576
CG6989	2.044
CG7015	5.446
CG7054	1.811
CG7130	2.247
CG7177	1.701
CG7246	2.487
CG7324	2.333
CG7382	1.541
CG7429	1.594
CG7439	2.001
CG7492	1.545
CG7506	1.589
CG7532	1.670
CG7542	1.570
CG7920	0.525
CG7935	0.621
CG8002	0.611
CG8012	0.629
CG8013	0.568
CG8058	0.624
CG8118	0.659
CG8237	0.633
CG8448	0.606
CG8453	0.384
CG8610	0.271
CG8611	0.424
CG8613	0.381
CG8628	0.448
CG8630	0.525
CG8673	0.555
CG8681	0.485
CG8726	0.563
CG8736	0.487
CG8790	0.433
CG8863	0.543
CG8896	0.620
CG8914	0.583
CG8961	0.518
CG9117	0.218
CG9171	0.647
CG9294	0.491
CG9307	0.654
CG9316	0.600
CG9394	0.509
CG9496	0.181
CG9528	0.611
CG9547	0.592
CG9550	0.621
CG9572	0.555
CG9580	0.487
CG9606	0.594
CG9691	0.661
CG9778	0.259
CG9834	0.661
CG9839	0.614
CG9863	0.422
CR318086	0.417
CR32864	0.221
L22585	0.642

CG7707	1.866
CG7730	1.915
CG7759	2.413
CG7808	2.562
CG7809	2.919
CG7845	1.746
CG78671	1.786
CG7903	1.638
CG7953	3.017
CG7963	2.298
CG7967	1.901
CG7991	2.451
CG8049	1.513
CG8085	2.835
CG8097	1.572
CG8314	1.522
CG8334	2.134
CG8345	3.068
CG8394	2.788
CG8416	2.240
CG8460	2.007
CG8474	1.679
CG8498	2.373
CG8509	1.771
CG8544	1.830
CG8597	1.557
CG8642	1.875
CG8730	1.512
CG8745	1.548
CG8828	1.698
CG8865	1.561
CG8866	1.586
CG8905	1.794
CG8925	2.060
CG8979	1.930
CG8986	1.810
CG9092	1.559
CG9093	1.701
CG9115	1.723
CG9240	1.603
CG9284	2.211
CG9333	1.548
CG9334	2.063
CG9436	2.210
CG9459	1.746
CG9494	1.539

CG9523	2.834
CG9539	1.544
CG9617	1.597
CG9668	1.641
CG9686	1.716
CG9862	3.097
CG9935	1.631
CG9953	1.542
CR30478	1.590
CR31621	3.464
CR40456	1.938